Chemical ligation for the ADP-ribosylation of the linker histone H1.2

Doctoral thesis

for obtaining the academic degree
Doctor of Natural Sciences
(Dr. rer. nat.)

Submitted by
Marcel Brakonier

at the

Universität Konstanz

Faculty of Sciences
Department of Chemistry

Konstanz, 2024

Dissertation der Universität Konstanz

Tag der mündlichen Prüfung: 24.01.2025

Prüfungsvorsitzender:	Prof. Dr. Martin Scheffner
Referent:	Prof. Dr. Andreas Marx
Referent:	Prof. Dr. Jörg Hartig

Die vorliegende Dissertation entstand in der Zeit von Oktober 2018 bis Juli 2024 unter der Leitung von Herrn Prof. Dr. Andreas Marx am Fachbereich Chemie der Universität Konstanz.

Acknowledgement / Danksagung

An dieser Stelle möchte ich mich herzlich bei einigen Menschen bedanken ohne deren Unterstützung dies nicht möglich gewesen wäre.
Mein größter Dank gilt Prof. Dr. Andreas Marx, der mir die Möglichkeit gegeben hat, dieses spannende und abwechslungsreiche Thema in seiner Arbeitsgruppe zu bearbeiten. Seine unermüdliche Unterstützung, sein umfangreiches Fachwissen und seine inspirierenden Ratschläge haben maßgeblich zum Gelingen dieser Arbeit beigetragen. Seine Geduld und sein Vertrauen in meine Fähigkeiten haben mir den Raum gegeben, eigene Ideen zu entwickeln und umzusetzen. Ohne seine ständige Ermutigung wäre diese Arbeit nicht in der jetzigen Form entstanden. Vielen Dank für alles!
Mein Dank gilt auch Prof. Dr. Jörg Hartig für die Übernahme meines Zweitgutachtens und Prof. Dr. Martin Scheffner für die Übernahme des Prüfungsvorsitzes. Vielen Dank dafür.
Besonderer Dank gilt auch Dr. Martin Mex, der während seiner Zeit in der Arbeitsgruppe die Grundlagen für diese Dissertation gelegt hat. Danke auch für die vielen Tipps, die Einführung in die Thematik und die guten Diskussionen. Ebenfalls zu erwähnen sind hierbei Dr. Philip Saumer und Dr. Simon Geigges für die Starthilfe in das H1 Thema und die Erklärung aller möglichen biochemischen Arbeitstechniken. Nicht zu vergessen ist auch Luisa Huber, die mir bei biochemischen Laborfragen immer mit Rat und Tat zur Seite stand.
Hierbei möchte ich mich auch bei Dr. Matthias Frese und Dr. Philip Saumer für die Korrekturen meiner Dissertation bedanken. Vielen Dank, dass Ihr dazu beigetragen habt diese Arbeit zu verbessern und insbesondere Matthias auch für die abwechslungsreichen Gespräche bei einem Feierabendbier.
Allen aktuellen und ehemaligen Mitgliedern der AG Marx möchte ich für die gute Arbeitsatmosphäre und die hilfreichen Diskussionen danken. Ein weiterer Dank geht an Dr. Philip Saumer, Florian Stumpf und Jakob Zwicker für diverse LC-MS Messungen. Ebenfalls zu erwähnen sind hierbei alle TAs und Festangestellten der AG Marx, die bei allen Arbeiten innerhalb und außerhalb des Labors unterstützend tätig waren. Insbesondere Petra Jakesch, die uns bei allen administrativen Angelegenheiten unterstützt.
Außerdem möchte ich mich bei Dr. Martin Mex, Dr. Moritz Welter, Dr. Daniel Hammler, Dr. Matthias Frese und Jakob Arnold für die angenehme und produktive Atmosphäre in der Chemie Box 2 bedanken.

Ich möchte mich auch bei allen Studierenden bedanken die ich während meiner Promotion betreut habe und die an meinem Projekt mitgewirkt haben: Saskia Ulm, Anna-Lena Ruopp, Gero Würthwein, Natalie Munding, Mina Bathen, Frederic Hallmann und Kristin Delloch.
Bedanken möchte ich mich auch bei Anke Friemel und Ulrich Haunz von der NMR Core Facility der Universität Konstanz für die Hilfe bei NMR-Messungen und die Unterstützung bei der Auswertung komplizierter Nukleotid NMR-Spektren.
Ein riesiges Dankeschön geht auch an alle meine Freunde. Eure Gesellschaft, die gemeinsamen Erlebnisse und die gemeinsamen Momente haben mir nicht nur Freude bereitet, sondern mich auch daran erinnert, wie wichtig gute Freunde sind. Für Entspannung sorgten dabei auch die regelmäßigen Ausflüge nach Meersburg oder Überlingen.
Meiner Familie, insbesondere meinen Eltern, bin ich zu besonderem Dank verpflichtet. Eure unermüdliche Unterstützung während des Studiums und der Promotion haben diese Arbeit erst möglich gemacht. Vielen Dank!
Luisa, dir gebührt mein größter Dank und meine tiefste Wertschätzung. Ohne deine unerschöpfliche Geduld, deinen wissenschaftlichen Sachverstand und dein großes Verständnis für schwierige Phasen hätte ich diese manchmal mühevolle Reise nicht geschafft.

Zusammenfassung und Ausblick

Posttranslationale Modifikationen (PTMs) von Histonen spielen eine zentrale Rolle in verschiedenen zellulären Prozessen einschließlich der DNA Reparatur, des Strukturaufbaus des Chromatins und der Regulation der Transkription.[1] Dazu gehört die ADP-Ribosylierung als Vertreter einer reversiblen PTM, die in einer Vielzahl von Proteinen im Zellkern und im Zytoplasma vorkommt. Diese Modifikation tritt bei allen vier Kernhistonen (H2A, H2B, H3 und H4) sowie dem Linker Histon (H1) auf, insbesondere im Zusammenhang mit der DNA-Reparatur und der DNA Weiterverarbeitung.[2] Trotz ihrer Bedeutung und weitverbreiteten Vorkommens ist die ADP-Ribosylierung von Linker-Histonen noch nicht ausreichend verstanden. Dies liegt daran, dass es nur wenige Methoden gibt, die eine ortsselektive ADP-Ribosylierung von Linker-Histonen ermöglichen. Dabei erschwert die hohe Anzahl an Lysinen im Linker-Histon die Selektivität der ADP-Ribosylierung mit konventionellen Modifikationsmethoden, da diese zu Nebenreaktionen und unerwünschten Modifikationsstellen führen. Der Nachweis von ADP-Ribosylierungsstellen im Linker-Histon wird durch die hohe Anzahl von Lysinen in der Proteinsequenz zusätzlich erschwert, da gängige Nachweismethoden mittels Massenspektrometrie eine Fragmentierung des Proteins vor der Messung erfordern, was im Falle des Linker-Histons zur Bildung kleiner, schwer nachweisbarer Fragmente führt.

In dieser Studie wurde eine neuartige Methode zur ortsselektiven Herstellung von ADP-ribosylierten Linker-Histonen durch Anwendung eines chemischen Ligationsansatzes entwickelt. Hierbei basierte der Modifizierungsprozess auf der Reaktion mit Cysteinresten, was im Falle des Linker-Histons die gezielte Einführung der ADP-Ribosylierung ermöglichte, da aufgrund des Fehlens natürlicher Cysteine in der Proteinsequenz nur gentechnisch eingebrachte Cysteine für die Reaktion zur Verfügung stehen. Die Cystein-Selektivität und die Stabilität der gebildeten Bindung wurden systematisch untersucht. In diesem Zusammenhang wurde eine alternative Syntheseroute für ein ADP-Ribose Dimer etabliert, das als Ausgangsmaterial für die Modifikation des Linker-Histons durch die innovative Proteinmodifikationsmethode verwendet wurde. Der funktionelle Einfluss der ADP-ribosylierten Linker-Histone auf die Bildung der Chromatinstruktur wurde durch Experimente zum Aufbau des Chromatosoms evaluiert. Rekombinante Kernhiston-Oktamere wurden mit nukleosomaler DNA kombiniert, um Nukleosome aufzubauen. Der anschließende Einbau der mono- und diADP-ribosylierten Linker-Histon-Varianten führte zur Bildung

verschiedener Chromatosom-Varianten, wobei der Einfluss der Modifikation untersucht werden konnte.

Um das anspruchsvolle Ziel einer cysteinselektiven Proteinmodifikation zu erreichen, wurde ein Thiocarbamat-basierter Linker für die Modifizierung verwendet. Auf diese Weise wurde die ortsselektive ADP-Ribosylierung des Linker-Histons H1.2 untersucht. Thiocarbamate und Dithiocarbamate werden zur selektiven Modifizierung von Cysteinresten in Proteinen verwendet.[3-6] Um dieses Strategie in dieser Arbeit zu realisieren wurde *S*-Ethyl α-Methylhydrazid Thiocarbamat (11.4) synthetisiert, welches eine Thiocarbamatfunktionalität für die Proteinmodifikation und eine Hydrazidfunktionalität für die Einführung eines Zielmoleküls, wie ADP-Ribose, enthält.[7] Durch ortsspezifische Mutagenese konnte ein Cystein in die Sequenz des Linker-Histons an einer bekannten ADP-Ribosylierungsstelle eingeführt werden, wodurch die Variante H1.2 S150C erzeugt wurde.[8] Um die Selektivität des Thiocarbamats für Cysteine zu untersuchen, wurde ein Modellsystem entwickelt, dass *S*-Ethyl α-Methylhydrazid Thiocarbamat funktionalisiertes Biotin (TC-Biotin) zur Kopplung an das Protein nutzt. Nach erfolgreicher TC-Biotin Synthese wurde dessen Eignung zur Modifizierung der Linker-Histon Variante H1.2 S150C untersucht. Die erfolgreiche Biotinylierung des Linker-Histons mit TC-Biotin konnte durch eine Western-Blot (WB) Analyse bestätigt werden, die eine konzentrationsabhängige Biotin-Modifikation des Linker-Histons nur in Gegenwart eines Cysteinrestes zeigte. Um die *in vitro* Anwendbarkeit der mit *S*-Ethyl α-Methylhydrazid Thiocarbamat modifizierten Proteine sicherzustellen, wurde die Stabilität der Verknüpfung in zellulärer Umgebung überprüft. Dies wurde durch Inkubation von biotinyliertem H1.2 S150C mit HEK293T Zelllysat und Analyse mittels WB verifiziert, wodurch die Stabilität der Biotin Modifikation unter diesen Bedingungen bestätigt wurde.

Die nachgewiesene Cystein-Selektivität der Thiocarbamat-Ligationsmethode konnte dann auf die ortsselektive ADP-Ribosylierung des Linker-Histons H1.2 angewendet werden. Zu diesem Zweck wurde *S*-Ethyl α-Methylhydrazid Thiocarbamat modifizierte mono ADP-Ribose (TC-mADPr) synthetisiert, wobei ein Hydrazon als Zwischenprodukt gebildet wurde. Die erfolgreiche mADP-Ribosylierung des Linker-Histons konnte durch Flüssigchromatographie-Massenspektrometrie und WB Analysen bestätigt werden. Der Vergleich der Ergebnisse unter Verwendung des Wildtyp Linker-Histons (H1.2 WT) bewies die Cystein-Selektivität des TC-mADPr, da in Abwesenheit des Cysteinrestes bei der Wildtyp Variante keine Modifikation auftrat. Die Stabilität des modifizierten Proteins unter den Bedingungen der Modifizierungsreaktion mit TC-mADPr konnte ebenfalls durch eine WB Analyse verifiziert werden. Diese Methode stellt den ersten berichteten Ansatz zur ortsselektiven mADP-

Ribosylierung des rekombinant exprimierten Linker-Histons ohne Nebenreaktionen dar und könnte auf andere Proteine ausgeweitet werden.

Um die Untersuchung eines ADP-Ribose Oligomers auf die Bildung der Chromatinstruktur zu ermöglichen, wurde eine optimierte Synthese des ADP-Ribose-Dimers (diADPr) mit freiem reduzierendem Ende entwickelt.[9-11] Nach der Glykosylierung der entsprechenden Donor- (13.1) und Akzeptormoleküle (13.2) wurde die stereochemische Inversion durch ein Oxidations-Reduktionsverfahren erreicht, was zur gewünschten Stereochemie des 2'-*O*-α-Ribosyl-Adenosin-Disaccharids (13.4) führte.[12-14] Durch strategische Anpassung der Schutzgruppen konnte eine Orthogonalität in das Molekül eingeführt werden, was die Anbringung von zwei unterschiedlichen Phosphatgruppen an den Enden ermöglichte und zur Bildung des bis-phosphorylierten 2'-*O*-α-Ribosyl-Adenosin (13.10) führte. Die Bildung der Pyrophosphatbindungen mit den Endgruppen, Ribose-*H*-Phosphonat (14.6) und Adenosin-*H*-Phosphonat (15.5), ermöglichte anschließend den schrittweisen Aufbau des geschützten diADPr. Schließlich führte die vollständige Entschützung zur Bildung von diADPr mit einem freien reduzierenden Ende, welches für die Proteinmodifizierungsreaktion geeignet ist.

Die zuvor beschriebene Strategie für die mADP-Ribosylierung des Linker-Histons wurde auf das synthetisierte diADPr mit freiem reduzierenden Ende angewendet. Hierzu wurde *S*-Ethyl α-Methylhydrazid Thiocarbamat (11.4) in das diADPr eingebracht, wodurch TC-diADPr erhalten wurde. Die erfolgreiche diADP-Ribosylierung der Linker-Histon Variante H1.2 S150C konnte durch LC-MS sowie durch WB Analysen bestätigt werden. Die Ergebnisse zur diADP-Ribosylierung des Linker-Histons repräsentiert den ersten dokumentierten ortsselektiven Einbau des kürzesten Oligomers der poly-ADP-Ribose (pADPr) in das rekombinante Linker Histon.

Der Einfluss der ADP-Ribosylierung des Linker-Histons auf die Bildung der Chromatinstruktur wurde in einem Experiment zur Chromatosombildung untersucht. Nukleosomale DNA, die für den Aufbau von Nukleosomen und die Bindung des Linker-Histons optimiert ist, wurde mittels Polymerase-Kettenreaktion sythetisiert.[15-18] Die Kombination der DNA mit rekombinanten Kernhiston-Oktameren ermöglichte die erfolgreiche Bildung von Nukleosomen.[19,20] Die rekombinanten Nukleosome wurden mit den ADP-ribosylierten Linker-Histonen inkubiert, um die entsprechenden Chromatosom-Varianten zu erhalten. Die quantitative Bildung von Chromatosomen und der Einbau der ADP-ribosylierten Linker-Histone in die Chromatinstruktur konnte durch native PAGE- und native PAGE-WB Analysen gezeigt werden. Der Einbau der mono- und diADP-ribosylierten Linker-Histone in das Chromatosom stellt die erste beschriebene Methode dar, ortsselektiv ADP-ribosylierte Linker-Histone in eine rekombinante Chromatinstruktur zu integrieren. Darüber hinaus

wurden die Auswirkungen der eingeführten Modifikationen auf die Chromatinstruktur durch Experimente zur Chromatosombildung untersucht. Es konnte gezeigt werden, dass die Bildung der Chromatosome in Abhängigkeit von der Kettenlänge der ADP-Ribose gehemmt wird. Dies wurde durch einen erhöhten Bedarf an ADP-ribosyliertem Linker-Histon zur quantitativen Ausbildung des Chromatosoms nachgewiesen, wobei ein stärkerer Effekt für das diADP-ribosylierte Linker-Histon im Vergleich zum mADP-ribosylierten Linker-Histon beobachtet wurde. Damit konnte der direkte Einfluss dieser anionischen Modifikation auf die Ausbildung der Chromatinstruktur in Abhängigkeit von der Länge der ADP-Ribose Kette gezeigt werden.

Mit der beschriebenen Synthese des *S*-Ethyl α-Methylhydrazid Thiocarbamats (11.4) und dem erfolgreichen Einbau von ADP-Ribose oder Biotin in das Linker-Histon, ermöglichen strukturelle Modifikationen am Thiocarbamat-Linker die Einführung der ADP-Ribose in einer ringgeschlossenen Konformation. Moyle und Muir beschrieben die ADP-Ribosylierung mit Hilfe einer *N*-Methylaminooxy-Funktionalität in der zu modifizierenden Aminosäure, die in der Bildung eines ADP-ribosylierten Oligopeptids mit geschlossenem Ring resultierte (**Scheme 4A**).[21] Durch die Anwendung dieses Konzepts auf die Thiocarbamat-Proteinmodifikation würde den Einbau einer ringgeschlossenen ADP-Ribose in ein Zielprotein ermöglichen und damit die native Bindung eines Serins an ADP-Ribose imitieren. Darüber hinaus ermöglicht die hier beschriebene Methode der cysteinselektiven Proteinmodifikation die Einführung weiterer PTMs in das Linker-Histon, die mit den üblicherweise verwendeten Methoden nur schwer zugänglich sind. Dies würde zu einem besseren Verständnis des Einflusses von PTMs auf das Linker-Histon selbst und deren Funktion im chromatosomalen Kontext beitragen. In diesem Zusammenhang ist auch die Einführung von Farbstoffen oder Funktionalitäten zur Immobilisierung in das Protein mit der hier etablierten Methode möglich.

Neben den Kernhistonen und dem Linker-Histon sind eine Vielzahl weiterer Zielproteine für die ADP-Ribosylierung bekannt. Einige dieser Proteine, wie z.B. Ubiquitin, besitzen ebenfalls keinen Cysteinrest in der Proteinsequenz, so dass diese Methode auch zur Modifizierung dieser Proteine eingesetzt werden kann.[22] Dies würde es ermöglichen, die Auswirkungen der ADP-Ribosylierung von Proteinen über das Linker-Histon hinaus zu untersuchen.

Aufgrund des nachgewiesenen Einflusses der ADP-Ribosylierung des Linker-Histons an Serin 150 können auch andere Modifikationsstellen in der globulären und N-terminalen Domäne wie z.B. Serin 54, mit der beschriebenen Thiocarbamat-Ligationsmethode untersucht werden.[8] Die Verwendung dieser ADP-ribosylierten Linker-Histone zur Untersuchung der Chromatosombildung würde den Einfluss anderer Modifikationsstellen auf

die Chromatinstruktur aufzeigen, die auf unterschiedlicher Weise an dessen Bildung beteiligt sind. Dies könnte generell zu einem besseren Verständnis in diesem Bereich beitragen.

Darüber hinaus können die ortsspezifischen ADP-ribosylierten Linker-Histone in einem Chromatosom-Bereich eingebaut werden, dass aus einer sequentiellen Anordnung mehrerer Nukleosome entlang eines DNA-Strangs besteht. Dies eröffnet die Möglichkeit, die Auswirkungen der ADP-Ribosylierung des Linker-Histons auf höhere Chromatinstrukturen und deren Funktion zu untersuchen.

Die hier beschriebene Methode zur Herstellung von mono- und diADP-ribosylierten Linker-Histonen ermöglicht die weitere Untersuchung des Interaktoms dieser PTM innerhalb der Chromatinstruktur mittels Affinitätsanreicherungs-Massenspektrometrie. Dazu kann am 5'-Ende der nukleosomalen DNA, welche für die Anreicherungsexperimente verwendet wird, eine chemische Funktionalität, wie z.B. Desthiobiotin, eingeführt werden. Auch die Identifizierung von Proteinen, die mit dem ADP-ribosylierten Linker-Histon innerhalb der Chromatinstruktur interagieren, würde das Verständnis dieser PTM und ihrer Funktion über die Beteiligung an der Bildung der Chromatinstruktur hinaus erweitern.[15]

Eine weitere Untersuchung des Histon-Codes und der kombinatorischen Wirkung verschiedener PTMs könnte durch die gleichzeitige Einführung einer zweiten ADP-Ribosylierungsstelle oder einer anderen PTM in dasselbe Linker-Histon erreicht werden. Dies könnte die Untersuchung des Zusammenspiels mehrerer PTMs bei der Bildung der Chromatinstruktur oder des Interaktoms im Chromatin ermöglichen.

Insgesamt wird die hier vorgestellte Methode zur cysteinselektiven mono- und diADP-Ribosylierung des Linker-Histons durch den Thiocarbamat-Ligationsansatz die chemische Werkzeugpalette zur Untersuchung von Histon-PTMs erheblich erweitern und wesentlich zu einem besseren Verständnis ihres Einflusses auf verschiedene zelluläre Prozesse beitragen. Darüber hinaus könnte die Anpassung des Chromatosombildungs Assay auf andere Linker-Histon PTMs zu einem besseren Verständnis im Zusammenhang mit der Ausbildung der Chromatinstruktur beitragen.

Contents

List of Abbreviations

Abbreviations of the International System of Units, chemical groups and formulas according to the IUPAC (International Union of Pure and Applied Chemistry) nomenclature are not listed.

abs.	absolute
ADP	adenosine diphosphate
AE-MS	affinity enrichment mass spectrometry
AMP	adenosine monophosphate
ARH	ADP-ribosyl hydrolase
ARTC	ecto ADP-ribosyl transferase
ARTD	ADP-ribosyl transferase
ATP	adenosine triphosphate
BCA	bicinchoninic acid assay
biotin-iodoacetamide	biotin polyethyleneoxide iodoacetamide
biotin-maleimide	*N*-biotinoyl-*N*'-(6-maleimidohexanoyl) hydrazide
bs	broad signal
BSA	bovine serum albumin
conc.	concentration
crDNA	competitor DNA
cryo-EM	cryogenic electron microscopy
CuAAC	copper (I) catalyzed azide-alkyne cycloaddition
d	doublet
DCA	dichloroacetic acid
DCE	dichloroethane
DCM	dichloromethane
dd	doublet of doublets
diADPr	dimeric ADP-ribose
DIPEA	di-*iso*-propylethylamine
DMAP	4-dimethylaminopyridine
DMF	*N*,*N*-dimethylformamide
DMSO	dimethyl sulfoxide
DMTr	dimethoxytrityl protecting group
DMTrCl	dimethoxytrityl chloride

DNA	deoxyribonucleic acid
dNTP	2'-deoxyribonucleoside-5'-triphosphate
E. coli	*Escherichia coli*
EDTA	ethylenediaminetetraacetic acid
e.g.	exempli gratia
ESI-MS	electrospray ionization mass spectrometry
ETD	electron transfer dissociation
EtOAc	ethyl acetate
EtOH	ethanol
ETT	5-ethylthiotetrazole
Fm	fluorenylmethyl protecting group
Fmoc	fluorenylmethoxycarbonyl protecting group (N-terminal)
GSH	glutathione
HPLC	high performance liquid chromatography
HRMS	high resolution mass spectrometry
HSB	high salt buffer
IMAC	immobilized metal affinity chromatography
IPTG	isopropyl β-D-1-thiogalactopyranoside
LC-MS	liquid chromatography mass spectrometry
LSB	low salt buffer
m	multiplet
m/z	mass-to-charge ratio
mADPr	monomeric ADP ribose
MeCN	acetonitrile
MeOH	methanol
MS	mass spectrometry
NAD^+	nicotinamide adenine dinucleotide
NCP	nucleosomal core particle
NMR	nuclear magnetic resonance
NP-40	Nonidet P40 Substitute
NRL	nucleosomal repeat length
pADPr	polymeric ADP-ribose
PAGE	polyacrylamide gel electrophoresis
PARG	poly ADP-ribose glycohydrolase
PARP	poly ADP-ribose polymerase

PBS	phosphate buffered saline
PCR	polymerase chain reaction
PE	petroleum ether
PMSF	phenylmethylsulfonyl fluoride
ppm	parts per million
PTM	post-translational modification
q	quartet
quin	quintet
RP-HPLC	reverse-phase high performance liquid chromatography
rpm	revolutions per minute
s	singlet
SDM	site-directed mutagenesis
SDS	sodium dodecyl sulfate
SPPS	solid phase peptide synthesis
t	triplet
TAE	tris-acetate EDTA
TBAF	tetrabutylammonium fluoride
TBDMSOTf	*tert*-butyl dimethylsilyl trifluoromethanesulfonate
TBDPS	*tert*-butyl diphenylsilyl protecting group
TBDPSCl	*tert*-butyl diphenylsilyl chloride
TBE	tris-borate EDTA
TC-biotin	thiocarbamate linker modified biotin
TC-diADPr	thiocarbamate linker modified dimeric ADP-ribose
TCEP	tris(2-carboxyethyl)-phosphine
TC-mADPr	thiocarbamate linker modified monomeric ADP-ribose
TEA	triethylamine
TEA·3HF	triethylamine trihydrofluoride
TEAA	triethylammonium acetate buffer
TEAB	triethylammonium bicarbonate buffer
TEV	tobacco etch virus
TFA	trifluoroacetic acid
THF	tetrahydrofuran
Thiocarbamate linker	*S*-Ethyl α-methylhydrazide thiocarbamate
TLC	thin layer chromatography
TMS-Im	trimethylsilyl imidazole

TrtCl	trityl chloride
WB	western blot
WT	wild type
δ	chemical shift [ppm]

List of Figures

List of Schemes

1 Introduction

1.1 Chromatin architecture

In eukaryotic cells, deoxyribonucleic acid (DNA) is the storage medium for genetic information. With an average size of 3 billion base pairs and a linear length of approximately 2 meters, the genomic DNA in the nucleus has to be packed densely to fit into the 10 µm nucleus.[23] This transformation is achieved by the associating the DNA with protein complexes resulting in the formation of a three-dimensional architecture, the chromatin (**Figure 1**).

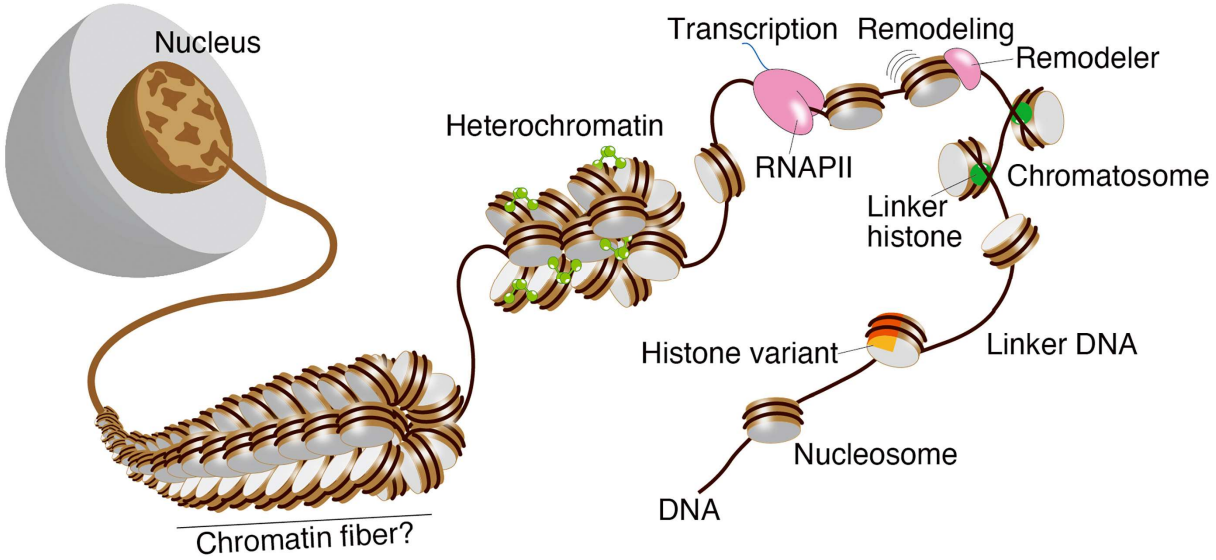

Figure 1. Hierarchical architecture of chromatin. The compaction of DNA in the cell nucleus begins with the association to the four core histones (H2A, H2B, H3 and H4) to the nucleosome with interspersed linker DNA. Compaction towards the chromatosome is achieved by the addition of the linker histone H1. Interactions between the chromatosomes lead to further compaction into heterochromatin and chromatids. Figure reprinted from 10.1016/j.bbagrm.2022.194851, with permission from Elsevier.

In addition to the establishment of a three-dimensional chromatin architecture within the cell nucleus, this structured DNA plays an important role in modulating essential cellular processes including DNA repair, transcriptional regulation and cell apoptosis.[1,24] The structured DNA within the chromatin consists of repeating units with each unit containing approximately 150 base pairs of DNA wrapped 1.65 times around the core histone octamer. The core histone octamer consists of two distinct types of core histone heterodimers, the H2A-H2B and H3-H4 heterodimers.[25,26] These core histones, with molecular weights ranging from

10 to 15 kilodaltons (kDa), contain a structured globular domain and unstructured N- and C-terminal regions. The core histone heterodimerization is induced by its globular domain, forming a histone folding motif. After two parts of each heterodimer assemble into the core histone octamer, the unstructured N-terminal regions of these histones project outward from the octamer and actively participate in protein-protein and protein-DNA interactions.[27,28] In addition, the abundance of positively charged residues on the surface of the core histones, combined with hydrogen bonding facilitates their strong binding to the negatively charged DNA strand. Nucleosomal core particles (NCPs), characterized by the DNA wrapped around one core histone octamer, contains one DNA base pair located between the entry and the exit of the DNA from the NCP. This base pair is called nucleosome dyad. This dyad serves as the central point of the DNA sequence within the NCP structure (**Figure 2**, left).[29,30] NCPs are separated by linker DNA with variable size and together form the nucleosome.[31]

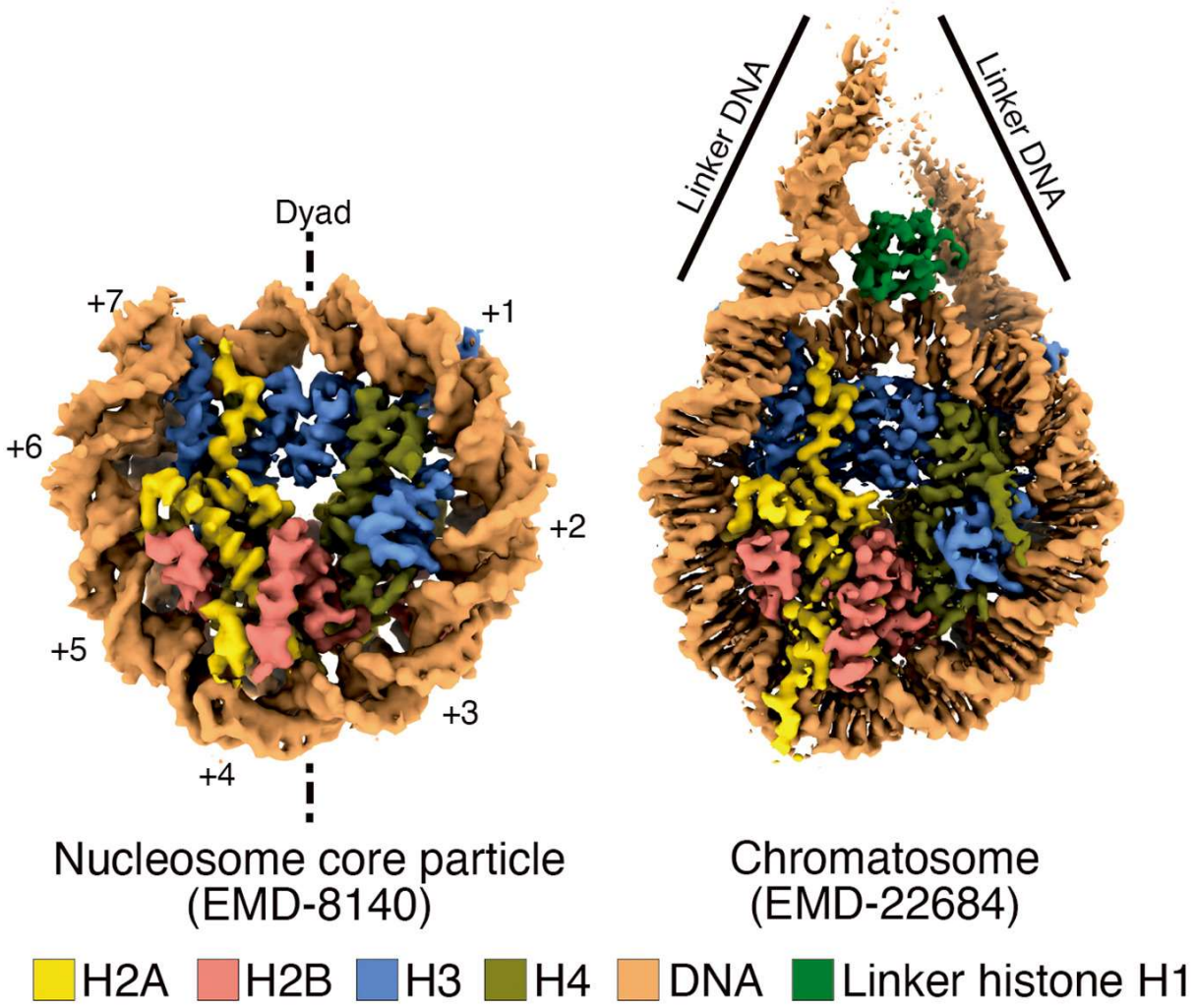

Figure 2. Structure of nucleosome core particle and chromatosome. Cryo-EM structures of NCP and chromatosome. Dyad marks the base pair located at the center of the linker DNA entrance and the exit. Figure reprinted from 10.1016/j.bbagrm.2022.194851, with permission from Elsevier.

Upon attachment of the linker histone H1 a condensed and repetitive chromatin structure called chromatosome is established. During this process of DNA compaction, ten base pairs of DNA at each end of the nucleosome become associated with the linker histone (**Figure 2**, right).[32] All histones, including the four core histones and the linker histone, bind to DNA through electrostatic interactions between cationic arginine and lysine residues of the histones and the anionic phosphate backbone of DNA.[33] Further assembly of chromatosomes results in an increased DNA compaction leading to the formation of the initial nucleosome array known as the 30 nm fiber.[34] This helical configuration of densely packed DNA has been a controversial topic in chromatin research, as the *in vivo* evidence for its structure is not clear.[35-37] Two models are proposed to solve this problem. The first model, termed the solenoid model, postulates the interconnection of nucleosomes forming a one-start helix.[38,39] Conversely, the second model proposes a zigzag two-start helix in which nucleosomes are arranged in two rows with linker DNA dispersed between the nucleosome stacks.[40] The architectural conformation of the 30 nm fiber is influenced by several factors including the nucleosome spacing, ionic strength and the interaction with linker histones. These diverse factors collectively shape the complex structure of chromatin at the 30 nm scale.[41] Furthermore, modulations of the assembly of higher order chromatin structures are determined by the non-uniform charge distribution on the surface of the NCPs. In particular, a cluster of seven amino acid side chains within the core histone H2A interacts with the N-terminus of the core histone H4.[37,42] Recent studies on the extension of the 30 nm fiber indicate that this higher order architecture is manifested predominantly within regions of several nucleosomes rather than in an extended form.[43-45] These studies suggest that such architectural complexity at larger length scales is directed by organized clusters of different sizes, such as zigzag structures, which are interrupted by disordered or heterogeneous regions.[44,46] These observations imply that chromatin is not a homogeneous entity, but rather a dynamically heterogeneous structure with diverse folding modes and localized structural differences.[47,48]

1.2 Linker histones

In contrast to the well-studied core histones, the linker histone H1 variants remain comparatively less understood in the field of chromatin remodeling. Linker histones are characterized as small proteins of approximately 200 amino acids in length. This highly basic protein consists of a globular domain of 70 amino acids, a short N-terminus (30 amino acids) and a lysine-rich C-terminus (100 amino acids). The globular domain itself forms a winged helical structure containing a helix-turn-helix motif that includes three α-helices and three β-strands (**Figure 3**).[49-51] In addition to the globular domain, the linker histone consists of a short unstructured tail at the N-terminus and an extended unstructured tail at the C-terminus. Working together with the core histones and several other proteins, linker histones play a key role in stabilizing higher order chromatin structures such as the chromatosome. The binding of 10 base pairs of linker DNA to both ends of the nucleosome lead to an increased stability and compaction, further contributing to the structural integrity of chromatin.[32,52]

In both humans and mice, a repertoire of 11 genes has been described for the linker histone family.[53] The somatic subtype of linker histones, including H1.1 – H1.5, exhibits widespread expression in various cell types and is encoded within the histone gene cluster together with the four core histones.[54,55] While the globular domain of the linker histone subtypes share structural homology, there is a considerable variability within the N- and C-terminal tails, providing a basis for functional specialization and differential regulation.[56]

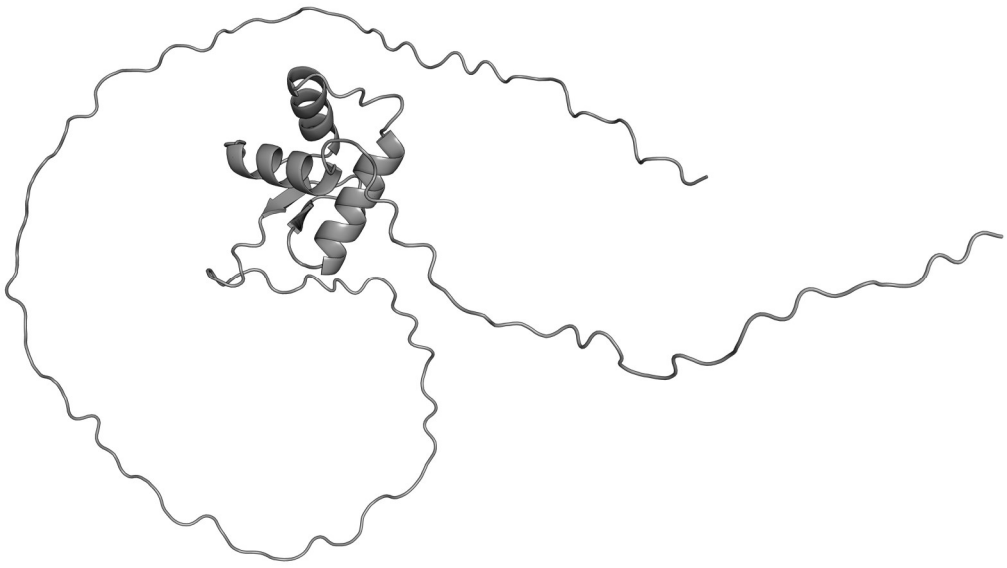

Figure 3. Tertiary structure of the linker histone H1.2. The winged helix structure of the globular domain, containing three α-helices (α_1, α_2, α_3) and three β-strands (β_1, β_2, β_3). Structure from AlphaFold prediction.

Despite sharing a common binding region for nucleosomes, each H1 variant exhibits distinct nucleosomal repeat lengths (NRLs), which describes the distance between two successive chromatosomes. *In vitro* studies of Drosophila embryo extracts have revealed the longest NRL for H1.4 and H1.5, a moderate NRL for H1.0, H1.2 and H1.3 and the shortest NRL for H1.1.[57] These differences in the affinity for chromatin of the H1 variants are due not only to sequence variation, but also to PTMs and the influence of competing proteins.[53,58] Beyond these variations, the precise modes of linker histone binding to nucleosomes remain the subject of ongoing research.[59] The initial elucidation of the structure of the nucleosome bound linker histone was achieved by solution nuclear magnetic resonance (NMR) spectroscopy, which revealed an asymmetric off-dyad binding configuration with the linker DNA engagement on one side (**Figure 4A**).[60] In contrast, the *in vitro* examination of 30 nm fibers using cryogenic electron microscopy (cryo-EM) revealed that the globular domain of the linker histone asymmetrically binds off-dyad to both linker DNA strands (**Figure 4B**).[61] Cryo-EM imaging and nanoscale modeling proposed a binding model in which the globular domain of the linker histone interacts symmetrically with both linker DNAs, specifically targeting the minor groove at the dyad.[62] Further insights from X-ray crystallography described this on-dyad binding mode for the nucleosome complexed with the globular domain of the linker histone (**Figure 4C**).[63] The combination of cryo-EM and X-ray crystallography techniques allowed the achievement of the first nucleosome structure incorporating the full-length linker histone H1.[64] The globular domain of H1 engages the nucleosome at the dyad with one α helix and two β-strands located at the C-terminus of the globular domain (**Figure 4D**). The flexible C-terminal domain of the linker histone interacts preferentially with the opposing linker DNA strand, thereby imparting significant asymmetry to the nucleosome.[64,65] In addition to the on-dyad and off-dyad binding modes, recent investigations have revealed a novel third non-dyad binding mode.[36] In this novel mode, a distinct binding site away from the nucleosome has been identified. In this scenario, the globular domain of the linker histone sits in a niche in between the 30 nm fibers and binds to the nucleosomal DNA, thereby enhancing the interlocking between the DNA strands.[36] These results for the different binding modes demonstrate the dynamic flexibility of the linker histone in both binding and orientation relative to the nucleosome. It is concluded that the establishment and dynamics of higher order structures are regulated by factors such as nucleosomal DNA characteristics and the linker histone subtype.[59,65] In addition to their central role in chromatin compaction, linker histones exert a significant regulatory influence on transcriptional activity.[66] Due to their ability to condense chromatin and prevent DNA transcription, linker histones are considered to be repressors of

transcriptional activity.[67] However, linker histones exhibit a sequence-dependent influence on the gene expression and therefore can also act as a positive regulator on transcription.[68,69]

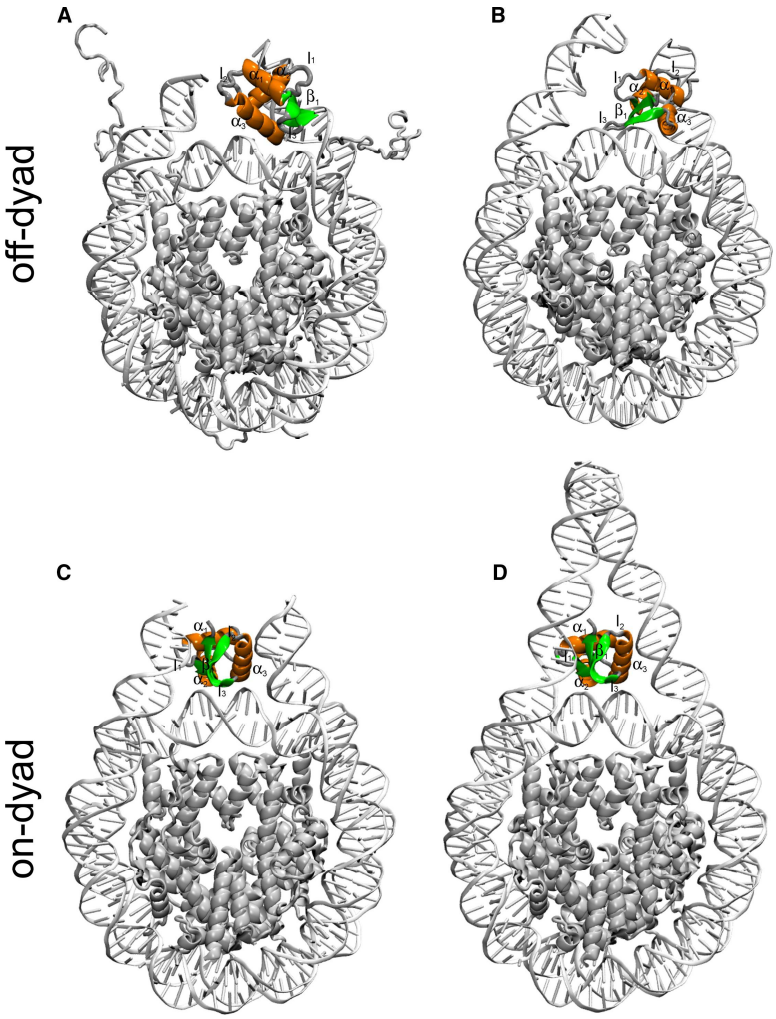

Figure 4. Modes of linker histone binding to the nucleosome. A. Asymmetric off-dyad binding.[60] **B.** Off-dyad binding to H1.4.[61] **C.** Symmetric on-dyad binding.[63] **D.** On-dyad binding to H1.[64] Nucleosomal DNA and core histone octamer depicted in grey, linker histone depicted in green and orange. Reprinted with CC-license (license number: 5790150850386) from[65], with permission from Elsevier.

Furthermore, linker histones participate in maintaining the genomic stability by the formation of higher order chromatin structures.[70] Thus, linker histones are essential for preventing DNA damage and facilitating DNA repair processes.[71] Disruption of the expression or regulation of the linker histones are associated with chromatin instability, divergent gene expression and DNA damage induced mutagenesis, highlighting their critical role in maintaining the genomic integrity.[72,73]

1.3 Post-translational modifications of histones

PTMs on histones, often described as their epigenetic marks, are a crucial element in the regulation of chromatin remodeling and gene expression.[74] These modifications include a variety of chemical functionalities on histones such as acetylation, methylation, phosphorylation, biotinylation, ubiquitination, adenosine-diphosphate (ADP)-ribosylation and others.[75] While extensive research has identified numerous modification sites and chemical modifications that occur on the four core histones, the characterization of PTMs on the linker histone H1 remains challenging.[76] The detection of PTMs with mass spectrometric (MS) methods is hindered by the high lysine content of the linker histone.[77] Nevertheless, extensive research in the field of linker histone PTMs has led to the identification of several PTMs, including acetylation, methylation, phosphorylation, ubiquitination, ADP-ribosylation, among others. However, the functional significance of these modifications remains largely unknown.[77,78] A selection of the most abundant PTMs and their location for the four core histones is shown in **Figure 5**.[75] These modifications occur on both the terminal regions and the globular domain of the histones. It is proposed that they serve as an epigenetic code, with each modification having a specific function.[79] These reversible modifications on histones promote, e.g. the recruitment of ATP-dependent enzymes that control the chromatin remodeling. Consequently, changes in the chromatin structure exert regulatory effects on transcription and gene expression.[80] The dynamics of histone PTMs – incorporation, maintenance and removal – are catalyzed by specialized enzymes called writers, readers and erasers.[81] The effect of the PTM on histones and the chromatin structure can either be direct or indirect. Directly acting PTMs serve as a platform for reader enzymes, thereby regulating cellular processes, often by structural alteration of the chromatin structure.[82,83] Conversely, indirectly acting PTMs require an intermediate step of binding a chromatin remodeling complex or effector proteins to affect cellular processes.[74,84] The epigenetic code of histone PTMs, often referred as the "histone code", describes a complex network of interactions among multiple PTMs, recognized by reader enzymes that trigger unique downstream effects and functions.[76,82] These reader enzymes with more than one binding domain for PTMs possess the ability to simultaneously engage one or more histone tail, thereby modulating the PTM functionality.[85]

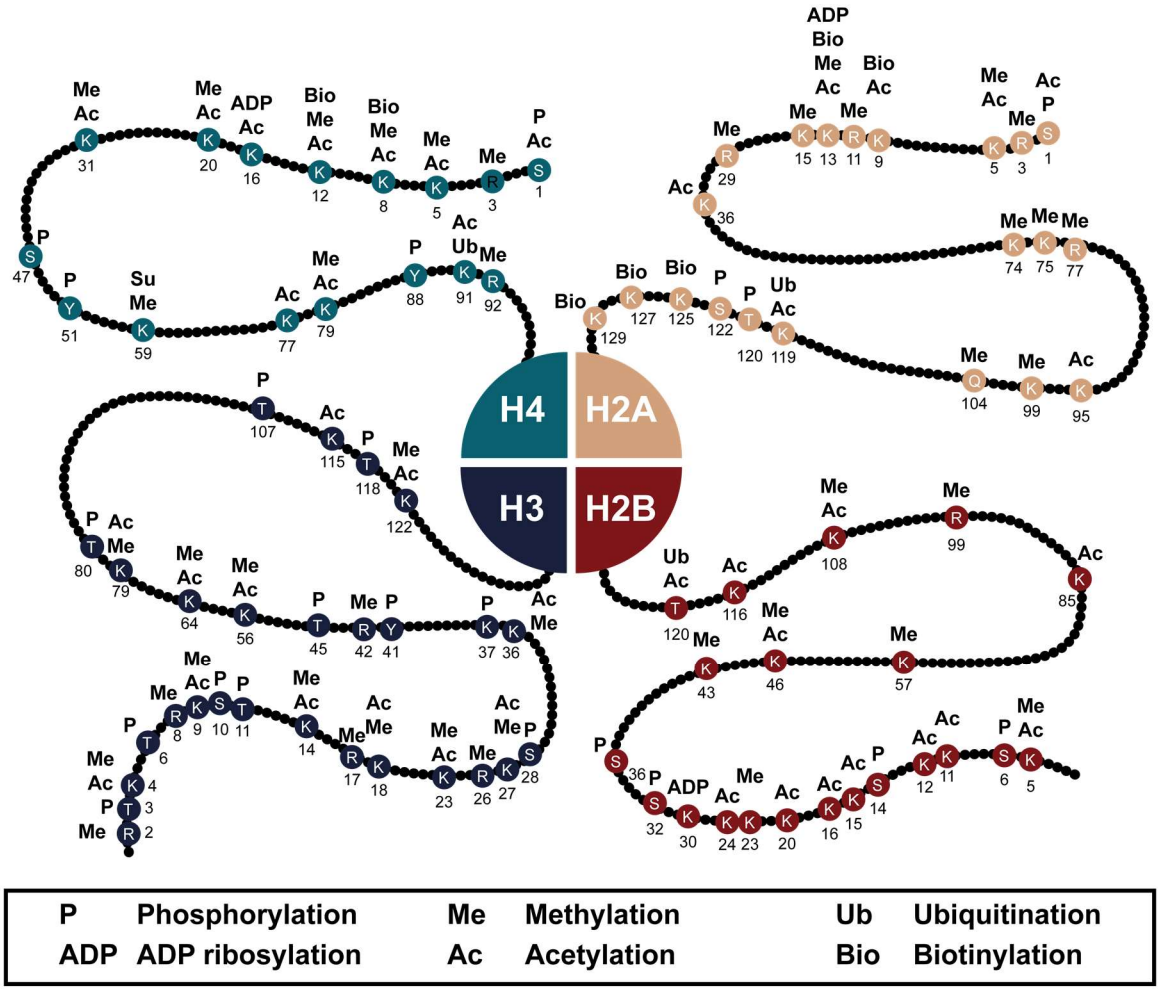

Figure 5. Post-translational modifications of the core histones. Post-translational modifications in the amino acid sequence (number at bottom, without starting methionine) for histones H2A, H2B, H3 and H4: phosphorylation (P), methylation (Me), ubiquitination (Ub), ADP-ribosylation (ADP), acetylation (Ac), biotinylation (Bio). Figure adapted from [75]

Moreover, beyond recognizing more than one PTM at a time, individual PTMs can exert regulatory effects on neighboring PTMs, either on the same histone tail or across different histone tails. This is enabled by the recruitment of writers or erasers, as exemplified by the GSK3-mediated phosphorylation, which requires an initial phosphorylation at the fourth amino acid residue from the modification site.[86] Conversely, there is a competitive relation between PTMs located on a single amino acid side chain, where bulky PTMs can block the modification site.[86] The interplay of these PTMs, in combination with various environmental conditions, plays a critical role in the chromatin architecture and function, thereby modulating the dynamics of gene expression.[87]

Lysine acetylation of histones is a highly dynamic PTM catalyzed by histone acetyltransferases as writers and histone deacetylases as erasers. Acetyltransferases use acetyl-coenzyme A as cofactor to transfer the acetyl moiety to the ε-amino group of the lysine.[88] This reversible PTM exerts regulatory control over numerous cellular processes, including transcriptional regulation, chromatin structure remodeling, cell apoptosis, DNA

repair and others.[89] Acetylation-induced neutralization of the positive charge on the lysine ε-amino group weakens the histone-DNA interaction within the chromatin, thereby increasing the DNA accessibility.[90] In addition, histone acetylation serves as binding platform for bromodomain-containing proteins, that recognize and bind acetylated lysines. The therefore induced recruitment of chromatin remodeling complexes and transcriptional co-activators promote chromatin decondensation and the assembly of the transcriptional machinery, resulting in increased gene expression.[91] In contrast, histone deacetylases catalyze the removal of the acetyl group from lysine residues, promoting chromatin compaction and transcriptional repression.[92] The interplay between histone acetylation and deacetylation is essential for the regulation of gene expression and a dysregulation of this balance has been associated with several diseases including cancer and metabolic syndromes.[93]

The phosphorylation of serine, threonine and tyrosine residues is a common PTM of histones.[94] This protein modification is catalyzed by kinases and involves the transfer of a phosphate from adenosine triphosphate (ATP) to the amino acid side chain, and its removal is regulated by enzymes called phosphatases.[95] As a result of histone phosphorylation, a negative charge is incorporated into the histone, directly affecting the histone-DNA interaction and thus the chromatin structure. In particular, both the terminal tails and the globular domain of the core histones and the linker histone can be phosphorylated.[75] In addition, histone phosphorylation serves as a recruitment signal for specific effectors such as BRCT (BRCA1 C-terminal), a phosphate-binding protein, involved in DNA damage response pathways.[96] Histone phosphatases, responsible for removing this PTM are less well studied than their writer counterpart, although playing a crucial role in regulating the reversible nature of histone phosphorylation. The dynamic balance between kinase and phosphatase activities regulates the histone phosphorylation levels and thereby modulating the chromatin structure in response to cellular changes.[97] In addition to changes in the chromatin structure, an imbalance between phosphorylation and dephosphorylation is associated with numerous diseases including cancer.[98]

Histone methylation, a frequent histone PTM, targets basic amino acid side chains, such as lysine, arginine and histidine residues.[99,100] These modifiable amino acids exhibit different methylation states, with lysine is susceptible to mono-, di- and trimethylation at their ε-amino group, arginines to mono-methylation or a symmetrically or asymmetrically di-methylation at their guanidinyl group.[101-103] In contrast to these multiple modifications, histidine residues are restricted exclusively to mono-methylation.[104] Histone methylation is catalyzed by histone methyltransferases using S-adensoyl-L-methionine as a substrate and is removed by demethylases such as Jumonji domain-containing lysine demethylase.[105,106] Notably,

chromatin effectors have the ability to recognize histone methylation patterns, thereby recruiting modulating enzymes affecting transcriptional regulation and chromatin remodeling processes.[107]

In contrast to small molecule modifications such as acetylation, methylation and phosphorylation, ubiquitination involves the attachment of a small protein, ubiquitin, to histones. Ubiquitin, consisting of 76 amino acids and is attached to lysine residues within the histone tails. The incorporation of this PTM is catalyzed by three enzymes, the ubiquitin activating enzyme (E1), the ubiquitin conjugating enzyme (E2) and the ubiquitin ligase (E3).[108] These modifiers determine both the site and the ubiquitination extent. Ubiquitination can occur in its monomeric and polymeric form, in which additional ubiquitin moieties are conjugated to one of the seven lysine residues of the previously bound ubiquitin, resulting in the formation of ubiquitin chains with distinct length.[109] Although the number of known modification sites for histone ubiquitination remains limited, lysine 119 in H2A and lysine 120 in H2B have been well studied.[110,111] In the dynamic process of the addition and removal of ubiquitin from histones, the protease catalyzed deubiquitination affects the chromatin structure and downstream DNA processes.[112]

Another important PTM that can occur in either a monomeric or polymeric form on histones is the ADP-ribosylation. This reversible protein modification involves the transfer of ADP-ribose from nicotinamide adenine dinucleotide (NAD^+) to the target protein. Predominantly, mono ADP-ribose is attached and serves as a binding platform for subsequent ADP-ribosylation events, resulting in the formation of poly ADP-ribosylated proteins.[113] Amino acid side chains known to accept this PTM include lysine, cysteine, arginine, glutamate, serine and others.[1,8] This protein modification, both for mono- and poly ADP-ribosylation of target proteins, is catalyzed by three families of enzymes: ADP-ribosyl transferases (ARTDs, also known as PARPs), ecto ADP-ribosyl-transferases (ARTCs) and sirtuins.[114] The removal of this PTM is catalyzed by ADP-ribosyl hydrolases (ARHs) and poly ADP-ribose glycohydrolases (PARGs).[114] In mammalian cells, four different hydrolases have been characterized for the removal of ADP-ribose (ARH1-3, PARG).[115] While ARH1 is exclusively active in cleaving the linkage between ADP-ribose and arginine, ARH2 lacks a hydrolase activity for the common targets in histones.[116,117] In contrast, ARH3 and PARG hydrolyze the *O*-glycosidic bond in poly ADP-ribose, resulting in a mono ADP-ribosylated protein that is subsequently processed by other enzymes.[118,119] Both the four core histones and the linker histone were found to be ADP-ribosylated.[120] Since all histones are mainly found in the nucleus, the enzymes responsible for histone ADP-ribosylation are likely to be localized there. In this context, the ARTDs are the only nuclear enzymes, with SIRT6, a sirtuins member, showing predominantly a deacetylase

activity rather than a ADP-ribosyltransferase activity.[121] The ARTD family consists of 18 members (ARTD1-18) with diverse cellular localizations, activities and functions. While ARTD1-3 are predominantly localized in the nucleus, ARTD4-6, ARTD9 and ARTD10 are also present in the cytoplasm.[122,123] To date, only ARTD1, ARTD3 and ARTD10 have been identified as enzymes that catalyze the mono- or poly ADP-ribosylation of histones.[124-126] The detection of ADP-ribosylated histones presents several challenges, including their low abundance and the technical difficulties associated with lysine-rich regions in some histones, complicating MS analysis.[127,128] Furthermore, the identification of modifications sites within histones is even more challenging. Identified ADP-ribosylated amino acids include the basic N-terminus, glutamate 2 in H2B, glutamates 2, 14 and 116 in the linker histone H1 and the C-terminal lysine.[120,129] Electron transfer dissociation (ETD) MS analysis of histone peptides in combination with ARTD1 revealed several lysines as modification sites on all core histones, including H2A K13, H2B K30, H3 K27 and K37, H4 K16.[125] Further ETD-MS studies have identified serine residues as targets for ADP-ribosylation events.[8] Specifically, modification sites in the N-terminal tail have been identified for the core histone H2B at serines 6 and 14, and for H3 at serines 10 and 28. Among the linker histone variants, modifications sites have been identified in different protein compartments. In the N-terminal region, serine 26 was found to be modified, while within the globular domain, serines 54 and 103 were identified. Additionally, the serines 112, 149 and 187 in the C-globular domain were also identified.[8] As a result of this PTM, the effect of ADP-ribosylation on the chromatin structure has been extensively investigated. Studies using protein modification with ARTD1 and an excess of NAD^+ have revealed ADP-ribosylation induced chromatin relaxation. However, in the absence of NAD^+, chromatin condensation was detected, which was suggested to be due to the binding of ARTD1 to the chromatin.[130,131] These experimental results were further confirmed by sedimentation velocity experiments in which poly ADP-ribosylated core histones within nucleosomes exhibited a relaxed compaction and subsequent addition of the linker histone failed to induce recondensation, indicating a decondensing effect of this PTM on higher order chromatin structures.[132] Chromatin relaxation induced by poly ADP-ribosylation leads to an increase in the accessibility of single-stranded DNA, as demonstrated by DNA digestion assays using micrococcal nuclease, resulting in faster DNA degradation for poly ADP-ribosylated chromatin.[133] It has been shown that ADP-ribosylation of the linker histone induces decoiling of the linker DNA rather than removing of the modified linker histone from the chromatin. This observation is attributed to the reduced affinity of the linker histone for the linker DNA upon ADP-ribosylation of its terminal regions, which may interfere with the formation of higher order chromatin structures.[134] The mechanism of chromatin remodeling induced by

histone ADP-ribosylation and the resulting increased accessibility of genomic DNA is closely linked to DNA damage repair pathways. Following DNA damage, the core histones H2B and H3 are the primary targets of histone ADP-ribosylation, whereas H4 and the linker histone H1 exhibit lower levels of modification.[135] ADP-ribosylation of the core histone H2B, a primary target of DNA damage induced histone modification, primarily affects changes in the chromatin structure rather than recruitment of processing enzymes.[123] Studies have shown that DNA cleavage by endo-exo-nucleases, such as micrococcal nuclease, results in highly ADP-ribosylated histones.[127] It has also been shown that histones are modified mainly in the vicinity of the cleavage site.[136] Radioimmunoassays have further elucidated a substantial increase in both mono- and poly ADP-ribosylation levels following DNA damage, attributed to the activation of ARTD1 by DNA lesions.[122,137] *In vitro* studies validated this response, demonstrating an increased enzymatic activity and self-modification rates of ARTD1 with poly ADP-ribose upon DNA damage.[138] Exposure of cells to genotoxic stress induces poly ADP-ribosylation of ARTD1, with only specific regions of ARTD1 being modified, indicating a localized response to DNA damage and site specific ADP-ribosylation of histones.[139]

The recognition of histone ADP-ribosylation by potential interacting proteins in the context of the DNA damage response is a subject of considerable interest. Several classes of binding domains for ADP-ribosylated proteins have been elucidated, of which the PAR-binding motif, the macrodomain, the WWE domain and the PAR-binding zinc finger domain have been extensively studied.[140,141] Enzymes with a PAR-binding motif are the most abundant readers of ADP-ribosylation. Analysis of interacting proteins, including histones, have revealed a 22-25 amino acid sequence that non-covalently interacts with poly ADP-ribose.[142] Reader enzymes bearing a macrodomain binding motif typically contain a conserved 140-190 amino acid cascade domain for poly ADP-ribose binding.[143] Human macrodomain-containing proteins are often involved in ADP-ribosylation events due to their ability to sense *O*-acetyl ADP-ribose along with mono- and poly ADP-ribose.[141] WWE domain-containing proteins, characterized by the presence of three highly conserved amino acids, show specific recognition of poly ADP-ribose. The observation that many WWE domain-containing enzymes also possess an E3 ligase or PARP catalytic domain suggest their involvement in ubiquitination and poly ADP-ribosylation events.[144] In particular, the E3 ubiquitin protein ligase RNF146 has been identified to regulate levels of poly ADP-ribosylated proteins by ubiquitination-mediated degradation, highlighting the role of the WWE domain in poly ADP-ribose recognition.[145,146] Enzymes with a PAR-binding zinc finger domain, originally recognized as binders for nucleic acids and proteins, have been identified as poly ADP-ribose markers.[147] The first evidence for their involvement came from the identification of this

domain in proteins essential for the localization of DNA damage in a poly ADP-ribose dependent manner.[148]

1.4 Chemical tools for ADP-ribosylation studies

As described in the previous section, ADP-ribosylation as a PTM of histones exerts a substantial influence on cellular processes such as DNA repair, transcriptional regulation and protein recruitment.[1] A comprehensive understanding of the mechanism and subcellular localization of ADP-ribosylation will improve the knowledge of potential targets, interacting partners and resulting effects. Therefore, the synthesis of site-specifically modified proteins and the chemical assembly of ADP-ribose are mandatory. From a chemical point of view, both the formation of site-specifically ADP-ribosylated proteins and the synthesis of ADP-ribose oligomers present significant challenges. The composite nature of these entities, which combine elements of synthetic chemistry related to nucleic acids, oligosaccharides and peptides requires solutions that arise from incompatibilities. Further complicating the issue is the incorporation of pyrophosphate linkages, a task that poses difficulties in achieving with high efficiency.[149]

1.4.1 Synthesis of mono ADP-ribosylated peptides

Mono ADP-ribosylated proteins, which represent the smallest introduced modification within this PTM, play key roles in numerous cellular processes.[150] To study this phenomenon in a biochemical context, several methods for the synthesis and evaluation of mono ADP-ribosylated peptides have been examined. The two major challenges in this process are the conjugation of mono ADP-ribose with nucleophilic amino acid side chains and the formation of pyrophosphate bond within the mono ADP-ribose. Solid phase peptide synthesis (SPPS) is the method of choice for incorporating this modification into the oligopeptide sequence. The incorporation of ribosyl moieties into amino acid side chains has been extensively investigated, driven by the requirement for a 1,2-*cis* configuration in the glycosidic linkage. Pioneering work by van der Heden van Noort *et al*. realized this by the synthesis of a SPPS-compatible ribosyl building blocks (**Scheme 1**).[151] The synthesis was initiated with the preparation of an appropriately protected β-D-ribosyl azide (1.1), which was reduced to the corresponding amine (1.2). Subsequent coupling with Z-Asp-OBn, mediated by EDC, allowed the transfer of the ribosyl moiety to the amino acid. The removal of the N- and C-terminal protecting groups from asparagine was followed by the introduction of a fluorenylmethyloxycarbonyl (Fmoc) protecting group at the N-terminus, yielded the α-linked building block used in the SPPS (1.4).

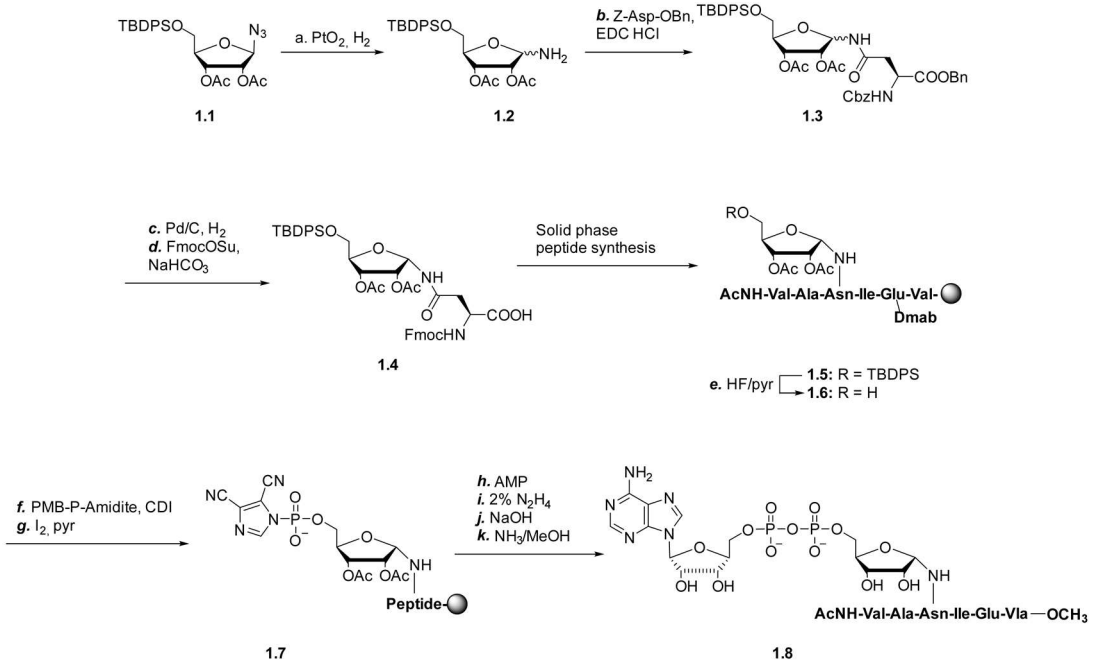

Scheme 1. Synthesis of mono ADP-ribosylated peptide. Ribosyl asparagine (1.4) used in SPPS to generate ribosylated oligopeptide (1.5). Phosphorylation and coupling to AMP yields mono ADP-ribosylated oligopeptide 1.8. Synthesis adapted from[151]. Figure adapted from[149]

Following SPPS, the ribosyl peptide (1.5) was desilylated with hydrogen fluoride to yield the free primary hydroxyl group (1.6). The immobilized peptide was then phosphorylated using di-*O*-PMB *N,N*-di-*iso*-propyl phosphoramidite with DCI activation. Subsequent oxidation with iodine provided the preactivated phosphorimidazolide (1.7). The following diphosphate coupling reaction with protected adenosine monophosphate (AMP) resulted in the formation of the mono ADP-ribosylated peptide. Deprotection and cleavage from the solid support yielded the deprotected mono ADP-ribosylated peptide (1.8), which was purified by high performance liquid chromatography (HPLC) and analyzed via liquid chromatography mass spectrometry (LC-MS). Analysis revealed the formation of by-products during the diphosphate coupling reaction. Despite changing to a solution AMP activation strategy, the side product formation was not reduced and no yield improvement was observed.[151] Given this limitation, Kistemaker *et al*. developed an alternative synthesis for the diphosphate coupling reactions during SPPS (**Scheme 2**).[152] This method involved a combination of phosphate (P^{V}) and phosphoramidite (P^{III}) chemistry, avoiding an on-resin phosphorylation by synthesizing a phosphorylated amino acid building block (2.3).

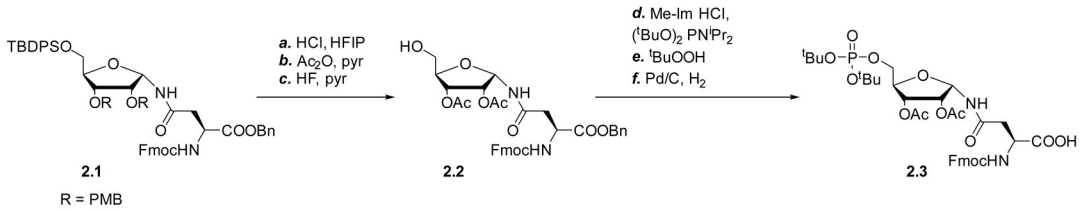

Scheme 2. Synthesis of the phosphorylated amino acid building block for SPPS. Protected ribosyl asparagine (2.2) used for phosphorylation prior to SPPS. Synthesis adapted from[152]. Figure adapted from[149]

Therefore, a protected ribosylated asparagine (2.1) was used as starting material. After exchanging the protecting groups for the secondary hydroxyl groups to acetyl and deprotecting the primary hydroxyl group with hydrogen fluoride, the intermediate (2.2) was obtained. The construction of the SPPS-compatible building block was realized by a phosphorylation reaction with di-*tert*-butyl-*N,N*-di-*iso*-propyl phosphoramidite followed by oxidation with *tert*-butyl hydroperoxide (tBuOOH). After C-terminal deprotection by hydrogenolysis, the desired phosphorylated SPPS building block (2.3) was obtained.[152]

This approach also enabled the preparation of a mono ADP-ribosylated peptide derived from the N-terminal region of the core histone H2B. For this purpose, an endogenous serine modification site from the native protein was used. The oligopeptide was synthesized via SPPS using the Fmoc protection strategy, with the phosphorylated ribosyl-serine (3.1) serving as the modified amino acid (**Scheme 3**).[153] Incorporation of the phosphorylated ribosyl serine (3.1) into the oligopeptide yielded the ribosyl peptide (3.4). To enable the diphosphate bond formation, the *tert*-butyl protecting groups of the phosphate were removed using trifluoroacetic acid (TFA), yielding the oligopeptide 3.5. This was then coupled with adenosine phosphoramidite (3.2) in the diphosphate coupling reaction using 5-ethylthiotetrazole (ETT) as the activator. P^{III} oxidation followed by removal of the cyanoethyl protecting group afforded the protected mono ADP-ribosylated peptide. Basic cleavage from the solid support and global deprotection resulted in the mono ADP-ribosylated peptide 3.6.[153] This procedure for generating a mono ADP-ribosylated peptide with serine as the amino acid target represents the first synthetic introduction of this PTM at a serine modification site in the sequence of a core histone.[151]

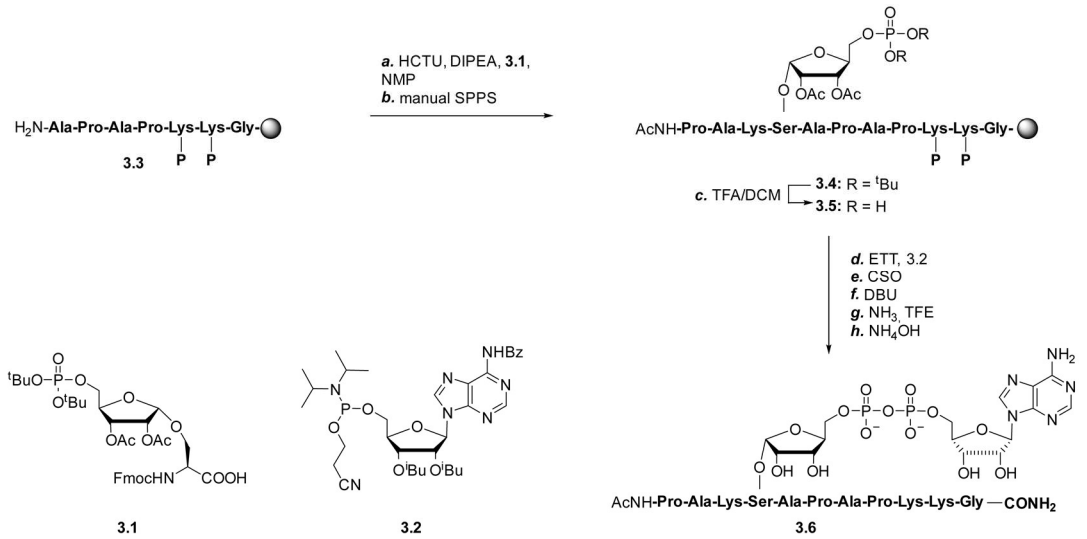

Scheme 3. Synthesis of mono ADP-ribosylated core histone H2B oligopeptide. Phosphorylated ribosyl asparagine (3.1) used in SPPS to generate ribosylated oligopeptide (3.5). Diphosphate coupling with 3.2 yields mono ADP-ribosylated oligopeptide derived from core histone H2B. Synthesis adapted from[153] Figure adapted from[149]

This achievement marks the first case of a site-specific introduction of mono ADP-ribose into the native core histone H2B sequence. Previous studies have relied primarily on asparagine and glutamine as stabilized variants of the amino acid targets aspartic acid and glutamic acid.[149,151] A related procedure was adapted from Hananya *et al.* to synthesize the full-length mono ADP-ribosylated core histones H2B and H3.[154] There, a phosphorylated ribosyl-serine was used in SPPS to generate ribosyl oligopeptides from these histones. Subsequent phosphate deprotection enabled the diphosphate coupling using ETT as an activator. After cleavage from the resin, the mono ADP-ribosylated oligopeptide was subjected to native chemical ligation with the remaining oligopeptide corresponding to the respective core histone. Using this method, native mono ADP-ribosylated core histones H2B and H3 were synthesized and subsequently used in biophysical and biochemical experiments.[154] Another semisynthetic approach to mono ADP-ribosylated histones was used to generate modified linker histones variants.[155] In this method, a peptide within the C-terminal region was enzymatically ADP-ribosylated at either serine 150 or 188. Native chemical ligation reactions were then used to link this modified peptide to the recombinant oligopeptide containing the N-terminus and the globular domain. A final ligation reaction to incorporate the remaining C-terminal domain, resulted in the formation of the mono ADP-ribosylated linker histone variants.[155]

Moyle and Muir introduced a post SPPS mono ADP-ribosylation method for an N-terminal oligopeptide derived from the core histone H2B (**Scheme 4A**).[21] In this method, glutamic acid residues were substituted with either aminooxy or *N*-methylaminooxy resulting in the corresponding oligopeptides 4.1 and 4.3. Subsequent modification of oligopeptide 4.1 with

mono ADP-ribose resulted in the formation of ring-closed mono ADP-ribosylated oligopeptide 4.2. The modification with the aminooxy oligopeptide 4.3 led to the formation of the ring-opened mono ADP-ribosylated oligopeptide 4.4 via an oxime intermediate. Although a complete conversion to 4.2 was achieved, the reaction leading to 4.4 also produced the ring-closed mono ADP-ribosylated oligopeptide as minor side product.[21] However, this method presents a notable drawback for generating full-length mono ADP-ribosylated histones. The N-terminal regions of the core histones, as well as the tails of the linker histone, are rich in lysine residues, leading to nonspecific and uncontrollable protein modifications via this approach.[149]

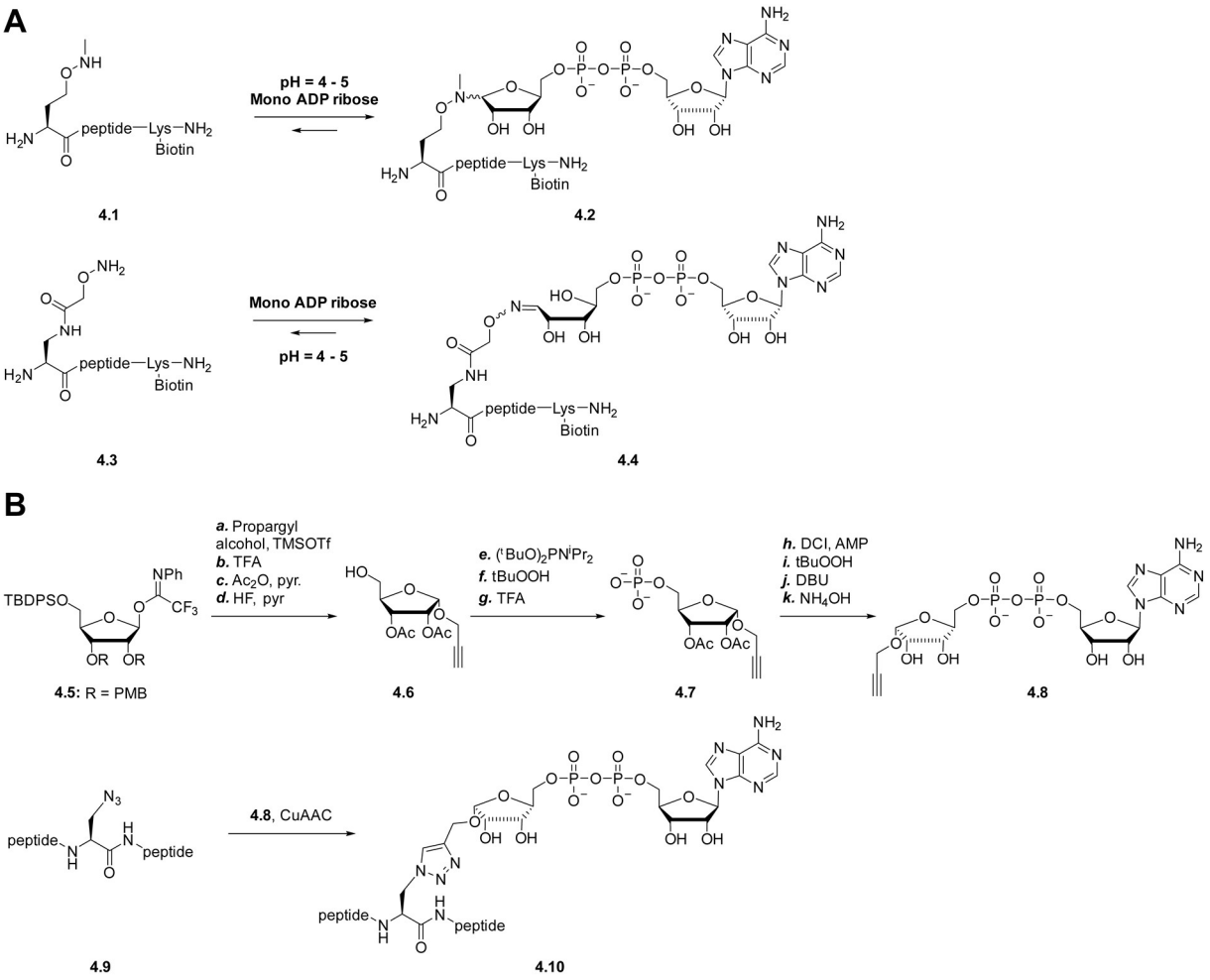

Scheme 4. Synthesis of mono ADP-ribosylated peptides by post SPPS methods. A. *O*-methylamino homoserine (included in oligopeptide 4.1) and 3-(2-aminooxy) acetylamino alanine (included in oligopeptide 4.3) modification of N-terminal H2B oligopeptide.[21] **B.** Triazole modification of N-terminal H2B oligopeptide by copper catalyzed azide alkyne cycloaddition (CuAAC).[156] Figure adapted from[149]

Liu *et al.* presented a method for the mono ADP-ribosylation of oligopeptides using copper catalyzed azide-alkyne cycloaddition (CuAAC).[156] The synthetic pathway for the alkyne modified ribose monophosphate (4.7), the alkyne modified mono ADP-ribose (4.8) and the mono ADP-ribosylated oligopeptide (4.10) are shown in **Scheme 4B**. The building block for

CuAAC was derived from 1'-*O*-(*N*-phenyl)-2,2,2-trifluoroacetimido-2',3'-di-*O*-PMB-5'-*O*-TBDPS β-D-ribose (4.5). The introduction of the CuAAC-compatible functional group was achieved by the reaction with propargyl alcohol, resulting in the formation of only the α-anomer of the product. Subsequent manipulation of the protecting groups resulted in the intermediate (4.6), which was phosphorylated with di-*tert*-butyl-*N,N*-di-*iso*-propyl phosphoramidite. Oxidation with tBuOOH and *tert*-butyl deprotection afforded compound 4.7. The diphosphate coupling reaction with adenosine phosphoramidite 3.2, resulted in the 1'-*O*-propargyl mono ADP-ribose (4.8) after deprotection. The CuAAC reaction involving 4.8 and 4.9 was performed at pH 7.6 using copper (II) sulfate, sodium ascorbate and a triazole ligand, yielding the triazole-linked mono ADP-ribosylated oligopeptide 4.10.

1.4.2 Synthesis of ADP-ribose oligomers

The synthesis of ADP-ribose oligomers involves the sequential formation of an α-glycosidic linkage between the anomeric carbon atom of a ribose and the 2'-hydroxyl group of an adenosine. In addition, a pyrophosphate bond has to be introduced between the primary alcohols of the ribose and the adenosine. To realize this synthesis, an internal building block is desirable. Given the need for both an α-glycosidic and a pyrophosphate linkage within the same molecule, a strategically designed building block should incorporate the α-glycosidic linkage, as repetitive glycosylation reactions are incompatible with retaining multiple pyrophosphate bonds.[149] Thus, the building block should contain the α-glycosidic linkage while the pyrophosphate linkage is introduced iteratively during the stepwise reaction to form ADP-ribose oligomers. All existing methods for the synthesis of ADP-ribose oligomers have adopted this approach.[9,10,149]

The first synthesis of an internal building block for ADP-ribose oligomers with a pre-introduced α-glycosidic linkage was achieved by Mikhailov *et al.* (**Scheme 5**).[13] In this synthesis, the glycosylation reaction used N^6-benzoyl-3',5'-*O*-(tetra-*iso*-propyl-disiloxane-1,3-diyl)-adenosine as glycosylation acceptor (5.1) and 1,2-di-*O*-acetyl-3,5-di-*O*-benzoyl-D-arabinofuranoside as glycosylation donor (5.2). The stereochemical outcome of this reaction is determined by the 2-*O*-benzoyl group of the donor due to its neighboring group participation. The subsequent transformation to the desired ribosyl-adenosine configuration is achieved by protecting group manipulation to the 2''-unprotected intermediate 5.4.

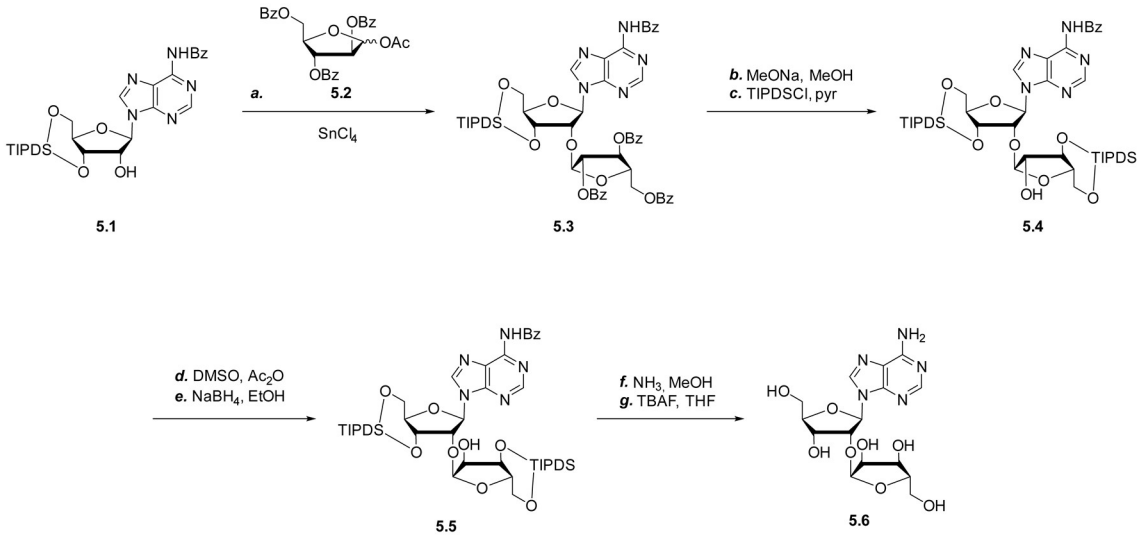

Scheme 5. Synthesis of an ADP-ribose building block with pre-introduced α-glycosidic linkage. Tin tetrachloride catalyzed glycosylation of N^6-benzoyl-3',5'-*O*-(tetra-*iso*-propyl-disiloxane-1,3-diyl)-adenosine (5.1) and 1',2'-di-*O*-acetyl-3',5'-di-*O*-benzoyl-D-arabinofuranoside (5.2). Stereochemical inversion and deprotection to give ribosyl-adenosine 5.6. Synthesis adapted from[13]. Figure adapted from[149]

The stereochemical inversion is achieved by an oxidation-reduction mechanism starting with an oxidation under Albright-Goldman oxidation conditions and is followed by the reduction of the ketone to the desired ribosyl-adenosine compound 5.5. Subsequent deprotection using methanolic ammonia and tetrabutylammonium fluoride (TBAF) resulted in the formation of the ribosyl-adenosine moiety 5.6.[13] Additionally, this glycosylation method, coupled with stereochemical inversion, has found application in the synthesis of potential PARP inhibitors by Zheng *et al*.[14] To avoid the necessity for a stereochemical inversion, several approaches have been developed such as a direct α-glycosylation. Van der Heden van Noort *et al.* investigated the glycosylation with 1-*O*-(*N*-phenyl)-2,2,2-trifluoroacetimido-2,3,5-tri-*O*-benzyl β-D-ribose (6.2) as glycosylation donor and *N*^{6}-di-benzoyl-3',5'-*O*-(tetra-*iso*-propyl-disiloxane-1,3-diyl)-adenosine (6.1) as glycosylation acceptor (**Scheme 6A**).[157] This α-selective glycosylation reaction, catalyzed by trimethylsilyl trifluoromethanesulfonate (TMSOTf), resulted in the formation of the ribosyl-adenosine moiety 6.3. Multiple protecting group manipulations yielded ribosyl-adenosine 6.4 with a 5'-TBDPS- and a 5''-DMT protected hydroxyl group. The orthogonality of these protecting groups is further needed to allows a stepwise reaction with the distinct termini to form ADP-ribose oligomers.[157]

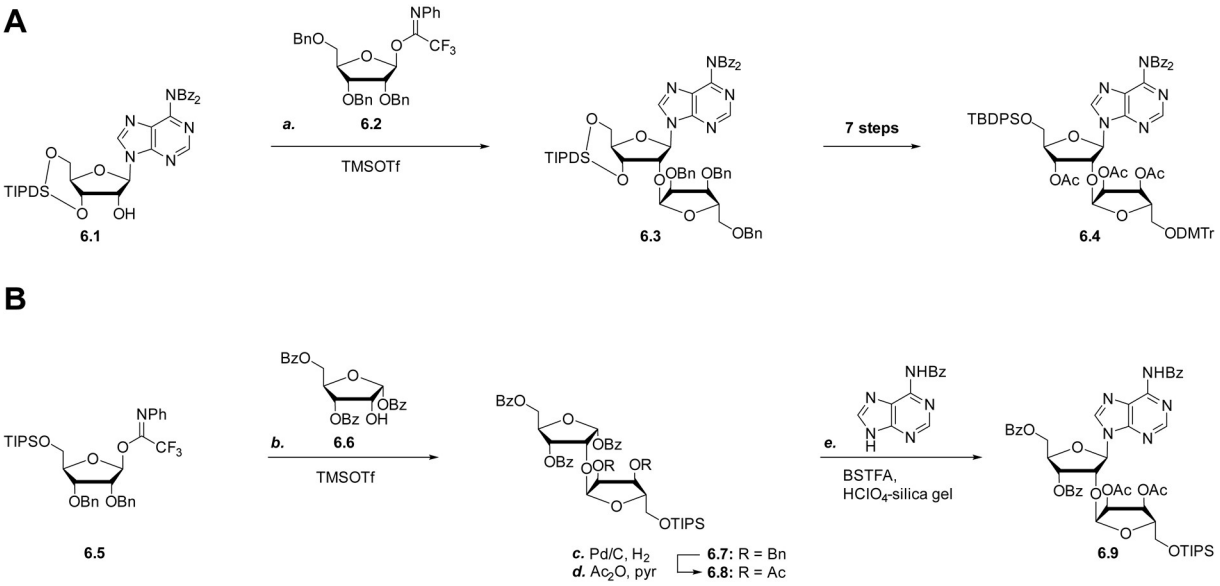

Scheme 6. Synthesis of ribosyl-adenosine building blocks. A. Glycosylation with 1-*O*-(*N*-phenyl)-2,2,2-trifluoroacetimido-2',3',5'-tri-*O*-benzoyl ribose (6.2) as glycosylation donor.[157] **B.** Synthesis with 1-*O*-(*N*-phenyl)-2,2,2-trifluoroacetamido-2',3'-di-O-benzyl-5'-tri-*iso*-propyl ribose (6.6) as glycosylation donor and subsequent Vorbrüggen glycosylation.[9] Figure adapted from[149]

In response to the demand for higher yields and improved scalability of glycosylation reactions, Kistemaker *et al.* developed a novel synthetic strategy, that expands the possibility of synthesizing larger ADP-ribose oligomers.[9] In this approach, the nucleobase adenine is introduced after the glycosylation via a Vorbrüggen type reaction (**Scheme 6B**).[9] Analogous to the previously described glycosylation method, this synthetic route involves the reaction of 1-*O*-(*N*-phenyl)-2,2,2-trifluoroacetimido-2,3-di-*O*-benzyl-5-*O*-tri-*iso*-propylsilyl-β-D-ribose (6.5) and 1,3,5-tri-*O*-benzoyl-α-D-ribose (6.6) to form the glycosylated disaccharide 6.7 with the desired α configuration. After changing the protecting groups on the 2''- and 3'' hydroxyl groups from benzyl to acetyl, the disaccharide (6.8) is reacted with N^6-benzoyladenine to give the ribosyl-adenosine building block (6.9).[9,149] This method of subsequent nucleobase introduction was adapted by Liu *et al.* to synthesize a branched ribosyl-adenosine -ribosyl building block.[158,159] The synthesis for the triphosphorylated *O*-α-D-ribofuranosyl-(1'''-2'')-*O*-α-D-ribofuranosyl-(1''-2')-adenosine-5',5'',5'''-tris(phosphate) (7.6) is shown in **Scheme 7**. Starting with disaccharide 6.7, protecting group manipulation afforded the 2'' unprotected disaccharide (7.1). Using the synthetic procedure for an α-glycosylation with 1-*O*-(*N*-phenyl)-2,2,2-trifluoroacetimido-2,3-di-*O*-benzyl-5-*O*-tri-*iso*-propylsilyl β-D-ribose (6.5) as glycosylation donor, the trisaccharide (7.2) with the introduced ribosyl linkage was obtained.[159] After adjusting the protecting group pattern of the trisaccharide, the nucleobase adenine was introduced via a similar Vorbrüggen type reaction as described in **Scheme 6B**, yielding the protected *O*-α-D-ribofuranosyl-(1'''-2'')-*O*-α-D-ribofuranosyl-(1''-2')-adenosine (7.4).

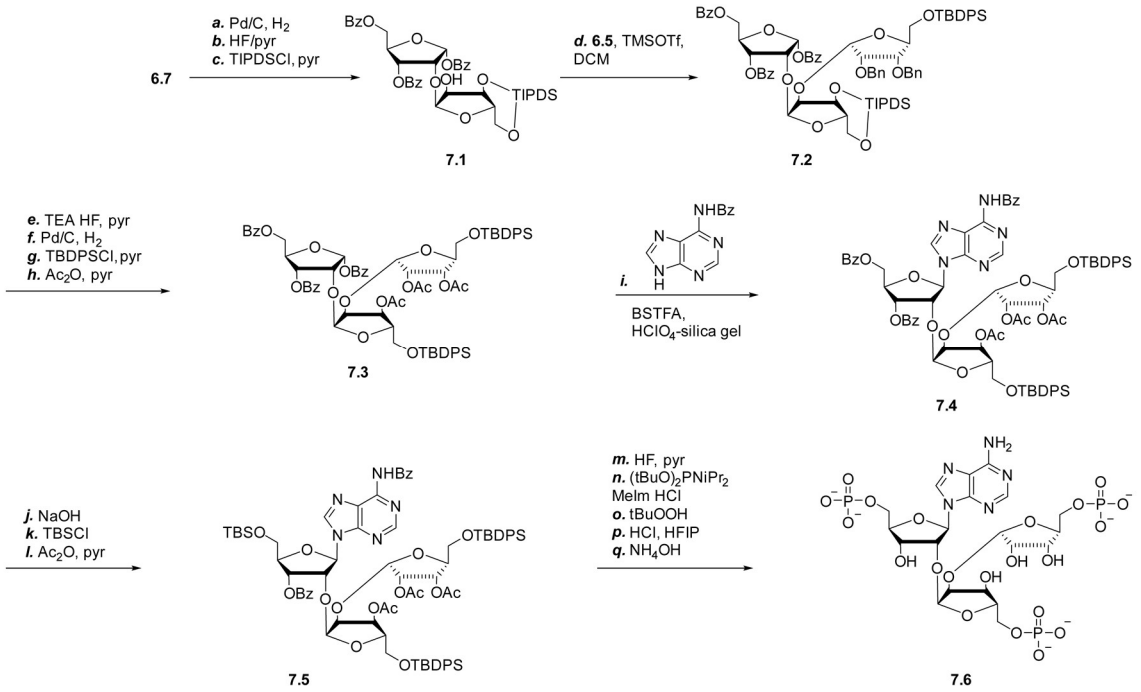

Scheme 7. Building block synthesis for branched ADP-ribose oligomers. Generation of 2' unprotected ribosyl-adenosine by protecting group manipulation. Branching point introduction by reaction of 7.1 with 1'-*O*-(*N*-phenyl)-2,2,2-trifluoroacetimido-2',3'-di-*O*-benzyl-5'-*O*-tri-*iso*-propylsilyl-β-D-ribose using TMSOTf as catalyst. Vorbrüggen type glycosylation to introduce adenine. Phosphorylation reaction to obtain triphosphorylated 7.6. Synthesis adapted from[159] Figure adapted from[149]

Subsequent protecting group manipulation yielded trisaccharide 7.5, which allowed a simultaneous 5', 5'' and 5''' hydroxyl deprotection while retaining all other protecting groups. Removal of these protecting groups by treatment with hydrogen fluoride allowed for phosphorylation with di-*tert*-butyl-*N,N*-di-*iso*-propyl phosphoramidite. Oxidation with tBuOOH and global deprotection resulted in the triphosphorylated ribosyl-adenosine -ribosyl (7.6).[159] Solution NMR studies of this compound revealed an identical linkage to that found in native branched ADP-ribose oligomers.[160,161]

Numerous methods for incorporating pyrophosphates into organic compounds such as nucleotides have been documented.[162-165] However, the synthesis of ADP-ribose oligomers requires the introduction of multiple of these linkages into a single molecule, which poses certain difficulties.[149]

A reported synthesis for an ADP-ribose dimer, which incorporates two pyrophosphate bonds within one molecule, was published by Lambrecht *et al.* (**Scheme 8**).[10] Starting with an α-linked ribosyl-adenosine building block (8.1), selective 5'-TBS deprotection allowed the introduction of a benzyl protected phosphate. Subsequent conversion of the allyl protecting groups of the secondary hydroxyl groups to TBS protecting groups yielded the monophosphorylated ribosyl-adenosine (8.2).

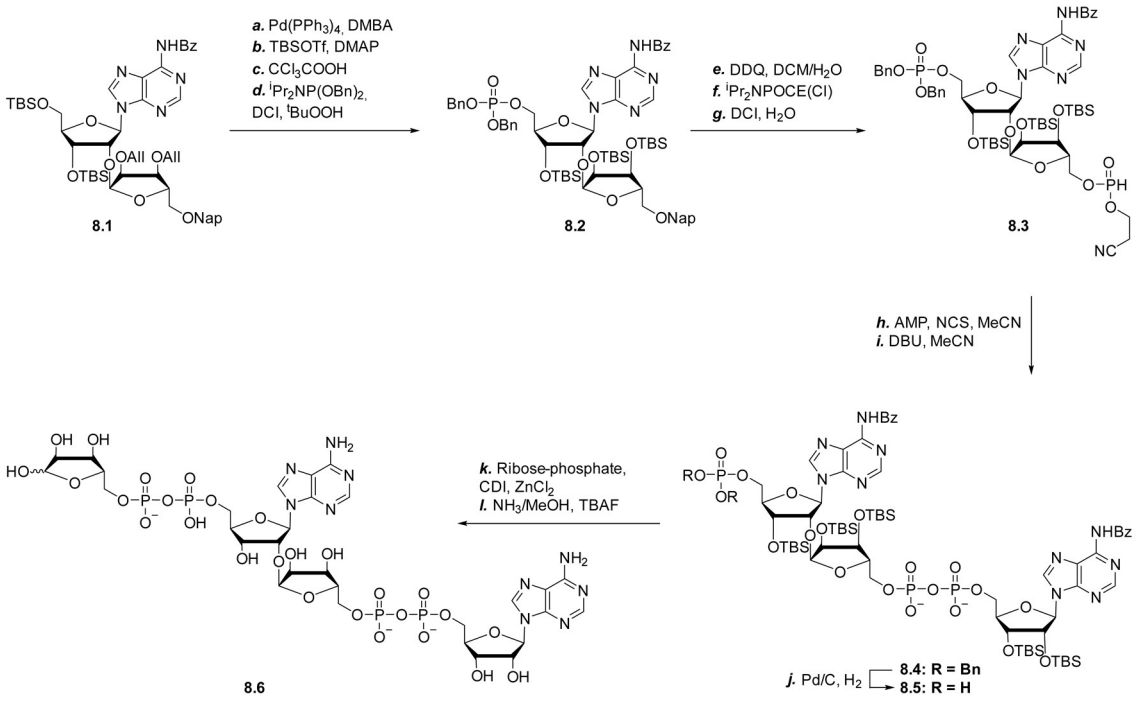

Scheme 8. Synthesis of ADP-ribose dimer. Selective 5' TBS deprotection and phosphorylation to 8.2. 5'' Nap deprotection and phosphoramidite introduction to compound 8.3. First diphosphate coupling by combination of P^{III} and P^{V} chemistry resulting in 8.4. Phosphate deprotection and second diphosphate coupling reaction to ADP-ribose dimer. Synthesis adapted from[10] Figure adapted from[149]

Cleavage of the naphthyl ether releases the 5''-hydroxyl group, enabling the incorporation of an *H*-phosphonate by reaction with 2-cyanoethyl-*N,N*-di-*iso*-propyl choro phosphoramidite. Hydrolysis of the intermediate gave the bis-phosphorylated ribosyl-adenosine (8.3). The pyrophosphate coupling reaction was performed by applying an Atherton-Todd type reaction, starting with the chlorination of the *H*-phosphonate with *N*-chlorosuccinimide followed by the condensation with adenosine monophosphate. Subsequent basic cleavage of the cyanoethyl phosphate protecting group afforded compound 8.4.[10] Hydrogenolysis of the benzyl phosphate protecting groups gave compound 8.5, which was used for the following second pyrophosphate bond formation. To introduce the second pyrophosphate bond, ribose monophosphate was preactivated with CDI to yield the corresponding phosphorimidazolide. Condensation with compound 8.5 and subsequent removal of all protecting groups afforded the ADP-ribose dimer (8.6), marking the first reported synthesis of an ADP-ribose dimer with the unprotected reducing end of the ribose.[10,149]

A different approach to the solution phase synthesis described above was demonstrated by a solid phase synthesis strategy published by Kistemaker *et al.*[9] This method not only enabled the production of ADP-ribose dimers, but also allows the generation of even longer oligomers. The synthesis of the bis-phosphorylated ribosyl-adenosine moiety and the solid phase synthesis strategy are shown in **Scheme 9**. This strategy combines P^{III} and P^{V} chemistry, which is well known for its utilization in SPPS for the introduction of pyrophosphate bonds

into mono ADP-ribosylated peptides.[153] Here, it was applied to iteratively introduce pyrophosphate bonds into a single molecule.[149] This requires the synthesis of a suitable ribosyl-adenosine building block (9.4) with a phosphoramidite at the 5'-hydroxyl group of the adenosine and a protected phosphate at the 5''-hydroxyl group of the ribose (**Scheme 9A**).

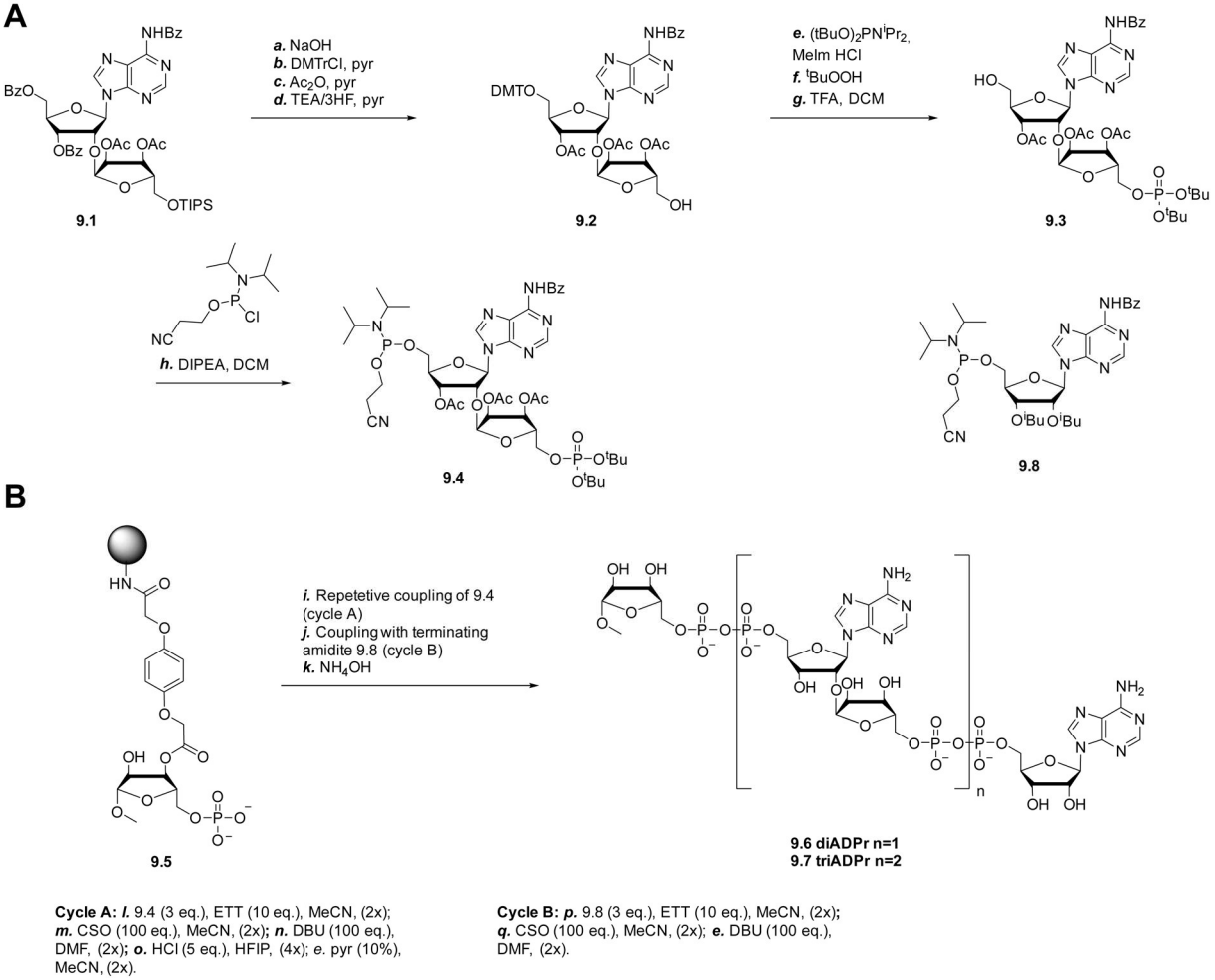

Scheme 9. Solid phase synthesis of ADP-ribose dimers and trimers. A. Synthesis of bis-phosphorylated ribosyl-adenosine building block applicable for solid phase synthesis. Introduction of protected P^{V} into 9.2 and deprotection of DMTr group to compound 9.3. P^{III} incorporation results in the bis-phosphorylated building block 9.4 used in solid phase synthesis. **B.** Solid phase strategy for the synthesis of ADP-ribose dimers and trimers. Chain elongation by cycle A with mono phosphorylated ribose immobilized on resin and 9.4. Termination reaction by cycle B and 9.8 as terminating reagent yielding ADP-ribose dimer or trimer.[9] Figure adapted from[149]

Starting with an orthogonal protected ribosyl-adenosine (9.1), manipulation of the protecting groups yielded the 5'-DMT and 5''-unprotected ribosyl-adenosine disaccharide (9.2). Phosphorylation with di-*O*-*tert*-butyl-*N,N*-di-*iso*-propyl phosphoramidite and subsequent oxidation was followed by acidic detritylation to give the monophosphorylated ribosyl-adenosine (9.3). The phosphoramidite was introduced by reaction with 2-cyanoethyl-*N,N*-di-*iso*-propyl phosphoramidite to give 9.4. The orthogonality in reactivity of the phosphates within this ribosyl-adenosine moiety makes it possible to perform a stepwise condensation

to ADP-ribose oligomers. Prior to solid phase synthesis, a controlled pore glass (CPG) solid support was modified with a Q-linker to functionalize the resin with a ribose monophosphate (9.5). The solid phase synthesis cycle is initiated by the pyrophosphate bond formation of the 5'-phosphoramidite (9.4) with the phosphate on the solid support (9.5). This diphosphate coupling reaction is catalyzed by the addition of ETT and after oxidation of the P^{III}-P^{V} intermediate, the cyanoethyl group is cleaved. Acidic deprotection of the *tert*-butyl groups allows a second round of pyrophosphate bond formation with the phosphoramidite building block to extend the ADP-ribose oligomer (**Scheme 9B**, cycle A). After these chain elongation, the extension is terminated by the reaction with the terminal adenosine phosphoramidite (9.8) using the same mechanism as for the previous pyrophosphate bond formation reactions (**Scheme 9B**, cycle B). Global deprotection and cleavage from the solid support by treatment with ammonia yields the ADP-ribose dimer (9.6) and trimer (9.7).[9,149] Furthermore, this solid phase synthesis approach for ADP-ribose oligomers was improved by Liu *et al.* to enable the preparation ADP-ribose oligomers up to the pentamer.[11]

1.5 Chemical protein modification methods at cysteines

Changes to proteins, such as PTMs, significantly change both their structure and function, leading to an increase in diversity of up to two orders of magnitude.[166] However, the introduction of modifications by organic synthesis is challenging due to the incompatibility between reaction conditions of organic synthesis and protein stability. In addition, it is crucial to achieve site specific modifications without side reaction in order to avoid complicated purification steps and evaluate the desired protein modification.[167] Established methods for chemical protein modification mainly target naturally occurring amino acids, including lysine, cysteine, serine, histidine and tyrosine as the site of modification.[168,169] Compared to methods using unnatural amino acids or enzymatic modifications, the use of naturally occurring amino acids avoids the need for genetic engineering to achieve the incorporation of the unnatural amino acid at the desired position in the protein sequence. Cysteine and lysine are commonly selected for protein modification reactions due to their high nucleophilicity.[170] While lysine is often used as a modification site, its high abundance in proteins often leads to non-specific modifications, resulting in heterogeneous modified proteins or in the blockage of functional sites. Strategies to prevent non-specific lysine modifications include the usage of differences in lysine reactivities within the protein sequence or using enzyme recognition sequences.[171,172] However, the widespread occurrence of most amino acids present challenges

in achieving site specific protein modifications, often resulting in modifications at multiple sites.[167]

In contrast to lysine modification reactions, cysteine modifications offer several advantages. The overall abundance of cysteine residues within a protein is comparatively low compared to lysine, making it a suitable target for chemical protein modification. In addition, the use of site-directed mutagenesis (SDM) prior to protein expression allows the simple introduction of a cysteine residue at a specific position within the protein sequence. The variety of PTMs that occur at cysteine residues underscores the diversity of the reactivity associated with this amino acid.[167] Manipulating the pH of the modification reaction can even direct the regioselectivity towards cysteine over lysine.[173] Among the electrophiles commonly used for cysteine modification reactions, maleimides and α-halocarbonyls have been extensively studied. The latter are often used as capping agents prior to digestion in protein sequencing.[174] However, α-halocarbonyls show major drawbacks in cysteine-selective protein modification reactions. Both histidine and terminal amino groups can potentially outcompete cysteine and lysine as primary modification targets under certain reaction conditions.[175] In contrast, maleimides exhibit higher regioselectivity, although they are susceptible to substituent exchange reactions with reactive thiols present in solution or derived from the protein. This tendency can lead to undesired side modification or release of the modifier.[176] Studies to improve the stability of cysteine modifications with maleimides have led to the development of ring-opened maleimides. The ring-opened structure results from hydrolysis and prevents target exchange reactions with thiols. However, this approach requires optimization of reaction conditions for each substrate.[177]

Disulfide bonds in proteins are used to preserve the tertiary and quaternary structure of the protein. Exploiting the principle of disulfide bond formation between a cysteine and a thiol, similar to those in native proteins, has been adapted for protein modification purposes. Due to the typically slow reaction rates of sulfide exchange reactions in the formation of new disulfide bonds, reagents have been developed to kinetically control and increase the reaction rate.[166] This strategy has found application in protein modifications using alkyl or aryl thiosulfates that selectively target cysteine residues.[178-180]

Another class of compounds potentially filling the gap of a cysteine-selective protein modification are dithiocarbamates. These compounds are used in diverse fields such as rubber curing, fungicides and pharmaceuticals.[181] In particular, disulfiram, marketed under the brand name Antabuse™ is used in the treatment of chronic alcoholism and acts by covalently modifying proteins at a cysteine residues (**Scheme 10**, left).

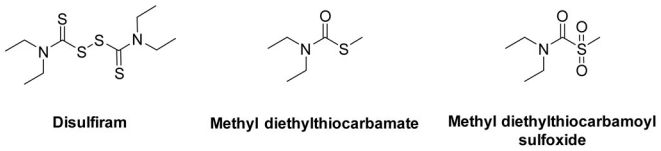

Scheme 10. Chemical structure of disulfiram and its metabolites.

The mechanism of action of disulfiram, which is characterized by its dimeric structure, relies on a metabolic pathway to receive methyl diethylthiocarbamate (**Scheme 10**, middle). This metabolite covalently modifies a cysteine residue within aldehyde dehydrogenase, thereby inhibiting its function.[182] Prior to covalent protein modification, methyl diethylthiocarbamate is oxidized to methyl diethylthiocarbamoyl sulfoxide (**Scheme 10**, right), an important step that activates its reactivity for cysteine residues. This controlled increase in the reactivity with cysteines makes this form of protein modification suitable for chemical protein modification approaches.

Another mechanism of a covalent cysteine modification by disulfiram involves the formation of disulfide bonds. There, the disulfide bond present in disulfiram is reduced by a reactive cysteine, resulting in the formation of a new disulfide bond and the release of diethylthiocarbamate.[3] This mechanism has been used by Laps *et al.* to form disulfide bonds in proteins such as conotoxin and the peptide hormone oxytocin.[4,5] Here, the active cysteine is oxidized to the corresponding disulfide by reaction with diethyldithiocarbamate and palladium. This disulfide intermediate serves as a precursor for the formation of an intramolecular disulfide bond with the target protein or peptide hormone.[4,5]

Similarly, thiocarbamates have been investigated for their potential to perform cysteine-selective reactions similar to dithiocarbamates. Hwang *et al.* used the thiocarbamate functional group to achieve thiol-selective reactions with coenzyme A.[6] Using desthiobiotin modified with a thiocarbamate linker, a molecular handle could be introduced into a protein. The activation of the desthiobiotin thiocarbamate to the corresponding sulfone promoted its reaction with the thiol in coenzyme A, resulting in the formation of a desthiobiotin-coenzyme A conjugate that can be used for protein modification reactions. Dithiocarbamates and thiocarbamates offer distinct advantages over conventional methods due to their enhanced selectivity towards cysteine residues. Strategic incorporation of an appropriately designed linker could enable a complete cysteine-selective method for the introduction of a variety of modification into proteins, including synthetically challenging PTMs such as ADP-ribosylation.

2 Objectives

PTMs of histones play an important role in the regulation of the chromatin architecture and many other cellular processes including transcriptional regulation.[1] Among the major targets of ADP-ribosylation during chromatin remodeling and DNA processing are the four core histones and the linker histone. Despite extensive studies on histone PTMs, the effects of the ADP-ribosylation of the linker histone remain largely unexplored due to the lack of suitable methods to generate and analyze the modified protein. The emerging role of ADP-ribosylated linker histones in processes beyond chromatin formation underlines the need to generate defined ADP-ribosylated linker histones to study their functional effects.

The aim of this work was to elucidate the influence of the site-selective ADP-ribosylation of the linker histone H1.2 on the chromatin structure formation. For this purpose, a novel chemical ligation approach based on a thiocarbamate as reactive group for the protein modification should be established for the ADP-ribosylation of the recombinantly expressed linker histone. The site selectivity and *in vitro* stability of the thiocarbamate ligation method will be investigated using a model system in which biotin is incorporated into the linker histone. The knowledge gained from this model system should then be applied to investigate and analyze the mono ADP-ribosylation of the recombinant protein at a known ADP-ribosylation site.

Since the ADP-ribosylation of histones yields both mono ADP-ribosylated proteins and their polymeric form, a suitable synthetic pathway for dimeric ADP-ribose with a free reducing end will be established. The thiocarbamate ligation approach should be verified for its applicability to the synthesized dimeric ADP-ribose, which would then allow for the investigation of the incorporation of oligomeric ADP-ribose into the recombinant linker histone.

The incorporation of the ADP-ribosylated linker histone variants into the chromatin structure will be studied by performing a chromatosome assembly assay. Here, nucleosomes are assembled from recombinant core histone octamer and nucleosomal DNA with a sequence optimized for linker histone binding. Thus, by using mono- and diADP-ribosylated linker histones for the assembly of the chromatosomes, it would be possible to investigate the effects

of linker histone ADP-ribosylation on the chromatin structure formation as well as to elucidate the impact of the ADP-ribose chain length in this process.

The research results presented in this thesis may contribute to a better understanding of the effects of site-selective ADP-ribosylation of linker histones on chromatin structure formation.

3 Results and Discussion

3.1 Biotinylation of the linker histone H1.2

PTMs of proteins alter their function and structure, resulting in a dramatic increase in the diversity of the proteome.[166] Studying the effects of different PTMs on target proteins is a compelling area of research in chemical biology. Here, it is desirable to closely mimic the native PTM of a protein in order to evaluate the direct influence of the introduced group.[166] In addition, the site-specific introduction of the PTM allows the investigation of a specific modification site and evaluate their impact. Protein ADP-ribosylation, especially histone ADP-ribosylation, is an extensively studied PTM due to its influence on the chromatin structure as well as on various cellular processes.[1] To date, the deliberate generation of ADP-ribosylated proteins has been challenging. Enzymatic protein modification with known ADP-ribosylating enzymes results in a heterogeneous mixture of modified proteins with different chain lengths and modification sites, requiring time-consuming purification procedures in order to obtain distinct modified proteins. Moreover, the modification of aspartic acid and glutamic acid as representatives for endogenous ADP-ribosylation sites results in the formation of an *O*-glycosidic linkage that is unstable in acidic environments, making it difficult to study using conventional methods.[149] Current synthetic approaches for the investigation of the protein ADP-ribosylation are predominantly based on SPPS strategies. The incorporation of modified amino acid building blocks with a phosphorylated ribose attached to an amino acid allows the site-selective modification of oligopeptides or small proteins (**Scheme 1**, **Scheme 3** and **Scheme 4**).[151-153] While these approaches offer flexibility in the selection of the target amino acid and the type of chemical linkage between the amino acid and the ribose, there are significant drawbacks, such as the limited achievable protein size when using SPPS and the complexity of synthesizing the amino acid building blocks. Alternatively, unnatural amino acids enable the formation of linkages to chemical modifications via reactions such as CuAAC. For example, the synthesis of 1'-propargyl mono ADP-ribose (4.8) coupled to an azido alanine containing oligopeptide allows site-selective incorporation of mADPr into an oligopeptide (**Scheme 4B**).[156] Similarly, the use of *O*-methylamino homoserine or 3-(2-aminooxy) acetylamino alanine renders a direct modification, resulting in the formation of modified

oligopeptides derived from the N-terminal region of the core histone H2B (**Scheme 4A**).[21] However, these methods are only suitable for the investigation of short ADP-ribosylated peptides due to the involvement of SPPS.

The investigation of the ADP-ribosylation of the linker histone H1.2 bears several challenges. In particular, the protein sequence contains numerous nucleophilic lysine residues, making a site-selective modification with an electrophile difficult. However, the absence of cysteine residue in the sequence of the linker histone H1.2 enables the deliberate introduction of modifications into the protein by using SDM. While methods using unnatural amino acids such as azido alanine require techniques like amber stop codon suppression, the incorporation of the natural amino acid cysteine into the protein sequence is more straightforward and simpler via SDM. Overall, cysteine is a well-studied amino acid for protein modification and therefore an ideal target for the purpose of deliberate ADP-ribosylation.[166] The linkage between the modifier and the cysteine should ideally mimic an endogenous linkage, as even minor changes in the linkage can significantly affect small modifications such as mADP-ribosylation. Hence, certain criteria must be fulfilled, including near-quantitative conversions to avoid complex purification procedures. Moreover, reactions for the modification introduction must occur under protein-compatible conditions, including low temperatures and aqueous buffer systems, to preserve the tertiary structure and more importantly the function of the protein.

3.1.1 Site-directed mutagenesis and expression of linker histone H1.2 S150C

Given these prerequisites, the investigation of a site-specific ADP-ribosylation of the linker histone started with the generation of a linker histone variant containing a cysteine at a known ADP-ribosylation site. Expression of the recombinant protein in *E. coli* provided the desired linker histone variant with a specific cysteine mutation site without the addition of any PTM. This allowed a detailed investigation of the subsequent incorporated modification on the structure and function of the protein. In this study, serine 150 (numbering including the starting methionine) in the C-terminal region was chosen as the modification site. ADP-ribosylation of the linker histone at this position has been previously shown to significantly influence chromatin structure and remodeling complexes.[8] Therefore, a codon-optimized sequence containing the point mutation for the exchange of serine to cysteine (H1.2 S150C) was generated by SDM. Additionally, the plasmid encoded a C-terminal His_6-tag for purification by immobilized metal affinity chromatography (IMAC). The plasmid containing the mutation for the cysteine was transformed into *E. coli* BL21 (DE3) cells. After induction of the recombinant protein expression with *iso*-propyl-β-D-thiogalactopyranosid (IPTG), the

linker histone variant H1.2 S150C was isolated from the inclusion bodies, purified by IMAC and analyzed by SDS-PAGE (**Figure 6A**).

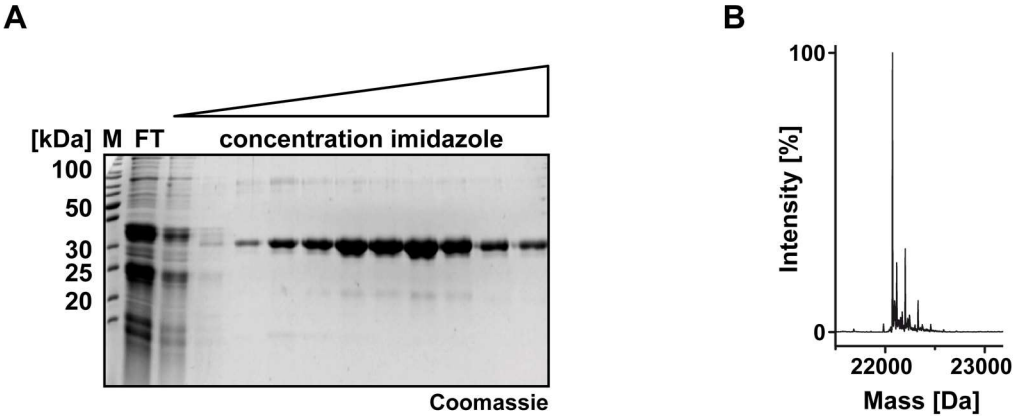

Figure 6. Analysis of the purification of the linker histone variant H1.2 S150C. A. SDS-PAGE gel analysis with Coomassie blue staining of immobilized metal affinity chromatography (IMAC) of the linker histone H1.2 S150C. Stepwise increase of imidazole concentration from 0 mM to 500 mM. **B.** Deconvoluted LC-MS analysis of the full-length protein. H1.2 S150C calculated 22072 Da, measured 22072 Da.

Proteins not bound to the cOmplete™ His-Tag purification resin (Roche) were removed by washing steps. Elution of the linker histone variant H1.2 S150C was achieved by gradually increasing the imidazole concentration (0 mM to 500 mM) in the elution buffer. The purity of the eluted fractions was analyzed by SDS-PAGE with Coomassie blue staining (**Figure 6A**). Moreover, the successful incorporation of the cysteine modification into the protein sequence was validated by full-length protein LC-MS analysis (**Figure 6B**). The measurement yielded a peak with a deconvoluted mass of 22072 Da for H1.2 S150C consistent with the calculated value of 22072 Da. This represents a mass shift of 16 Da relative to the mass of the H1.2 WT (22056 Da, **Figure S1** in the Appendix). This established expression system for the cysteine containing linker histone variant H1.2 S150C was used to further investigate the introduction of a cysteine-selective linker.

3.1.2 Synthesis of thiocarbamate linker modified biotin

The simple expression and purification procedure for the linker histone variant H1.2 S150C, combined with a cysteine-selective modification method, allows the site-selective incorporation of modifiers such as ADP-ribose into the protein. For this purpose, a thiocarbamate based linker developed by Dr. Martin Mex during his PhD studies in the group of Prof. Andreas Marx was used.[7] *S*-Ethyl α-methylhydrazide thiocarbamate (thiocarbamate linker, 11.4) was utilized as thiocarbamate containing modifier and the design was adapted from the structure of disulfiram, a drug used in the treatment of chronic alcoholism. Disulfiram is metabolized *in vivo* to the highly reactive methyl diethylthiocarbamoyl sulfoxide, which can covalently modify cysteines within the aldehyde dehydrogenase and therefore

inhibit the metabolism of ethanol.[182] The mechanism of this cysteine-selective protein modification is based on the activation of the thiocarbamate functionality by oxidation to the respective sulfone, which then undergoes a selective reaction with a thiol. This mechanism was also employed in the following protein modification reactions using the thiocarbamate linker. The synthesis of *S*-Ethyl α-methylhydrazide thiocarbamate (11.4) used in the protein modification reactions is shown in **Scheme 11**.

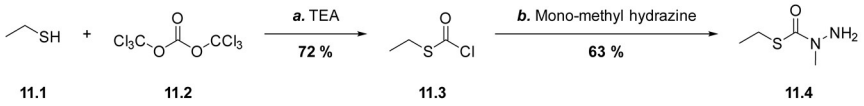

Scheme 11. Synthesis of *S*-Ethyl α-methylhydrazide thiocarbamate (11.4). ***a.*** TEA, THF, 0 °C, 1 h (72 %). ***b.*** Mono-methyl hydrazine, TEA, DCM, –80 °C to r.t., 16 h (63 %). For detailed regents and conditions, see **section 5.1.2.1**.

Starting with ethanethiol (11.1), a chloroformyl group was introduced by reaction with triphosgene (11.2) to give ethyl chlorothioformate (11.3). The crude product was then reacted in a subsequent synthesis with methylhydrazine to give the desired *S*-Ethyl α-methylhydrazide thiocarbamate (11.4). This synthesized linker contains two different chemical functionalities with different reactivities. First, the thiocarbamate functionality, which is used for cysteine-selective protein modification has been shown to be suitable for this purpose.[6,7] Second, the hydrazide functionality within the thiocarbamate linker enables the integration of various target molecules such as ADP-ribose or biotin. To further diversify the thiocarbamate linker with different modifiers, the reaction of ethyl chlorothioformate (11.3) with methylhydrazine instead of hydrazine was required to increase the stability. Thiocarbamates with an unsubstituted α-amine are susceptible to hydrolytic cleavage in their oxidized form, an issue that was avoided in compound 11.4.[183]

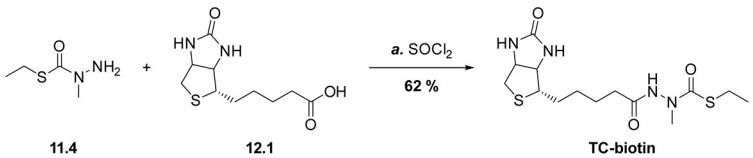

Scheme 12. Synthesis of TC-biotin. ***a.*** Thionyl chloride, MeCN, r.t., 20 h (62 %). For detailed reagents and conditions, see **section 5.1.2.2**.

To further investigate the cysteine selectivity and stability of the protein modification with the thiocarbamate linker (11.4), a model system of thiocarbamate-linker modified biotin (TC-biotin) was developed. The synthesis of TC-biotin is shown in **Scheme 12**. Biotin was coupled to the hydrazide functionality of the thiocarbamate linker by activation of biotin. This activation involved the reaction of biotin (12.1) with thionyl chloride in acetonitrile (MeCN)

to yield the acid chloride of biotin. The crude acid chloride of biotin was then reacted with *S*-Ethyl α-methylhydrazide thiocarbamate (11.4) to form TC-biotin in 62% yield.

3.1.3 Linker histone H1.2 S150C biotinylation

The synthesized TC-biotin was then subjected to linker histone modification reactions. The cysteine selectivity was evaluated by reactions with either the linker histone H1.2 WT or the cysteine containing variant H1.2 S150C. The linker histone H1.2 WT lacks a cysteine residue and therefore should not be able to undergo a putative cysteine-selective modification reaction. To enable the protein modification with TC-biotin by its thiocarbamate functionality, the thiocarbamate has to be oxidized. This activation procedure, shown in **Figure 7**, involved the conversion of the thiocarbamate to its sulfone derivative (oxTC-biotin) using Oxone™.[6] To investigate the cysteine selectivity of this protein modification, H1.2 S150C or H1.2 WT variants were incubated with increasing concentrations of the oxTC-biotin. Subsequent analysis included SDS-PAGE with Coomassie blue staining and WB analysis with ExtrAvidin Peroxidase (**Figure 7**).

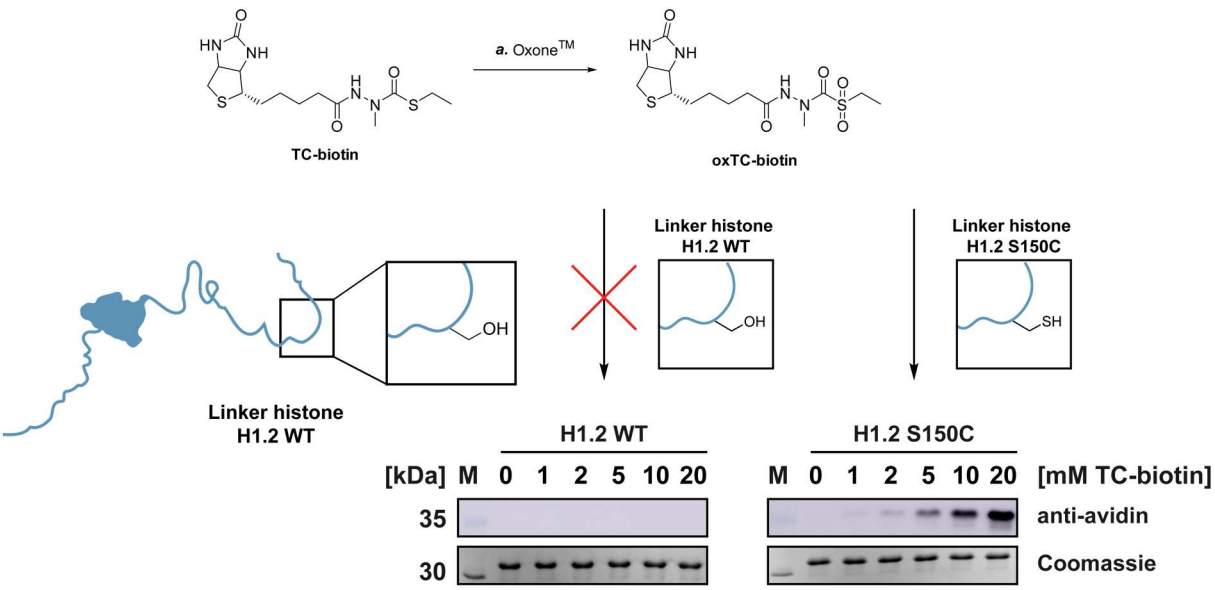

Figure 7. Biotinylation of linker histone H1.2 WT and S150C variant. Oxidation of TC-biotin to oxTC-biotin. Subsequent coupling to the linker histone H1.2 WT and cysteine containing variant H1.2 S150C. ***a.*** Oxone™ (10 mM in Milli-Q water, Merck), 25 °C, 2 h. OxTC-biotin was incubated with H1.2 WT or H1.2 S150C at 25 °C. Western Blot analysis (ExtrAvidin Peroxidase, Merck) and SDS-PAGE analysis of protein modification with oxTC-biotin and H1.2 WT and H1.2 S150C. For detailed reagents and conditions, see **sections 5.2.2.8** and **5.2.2.10**.

Incubation of H1.2 WT or H1.2 S150C with the activated oxTC-biotin was performed at 25 °C in Milli-Q water, with increasing concentrations of oxTC-biotin from 0 mM to 20 mM. The modification reactions were evaluated by SDS-PAGE with Coomassie blue staining and WB using ExtrAvidin Peroxidase, which selectively binds to biotin, serving as an indicator of the attachment of TC-biotin to the linker histone. For all modification reactions, Coomassie blue

stained SDS-PAGE gels showed bands of similar intensity. Notably, the incubation of H1.2 WT with activated oxTC-biotin should not result in protein modification due to the missing cysteine residue in the protein sequence. This is supported by absence of the corresponding bands in the WB analysis for the H1.2 WT using ExtrAvidin Peroxidase. In contrast, the WB analysis of the linker histone H1.2 S150C modification revealed a distinct band of the biotinylated protein starting at 5 mM TC-biotin with increasing intensity at higher oxTC-biotin concentrations. These results demonstrate the successful protein modification with TC-biotin and exclude the possibility of non-specific modifications of nucleophilic amino acid side chains such as lysine. This approach offers the distinct advantage over alternative techniques described in the literature, such as α-halocarbonyls or maleimide couplings, which tend to undergo non-specific modifications.[175]

The potential for non-specific modifications among the commonly used cysteine modification method and the developed thiocarbamate modification was further investigated. Therefore, the linker histone H1.2 WT was incubated with *N*-biotinoyl-*N*'-(6-maleimidohexanoyl) hydrazide (biotin-maleimide, 1 mM) as a maleimide derivative, biotin polyethyleneoxide iodoacetamide (biotin-iodoacetamide, 1 mM) as an α-halocarbonyl derivative and TC-biotin (2 mM).

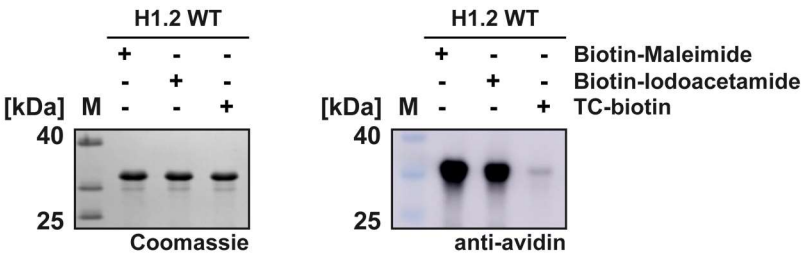

Figure 8. SDS-PAGE and WB analysis of linker histone H1.2 WT modifications. Linker histone H1.2 WT was incubated with biotin-maleimide, biotin-iodoacetamide or TC-biotin. Protein modifications were analyzed by SDS-PAGE with Coomassie blue staining and WB using ExtrAvidin Peroxidase (Merck). For detailed reagents and conditions, see **section 5.2.2.10**.

After incubation of H1.2 WT with the respective modifier, proteins were analyzed by SDS-PAGE with Coomassie blue staining and WB with ExtrAvidin Peroxidase (**Figure 8**). All histone H1.2 WT modification reactions showed bands of similar intensity on the Coomassie blue stained SDS-PAGE gel (**Figure 8**, left). However, upon WB analysis of these reactions, only the biotin-maleimide and biotin-iodoacetamide modification reactions showed distinct bands, demonstrating the non-specific property of these protein modification methods and further confirming the cysteine selectivity of the thiocarbamate linker method even when using an excess of TC-biotin compared to the other compounds tested. (**Figure 8**, right).

3.1.4 Stability analysis of the thiocarbamate ligation method

With the cysteine selectivity of this protein modification demonstrated by experiments with both the linker histone H1.2 WT and the cysteine containing variant H1.2 S150C, the stability of the formed linkage was investigated in a next step. The *in vitro* stability of the introduced protein modification was evaluated by incubation with HEK293T cell lysate.

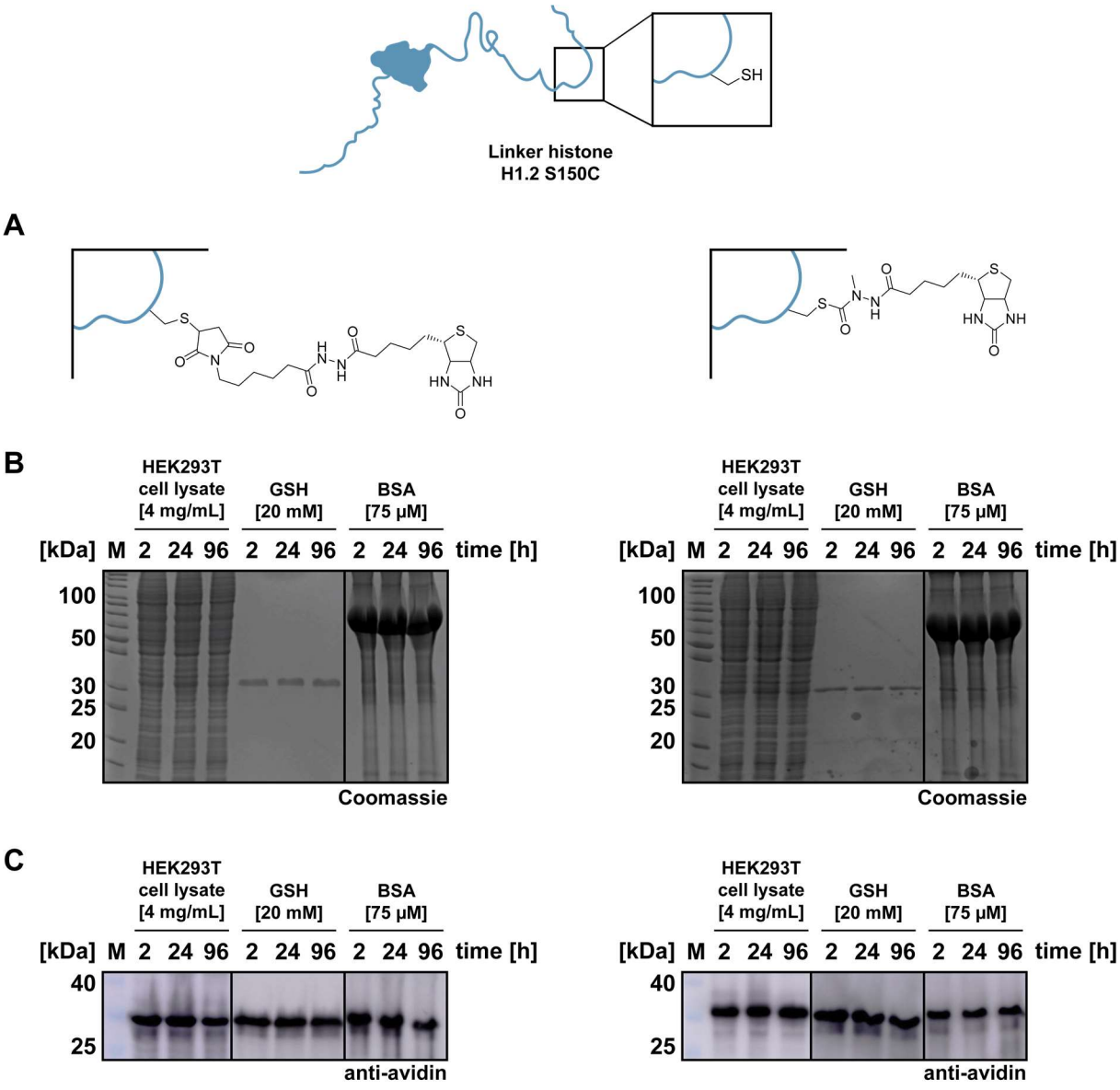

Figure 9. Stability assay of biotinylated linker histone H1.2 S150C. Linker histone was modified with *N*-biotinoyl-*N*'-(6-maleimidohexanoyl) hydrazide (biotin-maleimide, Merck) or TC-biotin. **A.** Schematic presentation of biotin-maleimide (left) and TC-biotin (right) linkage to H1.2 S150C. **B.** SDS-PAGE gel with Coomassie blue staining of the stability assay performed with HEK293T cell lysate (4 mg/mL), glutathione (GSH, 20 mM) and bovine serum albumin (BSA, 75 µM). Stability assay with biotin-maleimide (left) and TC-biotin (right) coupled to H1.2 S150C. **C.** WB analysis (ExtrAvidin Peroxidase, Merck) of the stability assay performed with HEK293T cell lysate (4 mg/mL), GSH (20 mM) BSA (75 µM). Stability assay with biotin-maleimide (left) and TC-biotin (right) coupled to H1.2 S150C. For detailed reagents and conditions, see **sections 5.2.2.8**, **5.2.2.9** and **5.2.2.11**.

To exclude potential thiol exchange reactions, a process observed in maleimide modified proteins, the stability of the formed linkage was investigated after incubation with glutathione (GSH) and an excess of bovine serum albumin (BSA).[184] Additionally to the biotinylation of H1.2 S150C with TC-biotin, a protein modification using biotin-maleimide and H1.2 S150C was used as a control (**Figure 9**). A schematic presentation of the different linker histone conjugates with either TC-biotin or biotin-maleimide to the cysteine residue of the linker histone are shown in **Figure 9A**. The biotinylated proteins were incubated with HEK293T cell lysate (4 mg/mL), GSH (20 mM) or BSA (75 µM). The samples were then subjected to SDS-PAGE with Coomassie blue staining and WB analysis using ExtrAvidin Peroxidase. Biotin-maleimide modified H1.2 S150C showed bands of consistent intensity in the WB analysis across all compounds tested and time points (**Figure 9C**, left). While maleimide-modified cysteines can undergo exchange reactions with reactive thiols, such reactions can be avoided by ring-opening hydrolysis.[177] The rate of this hydrolysis reaction depends on both the peptide and the succinimide applied in the modification reaction.[176] In the case of the biotin-maleimide and the linker histone H1.2 S150C used, this exchange reaction was not observed. However, since these samples served only as control to examine the stability of the TC-biotin protein modification, the exact mechanism underlying the stability of this linkage was not further investigated. Analogous to all compounds tested for the biotin-maleimide protein conjugate, TC-biotin modified H1.2 S150C showed bands of similar intensity in WB analysis during all conditions (**Figure 9C**, right). This new covalent protein modification method exhibits robust stability in HEK293T cell lysate along with no tendency towards thiol exchange reactions with GSH or BSA. An exchange would be indicated by the disappearance of the respective band in the WB analysis. The stability of the thiocarbamate linkage to the protein makes this method suitable for *in vitro* studies to investigate the influence of a site-selective protein modification by methods such as affinity enrichment approaches.

The thiocarbamate based protein modification method presented here was used to specifically generate a cysteine-biotin conjugate for the linker histone H1.2 S150C. First, *S*-Ethyl α-methylhydrazide thiocarbamate (11.4) was reacted with biotin to yield TC-biotin, which was subsequently incorporated into H1.2 S150C. (**Scheme 12** and **Figure 7**). The cysteine selectivity of the thiocarbamate linker was validated by experiments with H1.2 S150C and H1.2 WT, in which a protein modification only occurred in the presence of a cysteine residue in the protein sequence. This excludes non-specific modifications of nucleophilic amino acid side chains, especially lysine residues prevalent in the lysine-rich N-terminal region of the linker histone. Moreover, the stability of the formed linkage in HEK293T cell lysate demonstrated its *in vitro* stability, rendering this new protein

modification method applicable to cell lysate experiments such as affinity enrichment LC-MS/MS studies (**Figure 9**). In particular, with the cysteine selectivity demonstrated for the biotinylation of the linker histone H1.2 S150C, this method can be extended to PTMs of the linker histone such as ADP-ribosylation.

3.2 Mono ADP-ribosylation of the linker histone H1.2

The importance of the mADP-ribosylation on histones with a focus on the linker histone was highlighted in **section 1.3**. Nonetheless, further investigation into the site-selective introduction of this PTM on the linker histone is of particular interest. Current methods for protein mADP-ribosylation involve SPPS using ribosylated building blocks (**Scheme 1**[151] and **Scheme 3**[153]), which require native chemical ligation reactions in order to obtain the full-length modified protein. Alternatively, a different modification approach involves the incorporation of unnatural amino acids followed by protein modification reactions such as CuAAC (**Scheme 4**).[21,156] However, there is currently no established method for a site-specific ADP-ribosylation of the recombinantly expressed linker histones. The cysteine-selective thiocarbamate linker method, described for the biotinylation of the linker histone H1.2 S150C in **section 3.1**, promises to fill this gap by enabling site-selective protein modification without the use of unnatural amino acids or native chemical ligation reactions. This advancement would greatly contribute to increase the understanding of histone ADP-ribosylation and its effects on chromatin remodeling and the histone code. Following the incorporation of the thiocarbamate linker (11.4) into mADPr, the cysteine selectivity of this protein modification reaction was evaluated by reactions with the linker histone H1.2 WT and the cysteine containing variant H1.2 S150C.

The synthesis of thiocarbamate linker modified mADPr (TC-mADPr) was started with the reaction of mADPr and *S*-Ethyl α-methylhydrazide thiocarbamate (11.4) (**Figure 10A**). The mechanistic pathway for the introduction of the thiocarbamate linker into mADPr involved a hydrazone intermediate. Previous studies have shown that the formation of oximes in ligation reactions can be enhanced by multiple freeze-thaw cycles at –20 °C.[185] In this work, it was suspected that hydrazones, the amine analog of an oxime, would show a similar increase in product formation with this method. Application of this approach for the synthesis of TC-mADPr followed by the reduction of the hydrazone with $NaBH_3CN$ afforded the desired TC-mADPr in 88% yield.[7] Prior to the modification of a target protein with TC-mADPr, the incorporation of this PTM was enabled by the oxidation of the thiocarbamate functionality to the corresponding sulfone using Oxone™.[6] This oxidized TC-mADPr was then used directly in

the protein modification reactions. The site-selective mADP-ribosylation was investigated by modifying the cysteine-containing variant of the linker histone H1.2 S150C. The successful incorporation of mADPr into the linker histone H1.2 S150C using TC-mADPr was validated by LC-MS measurements of the full-length protein (**Figure 10B**).

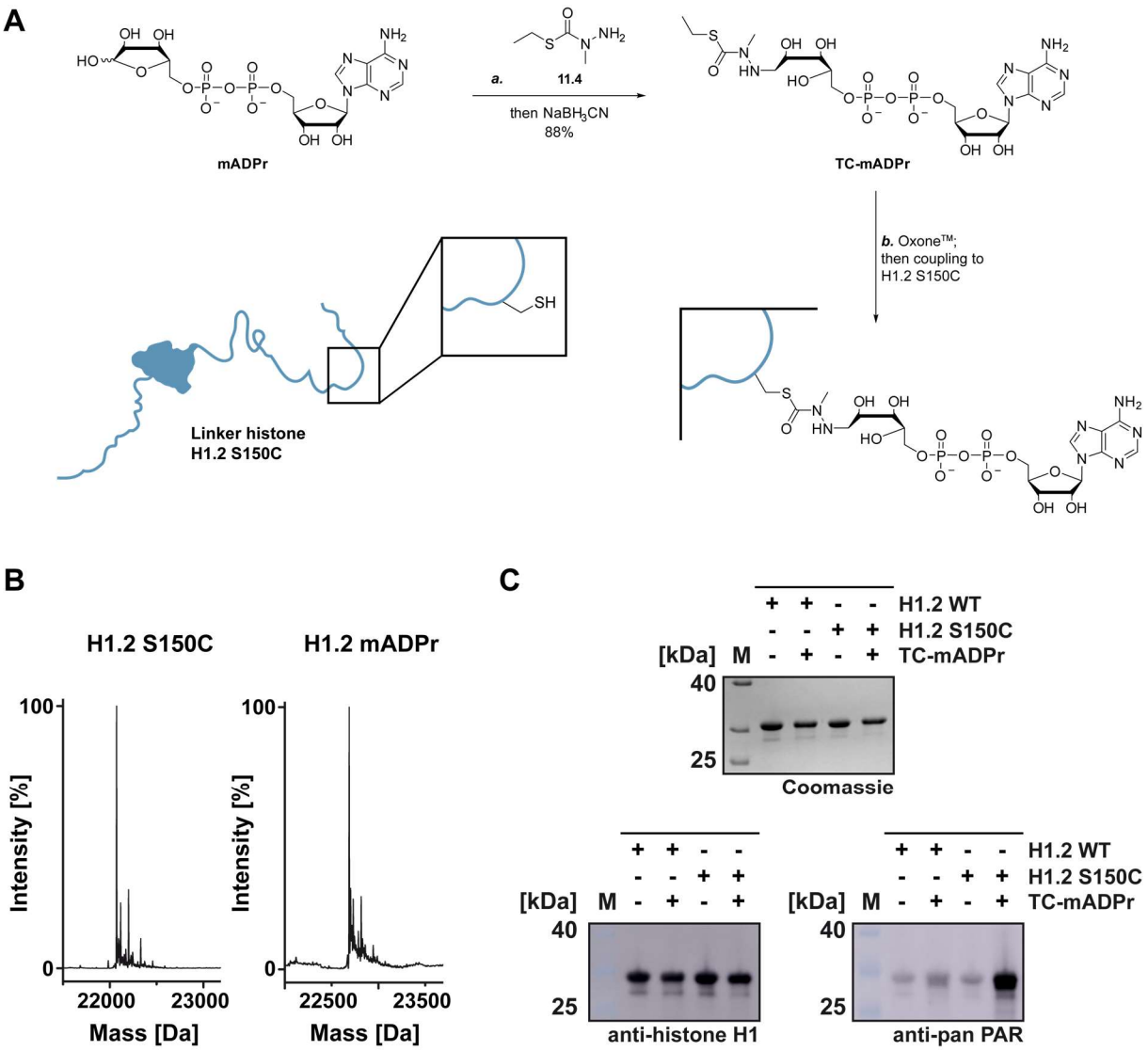

Figure 10. Synthesis of thiocarbamate linker modified mono ADP-ribose (TC-mADPr) and coupling to linker histone H1.2 S150C. A. Synthesis of thiocarbamate linker (11.4) with mono ADP ribose (mADPr). ***a.*** *S*-Ethyl α-methylhydrazide thiocarbamate (11.4), Milli-Q water, DMSO, AcOH, three freeze-thaw cycles (-20 °C), then $NaCNBH_3$, 4 °C, 18 h (88%). ***b.*** TC-mADPr was oxidized with Oxone™ (10 mM in Milli-Q water, Merck) and coupled to linker histone H1.2 S150C (4 °C, 16 h). **B.** Deconvoluted LC-MS analysis of full-length proteins. H1.2 S150C calculated 22072 Da, measured 22072 Da; H1.2 mADPr calculated 22687 Da, measured 22687 Da. **C.** SDS-PAGE gel with Coomassie blue staining and Western Blot analysis (anti-histone H1 and anti-pan-PAR binding reagent) of H1.2 WT, H1.2 WT and TC-mADPr, H1.2 S150C, H1.2 S150C and TC-mADPr. For detailed reagents and conditions, see **sections 5.1.2.3** and **5.2.2.7**.

The LC-MS analysis of the cysteine-containing linker histone variant H1.2 S150C resulted in a peak with a deconvoluted mass of 22072 Da (**Figure 10B**, left). After reaction of H1.2 S150C with TC-mADPr, LC-MS analysis revealed a peak with a deconvoluted mass of 22687 Da. The analyzed mass difference corresponds to a peak shift of 615 Da, which is consistent with the

expected mass increase resulting from the covalent linker histone modification (**Figure 11A**, 616 Da); note that 1 Da must be subtracted from the shown mass for the thiol proton of the cysteine, resulting in a net increase of 615 Da. The precise mass difference observed here for the deconvoluted masses of H1.2 S150C and H1.2 mADPr confirms the successful and covalent site-selective mADP-ribosylation, thus demonstrating the first method for the mADP-ribosylation of the recombinantly expressed linker histone. In addition to these results confirming the successful mADP-ribosylation of H1.2 S150C, the cysteine selectivity of the linker histone mADP-ribosylation was investigated by reacting TC-mADPr with both H1.2 WT and H1.2 S150C variants. Only the cysteine containing variant, H1.2 S150C, was expected to be modified, whereas H1.2 WT should remain unmodified upon reaction with TC-mADPr. After activation of TC-mADPr by oxidation to its corresponding sulfone, the linker histone variants H1.2 WT and H1.2 S150C were incubated with the activated TC-mADPr. Subsequent analysis of these protein modification reactions was performed by SDS-PAGE with Coomassie blue staining and WB using anti-histone H1 antibody and anti-pan PAR binding reagent (**Figure 10C**). The evaluation of the SDS-PAGE gel revealed bands of comparable intensity in all samples (**Figure 10C**, top), including H1.2 WT, H1.2 WT incubated with the activated TC-mADPr, H1.2 S150C and H1.2 S150C incubated with the activated TC-mADPr (from left to right). Moreover, the sample containing H1.2 S150C incubated with TC-mADPr showed a slight band shift to higher molecular weights compared to the unmodified H1.2 S150C sample. This altered migration behavior is caused by the covalent attachment of mADPr to the protein, having a different anionic nature and increased mass of the protein-mADPr conjugate. WB analysis using the anti-histone H1 antibody revealed signals of comparable intensity in all samples (**Figure 10C**, lower left). The uniform signal intensity observed confirms the stability of the linker histone under the conditions of the mADP-ribosylation reaction with TC-mADPr. To further verify the incorporation of mADPr into the linker histone H1.2 S150C and to exclude non-specific modifications at nucleophilic amino acid side chains, WB analysis was performed using the anti-pan PAR binding reagent (**Figure 10C**, lower right). In contrast to the WB results obtained with the anti-histone H1 antibody, WB evaluation using the anti-pan PAR binding reagent revealed a signal only for the reaction of H1.2 S150C with the activated TC-mADPr, confirming the successful mADP-ribosylation in the presence of a cysteine residue. The absence of a WB signal for the modification reaction involving H1.2 WT and TC-mADPr demonstrates that non-specific side reactions at nucleophilic amino acid side chains such as lysines can be excluded. These results, especially the presence of a WB signal for the reaction with H1.2 S150C and the absence of a signal for the reaction with H1.2 WT, validate the

cysteine-selective mADP-ribosylation of the linker histone H1.2 S150C using this thiocarbamate linker approach.

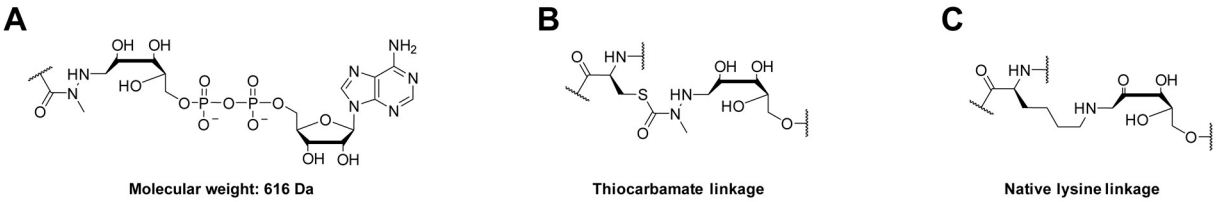

Figure 11. Molecular weight of the attached modification and the types of linkages for ADP-ribose. A. Chemical structure and molecular weight of the attached mADPr by TC-mADPr. **B.** Linkage of cysteine and the thiocarbamate modified mADPr. **C.** Natural linkage between lysine and mADPr in its ketamine form.

A crucial characteristic of linkers in ligation reactions, such as the thiocarbamate linker used in the protein modification reactions, is their similarity to native bonds, including both the attachment of the modifier and the length of the linker. The attachment of mADPr to a cysteine residue through the thiocarbamate ligation method is shown in **Figure 11B**. The ring-opened configuration resulting from the introduction of the thiocarbamate into the mADPr closely mirrors a natural mADP-ribosylation linkage to a lysine in its ketamine form (**Figure 11C**).[138] Notably, apart from this open ribose form, the number of atoms between the ribose and the peptide backbone remains constant, mimicking a native linkage. Compared to the commonly used maleimide method for a cysteine modification, which often relies on the use of extended linkers, the developed and established thiocarbamate linker approach avoids this drawback and makes this modification approach suitable for ADP-ribosylation studies.

In this section, a method for the cysteine-selective mADP-ribosylation of the linker histone variant H1.2 S150C was successfully described. The reaction of *S*-Ethyl α-methylhydrazide thiocarbamate (11.4) with mADPr afforded TC-mADPr in good yields (**Figure 10A**). Subsequent oxidation with Oxone™ allowed for a protein modification reaction. The successful incorporation and cysteine selectivity of the applied method was demonstrated by reactions of TC-mADPr with both H1.2 WT and H1.2 S150C. Validation of the introduced PTM was achieved by WB using the anti-pan PAR binding reagent and full-length protein LC-MS measurements (**Figure 10B** and **C**). The utilization of the described thiocarbamate linker approach for the mADP-ribosylation of the linker histone H1.2 S150C represents the first described method for a site-selective introduction of this PTM into the recombinant protein.

3.3 Synthesis of ADP-ribose dimer

In vivo ADP-ribosylation results not only in the covalent attachment of mADPr to the target protein, but also through the attachment of its polymeric form, pADPr. While mADP-ribosylation is more abundant in cells than pADP-ribosylation, the effect of the ADP-ribose chain length must not be ignored.[113] To investigate the impact of pADP-ribosylated proteins, several synthetic routes for short ADP-ribose oligomers have been developed.[9-11,149] Nonetheless, the utilization of these compounds in ADP-ribosylation studies of target proteins has not been realized yet. One reason for the limited use of these compounds is besides the complicated synthetic procedures, their inherent instability due to the presence of a free reducing end on the ribose moiety. Generally, the synthesis of suitable ADP-ribose oligomers requires handling of an unprotected anomeric center that is susceptible to degradation reactions. Previous works by Kistenmaker *et. al.* and Liu *et. al.* used methoxyacetals at the reducing end of the ribose to prevent degradation and increase the stability of the formed oligomers (**Scheme 9**).[9,11] However, these compounds are hindered at the binding site of a potential linker, making them unsuitable for protein modification studies. Lambrecht *et. al.* presented a method for synthesizing an ADP-ribose dimer (diADPr) with a free reducing end at the ribose, although this compound has not been evaluated for protein modification reactions beyond its initial synthesis.[10] In an effort to selectively modify a target protein for ADP-ribosylation with an ADP-ribose oligomer, an optimized synthesis route for the ADP-ribose dimer was developed and presented in the following. The application of the cysteine-selective thiocarbamate linker for the mADP-ribosylation of the linker histone in combination with an ADP-ribose dimer with free reducing end should allow the introduction of this ADP-ribose dimer to the linker histone. The design of the synthetic route was adapted by established procedures documented in the literature.[7,9,10,12,14]

3.3.1 Synthesis of 2'-*O*-α-ribosyl-adenosine building block

The synthesis of the desired ADP-ribose dimer requires the incorporation of several chemical functionalities that pose significant synthetic challenges. First, a 2'-*O*-α-glycosidic linkage between the adenosine and the ribose is fundamental. Second, the introduction of two pyrophosphate bonds is inevitable to yield the desired ADP-ribose dimer. For a streamlined approach, it is critical to determine which of these reactions is more challenging and requires harsher reaction conditions. Consequently, the synthetic approach was started with the introduction of the 2'-*O*-α-glycosidic linkage and the preparation of a bis-phosphorylated 2'-*O*-α-ribosyl-adenosine building block that could be used to form the pyrophosphate bonds with the respective ribose and adenosine termini. The synthesis route for the bis-

phosphorylated 2'-*O*-α-ribosyl-adenosine building block is illustrated in **Scheme 13**. The stereoselective glycosylation to generate the 2'-*O*-α-glycosidic linkage was performed via a tin tetrachloride catalyzed reaction involving N^6-benzoyl-3',5'-*O*-(tetra-*iso*-proylsiloxane-1,3-diyl)-adenosine (13.2) as glycosylation acceptor and 1,2-di-*O*-acetyl-3,5-di-*O*-benzoyl-D-arabinofuranose (13.1) as glycosylation donor.[12,186] The neighboring group participation of the 2-*O*-acetyl group in the arabinofuranose determined the stereochemical outcome of this reaction and provided the desired 2'-*O*-α configuration in the product. Due to the essential involvement and stereochemical control provided by the neighboring group, the outcome of this reaction was the 2'-*O*-α-arabinosyl-adenosine disaccharide (13.3).

In order to obtain the desired 2'-*O*-α-ribosyl-adenosine stereochemistry in the target compound, the inversion at the 2''-hydroxyl group was mandatory. This stereochemical inversion was successfully accomplished by an oxidation-reduction mechanism adapted from procedures by Mikhailov *et. al*.[12] and Zheng *et. al*.[14] The synthetic adaptation developed by Zheng *et. al.* by using 1,2-di-*O*-acetyl-3,5-di-*O*-benzoyl-D-arabinofuranose as the glycosylation donor allowed stereoselective deprotection of the 2'' hydroxyl group, which is essential for the stereochemical inversion, without requiring a global deprotection of the 2'-*O*-α-arabinosyl-adenosine moiety.[14] Hence, stereoselective hydrolysis of the 2''-*O*-acetyl protecting group using 5 mM K_2CO_3 in methanol allowed the application of the oxidation-reduction strategy. Oxidation of the free hydroxyl group to the ketone was performed under Albright-Goldman oxidation conditions.[187] Subsequent reduction of the resulting ketone with $NaBH_4$ afforded the desired 2'-*O*-α-ribosyl-adenosine moiety (13.4) in 44% yield over three synthesis steps. The approach outlined by Mikhailov *et. al.* used 1-*O*-acetyl-2,3,5-tri-*O*-benzoyl arabinofuranose as the glycosylation donor and required a global deprotection to perform the inversion of the stereochemistry at the 2''-hydroxyl group since a selective deprotection was not achievable.[12] In contrast to that, the protective group strategy employed in this synthesis allowed selective deprotection of the 2''-hydroxyl group while preserving all other protective groups and thus, allowing more selective syntheses for other purposes.[12]

The bridging tetra-*iso*-propyldisiloxan-1,3-diyl protecting group, known as the Markiewicz protecting group, was quantitatively cleaved using triethylamine trihydrofluoride as a fluorine donor, resulting in the formation of disaccharide 13.5.[188] Given the asymmetric structure of the ADP-ribose dimer, the introduction of orthogonally protected phosphates into the bis-phosphorylated 2'-*O*-α-ribosyl-adenosine building block was vital. The need to introduce orthogonality in subsequent syntheses required the introduction of a selective protecting group for the 5'-hydroxyl group. Therefore, a transient dimethoxytrityl (DMTr) protection was attached to the 5'-hydroxyl group, making it susceptible to acid-induced

cleavage. Selective hydrolysis of the 3''-*O*-benzoyl group was achieved by reaction with 50 mM K_2CO_3 in methanol, resulting in the formation of disaccharide triol 13.6 in 49% yield over three synthesis steps. The unprotected secondary hydroxyl groups were then silylated using *tert*-butyldimethylsilyl trifluoromethanesulfonate (TBDMSOTf) and di-*iso*-propyl ethylamine (DIPEA) as base.

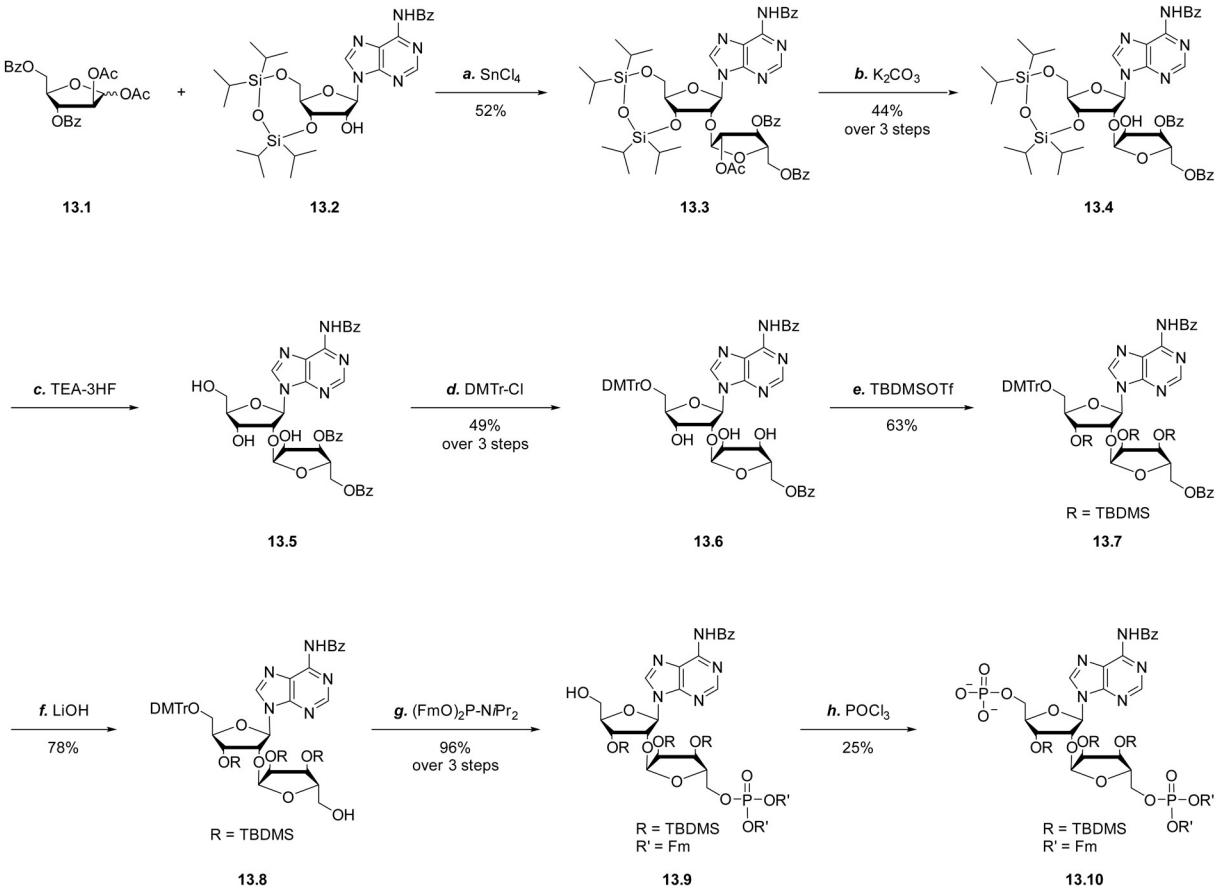

Scheme 13. Synthesis of bis-phosphorylated 2'-*O*-α-ribosyl-adenosine building block (13.10). ***a.*** $SnCl_4$, DCE, 4 °C, 48 h (52%). ***b.*** K_2CO_3, MeOH, 0 °C, 3 h; then Ac_2O, DMSO, r.t., 22 h; then $NaBH_4$, 0 °C, 2 h (44% over 3 steps). ***c.*** TEA-3HF, THF, 0 °C, 2 h. ***d.*** DMTr-Cl, pyridine, r.t., 18 h; then K_2CO_3, MeOH, 0 °C, 3 h (49% over 3 steps). ***e.*** TBDMSOTf, DIPEA, DMF, r.t., 16 h (63%). ***f.*** LiOH, EtOH, THF, r.t., 3 h (78%), ***g.*** $(FmO)_2$ P-N*i*Pr_2, tetrazole, DMF, r.t., 2 h; then tBuOOH, r.t., 0.5 h; then TFA, DCM, r.t., 2 h (96% over 3 steps). ***h.*** $POCl_3$, MeCN, pyridine, 0 °C, 3 h (25%). For detailed reagents and conditions, see **section 5.1.2.4.**

The protective group strategy employed here was adapted from the reported method described by Kistemaker *et. al*.[9] Changing the secondary hydroxyl protecting groups in the 2'-*O*-α-ribosyl-adenosine 13.7 from acetyl to TBDMS, as elucidated by Kistemaker *et. al.*, resulted in the formation of a less polar compound with the intention to simplify the purification in subsequent syntheses.[9] Following the basic saponification of the 5''-*O*-benzoyl protecting group catalyzed by lithium hydroxide, the disaccharide 13.8 was obtained in 78% yield, enabling the introduction of the first protected phosphate. Adopting a protective group strategy similar to that described by Kistemaker *et. al.*, orthogonality was efficiently

introduced at the ends of the molecule.[9] This synthetic step is crucial for the stepwise synthesis of the ADP-ribose dimer which is characterized by its distinct terminal moieties: the ribose and the adenosine. The stepwise synthesis of the desired ADP-ribose dimer required the incorporation of two phosphates with orthogonal protecting groups. Therefore, the first protected phosphate at the 5''-hydroxyl group was adapted from a reaction described by Liu *et. al*.[11,189] The initial introduction of the phosphate included the reaction with di-fluorenylmethyl-*N,N*-di-*iso*-propyl phosphoramidite ($(FmO)_2P\text{-}NiPr_2$) and tetrazole. Subsequent oxidation with tBuOOH afforded the fluorenylmethyl (Fm)-protected mono-phosphorylated disaccharide. The use of a Fm-protected phosphate in this synthesis step allowed acidic detritylation while preserving the phosphate protecting groups and the remaining hydroxyl protecting groups, resulting in the formation of the mono-phosphorylated disaccharide 13.9 in 96% yield over three synthesis steps. Phosphoryl chloride was used as phosphorylation reagent to introduce the second monophosphate at the 5'-hydroxyl group, avoiding a synthesis for deprotection to obtain the unprotected 5'-monophosphate used in the pyrophosphate bond formation. The bis-phosphorylated 2'-*O*-α-ribosyl-adenosine building block 13.10 was obtained in 25% yield. In contrast to the synthesis of a bis-phosphorylated 2'-*O*-α-ribosyl-adenosine moiety for the ADP-ribose dimer assembly reported by Dr. Martin Mex in his PhD thesis, which used a phosphordithioate and a tert-butyl protected phosphate, this approach offers the advantage of introducing an unprotected phosphate.[7] This modification makes the bis-phosphorylated 2'-*O*-α-ribosyl-adenosine building block (13.10) directly applicable to pyrophosphate coupling reactions, thereby streamlining the synthesis process.

3.3.2 Synthesis of terminal ribose-*H*-phosphonate

Diphosphate coupling reactions require the activation of one participating phosphate serving as electrophile. This is typically accomplished by the generation of phosphorimidazolides. Such intermediates own increased stability, improved reaction kinetics and lead to increased yields. A frequently employed method for producing phosphorimidazolides involves the reaction of a terminal phosphate with *N,N*-carbonyldiimidazole.[190] For the synthesis of the ADP-ribose dimer, starting from the bis-phosphorylated 2'-*O*-α-ribosyl-adenosine building block 13.10, the next synthesis step involved the synthesis of the two terminal moieties designed for the pyrophosphate bond formation. In the case of the unprotected 5'-monophosphate, directly applicable in a pyrophosphate coupling reaction, the initially introduced moiety is a ribose monophosphate. However, for the synthesis of the ADP-ribose dimer, a procedure for activating the phosphorus compound to the phosphorimidazolide derived from a ribose-*H*-phosphonate was adapted.[191]

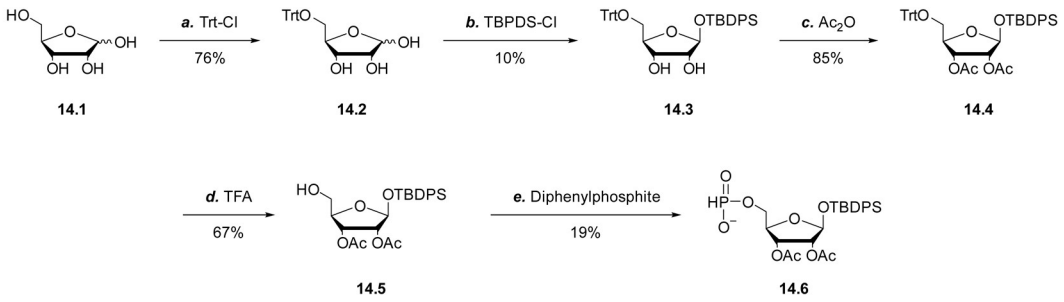

Scheme 14. Synthesis of 1-*O*-TBDPS-2,3-di-*O*-acetyl-5-*O*-*H*-phosphonate-β-D-ribose. ***a.*** Trt-Cl, pyridine, r.t., 18 h (76%). ***b.*** TBDPS-Cl, imidazole, DMF, r.t., 5 h (10%). ***c.*** Ac_2O, pyridine, r.t., 6 h (85%). ***d.*** TFA, triethylsilane, DCM, 0 °C, 3 h (67%). ***e.*** Diphenylphosphite, pyridine, 0 °C, 4 h (19%). For detailed reagents and conditions, see **section 5.1.2.5**.

The synthesis of the ribose-*H*-phosphonate using a suitable protecting group strategy is outlined in **Scheme 14**. The synthesis was started with D-ribose (14.1), which was 5-*O*-tritylated using trityl chloride (TrtCl). The choice of the protective group for the 1-hydroxyl group in this molecule was crucial to ensure the stability of the resulting ADP-ribose dimer, as its removal constitutes the final step in the synthesis pathway. Therefore, *tert*-butyldiphenylsilyl (TBDPS) was selected as protecting group due to its ability to be simultaneously deprotected with the protective groups on the secondary hydroxyl groups of the 2'-*O*-α-ribosyl-adenosine building block (13.10). The introduction of this protecting group was performed by reaction with *tert*-butyldimethylsilyl chloride (TBDPSCl) in the presence of imidazole. Implementation of a limited amount of TBDPSCl and conducting the reaction at low temperatures (0 °C) enabled a selective incorporation at the anomeric center of the D-ribose. Subsequent purification involved flash column chromatography to efficiently remove side products such as the 2-*O*- or 3-*O*-silylated D-ribose yielding the desired 1-*O*-TBDPS-5-*O*-Trt-β-D-ribose (14.3). Following the acetylation of the 2- and 3-hydroxyl groups with acetic anhydride and subsequent acidic detritylation, 1-*O*-TBDPS-2,3-di-*O*-acetyl-β-D-ribose (14.5) was obtained. The chosen protecting group strategy allowed for a controlled deprotection of the ADP-ribose dimer in which the acetyl deprotection is performed in conjunction with the removal of the N^6-benzoyl groups from the 2'-*O*-α-ribosyl-adenosine moiety (13.10) and the TBDPS group was cleaved simultaneously with the remaining silyl protecting groups.[10] The incorporation of the *H*-phosphonate functionality was realized by reaction of 14.5 with diphenylphosphite in pyridine. Subsequent hydrolysis in the presence of triethylamine yielded 1-*O*-TBDPS-2,3-di-*O*-acetyl-5-*O*-*H*-phosphonate-β-D-ribose (14.6) in 19% yield.[192]

3.3.3 Synthesis of terminal adenosine-*H*-phosphonate

Following the synthesis of the ribose-*H*-phosphonate moiety (14.6) required for the synthesis of the ADP-ribose dimer, the complementary adenosine-*H*-phosphonate derived from N^6-

benzoyladenosine was synthesized as depicted in **Scheme 15**. The synthesis of the adenosine-*H*-phosphonate was started with the tritylation of the 5'-hydroxyl group of N^6-benzoyl adenosine (15.1) utilizing DMTrCl. Subsequent acetylation of the secondary hydroxyl groups was achieved by reaction with acetic anhydride, resulting in the formation of N^6-benzoyl-2',3'-di-*O*-acetyl-5'-*O*-DMTr-adenosine (15.3) with a yield of 65%.

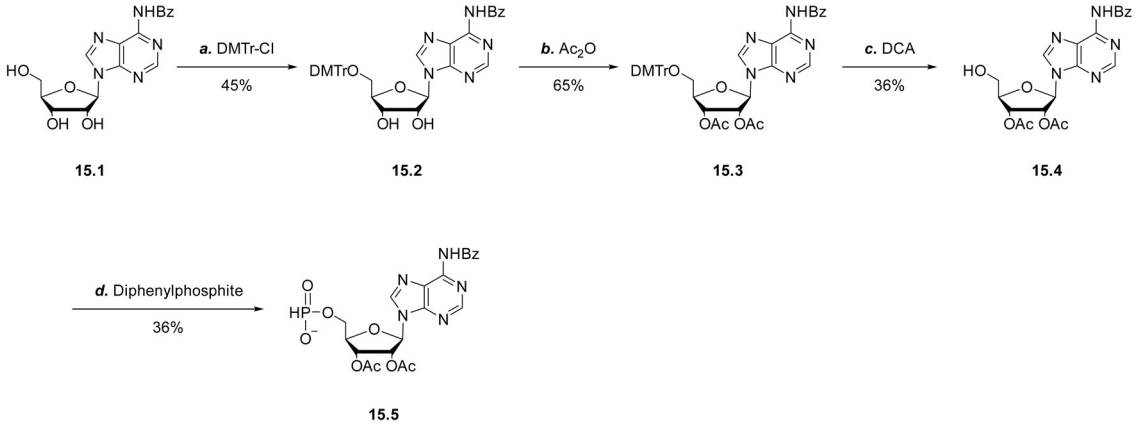

Scheme 15. Synthesis of N^6-benzoyl-2',3'-di-*O*-acetyl-5'-*O*-*H*-phosphonate-adenosine. ***a.*** DMTr-Cl, pyridine, r.t., 18 h (45%). ***b.*** Ac_2O, pyridine, r.t., 16 h (65%). ***c.*** DCA, DCM, r.t., 2 h (36%). ***d.*** Diphenylphosphite, pyridine, 0 °C, 0.5 h (36%). For detailed reagents and conditions, see **section 5.1.2.6**.

Acidic deprotection of the 5'-DMTr group employing dichloroacetic acid (DCA) afforded N^6-benzoyl-2',3'-di-*O*-acetyl-adenosine (15.4) in 36% yield. This compound served as the basis for the introduction of the *H*-phosphonate necessary for activation to the corresponding phosphorimidazolide and the pyrophosphate coupling reaction. The incorporation of the *H*-phosphonate moiety was achieved by reacting 15.4 with diphenylphosphite followed by hydrolysis, yielding N^6-benzoyl-2',3'-di-*O*-acetyl-5'-*O*-*H*-phosphonate-adenosine (15.5) in 36% yield.[192]

3.3.4 Synthesis of ADP-ribose dimer

After the successful synthesis of the 2'-*O*-α-ribosyl-adenosine building block (13.10) and the *H*-phosphonates for both termini (1-*O*-TBDPS-2,3-di-*O*-acetyl-5-*O*-*H*-phosphonate-β-D-ribose (14.6) and N^6-benzoyl-2',3'-di-*O*-acetyl-5'-*O*-*H*-phosphonate-adenosine (15.5)) the diphosphate coupling reactions were carried out to obtain the ADP-ribose dimer. The sequential assembly of the ADP-ribose dimer began with the reaction of the ribose-*H*-phosphonate 14.6 and the bis-phosphorylated 2'-*O*-α-ribosyl-adenosine building block (13.10). However, to find optimal conditions, activation studies were first performed with the respective phosphorimidazolide. The activation of compound 14.6 was accomplished by an Atherton-Todd type reaction with carbon tetrachloride and triethylamine to give the corresponding chlorophosphate intermediate.[193] Subsequently, this intermediate was

directly converted to 1-*O*-TBDPS-2,3-di-*O*-acetyl-5-*O*-phosphorimidazolide-β-D-ribose by reaction with trimethylsilyl-imidazole (TMS-Im) (**Figure 12A**).[191]

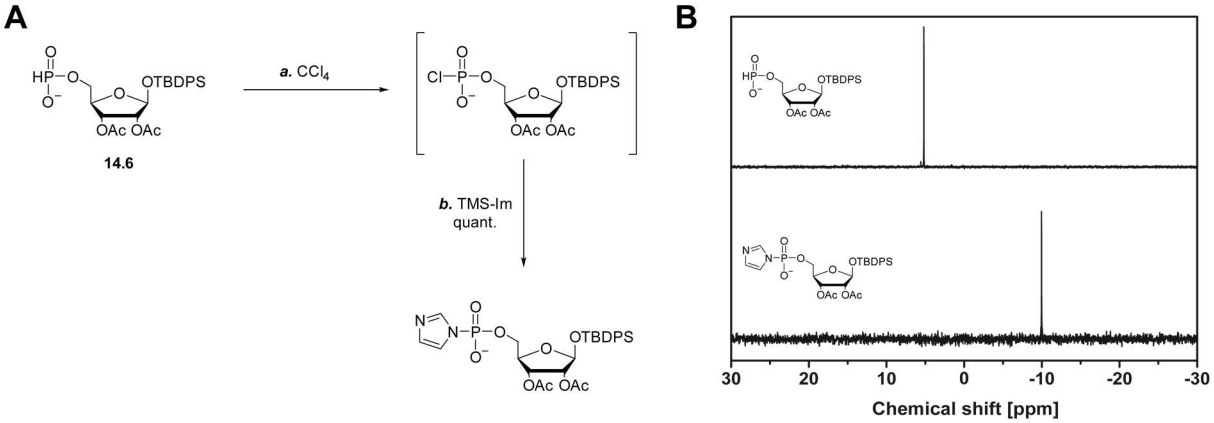

Figure 12. Synthesis and analysis of 1-*O*-TBDPS-2,3-di-*O*-acetyl-5-*O*-phosphorimidazolide-β-D-ribose. A. Synthesis of 1-*O*-TBDPS-2,3-di-*O*-acetyl-5-*O*-phosphorimidazolide-β-D-ribose. ***a.*** CCl_4, TEA, MeCN, r.t. 4 h. ***b.*** TMS-Im, r.t., 4 h (quant.). Reactions take place simultaneously. For detailed reagents and conditions, see **section 5.1.2.7**. **B.** ^{31}P-NMR analysis of H-phosphonate activation. Top: ^{31}P-NMR spectra of 1-*O*-TBDPS-2-di-*O*-acetyl-5-*O*-*H*-phosphonate-β-D-ribose. Bottom: ^{31}P-NMR reaction monitoring of the synthesis of 1-*O*-TBDPS-2,3-di-*O*-acetyl-5-*O*-phosphorimidazolide-β-D-ribose.

The reaction course of the synthesis of 1-*O*-TBDPS-2,3-di-*O*-acetyl-5-*O*-phosphorimidazolide-β-D-ribose was monitored by ^{31}P-NMR analysis (**Figure 12B**). The spectrum of the *H*-phosphonate 14.6 showed a peak with a chemical shift of 5.19 ppm (**Figure 12B**, top panel). Following the activation for 4 hours at room temperature, only a signal at –9.96 ppm was visible (**Figure 12B**, lower panel), corresponding to the 1-*O*-TBDPS-2,3-di-*O*-acetyl-5-*O*-phosphorimidazolide-β-D-ribose. This activated phosphate was subsequently subjected to a reaction with the bis-phosphorylated 2'-*O*-α-ribosyl-adenosine building block (13.10) to enable the formation of the initial pyrophosphate bond (**Figure 13A**). The pyrophosphate coupling reaction was carried out in *N,N*-dimethylformamide (DMF) over a period of 3 days at room temperature. The reaction progress of the pyrophosphate coupling reaction was monitored by ^{31}P-NMR spectroscopy (**Figure 13B**). To terminate the reaction prior to NMR analysis, samples were treated with 0.5 M triethylammonium bicarbonate buffer (TEAB). The spectrum of the 1-*O*-TBDPS-2,3-di-*O*-acetyl-5-*O*-phosphorimidazolide-β-D-ribose showed a single peak at –9.96 ppm (**Figure 13B**, top panel). The second starting material, the bis-phosphorylated 2'-*O*-α-ribosyl-adenosine building block 13.10, showed peaks at –0.01 ppm for the phosphate and –0.67 ppm for the Fm-protected phosphate (**Figure 13B**, middle panel).

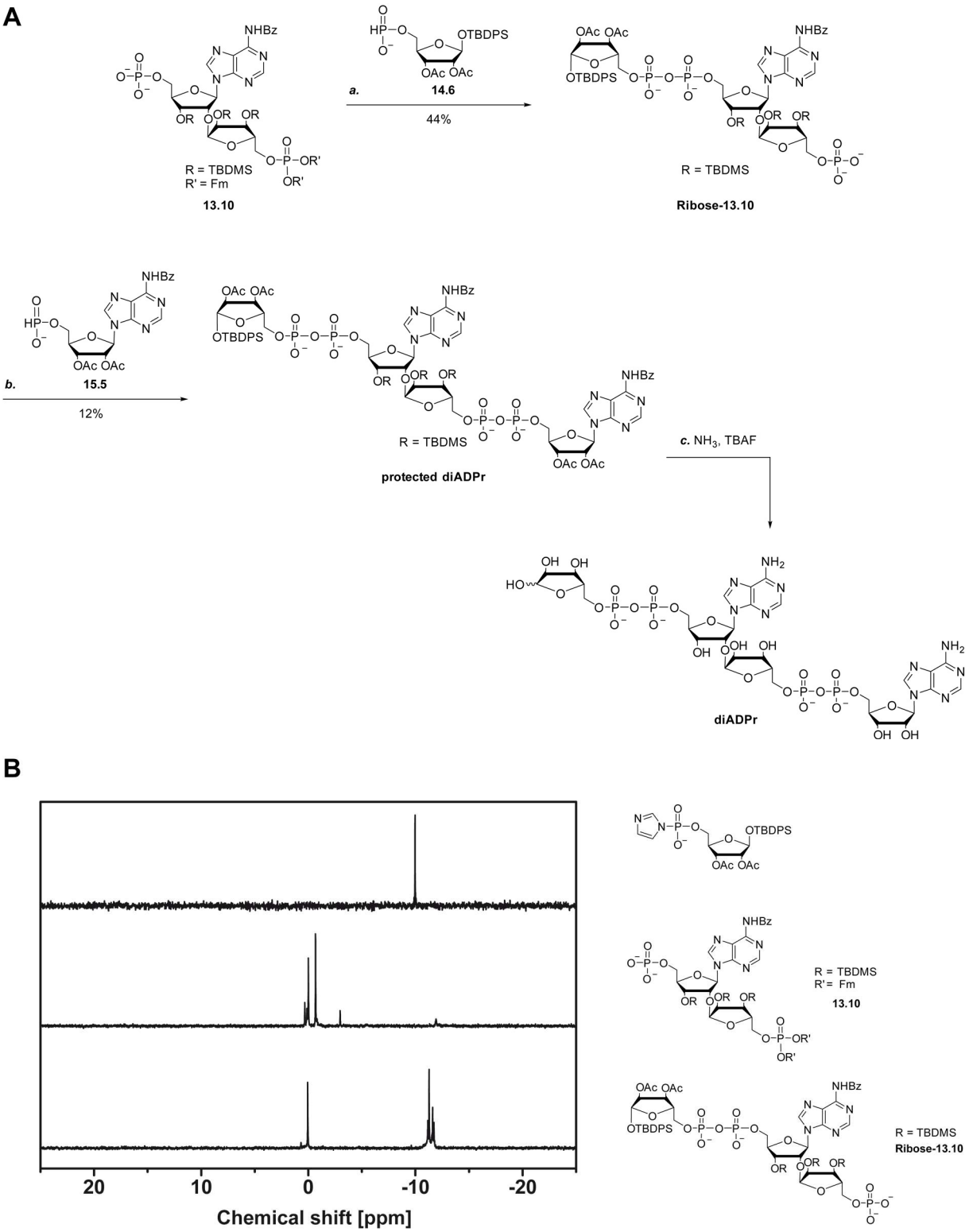

Figure 13. Pyrophosphate coupling reactions and deprotection to yield diADPr. A. ***a.*** 1-*O*-TBDPS-2,3-di-*O*-acetyl-5-*O*-*H*-phosphonate 14.6, TMS-imidazole, TEA, MeCN, CCl_4, r.t., 4 h; then DMF, r.t., 72 h (44%). ***b.*** N^6-benzoyl-2',3'-di-*O*-acetyl-5'-*O*-*H*-phosphonate-adenosine 15.5, TMS-imidazole, TEA, MeCN, CCl_4, r.t., 4 h; then DMF, r.t., 120 h (12%). ***c.*** NH_3 in MeOH, r.t., 18 h; then TBAF, THF, r.t., 3 h. For detailed reagents and conditions; see **section 5.1.2.7**. **B.** ^{31}P-NMR analysis of diphosphate coupling reaction. Top: ^{31}P-NMR spectrum of 1-*O*-TBDPS-2,3-di-*O*-acetyl-5-*O*-phosphorimidazolide-β-D-ribose. Middle: ^{31}P-NMR spectrum of bis-phosphorylated 2'-*O*-α-ribosyl-adenosine building block (13.10). Bottom: ^{31}P-NMR reaction monitoring of the synthesis of (1'-*O*-TBDPS-2',3'-di-*O*-acetyl-β-D-ribose)-N^6-benzoyl-[3''-*O*-TBDMS-2''-*O*-α-D-(2''',3'''-di-*O*-TBDMS-5'''-*O*-phosphate-ribofuranosyl]-adenosine (16.1) after 3 days.

The ^{31}P-NMR spectrum of the diphosphate coupling reaction after 3 days revealed two distinct types of peaks: a singlet at 0.05 ppm, indicative of a monophosphate, and a doublet of a doublet at −11.5 ppm corresponding to the formed pyrophosphate linkage (**Figure 13B**, lower panel). The chemical shift in the ^{31}P-NMR as well as the MS and ^{1}H-NMR measurements confirmed that the addition of 0.5 M TEAB buffer not only stopped the reaction but also led to the cleavage of the Fm phosphate protecting groups. This chemical reaction, started by the formation of the initial pyrophosphate bond followed by the subsequent cleavage of the Fm protecting groups, resulted in the formation of the compound ribose-13.10 (**Figure 13A**). In particular, the *in situ* removal of the Fm protecting groups offered a notable advantage over existing procedures by eliminating the need of a prior deprotection step before the second pyrophosphate coupling reaction, saving time and effort. The incorporation of the second pyrophosphate bond involved the reaction of ribose-13.10 with *N*^{6}-benzoyl-2',3'-di-*O*-acetyl-5'-*O*-*H*-phosphonate-adenosine (15.5). The adenosine-*H*-phosphonate was pre-activated prior to the pyrophosphate coupling by reaction with TMS-imidazole and triethylamine, resulting in the formation of the corresponding phosphorimidazolide via a reaction similar to the ribose activation. Notably, the incorporation of a second pyrophosphate bond within the same molecule is challenging due to repulsive effects, therefore requiring extended reaction times. Thus, the second pyrophosphate coupling reaction was performed in DMF over a period of 5 days at room temperature. This reaction yielded the protected ADP-ribose dimer (protected diADPr) in 12% yield. Global deprotection of the protected diADPr was achieved by a sequential process of treatment with methanolic ammonia and tetrabutylammonium fluoride (TBAF).[10] The precise sequence of the described treatments was essential to release the reducing end in the final synthesis step by cleaving the TBDPS protecting group. The ammonia treatment efficiently removed the *N*^{6}-benzoyl and *O*-acetyl protecting groups, while the TBAF reaction selectively removed *O*-TBDMS and the *O*-TBDPS protecting groups from the secondary hydroxyl groups and from the ribose at its reducing end, respectively. After HPLC purification, the fully deprotected ADP-ribose dimer (diADPr, **Figure 13A**) was obtained.

Here, an optimized synthetic pathway for the preparation of the ADP-ribose dimer (diADPr) with a free reducing end, differing form the procedure previously reported by Lambrecht *et. al.*[10], was presented. The glycosylation reaction was performed by the reaction of 1,2-di-*O*-acetyl-3,5-di-*O*-benzoyl-D-arabinofuranose (13.1) and *N*^{6}-benzoyl-3',5'-*O*-(tetra-*iso*-proylsiloxane-1,3-diyl)-adenosine (13.2), directed by the neighboring group participation of the 2-*O*-acetyl group, resulting in the formation of the 2'-*O*-α-glycosylated product.[12,186] Stereochemical inversion of the 2''-hydroxyl group by selective deprotection, oxidation and

reduction yielded the desired 2'-*O*-α-ribosyl-adenosine disaccharide (13.4). Strategic manipulation of the protecting groups introduced orthogonality at the termini, allowing the incorporation of orthogonally protected phosphates at the ends of the molecule to yield the bis-phosphorylated 2'-*O*-α-ribosyl-adenosine building block 13.10 (**Scheme 13**). By synthesizing both terminal groups, the 1-*O*-TBDPS-2,3-di-*O*-acetyl-5-*O*-*H*-phosphonate-β-D-ribose (14.6, **Scheme 14**) and N^6-benzoyl-2',3'-di-*O*-acetyl-5'-*O*-*H*-phosphonate-adenosine (15.5, **Scheme 15**), sequential pyrophosphate coupling reactions were performed after activation of the respective *H*-phosphonate, resulting in the formation of the protected diADPr (**Figure 13**).[191] Subsequent global cleavage of all protecting groups by sequential treatment with ammonia and TBAF yielded the unprotected ADP-ribose dimer (diADPr) with a free reducing end, making it suitable for the use in protein modification reactions with an appropriate method.

3.4 Di ADP-ribosylation of the linker histone H1.2

In addition to the formation of mono ADP-ribosylated proteins, certain ADP-ribosylating enzymes, such as ARTD1 and ARTD2, have the ability to catalyze the addition of multiple ADP-ribose units to the mADP-ribosylated substrate.[194] Moreover, specific reader enzymes have been identified that selectively recognize pADP-ribosylated proteins, such as the chromatin remodeling enzyme ALC1, which is known to bind exclusively to pADP-ribosylated proteins containing at least three ADP-ribose repeating units.[11,195] The alternative synthetic pathway for the generation of the ADP-ribose dimer with a free reducing end described in **section 3.3**, represents a promising approach for the production of ADP-ribosylated protein with the ADP-ribose dimer.

3.4.1 Synthesis of thiocarbamate linker modified ADP-ribose dimer

In combination with the method described in **section 3.2** for the preparation of the mADP-ribosylated linker histone H1.2 mADPr, the formation of a diADP-ribosylated linker histone H1.2 diADPr becomes achievable. Furthermore, the use of the cysteine selectivity of the thiocarbamate linker (11.4) ensures that non-specific modifications are avoided. The incorporation of the shortest ADP-ribose oligomers, the diADPr, into the PTM landscape of the linker histone would significantly improve the understanding of its effects on cellular processes. Following the reaction of the thiocarbamate linker (11.4) with the diADPr, the successful modification of the linker histone H1.2 S150C was evaluated.

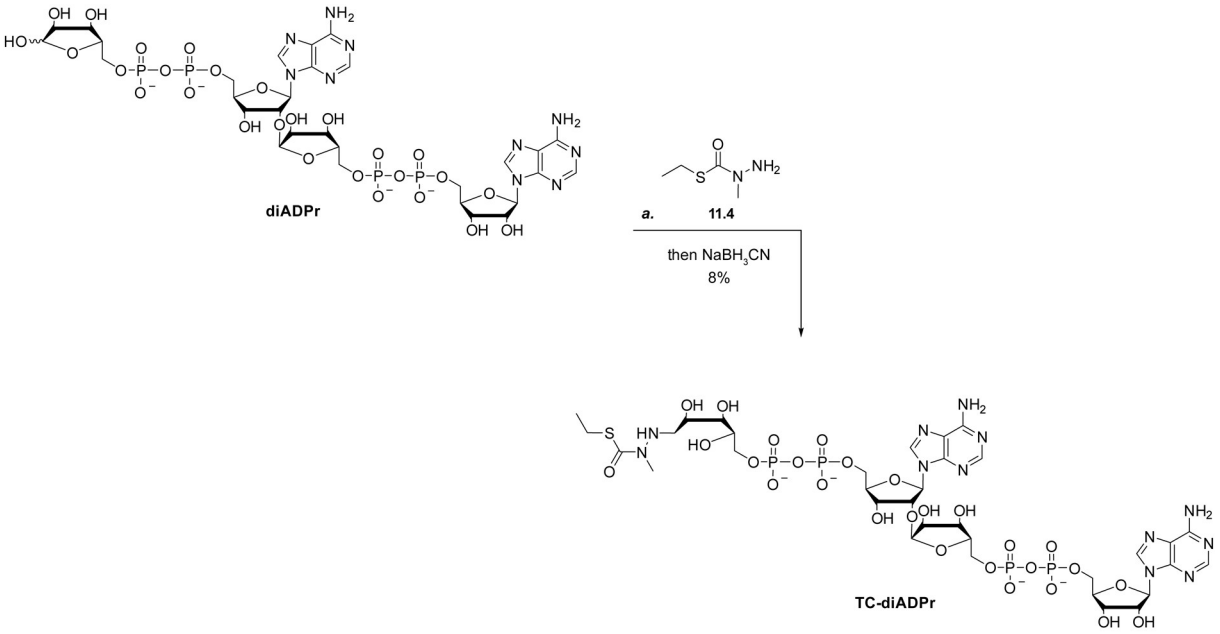

Scheme 16. Synthesis of TC-diADPr. ***a.*** *S*-Ethyl α-methylhydrazide thiocarbamate (11.4), Milli-Q water, AcOH, DMSO, 3 freeze-thaw cycles; then $NaBH_3CN$, 4 °C, 16 h (8% over 3 steps, deprotection with NH_3 and TBAF included). For detailed reagents and conditions, see **section 5.1.2.8**.

The synthetic pathway describing the reaction of the diADPr with *S*-Ethyl α-methylhydrazide thiocarbamate (11.4) is shown in **Scheme 16**. Analogous to the synthesis of TC-mADPr (**Figure 10A**), the reaction between diADPr and *S*-Ethyl α-methylhydrazide thiocarbamate (11.4) proceeded via the formation of a hydrazone intermediate. The formation of this intermediate is facilitated by subjecting the reaction mixture to multiple freeze-thaw cycles at –20 °C.[185] Subsequent reduction of the hydrazone intermediate with $NaBH_3CN$ resulted in the desired thiocarbamate linker modified diADPr (TC-diADPr) in 8% yield. This yield determination included the deprotection steps using methanolic ammonia and TBAF. The obtained TC-diADPr was then used in diADP-ribosylation reactions of the linker histone H1.2 S150C.

3.4.2 Linker histone diADP-ribosylation

Prior to the modification of the linker histone H1.2 S150C, the diADP-ribosylation was enabled by oxidation of TC-diADPr to the corresponding sulfone using Oxone™ [6] This activated TC-diADPr is then used directly in protein modification reactions with the linker histone variant H1.2 S150C. The modification process for the diADP-ribosylation is shown schematically in **Figure 14A**. Successful protein modification with TC-diADPr was evaluated by LC-MS measurements of the full-length protein (**Figure 14B**). The analysis displays both the measurements for the linker histone H1.2 S150C and the diADP-ribosylated linker histone H1.2 diADPr. The LC-MS measurement for the diADP-ribosylated linker histone resulted in a peak with a deconvoluted mass of 23228 Da indicating a shift of 1156 Da compared to the

unmodified H1.2 S150C. This corresponds to the mass of TC-diADPr attached to the cysteine residue of the linker histone H1.2 S150C. It should be noted that compared to the LC-MS measurement of H1.2 mADPr (**Figure 10B**), the quality of the measurement for H1.2 diADPr was compromised due to the instability of the introduced moiety under the LC-MS analytical conditions. In addition, the successful linker histone ADP-ribosylation with TC-diADPr was evaluated by SDS-PAGE with Coomassie blue staining and WB using anti-histone H1 antibody and anti-pan PAR binding reagent (**Figure 14C**). Analysis of the Coomassie blue stained SDS-PAGE gel revealed bands of similar intensity in all samples (**Figure 14C**, top), including H1.2 S150C, H1.2 mADPr, H1.2 diADPr (from left to right). The SDS-PAGE of the linker histone variant H1.2 mADPr showed a slight band shift to higher molecular weights, consistent with previous observations (**Figure 10C**, top). This is further supported for the linker histone H1.2 diADPr, which exhibited a distinct band shift to higher molecular weights in the SDS-PAGE gel, resulting from the covalent attachment of TC-diADPr. As previously described in **section 3.2**, the altered migration behavior is caused by the anionic nature of the diADPr and the increased mass of the protein-diADPr conjugate. WB analysis using the anti-histone H1 antibody revealed signals of uniform intensity in all samples analyzed (**Figure 14C**, lower left), furthermore confirming the stability of the linker histone during the modification with the developed thiocarbamate linker approach. The successful incorporation of TC-diADPr into the linker histone was confirmed by WB analysis using the anti-pan PAR binding reagent (**Figure 14C**, lower right). In contrast to the results obtained with the anti-histone H1 antibody, the anti-pan PAR binding reagent revealed signals exclusively for the H1.2 mADPr and H1.2 diADPr linker histone variants. This observation confirmed the efficient diADP-ribosylation of the linker histone H1.2 S150C using TC-diADPr. Differences in the WB signal intensities for H1.2 mADPr and H1.2 diADPr are attributed to the specificity of the anti-pan PAR binding reagent, which owns an increased affinity for oligo- and poly ADP-ribose compared to mono ADP-ribose.[196] Given the previously established cysteine selectivity of the thiocarbamate linker method, as demonstrated by the reactions of TC-biotin (**Figure 8**) and TC-mADPr (**Figure 10C**, lower right) with the linker histone H1.2 WT, further evaluation of the cysteine selectivity with TC-diADPr was considered as redundant. It was assumed that the presence of an additional ADP-ribose moiety in TC-diADPr compared to TC-mADPr would not be expected to alter the cysteine selectivity.

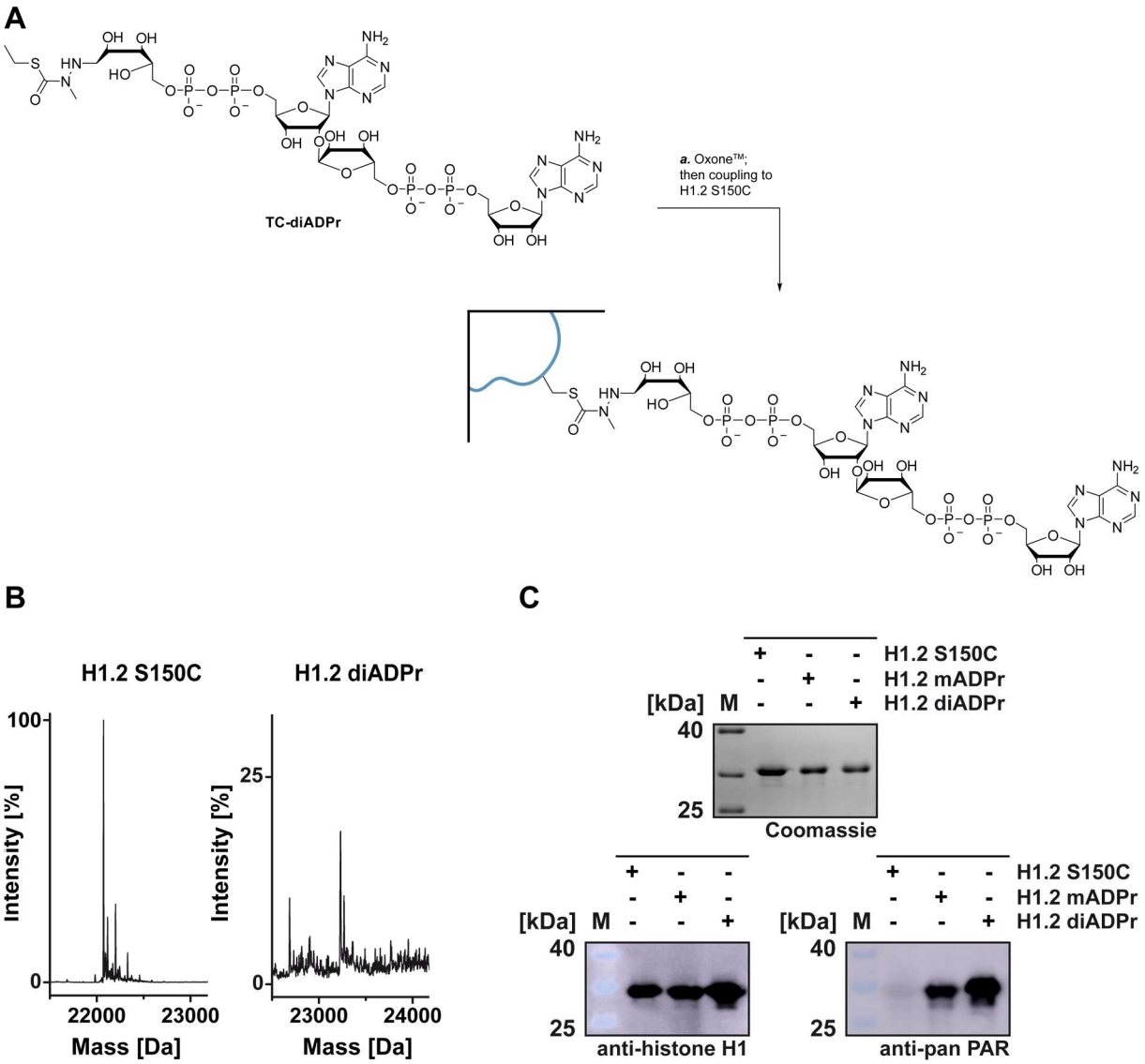

Figure 14. Preparation and analysis of the diADP-ribosylation of the linker histone H1.2 S150C. A. ***a.*** TC-diADPr was oxidized with Oxone™ (10 mM in Milli-Q water, Merck) and coupled to linker histone H1.2 S150C (4 °C, 16 h). **B.** Deconvoluted LC-MS analysis of full-length proteins. H1.2 S150C calculated 22072 Da, measured 22072 Da; H1.2 diADPr calculated 23230 Da, measured 23228 Da. **C.** SDS-PAGE gel with Coomassie blue staining (top) and Western Blot analysis (anti-histone H1 (bottom left) and anti-pan PAR binding reagent (bottom right)) of H1.2 S150C, H1.2 mADPr and H1.2 diADPr. For detailed reagents and conditions, see **section 5.2.2.7**.

The strategy for a cysteine-selective ADP-ribosylation of the linker histone H1.2 S150C, as described in **section 3.2** for the mADP-ribosylation, was successfully adapted to the diADP-ribosylation. The synthesis of TC-diADPr was achieved by the reaction of diADPr with *S*-Ethyl α-methylhydrazide thiocarbamate (11.4), yielding the desired product in moderate yields (**Scheme 16**). Subsequent activation of TC-diADPr by oxidation with Oxone™ enabled the modification of the linker histone H1.2 S150C. The successful incorporation of TC-diADPr was confirmed by full-length protein LC-MS measurements, as well as SDS-PAGE and WB analysis using the anti-pan PAR binding reagent and is shown in **Figure 14B** and **C**. Alongside to the first described incorporation of mADPr into the recombinantly expressed linker histone using

the thiocarbamate linker approach, this study marks the first reported incorporation of the shortest oligomer of pADPr into the linker histone yielding the formation of H1.2 diADPr. These two specific ADP-ribosylated linker histones enable a detailed investigation of the impact of this PTM on chromatin remodeling complexes and other cellular processes.

3.5 Chromatosome assembly assay

As reviewed in **section 1.1**, the compaction dynamics of DNA in eukaryotic cells are highly regulated for essential cellular processes, such as transcription, DNA repair and DNA packaging.[1,24] Many PTMs, in particular the ADP-ribosylation of histones, play a crucial role in modulating the higher order chromatin structure and thus directly influence DNA-based cellular processes (**section 1.3**). To study the impact of ADP-ribosylated histones on the chromatin structure, the development of a robust method to generate site specifically ADP-ribosylated histones is necessary. Currently, methods for the ADP-ribosylation of the four core histones and the linker histone rely on SPPS methods, that involve challenging syntheses and native chemical ligation procedures.[151,153] Given the direct impact of this PTM on the chromatin function and structure, the development of a method to generate ADP-ribosylated histones tailored for the incorporation into chromatin studies is essential. The developed method for a cysteine-selective mono- and diADP-ribosylation of the linker histone described in **sections 3.2** and **3.4** provides the first method to study the impact of this PTM on chromatosome formation and to gain insight into the interplay between the ADP-ribosylation and chromatin architecture. To accomplish this goal, a chromatosome assembly assay was developed that combined the ADP-ribosylated linker histone variants alongside with the nucleosome assembled from its recombinant parts. A schematic presentation of this assay is shown in **Figure 15**. The chromatosome assembly assay was started by the generation of the nucleosomal DNA by polymerase chain reaction (PCR). The core histone octamer, consisting of the recombinantly expressed core histones H2A, H2B, H3 and H4, was combined with the nucleosomal DNA to facilitate nucleosome formation.[15] The nucleosome was then incubated with the ADP-ribosylated linker histone variants to study their effect on the chromatin structure formation.

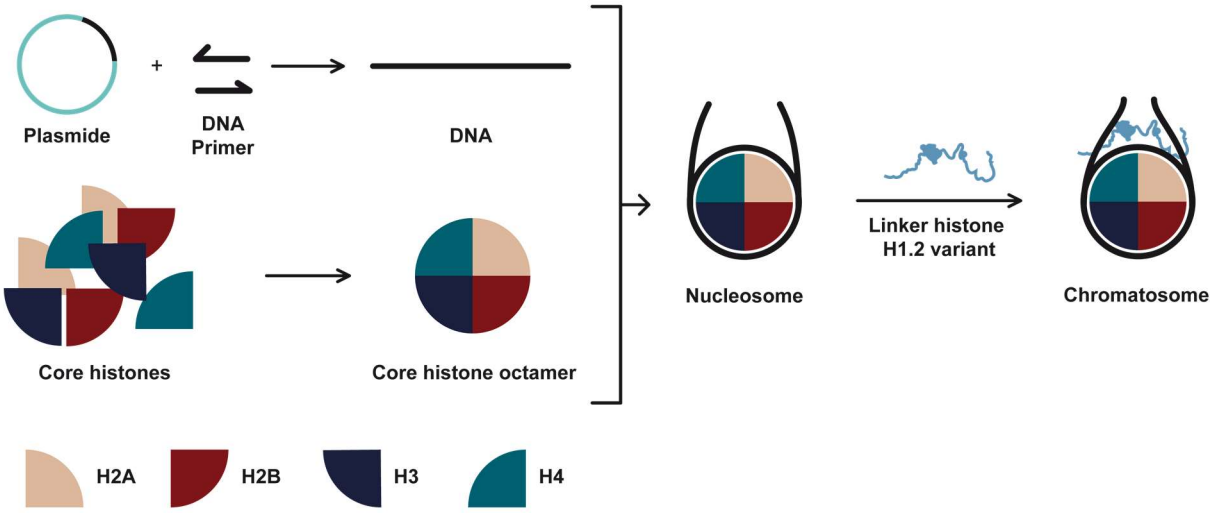

Figure 15. Chromatosome assembly assay. Nucleosomal DNA is synthesized via polymerase chain reaction (PCR). The core histone octamer is constructed using recombinantly expressed core histones H2A, H2B, H3 and H4. Stepwise salt dialysis employed to facilitate the assembly of the core histone octamer with the nucleosomal DNA, resulting in the nucleosome formation. Subsequent incubation with the linker histone H1.2 leads to the generation of the chromatosome.

3.5.1 Preparation of nucleosomal DNA

The nucleosome positioning sequence, which specifies the localization of nucleosomes within the DNA sequence, plays a crucial role in the generation of recombinant nucleosomes by promoting histone DNA interactions.[197] A DNA sequence based on the well-characterized "Wisdom 601" sequence was used for the chromatosome assembly assay. This 147 bp DNA sequence exhibits a high affinity for the binding of the core histone octamer, leading to the formation of recombinant nucleosomes.[16,17,198] To enable the assembly of recombinant nucleosomes into chromatosomes, the incorporation of a linker DNA of at least 11 bp at the ends of the "Wisdom 601" sequence is fundamental for linker histone binding. This was achieved by White *et. al.* by using a symmetric DNA sequence with 30 bp linker DNA at each side of the nucleosome positioning sequence derived from the "Wisdom 601" sequence. This resulted in a 207 bp nucleosomal DNA with enhanced binding to both the core histone octamer and the linker histone.[18] This optimized DNA sequence was also used in this work for the chromatosome assembly assay, cloned into a pUC-18 vector, and used as template for PCR amplification with the respective primers. PCR amplification to produce the nucleosomal DNA was performed on a large scale in 96-well plates using the Taq DNA polymerase (New England Biolabs). Purification of the PCR product was performed using Nucleospin Gel and PCR Clean-up Kit (Macherey-Nagel). The purified PCR product was subjected to agarose gel electrophoresis to confirm the desired size of the resulting DNA fragment (**Figure S2** in the Appendix).

3.5.2 Assembly of the core histone octamer

The expression and purification of the core histones and their assembly into the core histone octamer were performed by Dr. Philip Saumer and kindly provided for these studies.[198] Therefore, the DNA sequences corresponding to the core histones H2A, H2B, H3 and H4 were cloned into a pET-11a vector and subsequently induced for expression in *E. coli* BL21(DE3) cells according to a documented protocol.[199] Due to significantly reduced expression levels of the core histones H2B and H4, an improved coding sequence was used to improve protein expression and simplify the protein purification.[200] As a result, an N-terminal His_6-tag, followed by a TEV cleavage site was incorporated into the protein sequences. This optimized method facilitated the expression and purification of all four core histones with high purity and increased yields.[198] The expressed and purified core histones were then assembled into the core histone octamer under denaturing conditions. The denatured proteins were subjected to an unbalanced mixture with an excess of H2A and H2B, followed by dialysis refolding. After assembly of the core histone octamer, the excess of the H2A-H2B dimer was removed by size exclusion chromatography.[198]

3.5.3 Nucleosome assembly

The next step in the chromatosome assembly assay is the formation of recombinant nucleosomes. The method used to generate nucleosomes from its recombinant components is based on reconstitution processes. First, the core histone octamer and the nucleosomal DNA are combined in aqueous buffer solutions containing high salt concentrations, typically around 2 M NaCl (high salt buffer, HSB). This increased salt concentration inhibits interactions between the core histone octamer and the nucleosomal DNA.[19,20] Subsequent stepwise dialysis to lower salt concentrations with low salt buffer (LSB) enables the controlled emergence of interactions between the components of the octamer, such as the H2A-H2B dimer or the H3-H4 tetramer, and the nucleosomal DNA. This sequential process ultimately results in the formation of the nucleosome.[201] Further dialysis to physiological salt concentrations renders the recombinant nucleosomes suitable for *in vitro* applications. The nucleosome assembly was started by combining nucleosomal DNA with the core histone octamer in a buffer containing 2M NaCl and 0.05% (v/v) Nonidet™ P-40 Substitute. The inclusion of a detergent in the buffer was used to increase the stability of the resulting nucleosome.[202] Gradual reduction of the salt concentration to 50 mM NaCl by dialysis promoted the nucleosome formation (**Figure 16A**). The ideal ratio of core histone octamer to nucleosomal DNA for a quantitative nucleosome formation was determined by small-scale titration experiments while maintaining a constant nucleosomal DNA concentration. The

result of these nucleosome assemblies was analyzed by native PAGE with ethidium bromide staining (**Figure 16B**). The ratio of core histone octamer to nucleosomal DNA plays a crucial role in determining the transition state during the formation of the nucleosome. At very low ratios, residual free nucleosomal DNA may be present, potentially interfering in subsequent experiments or requiring difficult purification procedures.

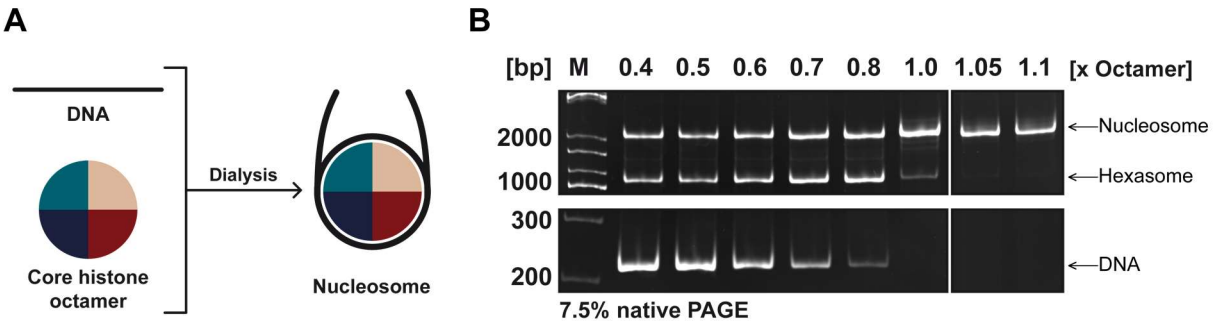

Figure 16. Preparation and analysis of the nucleosome assembly. A. Schematic presentation detailing the nucleosome assembly mechanism via stepwise salt dialysis involving the nucleosomal DNA and the core histone octamer. **B.** 7.5% native PAGE gel with ethidium bromide staining of the nucleosome assembly. For detailed reagents and conditions, see **section 5.2.2.14**.

This phenomenon was visible in the nucleosome assembly with a ratio of 0.4 equivalents of the core histone octamer per nucleosomal DNA (**Figure 16B**). An intensive band with a size of approximately 200 bp, corresponding to free nucleosomal DNA, was present up to a ratio of 1.0 equivalents of the core histone octamer per nucleosomal DNA. Moreover, even at this low concentration of the core histone octamer present at this ratio, the desired nucleosome was formed only to a small extent as evidenced by the band at approximately 2000 bp corresponding to the formed nucleosome. The additional band at 1000 bp indicates the formation of hexasomes, histone-DNA complexes lacking a H2A-H2B heterodimer. The formation of hexasomes can be caused by different mechanisms and represents an intermediate state during the assembly of nucleosomes.[203,204] This intermediate was observed up to a ratio of 1.05 equivalents of the core histone octamer per nucleosomal DNA. This suggests that this ratio is not sufficient to achieve complete nucleosome formation in a quantitative manner. By increasing the ratio to 1.1 equivalents of the core histone octamer per nucleosomal DNA a complete and quantitative nucleosome formation was achieved. This final ratio was then used as the basis for scaling up the assembly of recombinant nucleosomes in subsequent experiments. Further increases in the ratio of core histone octamer to nucleosomal DNA would result in sedimentation of the formed nucleosomes.

3.5.4 Chromatosome assembly

The combination of recombinant nucleosomes, successfully obtained in large quantities, with the prepared ADP-ribosylated linker histone variants H1.2 mADPr and H1.2 diADPr allows the investigation of the effects of mono- and diADP-ribose modifications on the chromatosome assembly. The chromatosome formation experiments were performed with the mono- and diADP-ribosylated linker histone variants and the unmodified cysteine containing variant H1.2 S150C. The schematic presentation of this assembly is shown in **Figure 17A**.

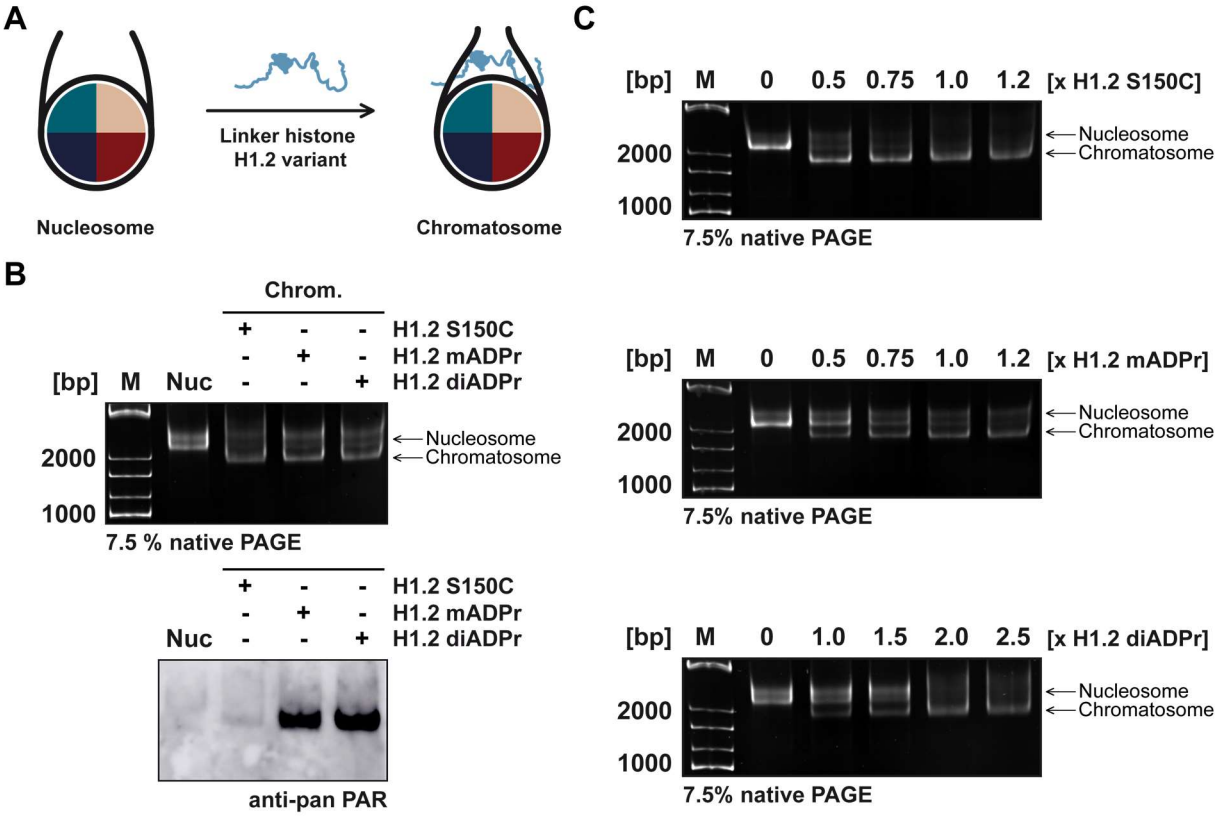

Figure 17. Preparation and analysis of chromatosome formation with H1.2 S150C, H1.2 mADPr and H1.2 diADPr. A. Schematic presentation of the chromatosome assembly with the respective linker histone H1.2 variants. **B.** 7.5% native PAGE gel (top) of nucleosome and assembled chromatosome with the linker histone variants H1.2 S150C, H1.2 mADPr and H1.2 diADPr. Native PAGE gel WB analysis (bottom) using the anti-pan PAR binding reagent for the nucleosome and the assembled chromatosomes with the linker histone variants H1.2 S150C, H1.2 mADPr and H1.2 diADPr. **C.** 7.5% native PAGE gels with ethidium bromide staining of the titration experiments for intact chromatosomes with the linker histone variants H1.2 S150C (top), H1.2 mADPr (middle) and H1.2 diADPr (bottom).

For these experiments, the recombinant nucleosomes were combined with the appropriate linker histone variant (H1.2 S150C, H1.2 mADPr and H1.2 diADPr), followed by incubation at 19.5 °C for 35 minutes in LSB. The evaluation of the quantitative chromatosome formation and the incorporation of the ADP-ribosylated linker histone variants in the chromatosome was performed by native PAGE with ethidium bromide staining and native PAGE WB analysis

using the anti-pan PAR binding reagent (**Figure 17B**). It is of note that all linker histone variants used for chromatosome formation experiments were successfully incorporated into the chromatosome structure, as shown by the band shift to a smaller size compared to the nucleosome band observed in the native PAGE (**Figure 17B**, top). In contrast to the nucleosome, the chromatosome showed an increased migration behavior in native PAGE due to its more condensed structure after the addition of the linker histone.[205] Native PAGE WB analysis with the anti-pan PAR binding reagent was used to investigate the incorporation of the ADP-ribosylated linker histone variants into the chromatin structure (**Figure 17B**, bottom). This analysis revealed detectable WB signals exclusively for the chromatosomes prepared with the ADP-ribosylated linker histones H1.2 mADPr and H1.2 diADPr. The results of the quantitative formation of the chromatosome, coupled with the confirmed incorporation of the ADP-ribosylated linker histones shown in **Figure 17B**, represents the first reported incorporation of site-specifically ADP-ribosylated linker histones into a chromatin structure. Furthermore, the confirmed incorporation of the ADP-ribosylated linker histones by the thiocarbamate ligation approach into the chromatosome renders this method suitable for the application in the chromatosome assembly assay.

The ADP-ribosylation of the linker histone has been associated to chromatin remodeling, as demonstrated for ADP-ribosylated core histones and the PARP-dependent *in vitro* decondensation of chromatin.[132,206-208] To investigate the effect of the linker histone ADP-ribosylation on the chromatin structure, chromatosome formation experiments were performed using the mono- and diADP-ribosylated linker histone variants and the unmodified cysteine containing variant H1.2 S150C. Nucleosomes were incubated with increasing concentrations of the respective linker histone and subsequently analyzed by native PAGE with ethidium bromide staining (**Figure 17C**). The chromatosome assembly with the unmodified linker histone variant H1.2 S150C required 1.0 equivalents of the linker histone to achieve quantitative chromatosome formation (**Figure 17C**, top). The quantitative transition from the nucleosome to the chromatosome can be seen by the complete disappearance of the nucleosome band and the formation of the respective chromatosome band in the native PAGE gel. Contrary to this result, the chromatosome assembly with H1.2 mADPr required 1.2 equivalents of the linker histone to obtain a complete chromatosome formation (**Figure 17C**, middle). This change in the amount of the linker histone required for the chromatosome formation demonstrates the direct influence of the mADP-ribosylation and the partly inhibitory effect of the linker histone PTM on the formation of the chromatin structure. In contrast to this observation, a study by Hananya *et al.* reported that the mADP-ribosylation of the core histones does not interfere with the chromatin

structure formation.[154] The chromatosome assembly was further disrupted when H1.2 diADPr was used, as evidenced by the requirement of 2.0 equivalents for complete chromatosome formation (**Figure 17C**, bottom). The differences in the results for the chromatosome formation by using either the mono- or the diADP-ribosylated linker histone demonstrate the dependence of the chain length of this PTM on the chromatosome assembly. This is consistent with the observation of Tashiro *et al.* regarding the effect of linker histone ADP-ribosylation and its role in hindering chromatosome structure formation.[155] The resulting inhibition of the chromatosome formation upon ADP-ribosylation of the linker histone may be contributed to the anionic nature of the ADP-ribose modification resulting in repulsive interactions with the negatively charged DNA, ultimately leading to the decondensation of the higher order chromatin structure.[209] In response to DNA damage, histones undergo extensive ADP-ribosylation events, resulting in chromatin decondensation and increased DNA accessibility to the DNA damage repair machinery.[209] This is consistent with the observed inhibition of the chromatosome formation upon mono- and diADP-ribosylation of the linker histone. In addition to repulsive effects between the DNA and the ADP-ribose modification leading to the decondensation of the chromatin, ADP-ribosylation of the linker histone can promote binding of the anionic ADP-ribose to the positively charged core histones. This in turn increases the decondensation of the chromatin structure.[210]

The importance of the ADP-ribosylation as a PTM of the linker histone was highlighted in **section 1.3**. To improve the understanding of the effects of this PTM on chromatin structure formation, mono- and diADP-ribosylated linker histones, H1.2 mADPr and H1.2 diADPr, were incorporated into a chromatosome assembly assay. First, nucleosomes were assembled by combining the prepared nucleosomal DNA with the recombinant core histone octamer (**Figure 16**).[15-20] These nucleosomes were then incubated with the respective linker histone variant to enable the chromatosome assembly. The achievement of both quantitative chromatosome formation and incorporation of the modified proteins was verified by native PAGE and WB analysis (**Figure 17B**). The incorporation of the modified linker histones into a chromatosome represents the first described method for the introduction of site-selectively mono- and diADP-ribosylated linker histones into the chromatin structure. Furthermore, the dependence of the ADP-ribose chain length on the quantitative chromatosome assembly was revealed by chromatosome formation experiments, demonstrating the direct influence of the linker histone ADP-ribosylation on the chromatin structure formation (**Figure 17C**). With these results and the approach to site selectively introduce ADP-ribose into the linker histone H1.2, a detailed investigation of the impact of ADP-ribosylated histones on the chromatin remodeling machinery by affinity enrichment methods becomes feasible.

4 Summary and Outlook

PTMs of histones play a crucial role in various cellular processes such as DNA repair, chromatin remodeling and transcriptional regulation.[1] Among these PTMs, the ADP-ribosylation occurs on a variety of proteins in the nucleus and the cytoplasm. This modification targets all four core histones (H2A, H2B, H3 and H4) as well as the linker histone (H1), most notably in the context of DNA repair and DNA processing.[2] Despite its importance and widespread occurrence, linker histone ADP-ribosylation remains poorly understood due to the lack of methods that allow the site-selective ADP-ribosylation of linker histones. The high number of lysines in the linker histone sequence complicates the selectivity of the ADP-ribosylation with conventional modification methods, leading to side reactions and unwanted modification sites. Detection of ADP-ribosylation sites in the linker histone is further complicated by the high number of lysines in the protein sequence, since common detection methods such as LC-MS require fragmentation of the protein prior to measurement, which in the case of the linker histone leads to the formation of small fragments that are difficult to detect.

In this study, a novel method to site-selectively generate ADP-ribosylated linker histones was developed by applying a chemical ligation approach. The modification process was based on the reaction with cysteine residues, which in the case of the linker histone allowed the targeted introduction of the ADP-ribosylation, as due to the lack of natural cysteines in the protein sequence only genetically engineered cysteines are available for the reaction. After successful implementation of this strategy, the cysteine selectivity and the stability of the formed linkage was investigated. For further functional studies, an alternative synthetic pathway for an ADP-ribose dimer was established, allowing the modification of the linker histone by the innovative protein modification method. The functional impact of the ADP-ribosylated linker histones on the chromatin structure formation was evaluated by chromatosome formation experiments. Recombinant core histone octamers were combined with nucleosomal DNA to assemble nucleosomes. Subsequent incorporation of the mono- and diADP-ribosylated linker histone variants resulted in the formation of distinct chromatosomes, on which the influence of the modification was studied.

To achieve the ambitious objective of cysteine-selective protein modification, a thiocarbamate based linker was used for the incorporation. This was applied to investigate the site-selective ADP-ribosylation of the linker histone H1.2. Thiocarbamates and dithiocarbamates are known to selectively modify cysteine residues in proteins.[3-6] Therefore, *S*-Ethyl α-methylhydrazide thiocarbamate (11.4) was synthesized containing a thiocarbamate functionality for protein modification and a hydrazide functionality for the introduction of a target molecule, such as ADP-ribose.[7] SDM was used to insert a cysteine into the linker histone sequence at a known ADP-ribosylation site, resulting in the H1.2 S150C variant.[8] To evaluate the selectivity of the thiocarbamate for cysteine, a model system with *S*-Ethyl α-methylhydrazide thiocarbamate functionalized biotin (TC-biotin) was developed. After successful synthesis of TC-biotin, its applicability for the modification of the linker histone variant H1.2 S150C was evaluated. The successful biotinylation of the linker histone with TC-biotin was confirmed by WB analysis, which revealed a concentration-dependent biotin modification of the linker histone exclusively in the presence of a cysteine residue. To ensure the *in vitro* applicability of the proteins modified with *S*-Ethyl α-methylhydrazide thiocarbamate, the stability of the linkage in cell lysate was examined. This was verified by incubating the biotinylated H1.2 S150C with HEK293T cell lysate and analyzing by WB, confirming the stability of the TC-biotin modification under these conditions.

The demonstrated cysteine selectivity of the thiocarbamate ligation method allowed its extension to the site-selective ADP-ribosylation of the linker histone H1.2. Therefore, *S*-Ethyl α-methylhydrazide thiocarbamate modified mono ADP-ribose (TC-mADPr) was synthesized via a hydrazone intermediate. Successful mADP-ribosylation of the linker histone was confirmed by full-length protein LC-MS measurements and WB analysis. Comparison of the results with H1.2 WT proved the cysteine selectivity of TC-mADPr, as no modification occurred for the wild-type variant due to the absence of a cysteine residue. The stability of the protein under the modification reaction conditions with TC-mADPr was also confirmed by WB analysis. This method represents the first reported approach for the site-selective mADP-ribosylation of the recombinantly expressed linker histone without side reactions and could be extended to other proteins.

To investigate the influence of an ADP-ribose oligomer on the chromatin structure formation, an optimized synthesis route for the diADPr was developed.[9-11] Following the glycosylation of the respective donor (13.1) and acceptor (13.2) molecules, stereochemical inversion was achieved by an oxidation-reduction procedure, resulting in the desired stereochemistry of the 2'-*O*-α-ribosyl-adenosine disaccharide (13.4).[12-14] Strategic manipulation of the protecting groups introduced orthogonality into the molecule. This allowed the incorporation of two

distinct phosphate moieties at the termini to yield the bis-phosphorylated 2'-*O*-α-ribosyl-adenosine building block (13.10). The formation of pyrophosphate bonds with the terminal groups, the ribose-*H*-phosphonate (14.6) and the adenosine-*H*-phosphonate (15.5) enabled the stepwise assembly of the protected diADPr. Finally, global deprotection resulted in the formation of diADPr with a free reducing end suitable for protein modification reactions.

The strategy for the mADP-ribosylation of the linker histone was adapted to the synthesized diADPr with a free reducing end. This was achieved by introducing the *S*-Ethyl α-methylhydrazide thiocarbamate (11.4) into the diADPr yielding TC-diADPr. The successful diADP-ribosylation of the linker histone variant H1.2 S150C was verified by full-length protein LC-MS measurements, as well as SDS-PAGE and WB analysis. These results on the diADP-ribosylation of the linker histone mark the first reported incorporation of the shortest oligomer of pADPr into the recombinant linker histone.

The influence of ADP-ribosylation of the linker histone on the chromatin structure formation was investigated using a chromatosome assembly assay. The nucleosomal DNA, which is optimized for the nucleosome assembly and the binding of the linker histone, was prepared by PCR.[15-18] The combination of the DNA with the recombinant core histone octamer enabled the assembly of nucleosomes.[19,20] The recombinant nucleosomes were incubated with the ADP-ribosylated linker histones to form chromatosomes. The quantitative formation of chromatosomes and the incorporation of the ADP-ribosylated linker histones into the chromatin structure was verified by native PAGE and native PAGE WB analysis. The incorporation of the mono- and diADP-ribosylated linker histones into the chromatosome represents the first described method for assembling a recombinant chromatin structure with site-selective ADP-ribosylated linker histones. Moreover, the impact of the introduced modification on the chromatin structure was investigated by experiments on the chromatosome formation. Here, it was shown that the chromatosome formation is hindered depending on the chain length of the ADP-ribose This was demonstrated by an increased requirement for ADP-ribosylated linker histone to achieve quantitative chromatosome formation, with the effect being more pronounced for the diADP-ribosylated linker histone compared to the mADP-ribosylated linker histone. Hence, the direct influence of this anionic modification on the formation of the chromatin structure, depending on the length of the ADP-ribose chain, was elucidated.

With the described synthesis of the *S*-Ethyl α-methylhydrazide thiocarbamate (11.4) linker and the developed method to incorporate either ADP-ribose or biotin into the linker histone H1.2 S150C, the ADP-ribose moiety could be incorporated in its ring-closed form by structural modifications of the thiocarbamate linker molecule. Moyle and Muir reported an ADP-

ribosylation using an *N*-methyl aminooxy functionality in the amino acid to be modified, resulting in the formation of a ring-closed modified ADP-ribose (**Scheme 4A**).[21] Adapting this to the thiocarbamate ligation approach would enable the incorporation of a ring-closed ADP-ribose into a target protein, mimicking the native binding of a serine to the ADP-ribose. Furthermore, the described cysteine-selective method for protein modifications could facilitate the introduction of other PTMs into the linker histone, which are challenging to achieve with commonly used methods. This would contribute to a better understanding of the influence of PTMs on linker histones themselves and their function in the chromatosomal context. Within this setting, the introduction of dyes or a molecular handle into the protein is also feasible using the herein established method.

In addition to the core histones and the linker histone, a wide variety of other target protein for ADP-ribosylation are known. Some of these, such as ubiquitin, also lack a cysteine residue in their sequence, rendering this method applicable to modify these proteins.[22] This would permit the investigation of the effects of protein ADP-ribosylation beyond the linker histone.

Based on the demonstrated influence of the ADP-ribosylation of the linker histone at serine 150, other modification sites in the globular and the N-terminal domains, such as serine 54, can also be investigated applying the described thiocarbamate ligation method.[8] Using these ADP-ribosylated linker histones to study the chromatosome formation would reveal the influence of other modification sites on the chromatin structure that are involved in its formation in different ways. This could contribute to a better understanding of the field in general.

Furthermore, the site-specific ADP-ribosylated linker histones can be incorporated into a chromatosome array, which consists of a sequential arrangement of multiple nucleosomes along the same DNA strand. This opens the possibility to study the effects of the ADP-ribosylation of the linker histone on higher order chromatin structure and function.

The method described here for the generation of mono- and diADP-ribosylated linker histones allows further investigation of the interactome of these PTMs within the chromatin structure by an affinity enrichment mass spectrometry (AE-MS) approach. A molecular handle, such as desthiobiotin, can be introduced at the 5'-terminus of the nucleosomal DNA used for an affinity enrichment protocol. Also, the identification of proteins that interact with the ADP-ribosylated linker histone within the chromatin structure would expand the knowledge of this PTM and its function beyond its involvement in chromatin structure formation.[15]

Further investigation of the histone code and the combinatorial effect of different PTMs might be achieved by simultaneously introducing a second ADP-ribosylation site or another PTM

into the same linker histone. This could allow to study the interplay of multiple PTMs on the formation of the chromatin structure or the interactome in the chromatin.

Overall, the method presented here for the cysteine-selective mono- and diADP-ribosylation of the linker histone using the thiocarbamate ligation approach will considerably expand the chemical toolbox for the investigation of histone PTMs and contribute substantially to a better understanding of their influence on various cellular processes. Furthermore, the adaptation of the chromatosome assembly assay to other linker histone PTMs might contribute to a better understanding of histone PTMs in the context of chromatin structure formation.

5 Materials and Methods

5.1 Chemical synthesis

5.1.1 Materials

All reactions were carried out using standard laboratory techniques. Oxygen or moisture sensitive reactions were performed using nitrogen as an inert atmosphere and the appropriate anhydrous solvent (VWR). All commercially available chemicals were purchased from Sigma-Aldrich/Merck, TCI, VWR, Carl Roth, ABCR, Acros Organics or Fluka and used without further purification. Chromatography solvents were p.A., absolute or HPLC grade and technical solvents were distilled before to use. Buffer for HPLC was prepared with water from a Milli-Q purification system (Merck).

5.1.1.1 HPLC buffer solution

Triethylammonium bicarbonate (TEAB) buffer for analytical and preparative HPLC was prepared as followed. Milli-Q water (3.5 L) and triethylamine (TEA, 700 mL, 5 mol) were flushed with carbon dioxide (5 kg, from dry ice) while stirring. This process was continued to pH 7.5, then filled up to 5 L with Milli-Q water and stored at 4 °C to yield 1M TEAB buffer.
Triethylammonium acetate (TEAA) buffer was prepared by adding TEA (139 mL, 1 mol) and acetic acid (57 mL, 1 mol) to 500 mL Milli-Q water. The pH was adjusted to 7.0 and made up to 1 L with Milli-Q water to give 1M TEAA buffer.

5.1.1.2 Instrumental analysis

Nuclear magnetic resonance (NMR) spectra were performed on a Bruker Avance III 400 MHz or JEOL ECZ 500R at room temperature. All spectra were measured in $CDCl_3$, DMSO-d_6, DMF-d_7, MeOD or D_2O as solvent. Calibration was performed using the internal standard of the corresponding solvent peak ($CDCl_3$ δ 7.26 ppm, DMSO-d_6 δ 2.50 ppm, DMF-d_7 δ 2.74 ppm, MeOD δ 3.31 ppm, D_2O δ 4.79 ppm). Chemical shifts are given in parts per million (ppm) and coupling constants in Hertz (Hz). NMR spectra were analyzed using MestreNova 14.0.0

(MestreLab Research S.L.) according to the following convention: s (singlet), d (doublet), t (triplet), q (quadruplet), p (quintet), m (multiplet), bs (broad signal).

Low resolution electron spray ionization (LR-ESI-MS) mass measurements were conducted on a Bruker Daltronics amaZonSL with an external sodium format calibrant. High resolution electron spray ionization mass spectrometry (HR-ESI-MS) was performed on an Agilent 6546 QTOF mass spectrometer coupled to an Infinity II 1260 system with an external sodium format calibrant.

5.1.1.3 Chromatographic analysis

Thin layer chromatography (TLC) was performed on silica gel coated aluminum sheets (Type 60 F_{254}, 0.2 mm silica, Merck) and the analyzed compounds were visualized by UV-light (254 nm) or by staining with ceric ammonium molybdate solution (3.2 mM ceric ammonium sulfate, 40 mM ammonium molybdate in 1.1 M sulfuric acid).

Silica gel column chromatography was performed at elevated pressure (0.3 bar) using silica gel (Silica gel 60 M, pore size 40 – 63 µm, Macherey-Nagel). The solvent mixtures used as the mobile phase are indicated in the experimental procedure for each purification.

Reverse-phase high performance liquid chromatography (HPLC) was performed using Shimadzu systems equipped with LC 20AT pumps, CBM 20A controller and a SPD M20A detector. Different HPLC columns were used depending on the amount and the polarity of the compounds: 250/21 Nucleodur C_{18} HTec (5µm, flow rate: 15 mL/min, Macherey-Nagel), 250/10 Nucleodur C_{18} HTec (5µm, flow rate: 8 mL/min, Macherey-Nagel), 250/16 Nucleodur C_{18} Pyramid (5µm, flow rate: 15 mL/min, Macherey-Nagel), 250/10 Nucleodur C_{18} Pyramid (5 µm, flow rate 6 mL/min).

5.1.2 Methods

5.1.2.1 Synthesis of thiocarbamate linker

Ethyl chlorothioformate (11.3)

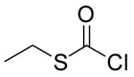

11.3

Ethanethiol (2.38 mL, 32.29 mmol) and TEA (1.49 mL, 10.73 mmol) were dissolved in anhydrous tetrahydrofuran (THF, 180 mL) and cooled to 0 °C. A solution of triphosgene in anhydrous THF (15 mL, 0.7 M) was added over a period of 20 minutes. The solution was stirred at 0 °C for 30 minutes and at room temperature for another 30 minutes. The resulting precipitate was filtered off and washed with diethyl ether. The combined organic phases were concentrated under reduced pressure to give 2.88 g of ethyl chlorothioformate (23.18 mmol, 72%). The crude product was used in the next synthesis without further purification.

***S*-Ethyl α-methylhydrazide thiocarbamate (11.4)**

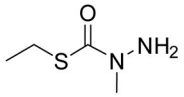

11.4

Methylhydrazine (1.51 mL, 28.99 mmol) and TEA (4.44 mL, 31.87 mmol) were dissolved in anhydrous dichloromethane (DCM, 35 mL) and cooled to –80 °C. Ethyl chlorothioformate (2.88 g, 23.18 mmol) dissolved in anhydrous DCM (13 mL) and added to the reaction mixture over a period of 20 minutes. The reaction mixture was warmed to room temperature and stirred for 16 hours. The reaction was diluted with DCM (100 mL) and washed with water (2x 50 mL) and brine (50 mL). The organic phase was dried over Na_2SO_4 and concentrated under reduced pressure to give 1.96 g of *S*-Ethyl α-methylhydrazide thiocarbamate (14.60 mmol, 63%).

^{1}H-NMR (400 MHz, Chloroform-*d*) δ (ppm) 3.91 (bs, 2H, NH_2), 3.16 (s, 3H, N-CH_3), 2.76 (q, 2H, CH_2), 1.23 (t, 3H, CH_3).

^{13}C NMR (101 MHz, Chloroform-*d*) δ (ppm) 125.18, 39.11, 24.32, 15.27.

5.1.2.2 Synthesis of thiocarbamate linker modified biotin

Thiocarbamate linker modified biotin (TC-biotin)

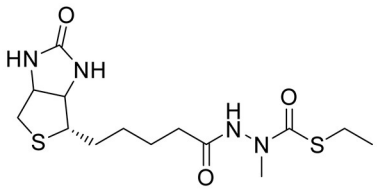

TC-biotin

Biotin (0.20 g, 0.82 mmol) was suspended in MeCN (3 mL) and thionyl chloride (0.5 mL, 6.9 mmol) was added. The reaction mixture was stirred at room temperature for 2 hours until the solution became clear. The solvent was removed under reduced pressure and the residue was dissolved in MeCN (3 mL). *S*-Ethyl α-methylhydrazide thiocarbamate (0.22 g, 1.64 mmol), dissolved in MeCN (1 mL), was added to the pre-activated biotin. This mixture was stirred at room temperature for 18 hours. The solvent was removed under reduced pressure and the residue was taken up in DCM (50 mL). The organic phase was washed with water (2x 25 mL) and the combined aqueous phases were lyophilized, yielding 0.18 g of the TC-biotin (0.51 mmol, 62 %).

^{1}H NMR (400 MHz, DMSO-d_6) δ (ppm) 10.3 (s, 1H, NH), 6.55 (bs, 1H, NH), 4.31 (dd, J = 7.7, 4.9 Hz, 1H, H-2), 4.13 (dd, J = 7.7, 4.4 Hz, 1H, H-5), 3.96 (bs, 1H, NH), 3.13 – 3.04 (m, 1H, H-4), 3.02 (s, 3H, N-CH_3), 2.82 (dd, J = 12.5, 5.1 Hz, 1H, H-3a), 2.70 (qd, J = 7.3, 3.9 Hz, 2H, Et-CH_2), 2.58 (d, J = 12.4 Hz, 1H, H-3b), 2.13 (t, J = 7.4 Hz, 2H, CH_2), 1.67 – 1.28 (m, 6H, 3x CH_2,), 1.15 (t, J = 7.3 Hz, 3H, CH_3).

5.1.2.3 Synthesis of thiocarbamate linker modified ADP-ribose monomer

Thiocarbamate linker modified ADP-ribose monomer (TC-mADPr)

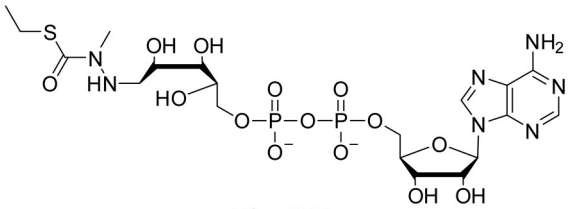

TC-mADPr

Monomeric adenosine diphosphate-ribose (mADPr, 45 mg, 0.08 mmol) was dissolved in Milli-Q water (5mL). Acetic acid (0.1 mL) and *S*-Ethyl α-methylhydrazide thiocarbamate (0.48 mL, 1 M in DMSO) were added followed by the addition of dimethyl sulfoxide (DMSO, 1.2 mL). The reaction mixture was freeze-thawed three times at –20 °C. Sodium cyanoborohydride (0.1 g, 1.6 mmol) was added and stirred at 4 °C for 18 hours. The solvent was removed under reduced pressure and the crude product was purified by RP-HPLC (Nucleodur C_{18} HTec, 50 mM TEAB, MeCN). After lyophilization 46 mg of TC-mADPr (0.07 mmol, 88%) was obtained.

^{1}H NMR (400 MHz, Methanol-d_4) δ (ppm) 8.55 (s, 1H, H-8), 8.15 (s, 1H, H-2), 6.06 (d, J = 5.6 Hz, 1H, H-1''), 4.64 (t, J = 5.4 Hz, 1H, H-2''), 4.48 – 4.44 (m, 1H, H-3''), 4.22 – 4.14 (m, 5H, H-1', H-2', H-5''), 3.92 – 3.84 (m, 2H, H-5'), 3.80 – 3.75 (m, 1H, H-4''), 3.66 (t, J = 6.6 Hz, 1H, H-3'), 3.07 (s, 3H, N-CH_3), 2.91 (dd, J = 11.5, 8.0 Hz, 1H, H-4'), 2.63 (q, J = 7.5 Hz, 2H, Et-CH_2), 1.16 (t, J = 7.3 Hz, 3H, Et-CH_3).

^{31}P NMR (162 MHz, Methanol-d_4) δ (ppm) -11.38 (dd, J = 143.1, 21.9 Hz).

5.1.2.4 Synthesis of bis-phosphorylated 2'-*O*-α-ribosyl-adenosine building block

N^6-benzoyl-[3',5'-*O*-(1,1,3,3-tetra-*iso*-propyl-disiloxane-1,3-diyl)-2'-*O*-α-D-(2''-*O*-acetyl-3'',5''-di-*O*-benzoyl-arabinofuranosyl)] –adenosine (13.3)

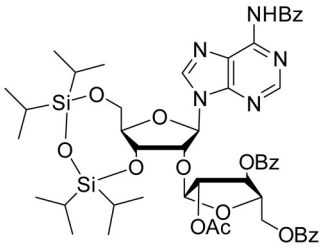

13.3

1,2-di-*O*-acetyl-3,5-di-*O*-benzoyl-D-arabinofuranoside (glycosylation donor) (5.64 g, 12.75 mmol) was stirred with $SnCl_4$ (3.3 mL, 28.25 mmol) in anhydrous dichloroethane (DCE, 50 mL) at 0 °C for 10 minutes. N^6-benzoyl-3',5'-*O*-(tetra-*iso*-propyl-disiloxane-1,3-diyl)-adenosine (glycosylation acceptor) (6.02 g, 9.81 mmol) dissolved in anhydrous DCE (100 mL) was added dropwise and the reaction mixture was stirred at 4 °C for 48 hours. Sat. aq. $NaHCO_3$ (130 mL) was added and the resulting suspension was stirred at 0 °C for 30 minutes. The solid was separated from the solution by centrifugation. The phases were separated and the organic phase was washed with water (200 mL), dried over Na_2SO_4 and concentrated under reduced pressure. The crude product was purified by silica gel column chromatography (petroleum ether/ethyl acetate (PE/EtOAc) 3/1 to 1/1), yielding 5.15 g of N^6-benzoyl-[3',5'-*O*-(1,1,3,3-tetra-*iso*-propyl-disiloxane-1,3-diyl)-2'-*O*-α-D-(2''-*O*-acetyl-3'',5''-di-*O*-benzoyl-arabinofuranosyl)] -adenosine (5.17 mmol, 52 %) as a white foam.

^{1}H-NMR (400 MHz, Chloroform-*d*) δ (ppm) 8.99 (s, 1H, H-2), 8.78 (s, 1H, H-8), 8.07 (d, *J* = 7.3 Hz, 4H, arom. Bz), 8.02 (d, *J* = 7.3 Hz, 2H, arom. Bz), 7.64 – 7.49 (m, 5H, arom. Bz), 7.46 - 7.37 (m, 4H, arom. Bz), 6.18 (s, 1H, H-1'), 5.67 (s, 1H, H-1''), 5.48 (s, 1H, H-2''), 5.45 (d, *J* = 4.7 Hz, 1H, H-3''), 4.82 – 4.69 (m, 2H, H-2', H-3'), 4.69 – 4.57 (m, 3H, H-4'', H-5''), 4.30 (d, *J* = 13.4 Hz, 1H, H-5'a), 4.24 (d, *J* = 9.4 Hz, 1H, H-4'), 3.99 (dd, *J* = 13.4, 2.3 Hz, 1H, H-5'b), 2.13 (s, 3H, Ac), 1.13 - 0.77 (m, 28H, Si^{i}Pr).

N^6-benzoyl-[3',5'-*O*-(1,1,3,3-tetra-*iso*-propyl-disiloxane-1,3-diyl)-2'-*O*-α-D-(3'',5''-di-*O*-benzoyl-arabinofuranosyl)] –adenosine

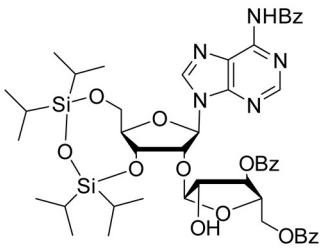

N^6-benzoyl-[3',5'-*O*-(1,1,3,3-tetra-*iso*-propyl-disiloxane-1,3-diyl)-2'-*O*-α-D-(2''-*O*-acetyl-3'',5''-di-*O*-benzoyl-arabinofuranosyl)] –adenosine (11.91 g, 11.96 mmol) was stirred with a 5 mM K_2CO_3 solution in methanol (MeOH, 500 mL) at 0 °C for 3 hours. Hydrogen chloride solution (0.25 mL, 37 %) was added and the mixture was stirred at 0 °C for another 10 minutes. The solvent was removed under reduced pressure, the residue was dissolved in EtOAc (500 mL) and washed with water (200 mL) and brine (200 mL). The organic phase was dried over Na_2SO_4 and concentrated under reduced pressure. The crude product was used in the next synthesis without further purification.

N^6-benzoyl-[3',5'-*O*-(1,1,3,3-tetra-*iso*-propyl-disiloxane-1,3-diyl)-2'-*O*-α-D-(3'',5''-di-*O*-benzoyl-ribofuranosyl)] –adenosine (13.4)

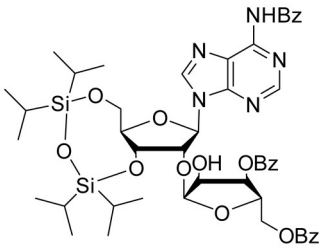

13.4

The crude product was stirred with acetic anhydride (2.10 mL, 22.22 mmol) in anhydrous DMSO (35 mL) under nitrogen atmosphere at room temperature for 22 hours. Abs. ethanol (EtOH, 80 mL) was added and the reaction mixture was stirred at 0 °C for 20 minutes. Sodium borohydride (0.83 g, 21.94 mmol) was added and the mixture was stirred for another 2 hours. After adding acetone (8 mL) and brine (100 mL), the mixture was extracted with EtOAc (300 mL). The organic phase was washed with brine (100 mL) and water (100 mL), dried over Na_2SO_4 and concentrated under reduced pressure. The crude product was purified by silica gel column chromatography (DCM/MeOH 99/1 to 97.5/2.5), yielding 5.03 g of N^6-benzoyl-[3',5'-*O*-(1,1,3,3-tetra-*iso*-propyl-disiloxane-1,3-diyl)-2'-*O*-α-D-(3'',5''-di-*O*-benzoyl-ribofuranosyl)] –adenosine (5.28 mmol, 44 % in 3 steps) as a white foam.

^{1}H-NMR (400 MHz, Chloroform-*d*) δ (ppm) 8.98 (s, 1H, H-2), 8.79 (s, 1H, H-8), 8.16 – 8.09 (m, 2H, arom. Bz), 8.02 (dd, *J* = 8.1, 1.5 Hz, 4H, arom. Bz), 7.64 – 7.50 (m, 5H, arom. Bz), 7.44 (td, *J* = 7.8, 3.2 Hz, 4H, arom. Bz), 6.20 (s, 1H, H-1'), 5.72 (d, *J* = 4.2 Hz, 1H, H-1''), 5.47 (dd, *J* = 7.2, 2.9 Hz, 1H, H-3''), 4.68 – 4.50 (m, 6H, H-2', H-2'', H-3', H-4'', H-5''), 4.32 (d, *J* = 13.4 Hz, 1H, H-5'a), 4.24 (d, *J* = 9.4 Hz, 1H, H-4'), 3.99 (dd, *J* = 13.4, 2.5 Hz, 1H, H-5'b), 1.14 - 0.94 (m, 28H, Si^{i}Pr).

N^6-benzoyl-2'-*O*-α-D-(3'',5''-di-*O*-benzoyl-ribofuranosyl) –adenosine (13.5)

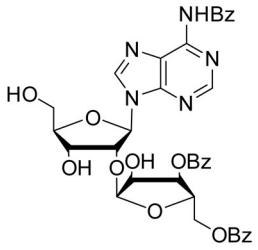

13.5

N^6-benzoyl-[3',5'-*O*-(1,1,3,3-tetra-*iso*-propyl-disiloxane-1,3-diyl)-2'-*O*-α-D-(3'',5''-di-*O*-benzoyl-ribofuranosyl)] –adenosine (4.05 g, 4.24 mmol) was stirred with triethylamine trihydrofluoride (TEA·3HF, 1 mL, 37 % HF) in anhydrous THF (35 mL) at 0 °C for 3 hours. Sat. aq. $NaHCO_3$ (50 mL) was added and the mixture was extracted with EtOAc (2x 150 mL). The organic phase was dried over Na_2SO_4, concentrated to dryness and used for the next synthesis without further purification.

N^6-benzoyl-[5'-*O*-(4,4'-dimethoxytrityl)-2'-*O*-α-D-(5''-*O*-benzoyl-ribofuranosyl)] –adenosine (13.6)

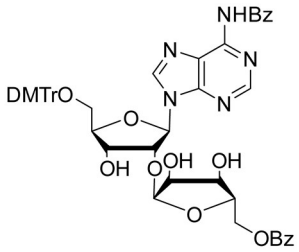

13.6

N^6-benzoyl-2'-*O*-α-D-(3'',5''-di-*O*-benzoyl-ribofuranosyl) –adenosine (2.81 g, 3.95 mmol) was stirred with dimethoxytrityl chloride (DMTrCl, 1.93 g, 5.69 mmol) in anhydrous pyridine (14 mL) at room temperature under nitrogen atmosphere for 16 hours. Abs. MeOH (3 mL) was added and the solvent was removed under reduced pressure. The residue was dissolved in EtOAc (200 mL), washed with sat. aq. $NaHCO_3$ (70 mL), dried over Na_2SO_4 and the solvent was removed under reduced pressure. The residue was dissolved in pyridine (20 mL), a 50 mM K_2CO_3 solution in MeOH (38 mL) was added and stirred at 0 °C for 3.5 hours. The

mixture was diluted with EtOAc (200 mL), washed with sat. aq. $NaHCO_3$ (50 mL) and brine (50 mL), dried over Na_2SO_4 and concentrated under reduced pressure. The crude product was purified by silica gel column chromatography (DCM/MeOH 100/1 to 50/1 to 25/1, 0.5 % TEA), yielding 1.96 g of *N*^{6}-benzoyl-[5'-*O*-(4,4'-dimethoxytrityl)-2'-*O*-α-D-(5''-*O*-benzoyl-ribofuranosyl)] –adenosine (2.15 mmol, 49 % in 3 steps).

^{1}H-NMR (400 MHz, DMSO-*d*$_6$) δ (ppm) 11.24 (s, 1H, NH), 8.68 (s, 1H, H-2), 8.63 (s, 1H, H-8), 8.07 – 8.03 (m, 2H, arom. Bz), 7.95 – 7.90 (m, 2H, arom. Bz), 7.64 (t, *J* = 7.3, 2H, DMTr), 7.55 (t, *J* = 7.6 Hz, 2H, arom. Bz), 7.49 (t, *J* = 7.7 Hz, 2H, arom. Bz), 7.36 (d, *J* = 7.5 Hz, 2H, DMTr), 7.26 – 7.20 (m, 7H, arom. Bz, DMTr), 6.81 (t, *J* = 9.0 Hz, 4H, DMTr), 6.27 (d, *J* = 4.1 Hz, 1H, H-1'), 5.22 (d, *J* = 4.1 Hz, 1H, H-1''), 5.16 (d, *J* = 6.7 Hz, 1H, C-2'' OH), 5.09 (t, *J* = 4.7 Hz, 1H, H-2'), 5.02 (d, *J* = 6.2 Hz, 1H, C-3' OH), 4.80 (d, *J* = 9.0 Hz, 1H, C-3'' OH), 4.58 (q, *J* = 5.5 Hz, 1H, H-3'), 4.42 – 4.29 (m, 3H, H-4'', H-5''), 4.21 (td, *J* = 5.4, 3.4 Hz, 1H, H-4'), 4.03 (q, *J* = 6.3, 5.9 Hz, 1H, H-2''), 3.98 (d, *J* = 5.5 Hz, 1H, H-3''), 3.71 (d, *J* = 2.1 Hz, 6H, -OCH_3), 3.30 - 3.18 (m, 2H, H-5').

N^6-benzoyl-[3'-*O*-TBDMS-5'-*O*-(4,4'-dimethoxytrityl)-2'-*O*-α-D-(2''-3''-di-*O*-TBDMS-5''-*O*-benzoyl-ribofuranosyl)] –adenosine (13.7)

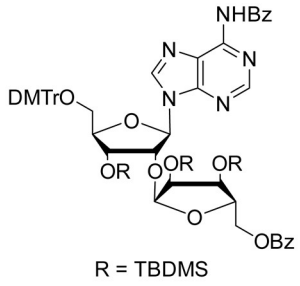

13.7

N^6-benzoyl-[5'-*O*-(4,4'-dimethoxytrityl)-2'-*O*-α-D-(5''-*O*-benzoyl-ribofuranosyl)] –adenosine (1.68 g, 1.85 mmol) was added to anhydrous DIPEA (2.10 mL, 12.06 mmol) and 4-dimethylaminopyridine (DMAP, 0.09 g, 0.74 mmol) in anhydrous *N,N*-dimethylformamide (DMF, 5mL) under nitrogen atmosphere at 0 °C. *Tert*-butyldimethylsilyltrifluoromethane sulfonate (TBDMSOTf, 1.3 mL, 5.66 mmol) was slowly added and the reaction mixture was stirred at 0 °C for 30 minutes and for another 4 hours at room temperature. The solution was diluted with EtOAc (80 mL), washed with sat. aq. $NaHCO_3$ (40 mL) and brine (40 mL). The organic phase was dried over Na_2SO_4, concentrated under reduced pressure and the crude product was purified by silica gel column chromatography (PE/EtOAc 2/1, 0.5 % TEA) to give 1.47 g of *N*^{6}-benzoyl-[3'-*O*-TBDMS-5'-*O*-(4,4'-dimethoxytrityl)-2'-*O*-α-D-(2''-3''-di-*O*-TBDMS-5'''-*O*-benzoyl-ribofuranosyl)] -adenosine (1.17 mmol, 63 %).

^{1}H-NMR (400 MHz, DMSO-*d*$_6$) δ (ppm) 11.20 (s, 1H, NH), 8.66 (s, 1H, H-2), 8.63 (s, 1H, H-8), 8.02 (d, *J* = 7.7 Hz, 2H, arom. Bz), 7.94 (d, *J* = 7.7 Hz, 2H, arom. Bz), 7.68 – 7.59 (m, 2H, DMTr),

7.54 (t, *J* = 7.5 Hz, 2H, arom. Bz), 7.48 (t, *J* = 7.6 Hz, 2H, arom. Bz), 7.29 (d, *J* = 7.7 Hz, 2H, DMTr), 7.25 – 7.11 (m, 7H, arom. Bz, DMTr), 6.80 (dd, *J* = 8.9, 2.3 Hz, 4H, DMTr), 6.21 (d, *J* = 3.9 Hz, 1H, H-1'), 5.26 (d, *J* = 2.8 Hz, 1H, H-1''), 5.08 (t, *J* = 4.4 Hz, 1H, H-2'), 4.76 (t, *J* = 5.0 Hz, 1H, H-3'), 4.53 (m, 1H, H-5''a), 4.32 – 4.24 (m, 1H, H-4''), 4.20 (dd, *J* = 11.8, 6.0 Hz, 1H, H-5''b), 4.14 (d, *J* = 5.0 Hz, 1H, H-4'), 4.09 (d, *J* = 6.2 Hz, 2H, H-2'', H-3''), 3.70 (s, 6H, -CH_3), 3.41 – 3.33 (m, 1H, H-5'a), 3.07 (dd, *J* = 10.8, 4.7 Hz, 1H, H-5'b), 0.89 – 0.76 (m, 27H, Si^{t}Bu), 0.07 (s, *J* = 6.3 Hz, 18H, $SiCH_3$).

N^6-benzoyl-[3'-*O*-TBDMS-5'-*O*-(4,4'-dimethoxytrityl)-2'-*O*-α-D-(2''-3''-di-*O*-TBDMS-ribofuranosyl)] –adenosine (13.8)

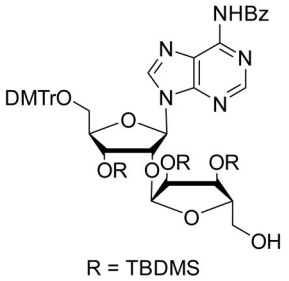

13.8

N^6-benzoyl-[3'-*O*-TBDMS-5'-O-(4,4'-dimethoxytrityl)-2'-*O*-α-D-(2''-3''-di-*O*-TBDMS-5''-*O*-benzoyl-ribofuranosyl)] –adenosine (1.47 g, 1.17 mmol) was dissolved in THF (10 mL). A 1 M LiOH solution in abs. EtOH (5 mL) was added and the mixture was stirred at 0 °C for 30 minutes and for another 3 hours at room temperature. The reaction mixture was diluted with EtOAc (60 mL), washed with water (30 mL) and sat. aq. $NaHCO_3$ (30 mL). The organic phase was dried over Na_2SO_4 and concentrated under reduced pressure. The crude product was purified by silica gel column chromatography (PE/EtOAc 2/1 to 1/1, 0.5 % TEA), to give 1.04 g of N^6-benzoyl-[3'-*O*-TBDMS-5'-*O*-(4,4'-dimethoxytrityl)-2'-*O*-α-D-(2''-3''-di-*O*-TBDMS-ribofuranosyl)] –adenosine (0.91 mmol, 78 %).

^{1}H-NMR (400 MHz, DMSO-d_6) δ (ppm) 8.69 (s, 1H, H-2), 8.62 (s, 1H, H-8), 8.06 – 7.99 (m, 2H, arom. Bz), 7.68 – 7.60 (m, 1H, arom. Bz), 7.54 (dd, *J* = 8.3, 6.9 Hz, 2H, arom. Bz), 7.34 – 7.27 (m, 2H, DMTr), 7.24 (t, *J* = 7.1 Hz, 2H, DMTr), 7.18 (ddd, *J* = 8.8, 4.5, 1.9 Hz, 5H, DMTr), 6.87 – 6.77 (m, 4H, DMTr), 6.21 (d, *J* = 3.9 Hz, 1H, H-1'), 5.10 (d, *J* = 3.4 Hz, 1H, H-1''), 5.06 (t, *J* = 4.3 Hz, 1H, H-2''), 4.78 (t, *J* = 5.1 Hz, 1H, H-3'), 4.64 (dd, *J* = 6.2, 4.6 Hz, 1H, C-5'' OH), 4.15 (q, *J* = 4.7 Hz, 1H, H-4'), 4.08 – 3.92 (m, 3H, H-2', H-3'', H-4''), 3.71 (d, *J* = 1.4 Hz, 6H, -CH_3), 3.56 – 3.47 (m, 1H, H-5'a), 3.38 (dd, *J* = 10.1, 6.1 Hz, 2H, H-5''), 3.10 (dd, *J* = 10.7, 4.9 Hz, 1H, H-5'b), 0.89 – 0.79 (m, 27H, Si^{t}Bu), 0.12 (s, 17H, $SiCH_3$).

N^6-benzoyl-[3'-*O*-TBDMS-2'-*O*-α-D-(2''-3''-di-*O*-TBDMS-5''-*O*-(di-fluorenylmethyl)-phosphoryl-ribofuranosyl)] –adenosine (13.9)

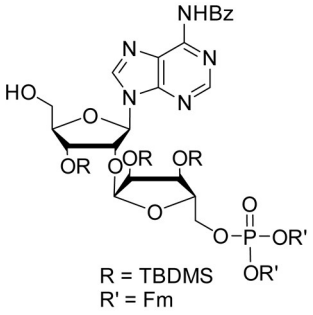

13.9

N^6-benzoyl-[3'-*O*-TBDMS-5'-*O*-(4,4'-dimethoxytrityl)-2'-*O*-α-D-(2''-3''-di-*O*-TBDMS-ribofuranosyl)] –adenosine (1.04 g, 0.91 mmol) was predried *in vacuo* and dissolved in anhydrous DMF (17 mL). Tetrazole (5.96 mL, 0.45 M in MeCN) and di-fluorenylmethyl *N,N*-di-*iso*-propyl phosphoramidite (7.26 mL, 0.91 mmol) were added and stirred for 2 hours at room temperature. Then tBuOOH (4.26 mL, 5.5 M in decane) was added and stirred for 30 minutes. The reaction was terminated with sat. aq. $NaHCO_3$ (20 mL) and extracted with EtOAc (20 mL). The organic phase was dried over Na_2SO_4 and concentrated under reduced pressure. The crude product was dissolved in DCM (55 mL), DCA (2.2 mL) was added and stirred at room temperature for 3 hours. Sat. aq. $NaHCO_3$ (30 mL) was added and the mixture was extracted with EtOAc (2x 30 mL). The organic phase was dried over Na_2SO_4 and concentrated under reduced pressure. The crude product was purified by silica gel column chromatography (DCM/MeOH 100/0 to 98/2) to give 1,12 g of N^6-benzoyl-[3'-*O*-TBDMS-2'-*O*-α-D-(2''-3''-di-*O*-TBDMS-5''-*O*-(di-fluorenylmethyl)-phosphoryl-ribofuranosyl)] –adenosine (0.88 mmol, 96 % in 2 steps).

^{1}H-NMR (400 MHz, Chloroform-*d*) δ (ppm) 8.71 (s, 1H, H-2), 8.07 (s, 1H, H-8), 8.01 (d, J = 7.6 Hz, 2H, arom. Bz), 7.70 (dt, J = 6.9, 14.5 Hz, 4H, arom. Bz, Fm), 7.60 (d, J = 7.4 Hz, 1H, Fm), 7.50 (m, 6H, Fm), 7.34 (dt, J = 7.2, 24.9 Hz, 4H, Fm), 7.23 (dd, J = 6.72, 14.35 Hz, 4H, Fm), 6.05 (d, J = 7.6 Hz 1H, H-1'), 4.97 (dd, J = 4.39, 7.81 Hz, 1H, H-1''), 4.86 (d, J = 3.31 Hz, 1H, H-2''), 4.56 (s, 1H, H-3'), 4.33 – 4.04 (m, 8H, H-2', H-4', H-5', H-3'', H-4'', H-5''), 3.85 (q, J = 5.0, 4.5 Hz, 2H, Fm), 3.67 (d, J = 2.8 Hz, 2H, Fm) 0.99 – 0.73 (m, 27H, Si^{t}Bu), 0.23 – -0.17 (m, 18H, $SiCH_3$).

^{31}P NMR (162 MHz, Chloroform-*d*) δ (ppm) -1.34 (s, 1P).

N^6-benzoyl-[3'-*O*-TBDMS-5'-*O*-phosphate-2'-*O*-α-D-(2''-3''-di-*O*-TBDMS-5''-*O*-(di-fluorenylmethyl)-phosphoryl-ribofuranosyl)] –adenosine (13.10)

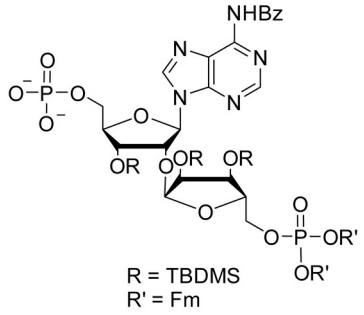

13.10

N^6-benzoyl-[3'-*O*-TBDMS-2'-*O*-α-D-(2''-3''-di-*O*-TBDMS-5''-*O*-(di-fluorenylmethyl)-phosphoryl-ribofuranosyl)] –adenosine (0.05 g, 0.04 mmol) was dissolved in anhydrous MeCN (5 mL) and cooled to 0 °C. $POCl_3$ (5 µL, 0.05 mmol) was added, followed by the addition of a catalytic amount of anhydrous pyridine. The reaction mixture was stirred at 0 °C for 4 hours and the reaction was terminated by the addition of 50 mM TEAB buffer. The solvent was removed under reduced pressure and the crude product was purified by RP-HPLC (Nucleodur C_{18} Pyramid, 50 mM TEAB, MeCN). After lyophilization, 17 mg of N^6-benzoyl-[3'-*O*-TBDMS-5'-*O*-phosphate-2'-*O*-α-D-(2''-3''-di-*O*-TBDMS-5''-*O*-(di-fluorenylmethyl)-phosphoryl-ribofuranosyl)] –adenosine (0.01 mmol, 25 %) was isolated.

^{1}H-NMR (400 MHz, Methanol-d_4) δ (ppm) 8.80 (s, 1H, H-2), 8.63 (s, 1H, H-8), 8.10 – 8.04 (m, 2H, arom. Bz), 7.76 – 7.68 (m, 5H, arom. Bz, Fm), 7.65 (ddq, J = 6.9, 4.1, 1.3 Hz, 2H, Fm), 7.60 – 7.54 (m, 2H, Fm), 7.49 – 7.15 (m, 10H, Fm), 6.30 (dd, J = 4.0, 2.4 Hz, 1H, H-1'), 5.24 (d, J = 3.9 Hz, 1H, H-1''), 4.68 (t, J = 4.1 Hz, 1H, H-2''), 4.59 (ddd, J = 6.9, 4.6, 2.7 Hz, 1H, H-3'), 4.36 - 3.85 (m, 14H, H-2', H-4', H-5', H-3'', H-4'', H-5'', Fm), 0.94 – 0.80 (m, 27H, Si^{t}Bu), 0.15 – 0.02 (m, 18H, $SiCH_3$).

^{31}P NMR (162 MHz, Methanol-d_4) δ (ppm) -0.01 (s, 1P), -0.67 (s, 1P).

5.1.2.5 Synthesis of 1-*O*-TBDPS-2,3-di-*O*-acetyl-5-*O*-*H*-phosphonate-β-D-ribose

5-*O*-triphenylmethyl-D-ribose (14.2)

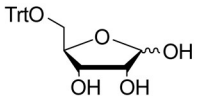

14.2

D-ribose (5 g, 33.3 mmol) was dissolved in pyridine (20 mL) and Trt-Cl (8.8 g, 31.64 mmol) was added. The reaction mixture was stirred for 18 hours at room temperature. The solvent was removed under reduced pressure and the residue was dissolved in DCM (50 mL), extracted with water (2x 50 mL) and brine (2x 50 mL). The organic phase was dried over $MgSO_4$ and concentrated under reduced pressure. The crude product was dissolved in DCM (9.5 mL) and under vigorous stirring added to cyclohexane (32 mL). After 1 hour, the resulting crystalline precipitate formed was filtered off and 9.91 g of 5-*O*-triphenylmethyl-D-ribose (25.3 mmol, 76 %) was isolated.

^{1}H NMR (500 MHz, Chloroform-*d*) δ (ppm) 7.47 – 7.10 (m, 15H, Trt), 5.38 (d, J = 4.3 Hz, 0.8H, H-1'β), 5.28 – 5.24 (m, 0.2H; H-1α), 4.34 (t, J = 5.5 Hz, 0.2H, H-3α), 4.21 (t, J = 3.8 Hz, 1.6H, H-2β, H-4β), 4.03 (ddd, J = 8.9, 4.6, 2.6 Hz, 1.2H, H-2α, H-4'α, H-3β), 3.39 – 3.34 (m, 0.2H, H-5aα), 3.28 (dd, J = 10.2, 4.0 Hz, 1H, H-5bα, H-5aβ), 3.12 (dd, J = 10.2, 3.9 Hz, 0.8H, H-5bβ).

1-*O*-TBDPS-5-*O*-triphenylmethyl-β-D-ribose (14.3)

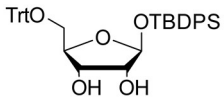

14.3

5-*O*-triphenylmethyl-D-ribose (2.72 g, 6.93 mmol) and imidazole (0.94 g, 13.86 mmol) were dissolved in anhydrous DMF (40 mL) at 0 °C. TBDPSCl (1.35 mL, 5.19 mmol) was added over 20 minutes and the reaction mixture was stirred at 0 °C for 5 hours. Sat. aq. NH_4Cl (100 mL) was added and the solvent mixture was extracted with DCM (150 mL). The organic phase was dried over $MgSO_4$ and concentrated under reduced pressure. The crude product was purified by silica gel column chromatography (PE/EtOAc 5/1 to 1/3), to give 0.45 g of 1-*O*-TBDPS-5-*O*-triphenylmethyl-β-D-ribose (0.72 mmol, 10 %) as white powder.

^{1}H NMR (400 MHz, DMSO-d_6) δ (ppm) 7.71 – 7.21 (m, 25H, Trt, Ph), 5.09 (s, 1H, H-1), 5.05 (d, J = 4.4 Hz, 1H, OH), 4.86 (d, J = 6.9 Hz, 1H, OH), 4.08 (q, J = 7.2 Hz, 1H, H-3), 3.96 (d, J = 9.4 Hz, 1H, H-4), 3.83 (t, J = 4.4 Hz, 1H, H-2), 3.25 (dd, J = 9.9, 3.3 Hz, 1H, H-5a), 3.06 (dd, J = 9.7, 6.0 Hz, 1H, H-5b), 0.91 (s, 9H, Si^{t}Bu).

1-*O*-TBDPS-2,3-di-*O*-acetyl-5-*O*-triphenylmethyl-β-D-ribose (14.4)

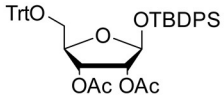

14.4

1-*O*-TBDPS-5-*O*-triphenylmethyl-β-D-ribose (0.45 g, 0.72 mmol) was dissolved in anhydrous pyridine (27 mL), acetic anhydride (1.35 mL, 14.38 mmol) was added and the reaction mixture was stirred for 6 hours at room temperature. The solvent was removed under reduced pressure and the residue was dissolved in DCM (30 mL). The organic phase was washed with water (2x 25 mL), brine (2x 25 mL), dried over $MgSO_4$ and concentrated under reduced pressure. The crude product was purified by silica gel column chromatography (PE/EtOAc 6/1), to give 0.44 g of 1-*O*-TBDPS-2,3-di-*O*-acetyl-5-*O*-triphenylmethyl-β-D-ribose (0.611 mmol, 85 %).

^{1}H NMR (500 MHz, Chloroform-*d*) δ (ppm) 7.68 – 7.19 (m, 25H, Trt, Ph), 5.46 (dd, J = 6.3, 4.7 Hz, 1H, H-4), 5.33 (dd, J = 4.7, 1.5 Hz, 1H, H-3), 5.27 (d, J = 1.5 Hz, 1H, H-1), 4.27 (q, J = 5.9 Hz, 1H, H-2), 3.40 – 3.29 (m, 2H, H-5), 2.03 (s, 3H, Ac), 1.99 (s, 3H, Ac), 0.96 (s, 9H, Si^{t}Bu).

1-*O*-TBDPS-2,3-di-*O*-acetyl-β-D-ribose (14.5)

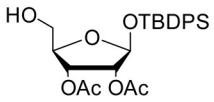

14.5

1-*O*-TBDPS-2,3-di-*O*-acetyl-5-*O*-triphenylmethyl-β-D-ribose (0.31 g, 0.43 mmol) was dissolved in DCM (10 mL) and cooled to 0 °C. Triethylsilane (0.27 mL, 1.71 mmol) and trifluoroacetic acid (TFA, 0.1 mL, 0.86 mmol) were added and the reaction mixture was stirred at 0 °C for 3 hours. Sat. aq. $NaHCO_3$ (150 mL) was added and the mixture was extracted with DCM (50 mL). The organic phase was dried over $MgSO_4$ and concentrated under reduced pressure. The crude product was purified by silica gel column chromatography (DCM/MeOH 99/1), yielding 0.14 g of 1-*O*-TBDPS-2,3-di-*O*-acetyl-β-D-ribose (0.29 mmol, 67 %).

^{1}H NMR (400 MHz, Chloroform-*d*) δ (ppm) 7.74 – 7.36 (m, 10H, Ph), 5.56 – 5.50 (m, 1H, H-4), 5.33 (s, 1H, H-1), 5.29 (d, J = 4.8 Hz, 1H, H-3), 4.17 (dt, J = 6.3, 3.2 Hz, 1H, H-2), 3.82 (d, J = 12.3 Hz, 1H, H-5a), 3.71 – 3.63 (m, 1H, H-5b), 2.05 (s, 3H, Ac), 2.01 (s, 3H, Ac), 1.09 (d, J = 2.1 Hz, 9H, Si^{t}Bu).

1-*O*-TBDPS-2,3-di-*O*-acetyl-5-*O*-*H*-phosphonate-β-D-ribose (14.6)

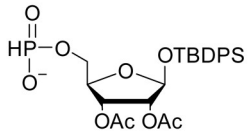

14.6

1-*O*-TBDPS-2,3-di-*O*-acetyl-β-D-ribose (0.19 g, 0.40 mmol) was dissolved in anhydrous pyridine (5 mL), cooled to 0 °C and diphenylphosphite (0.23 mL, 1.21 mmol) was added. The reaction mixture was stirred at 0 °C for 4 hours and TEA/water (10 mL, 1/1 v/v) was added and the solvent was removed under reduced pressure. The crude product was purified by RP-HPLC (Nucleodur C_{18} HTec, 50 mM TEAB, MeCN) and after lyophilization, 41 mg of 1-*O*-TBDPS-2,3-di-*O*-acetyl-5-*O*-*H*-phosphonate-β-D-ribose (0.08 mmol, 19 %) was isolated.

^{1}H NMR (400 MHz, Methanol-d_4) δ (ppm) 7.75 – 7.72 (m, 2H, Ph), 7.68 – 7.65 (m, 2H, Ph), 7.58 (s, 0.5H, P-H), 7.48 – 7.35 (m, 6H, Ph), 6.03 (s, 0.5H, P-H), 5.41 (dd, *J* = 6.5, 4.9 Hz, 1H, H-4), 5.27 (dd, *J* = 4.9, 1.6 Hz, 1H, H-3), 5.22 (d, *J* = 1.6 Hz, 1H, H-1), 4.26 - 4.20 (m, 1H, H-2), 4.08 - 4.02 (m, 2H, H 5), 2.03 (s, 3H, Ac), 1.98 (s, 3H, Ac), 1.08 (s, 9H, Si^{t}Bu).

^{31}P NMR (162 MHz, Methanol-d_4) δ (ppm) 5.19 (s, 1P).

5.1.2.6 Synthesis of N^6-benzoyl-2',3'-di-*O*-acetyl-5'-*O*-*H*-phosphonate-adenosine

N^6-benzoyl-5'-*O*-(4,4'-dimethoxytrityl)–adenosine (15.2)

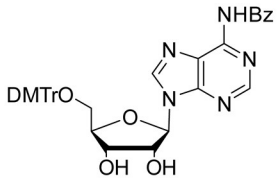

15.2

N^6-benzoyl–adenosine (3.0 g, 8.08 mmol) was dissolved in anhydrous pyridine (50 mL), DMTrCl (3.28 g, 9.69 mmol) was added and the mixture was stirred at room temperature for 2 hours. The reaction mixture was diluted with DCM (250 mL) and the organic phase was washed with sat. $NaHCO_3$ (150 mL) and brine (150 mL), dried over Na_2SO_4 and concentrated under reduced pressure. The crude product was purified by silica gel column chromatography (DCM/MeOH 98/2, 0.5 % TEA) to give 2.45 g of N^6-benzoyl-5'-*O*-(4,4'-dimethoxytrityl)–adenosine (3.63 mmol, 45 %).

^{1}H NMR (400 MHz DMSO-d_6) δ (ppm) 11.20 (bs, 1H, NH), 8.68 (s, 1H, H-8), 8.59 (s, 1H, H-2), 8.10 – 7.97 (m, 2H, arom. Bz), 7.68 – 7.49 (m, 3H, arom. Bz, DMTr), 7.36 (d, *J* = 7.4 Hz, 2H, arom. Bz), 7.24 (dd, *J* = 8.7, 3.0 Hz, 7H, DMTr), 6.83 (dd, *J* = 8.5, 5.6 Hz, 4H, DMTr), 6.07 (d, *J* = 4.7 Hz, 1H, H-1'), 5.62 (d, *J* = 5.7 Hz, 1H, OH), 5.27 (d, *J* = 5.6 Hz, 1H, OH), 4.79 (t, *J* = 5.0 Hz, 1H, H-2'), 4.33 (t, *J* = 5.1 Hz, 1H, H-3'), 4.12 (q, *J* = 4.7 Hz, 1H, H-4'), 3.72 (d, *J* = 1.4 Hz, 6H, OCH_3), 3.25 (d, *J* = 4.6 Hz, 2H, H-5').

N^6-benzoyl-2',3'-di-*O*-acetyl-5'-*O*-(4,4'-dimethoxytrityl)–adenosine (15.3)

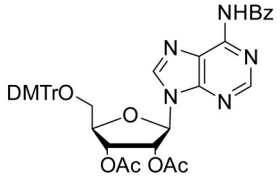

15.3

N^6-benzoyl-5'-*O*-(4,4'-dimethoxytrityl)–adenosine (2.45 g, 3.63 mmol) was dissolved in anhydrous pyridine (90 mL), acetic anhydride (0.86 mL) was added and the reaction was stirred at room temperature for 16 hours. DCM (250 mL) was added and the organic phase was washed with sat. aq. $NaHCO_3$ (100 mL), brine (100 mL), dried over Na_2SO_4 and concentrated under reduced pressure. The crude product was purified by silica gel column chromatography (DCM/MeOH 98/2, 0.5 % TEA), yielding 1.74 g of N^6-benzoyl-2',3'-di-*O*-acetyl-5'-*O*-(4,4'-dimethoxytrityl)–adenosine (2.36 mmol, 65 %).

^{1}H NMR (400 MHz, DMSO-d_6) δ (ppm) 11.26 (s, 1H, NH), 8.63 (s, 1H, H-8), 8.62 (s, 1H, H-2), 8.05 (d, *J* = 7.6 Hz, 2H, arom. Bz), 7.65 (t, *J* = 7.4 Hz, 1H, arom. Bz), 7.55 (t, *J* = 7.6 Hz, 2H,

arom. Bz), 7.44 – 7.14 (m, 9H, DMTr), 6.86 – 6.79 (m, 4H, DMTr), 6.35 (d, *J* = 5.4 Hz, 1H, H-1'), 6.22 (t, *J* = 5.7 Hz, 1H, H-2'), 5.75 (t, *J* = 5.3 Hz, 1H, H-3'), 4.33 (q, *J* = 4.6 Hz, 1H, H-4'), 3.72 (d, *J* = 1.5 Hz, 6H, OCH_3), 3.36 – 3.32 (m, 2H, H-5'), 2.11 (s, 3H, Ac), 2.05 (s, 3H, Ac).

N^6-benzoyl-2',3'-di-*O*-acetyl–adenosine (15.4)

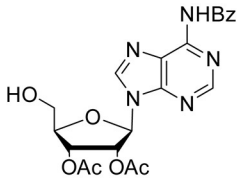

15.4

N^6-benzoyl-2',3'-di-*O*-acetyl-5'-*O*-(4,4'-dimethoxytrityl)–adenosine (1.74 g, 2.36 mmol) was dissolved in DCM (115 mL), DCA (5.7 mL) was added and stirred at room temperature for 2 hours. The reaction mixture was diluted with DCM (250 mL) and the organic phase was washed with water (150 mL) and sat. aq. $NaHCO_3$ (150 mL). The organic phase was dried over $MgSO_4$ and concentrated under reduced pressure. The crude product was purified by silica gel column chromatography (DCM/MeOH 97/3) to give 0.39 g of N^6-benzoyl-2',3'-di-*O*-acetyl–adenosine (0.87 mmol, 36 %).

^{1}H NMR (400 MHz, DMSO-d_6) δ (ppm) 11.62 (bs, 1H, NH), 9.13 (s, 1H, H-8), 9,08 (s, 1H, H-2), 8.45 – 8.33 (m, 2H, arom. Bz), 8.00 (t, *J* = 7.4 Hz, 1H, arom. Bz), 7.90 (t, *J* = 7.6 Hz, 2H, arom. Bz), 6.70 (d, *J* = 6.5 Hz, 1H, H-1'), 6.35 (t, *J* = 6.1 Hz, 1H, H-2'), 5.91 (dd, *J* = 5.8, 3.0 Hz, 1H, H-3'), 5.76 (t, *J* = 5.6 Hz, 1H, H-4'), 4.62 (q, *J* = 3.6 Hz, 1H, OH), 4.16 – 3.96 (m, 2H, H-5'), 2.50 (s, 3H, Ac), 2.36 (s, 3H, Ac).

N^6-benzoyl-2',3'-di-*O*-acetyl-5'-*O*-*H*-phosphonate–adenosine (15.5)

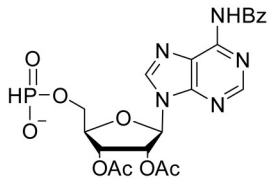

15.5

N^6-benzoyl-2',3'-di-*O*-acetyl–adenosine (0.39 g, 0.87 mmol) was dissolved in anhydrous pyridine (11 mL), diphenylphosphite (0.49 mL, 2.61 mmol) was added and the reaction mixture was stirred at 0 °C for 30 minutes. TEA/water (2.2 mL, 1/1 v/v) was added and the solvent was removed under reduced pressure. The crude product was purified by RP-HPLC (Nucleodur C_{18} Pyramid, 50 mM TEAB, MeCN), yielding 0.22 g of N^6-benzoyl-2',3'-di-*O*-acetyl-5'-*O*-*H*-phosphonate–adenosine (0.31 mmol, 36 %) after lyophilization.

^{1}H NMR (400 MHz, Methanol-d_4) δ (ppm) 8.78 (s, 1H, H-8), 8.74 (s, 1H, H-2), 8.11 – 8.05 (m, 2H, arom. Bz), 7.69 – 7.62 (m, 1H, arom. Bz), 7.61 – 7.53 (m, 2.5H, arom. Bz, H-P), 6.42 (d, *J* = 6.1 Hz, 1H, H-1'), 6.03 (s, 0.5H, H-P), 5.97 (t, *J* = 5.8 Hz, 1H, H-2'), 5.71 (dd, *J* = 5.6, 3.6 Hz, 1H, H-3'), 4.47 (qd, *J* = 3.5, 1.1 Hz, 1H, H-4'), 4.17 (qdt, *J* = 10.7, 7.0, 3.4 Hz, 2H, H-5'), 2.17 (s, 3H, Ac), 2.03 (s, 3H, Ac).

^{31}P NMR (162 MHz, Methanol-d_4) δ (ppm) 4.90 (s,1P).

5.1.2.7 Synthesis of ADP-ribose dimer

(1'-*O*-TBDPS-2',3'-di-*O*-acetyl-β-D-ribose)- N^6-benzoyl- [3''-*O*-TBDMS-2''-*O*-α-D-(2''',3'''-di-*O*-TBDMS-5'''-*O*-phosphate -ribofuranosyl] –adenosine (Ribose-13.10)

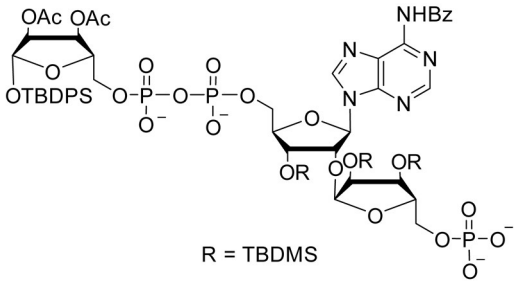

Ribose-13.10

1'-*O*-TBDPS-2',3'-di-*O*-acetyl-5'-*O*-*H*-phosphonate-β-D-ribose (48 mg, 0.09 mmol) was dissolved in MeCN (10 mL) and carbon tetrachloride (10 mL). TEA (44 µL, 0.32 mmol) and TMS-Im (27 µL, 0.18 mmol) were added and the reaction mixture was stirred at room temperature for 4 hours. The solvent was removed under reduced pressure and the residue was co-evaporated with MeCN (2x 10 mL), dissolved in *N,N*-dimethylformamide (6.5 mL) and added to N^6-benzoyl-[3'-*O*-TBDMS-5'-*O*-phosphate-2'-*O*-α-D-(2''-3''-di-*O*-TBDMS-5''-*O*-(di-fluorenylmethyl)-phosphoryl-ribofuranosyl)] –adenosine (49 mg, 0.03 mmol). The reaction mixture was stirred for 72 hours at room temperature. TEAB buffer (25 mL, 0.5 M) was added and the solvent was removed under reduced pressure. The residue was dissolved in DCM (25 mL) and washed with water (2x 25 mL). The organic phase was dried over $MgSO_4$ and concentrated under reduced pressure, to give 24 mg of (1'-*O*-TBDPS-2',3'-di-*O*-acetyl-β-D-ribose)- N^6-benzoyl- [3''-*O*-TBDMS-2''-*O*-α-D-(2''',3'''-di-*O*-TBDMS-5'''-*O*-phosphate -ribofuranosyl] –adenosine (0.016 mmol, 44 %) as a crude product, which was used for the next synthesis without further purification.

(1'-*O*-TBDPS-2',3'-di-*O*-acetyl-β-D-ribose)- N^6-benzoyl- [3''-*O*-TBDMS-2''-*O*-α-D-(2''',3'''-di-*O*-TBDMS-ribose- N^6-benzoyl-(2'''',3''''-di-*O*-acetyl) adenosine dinucleotide] – adenosine dinucleotide (protected diADPr)

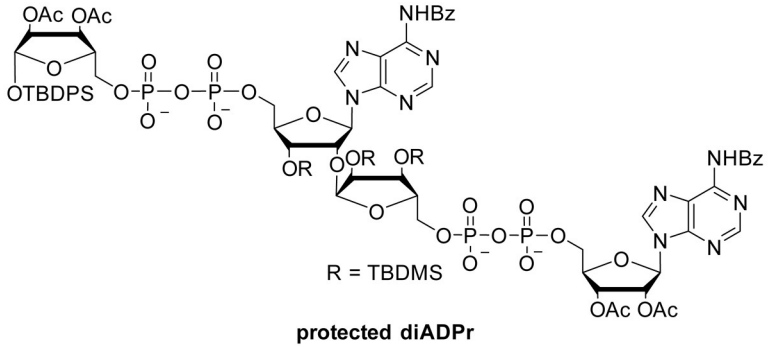

protected diADPr

N^6-benzoyl-2',3'-di-*O*-acetyl-5'-*O*-*H*-phosphonate–adenosine (20 mg, 0.04 mmol) was dissolved in MeCN (6 mL) and carbon tetrachloride (6 mL). TEA (19 µL, 0.14 mmol) and TMS-Im (11.8 µL, 0.08 mmol) were added and the reaction mixture was stirred at room temperature for 4 hours. The solvent was removed under reduced pressure and the residue was co-evaporated with MeCN (2x 5 mL), dissolved in DMF (4 mL) and added to (1'-*O*-TBDPS-2',3'-di-*O*-acetyl-β-D-ribose)- *N*^{6}-benzoyl- [3''-*O*-TBDMS-2''-*O*-α-D-(2''',3'''-di-*O*-TBDMS-5'''-*O*-phosphate -ribofuranosyl] –adenosine (24 mg, 0.016 mmol). The reaction mixture was stirred at room temperature for 120 hours. TEAB buffer (15 mL, 50 mM) was added and the solvent was removed under reduced pressure. The residue was dissolved in DCM (10 mL) and washed with water (2x 10 mL). The organic phase was dried over $MgSO_4$ concentrated under reduced pressure, yielding 4 mg of (1'-*O*-TBDPS-2',3'-di-*O*-acetyl-β-D-ribose)- *N*^{6}-benzoyl- [3''-*O*-TBDMS-2''-*O*-α-D-(2''',3'''-di-*O*-TBDMS-ribose- *N*^{6}-benzoyl-(2'''',3''''-di-*O*-acetyl) adenosine dinucleotide] –adenosine dinucleotide (0.002 mmol, 12 %) as crude product, which was used in the next synthesis without further purification.

D-ribose adenosine dinucleotide-2''-*O*-α-D-ribose adenosine dinucleotide (diADPr)

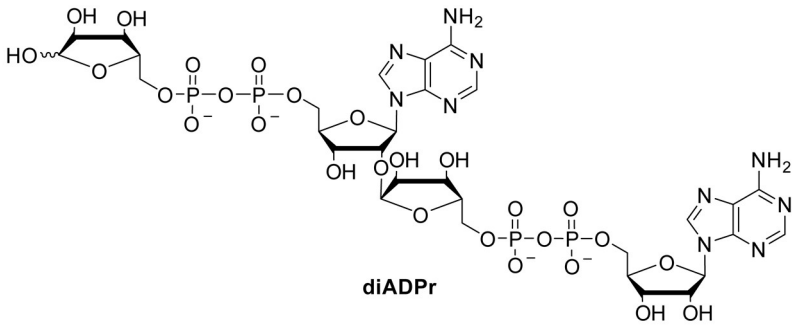

(1'-*O*-TBDPS-2',3'-di-*O*-acetyl-β-D-ribose)- *N*^{6}-benzoyl- [3''-*O*-TBDMS-2''-*O*-α-D-(2''',3'''-di-*O*-TBDMS-ribose- *N*^{6}-benzoyl-(2'''',3''''-di-*O*-acetyl) adenosine dinucleotide] –adenosine dinucleotide (4 mg, 0.002 mmol) was dissolved in methanolic ammonia (8 mL, 6 M) and stirred at room temperature for 18 hours. The solvent was removed under reduced pressure and the residue was co-evaporated with MeOH/TEA (10 mL, 9/1 v/v) and MeCN (10 mL). The residue was dissolved in THF (4 mL), TBAF (0.8 mL, 1.0 M in THF) was added and the reaction mixture was stirred at room temperature for 18 hours. The reaction was concentrated to 0.2 mL and aq. NaOAc (0.8 mL, 3 M) was added. The mixture was aliquoted to 0.1 mL in Eppendorf tubes and abs. EtOH (0.9 mL) was added. The tubes were cooled to –78 °C for 30 minutes and centrifuged (20 min., 14000 rcf, 4 °C). The supernatants were discarded and the pellets were resuspended in abs. EtOH (1mL). The tubes were again cooled to –78 °C for 30 minutes and centrifuged (20 min., 14000 rcf, 4 °C). All combined pellets were dissolved in Milli-Q water (0.8 mL) and purified by RP-HPLC (Nucleodur C_{18} Pyramid, 50 mM TEAB, MeCN).

The product was obtained as mixture with the de-ribosylated by-product, which was used for the next synthesis without separation, as the by-product is not reactive in the following reaction.

^{1}H NMR (400 MHz, Deuterium oxide) δ (ppm) 8.37 (s, 1H), 8.26 (s, 1H), 8.17 (s, 1H), 8.16 (s, 1H), 6.22 (d, J = 6.3 Hz, 1H), 6.08 (d, J = 4.6 Hz, 1H), 5.28 – 5.19 (m, 2H), 5.08 (d, J = 3.8 Hz, 1H), 4.91 (t, J = 5.8 Hz, 1H), 4.64 (t, J = 5.1 Hz, 1H), 4.59 – 4.52 (m, 3H), 4.43 – 4.30 (m, 6H), 4.29 – 4.14 (m, 9H), 4.10 – 3.99 (m, 6H).

^{31}P NMR (162 MHz, Deuterium Oxide) δ (ppm) -11.34 (m, 4P).

HRMS (ESI): m/z calcd for $C_{30}H_{42}N_{10}O_{27}P_4^{2-}$: 549.0580^{2-} [M-2H]; found 549.0599^{2-}.

5.1.2.8 Synthesis of thiocarbamate linker modified ADP-ribose dimer

Thiocarbamate linker modified ADP-ribose dimer (TC-diADPr)

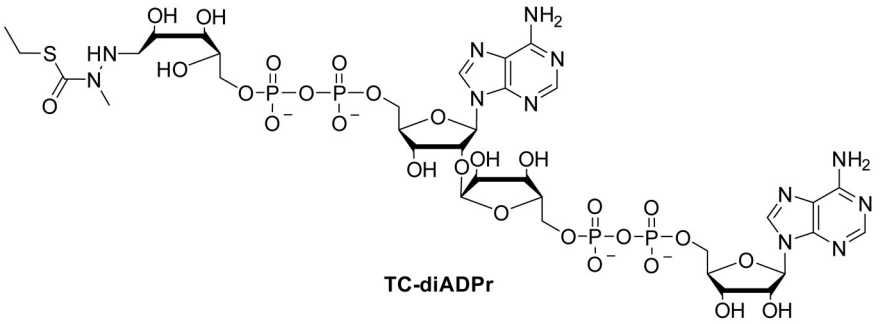

D-ribose adenosine dinucleotide-2''-*O*-α-D-ribose adenosine dinucleotide (0.36 mg, 0.33 µmol) was dissolved in Milli-Q water (1.7 mL). Acetic acid (0.1 mL) and *S*-Ethyl α-methylhydrazide thiocarbamate (22 µL, 1 M in DMSO) were added, followed by 50 µL DMSO. The mixture was freeze-thawed three times at –20 °C. Sodium cyanoborohydride (2.1 mg, 0.03 mmol) was added and the reaction mixture was stirred at 4 °C for 18 hours. The solvent was removed under reduced pressure and the crude product was purified by RP-HPLC (C_{18} HTec, 50 mM TEAB, MeCN). After lyophilization 0.034 mg of TC-diADPr (0.028 µmol, 8 %) was obtained.

LRMS (ESI): m/z calcd for $C_{34}H_{50}N_{12}O_{27}P_4S^{1-}$: 1217.18^{1-} [M-1H]; found 1217.19^{1-}.

5.2 Biochemical methods

5.2.1 Materials

Unless otherwise stated, water for biochemical methods was obtained from a Milli-Q purification system (Merck). All standard buffer chemicals were purchased in biological grade from Sigma-Aldrich/Merck, TCI, VWR, Carl Roth, ABCR, Acros Organics or Fluka. Mass spectrometry chemicals and solvents were purchased in LC-MS or UHPLC-MS grade.

5.2.1.1 Media and buffer solutions

Buffer were filtered through 0.4 µm pore size filters and bacterial culture media were autoclaved prior to use.

Buffer solution	**Composition**
Media	
LB medium	20 g/L LB broth, Carbenicillin 100 µg/mL
SOB medium	10 mM NaCl
	10 mM $MgCl_2$
	10 mM $MgSO_4$
	2 % (wt/v) tryptone
	0.5 % (wt/v) yeast extract
SOC medium	SOB medium
	20 mM glucose

Buffer solution	**Composition**
Protein purification	
Inclusion body buffer 1 (IB^+)	50 mM Tris HCl, pH 8.5
	100 mM NaCl
	1 mM EDTA
	1 % (v/v) Triton X-100
Inclusion body buffer 2 (IB^-)	50 mM Tris HCl, pH 8.5
	100 mM NaCl
	1 mM EDTA
Urea extraction buffer	50 mM Tris HCl, pH 7.0
	1 M NaCl
	6 M urea
	10 mM β-mercaptoethanol

Elution buffer with imidazole	50 mM Tris HCl, pH 7.5
	1 M NaCl
	6 M urea
	8 mM to 1 M imidazole
Elution buffer without imidazole	50 mM Tris HCl, pH 7.5
	1M NaCl
	6 M urea
Core histone lysis buffer 1	50 mM Tris HCl, pH 7.5
	100 mM NaCl
	1 mM EDTA
	1 mM PMSF
	5 mM β-mercaptoethanol
	1 % (v/v) Triton X-100
Core histone lysis buffer 2	50 mM Tris HCl, 7.5
	100 mM NaCl
	1 mM EDTA
	1 mM PMSF
	5 mM β-mercaptoethanol
Core histone unfolding buffer	20 mM Tris HCl, pH 7.5
	7 M guanidine HCl
	5 mM β-mercaptoethanol
10x SA buffer	400 mM NaOAc
	10 mM EDTA
	100 mM L-lysine
SAU 200/1000	1x SA buffer
	200 or 1000 mM NaCl
	7 M urea
	5 mM β-mercaptoethanol
TEV cleavage buffer	25 mM Tris HCl, pH 7.5
	150 mM NaCl
	1 mM DTT
PBS	137 mM NaCl
	2.7 mM KCl
	10 mM Na_2HPO_4
	1.8 mM KH_2PO_4

Buffer solution	**Composition**
Gel electrophoresis & Western Blot	
TAE	40 mM Tris HCl, pH 7.5 20 mM acetic acid 1 mM EDTA
Agarose gel (x %)	X % Agarose in 1x TAE and 0.5 µg/ml Ethidium bromide
10x TBE	900 mM Tris HCl, pH 8.3 900 mM boric acid 40 mM EDTA
10x SDS-PAGE running buffer	250 mM Tris HCl, pH 8.9 2 M glycine 1 % (wt/v) SDS
SDS-PAGE separating gel (x %)	X % (v/v) acrylamide/bisacrylamide (37.5:1) 375 mM Tris HCl, pH 8.8 0.1 % (wt/v) SDS 0.1 % (wt/v) APS 0.1 % (wt/v) TEMED
SDS-PAGE stacking gel (5 %)	5 % (v/v) acrylamide/bisacrylamide (37.5:1) 129 mM Tris HCl, pH 8.8 0.1 % (wt/v) SDS 0.1 % (wt/v) APS 0.1 % (wt/v) TEMED bromophenol blue
Native PAGE gel (7.5 %)	7.5 % (v/v) acrylamide/bisacrylamide (37.5:1) 0.8x TBE 0.16 % APS 0.08 % TEMED
6x SDS-PAGE loading dye	225 mM Tris HCl, pH 6.8 50 % (v/v) glycerol 5 % (wt/v) SDS

Coomassie staining solution	0.115 % (wt/v) Coomassie Brilliant blue R250 10 % (v/v) acetic acid 50 % (v/v) methanol
Coomassie destaining solution	10 % (v/v) acetic acid 50 % (v/v) methanol
20x Western blot transfer buffer	250 mM Tris HCl, pH 8.3 2 M glycine
20x TNE	200 mM Tris HCl, pH 7.6 50 mM EDTA 1 M NaCl
TNE-T	1x TNE 0.1 % (v/v) Tween 20
Western blot blocking solution	1x TNE-T 5 % (wt/v) milk powder

Buffer solution	**Composition**
Octamer assembly	
Octamer unfolding buffer	20 mM Tris HCl, pH 7.5 5 mM DTT 7 M guanidine HCl
Octamer refolding buffer	10 mM Tris HCl, pH 7.5 2 M NaCl 1 mM EDTA 5 mM β-mercaptoethanol

Buffer solution	**Composition**
Nucleosome and Chromatosome assembly	
Low salt buffer (LSB)	10 mM Tris HCl, pH 7.5 50 mM NaCl 1 mM EDTA 1 mM β-mercaptoethanol 0.05 % (v/v) Nonidet™ P-40 Substitute
High salt buffer (HSB)	10 mM Tris HCl, pH 7.5 2 M NaCl

	1 mM EDTA 1 mM β-mercaptoethanol 0.05 % (v/v) Nonidet™ P-40 Substitute

Buffer solution	**Composition**
Affinity enrichment	
HEK 293T lysis buffer	1x LSB 1x Roche cOmplete EDTA free Protease Inhibitor Cocktail 2 mM $MgCl_2$
Elution buffer	1x LSB without Nonidet™ P-40 Substitute 0.8 mM biotin

Buffer solution	**Composition**
Protein modification	
PARylation buffer, pH 7.5	0.15 M NaH_2PO_4 0.1 M NaCl

5.2.1.2 Oligonucleotides

Oligonucleotide	**5'- 3' Sequence**
H1.2 WT fw.	GCAACCCCGAAAAAAAGCGCAAAAAAAACG
H1.2 WT rev.	CGTTTTTTTTGCGCTTTTTTTCGGGGTTGC
H1.2 S150C fw.	GCAACCCCGAAAAAATGCGCAAAAAAAACG
H1.2 S150C rev.	CGTTTTTTTTGCGCATTTTTTCGGGGTTGC
Nuc. DNA fw.	ATCTAATACTAGGACCCTATACGC
Nuc. DNA rev.	TTTTTTTTTTTATCATTAATATGAATTCGGATCCACATG

Oligonucleotides were purchased from Biomers with RP-cartridge purification, although 5'-modified oligonucleotides purified by HPLC.

5.2.1.3 Plasmid constructs

Plasmid	Comment	Resistance	Origin
pET-11a H2A	-	Amp/Carb	Dr. Philip Saumer
pET-15b His_6-TEV-H2B	-	Amp/Carb	Dr. Philip Saumer
pET-11a H3	-	Amp/Carb	Dr. Philip Saumer
pET-15b His_6-TEV-H4	Traceless TEV cleavage site	Amp/Carb	Dr. Philip Saumer
pET-11a H1.2WT His_6	-	Amp/Carb	Dr. Simon Geigges
pUC-18 S3030	Contains nucleosomal DNA	Amp/Carb	Dr. Philip Saumer

5.2.1.4 Antibodies

No.	Antigen	Origin Species	Dilution	Supplier
1	Anti-histone H1	Rabbit, polyclonal	1:10000	Abcam ab17677
2	Anti-pan ADP-ribose binding reagent	Rabbit	1:5000	Merck
3	Anti-rabbit HRP		1:25000	Dianova
4	ExtrAvidin peroxidase	Chicken	1:400000	Merck

5.2.1.5 Chemicals/Enzymes

Chemical/Enzyme	Supplier
Acrylamide/Bisacrylamide (37.5;1), Rotiphorese Gel 30	Carl Roth
Agarose LE	Biozym
Biotin	TCI
BSA Standard (2 mg/mL)	Thermo Fisher Scientific
cOmplete EDTA free Protease Inhibitor Cocktail	Roche
cOmplete His-Tag purification resin	Roche
Core histone H4	Histonesource.com
dNTPs	Jena Bioscience
Ethidium bromide (1 %)	Carl Roth
GeneRuler 1kb DNA ladder	Thermo Fisher Scientific

Isopropyl-β-D-thiogalactopyranoside (IPTG)	Thermo Fisher Scientific
Linker histone H1, calf thymus	Merck
Milk powder (blotting grade)	Carl Roth
Nonidet™ P-40 Substitute	Fluka
PageRuler Prestained Protein Ladder	Thermo Fisher Scientific
PageRuler Unstained Protein Ladder	Thermo Fisher Scientific
Pierce ECL Western Blotting Substrate	Thermo Fisher Scientific
Pierce Protein G magnetic beads	Thermo Fisher Scientific
Pierce SuperSignal West Femto Maximum Sensitivity Substrate	Thermo Fisher Scientific
Roti-Quant 5x	Carl Roth
Taq polymerase	NEB
TriDye 100 bp DNA Ladder	NEB
TriDye 1 kb Plus DNA Ladder	NEB
Trypsin (sequencing grade)	Promega

5.2.1.6 Kits

Kit	**Supplier**
NucleoSpin Gel and PCR Clean-up Kit	Macherey-Nagel
Pierce BCA protein assay Kit	Thermo Fisher Scientific
QIAprep Spin Miniprep Kit	Qiagen
QIAquick Gel Extracktion Kit	Qiagen

5.2.1.7 Disposals

Product	**Supplier**
µ-C18 Zip Tips	Merck
96 PCR Plate non-skirted standard profile	VWR
Amersham Hybond 0.2 µm PVDF membrane	GE Healthcare
Amicon centrifugal tubes	Merck
Cuvettes	Carl Roth
Eppendorf tubes (1.5 mL, 2 mL)	Sarstedt
Eppendorf tubes(0.6 mL), siliconized PP	Biozym

Eppendorf tubes(1.5 mL, 2 mL), siliconized PP	Merck
Falcon tubes (15 mL, 50 mL)	Carl Roth
HiPPR detergent removal columns	Thermo Fisher Scientific
MS vials (250 µL)	Infochroma AG
Strip tubes for PCR	Thermo Fisher Scientific
PCR tubes	TreffLab
Pipette tips	Starlab
Serological pipettes	Sarstedt
Snakeskin dialysis tubing	Thermo Fisher Scientific
Syringe filter (0.2 µm, 0.45 µm)	Carl Roth
Vivaspin centrifugal filters	Sartorius

5.2.1.8 Equipment

Equipment	**Type**	**Supplier**
Electrophoresis Power Supply	PowerPac Basic	BioRad
Electrophoresis Power Supply	PowerPac 3000	BioRad
Electrophoresis cell	Mini-Protean II	BioRad
Centrifuge	Sorvall LYNX 4000	Thermo Fisher Scientific
Centrifuge	Multifuge 4 KR	Heraeus
Centrifuge	Primo R	Heraeus
Centrifuge	Centrifuge 5810 R	Eppendorf
Gel imager	AI600	Amersham, GE
Mass spectrometer	6546 LC/Q-TOF	Agilent
Mass spectrometer	Q-Exavtive HF	Thermo Fisher Scientific
Nanodrop	ND-1000	Peqlab
PCR cycler	LifeECO	Bioer
Photometer	BioPhotometer	Eppendorf
Pipettes	Research	Eppendorf
Sonifier	MS72 Sonotrode, HS2200 Sonifier 250	Bandelin Sonoplus Branson
Thermocycler	T1	Biometra
UHPLC	Easy nLC 1200	Thermo Fisher Scientific
UV imager	GelDoc Go	BioRad

5.2.2 Methods

5.2.2.1 Agarose gel electrophoresis

Agarose gel electrophoresis was performed using 0.8 % (wt/v) or 2.5 % (wt/v) agarose in 1x TAE buffer with ethidium bromide (5 µg/mL) added for DNA staining. DNA samples were mixed with 6x DNA loading dye (NEB) to a final concentration of 1x loading dye. Reading was performed on a GelDoc Go imager (BioRad). Preparative agarose gels were used to purify PCR products by band excision and clean up using NucleoSpin Gel and PCR Clean up kit (Macherey-Nagel).

5.2.2.2 SDS-PAGE

SDS-PAGE was used to analyze and separate proteins using a combination of a 5 % stacking gel and a 12.5 – 18 % resolving gel. Samples were mixed with 6x SDS loading dye to a final concentration of 1x loading dye and were incubated at 95 °C for 5 minutes. Electrophoresis was performed at 30 mA for 30 minutes (12.5 – 15 % gels) or at 30 mA for 105 minutes (18 % gels) in 1x SDS running gel buffer. For protein size comparison either the stained or the unstained PageRuler (Thermo Fisher Scientific) protein ladder was used. Proteins were visualized by Coomassie blue staining. Gels were incubated in Coomassie blue staining solution for 20 minutes followed by destaining in destaining solution for 30 minutes. Gels were incubated in Milli-Q water for 2 hours prior to imaging (Amersham Imager 600, GE Healthcare).

5.2.2.3 Western-blot

Detection of proteins or post-translational modifications of proteins was performed by Western blot analysis using specific antibodies. For this purpose, proteins from the SDS-PAGE gel were electrochemically transferred to a 0.2 µm PVDF membrane (Amersham) in 1x Western blot transfer buffer by applying 60 V for 90 minutes. The membrane was blocked with Western blot blocking solution at room temperature for 1 hour or at 4 °C overnight, followed by the addition of the primary antibody. This was incubated either at room temperature for 1 hours or at 4 °C overnight. The appropriate peroxidase-conjugated secondary antibody was added and incubated at room temperature for 1 hour. Chemiluminescence readout using ECL Western blotting Substrate or, for low intensity, SuperSignal Substrate (Thermo Fisher Scientific) was performed using an Amersham Imager 600 (GE Healthcare).

5.2.2.4 Native-PAGE

Nucleosome and chromatosome samples were analyzed by native PAGE using 7.5 % separating gels. First, the gel was pre-run without samples at 90 V for 1 hour in 0.5x TBE buffer. Samples were mixed with 50 % glycerol to a final concentration of 10 % glycerol and electrophoresed at 85 V for 2 hours in 0.5x TBE buffer. Followed to electrophoresis, DNA was stained with ethidium bromide (0.1 % v/v) in 0.5x TBE buffer for 15 minutes followed by destaining for 15 minutes in 0.5x TBE buffer. DNA was visualized using a GelDoc Go imager (BioRad).

5.2.2.5 Site-directed mutagenesis to introduce S150C in linker histone H1.2

Site-directed mutagenesis was performed using *Pfu Turbo* DNA polymerase (Agilent) under the manufacturer's conditions. The reaction mix contained 200 µM dNTPs (each), 0.26 µM primers (forward and reverse), 10 ng template and 0.05 U/µL *Pfu Turbo* DNA polymerase in 1x cloned Pfu reaction buffer. After DpnI (NEB) digestion at 37 °C for 90 minutes in 1x CutSmart buffer, the PCR product was analyzed via a 0.8 % agarose gel and purified using the NucleoSpin Gel and PCR Clean-up Kit (Macherey-Nagel). The purified DNA template (100 ng) was transformed into chemically competent *E. coli* XL10 gold cells (100 µL). Here, cells were incubated on ice for 5 minutes then heat shocked at 42 °C for 45 seconds and incubated on ice for 5 minutes. The cell mix was added to SOC medium (10 mM NaCl, 10 mM $MgCl_2$, 10 mM $MgSO_4$, 2 % tryptone (wt/v), 0.5 % yeast extract (wt/v), 20 mM glucose) at 37 °C for 1 hour prior to plating on LB agar plates containing carbenicillin disodium salt (100 mg/L). After overnight incubation at 37 °C, a single cell colony was picked and incubated in LB medium (containing 100 µg/mL carbenicillin disodium salt) at 37 °C. Cells were harvested and plasmids were isolated by using the QIAprep Spin Miniprep Kit (Qiagen) following the manufacturer's protocol. The sequences of the isolated DNA were verified by Sanger sequencing (GATC Biotech AG). The DNA plasmid (100 ng) was transformed into electrochemically competent *E. coli* BL21 (DE3) cells by electroporation using Gene Pulser cuvettes (0.1 cm gap, BioRad) and default settings for bacterial cells (Gene Pulser Xcell Electroporation System 1800 Vm, 5 ms, 200 Ω). After incubation on ice for 5 minutes, the cell suspension was mixed with SOC medium and incubated at 37 °C for 45 minutes. Cells were plated on LB agar places containing carbenicillin disodium salt and incubated overnight at 37 °C. A single cell colony was picked for overnight culture in 10 mL LB medium containing 100 µg/mL carbenicillin disodium salt (100 mg/L). 500 µL cells were mixed with 500 µL glycerol and stored at –80 °C.

5.2.2.6 Production and purification of linker histone H1.2 variants

1 L LB medium (containing 100 µg/mL carbenicillin disodium salt) was inoculated with 10 mL of overnight culture and incubated at 37 °C. The expression of the recombinant protein was induced by the addition of 1 mM IPTG at OD_{600} = 0.6 – 0.8. After incubation at 37 °C for 4 hours, cells were harvested by centrifugation (20 minutes, 4000 rpm, 4 °C). Cell pellets were resuspended in 20 mL inclusion body buffer 1 (50 mM Tris-HCl pH 8.5, 100 mM NaCl, 1 mM EDTA, 1 % (v/v) Triton X-100, 2 mM PMSF) and sonicated (3x 1 min, 8 cycles, 20 % power). After centrifugation (20 minutes, 17000 rpm, 4 °C), the cell pellet was washed once with 20 mL inclusion body buffer 1 and twice with 20 mL inclusion body buffer 2 (50 mM Tris-HCl pH 8.5, 100 mM NaCl, 1 mM EDTA). Inclusion bodies containing the respective linker histone H1.2 variant were macerated with 15 mL urea-containing buffer A (50 mM Tris-HCl pH 7.0, 1 M NaCl, 6 M urea, 10 mM β-mercaptoethanol) at 4 °C overnight in an overhead roller. After centrifugation (30 minutes, 21000 rpm, 4 °C), the supernatant was incubated with calibrated cOmplete His-Tag purification resin (Roche) supplemented with 5 mM imidazole at 4 °C overnight in an overhead roller. For bead calibration, 1 mL beads were washed 4 times with 15 mL urea-containing buffer A by alternate mixing and centrifugation (7 minutes, 800 rpm, 4 °C). The protein bead solution was applied onto a 15 mL chromatography column and the flow through was collected. After washing with 5 mL elution buffer (50 mM Tris-HCl pH 7.5, 1 M NaCl, 6 M urea), the linker histone variant was eluted and fractionated using a gradient from 8 mM to 500 mM imidazole in the elution buffer. Protein purification was analyzed by SDS-PAGE. Fractions containing the protein were combined and dialyzed (Snakeskin, 3500 MWCO, Thermo Fisher Scientific) against 5 L Milli-Q water, concentrated using an Amicon-Ultra 15 filter tube (10000 MWCO, Merck) and the final protein concentration was determined by the implementing the Pierce BCA Assay Kit (Thermo Fisher Scientific) following the manufacturer's protocol. The protein was aliquoted and stored at –20 °C.

5.2.2.7 ADP-ribosylation of linker histone H1.2 S150C

Thiocarbamate linker-modified ADP-ribose (TC-mADPr, TC-diADPr, 10 mM in Milli-Q water) was oxidized using the Oxone™ monopersulfate compound (10 mM, Merck) in Milli-Q water at 25 °C for 2 hours. Linker histone H1.2 S150C (500 µg/mL) was reduced with tris(2-carboxylethyl)-phosphine (TCEP, 2 mM, ABCR) in 1x PARylation buffer at 37 °C for 30 minutes. After combining 40 µL of the reduced protein (final concentration 400 µg/mL, 18 nM) and 10 µL of the oxidized thiocarbamate linker-modified ADP-ribose (final concentration 2 mM), the reaction mixture (50 µL) was incubated at 4 °C overnight. Protein

ADP-ribosylation was analyzed by SDS-PAGE, Western blotting (anti-pan PAR binding reagent, Merck) and full-length protein LC-MS measurements.

5.2.2.8 Biotinylation of linker histone H1.2 S150C with TC-biotin

TC-biotin (1 – 20 mM in DMSO) was oxidized using the Oxone™ monopersulfate compound (10 mM in Milli-Q water, Merck) at 25 °C for 2 hours. Linker histone H1.2 S150C (500 µg/mL) was reduced with TCEP (2 mM, ABCR) in 1x PARylation buffer at 37 °C for 30 minutes. After combining 24 µL of the reduced protein (final concentration 400 µg/mL, 18 nM) and 6 µL of the oxidized TC-biotin in indicated concentrations the reaction mixture (30 µL) was incubated at 25 °C overnight. Protein biotinylation was analyzed by SDS-PAGE and Western Blotting (ExtrAvidin Peroxidase, Merck).

5.2.2.9 Biotinylation of linker histone H1.2 S150C with biotin-maleimide

Linker histone H1.2 S150C (500 µg/mL) was reduced with TCEP (2 mM, ABCR) in Milli-Q water for 30 minutes at 37 °C. The reduced H1.2 S150C (final concentration 400 µg/mL) was combined with N-biotinoyl-N'-(6-maleimidohexanoyl) hydrazide (biotin-maleimide, final concentration 1 mM) and incubated at 30 °C for 1 hour. Protein biotinylation was analyzed by SDS-PAGE and Western blotting (ExtrAvidin Peroxidase, Merck).

5.2.2.10 Biotinylation of linker histone H1.2 WT

Linker histone H1.2 WT was subjected to the same reduction procedure as for the cysteine containing variant H1.2 S150C. H1.2 WT (500 µg/mL) was treated with TCEP (2 mM, ABCR) for 30 minutes at 37 °C in either 1x PARylation buffer (for TC-biotin) or in Milli-Q water (for biotin-maleimide and biotin-iodoacetamide).

For TC-biotin modification: TC-biotin (10 mM in DMSO) was oxidized using the Oxone™ monopersulfate compound (10 mM in Milli-Q water, Merck) at 25 °C for 2 hours. After combining the H1.2 WT (final concentration 400 µg/mL) and the ox. TC-biotin (final concentration 5 mM) the reaction mixture was incubated at 25 °C overnight.

For biotin-maleimide modification: Biotin-maleimide (final concentration 1 mM) was mixed with H1.2 WT (final concentration 400 µg/mL) and incubated at 30 °C for 1 hour.

For biotin-iodoacetamide modification: Biotin polyethyleneoxide iodoacetamide (final concentration 1 mM) was incubated with H1.2 WT (final concentration 400 µg/mL) at room temperature for 30 minutes in the dark.

All samples were analyzed by SDS-PAGE and Western blotting (ExtrAvidin Peroxidase, Merck).

5.2.2.11 Thiocarbamate linker stability assay

Modified proteins (either with TC-biotin or with biotin-maleimide, final concentration 100 µg/mL) were mixed with HEK293T cell lysate (final concentration 4 mg/mL in lysis buffer), GSH (final concentration 20 mM in Milli-Q water) or BSA (final concentration 75 µM in Milli-Q water). Samples were incubated at 37 °C for the indicated times. After each time point, a sample (10 µL) was taken and the reaction was terminated by adding 6x SDS-PAGE loading dye (2 µL) and heating to 95 °C for 5 minutes. Samples were analyzed by 12.5 % SDS-PAGE and Western blotting (ExtrAvidin Peroxidase, Merck).

5.2.2.12 Core histone expression, purification and octamer assembly

Core histones were expressed, purified and assembled to the core histone octamer by Dr. Philip Saumer and kindly provided for this thesis.[15,198]

Core histones were expressed and purified according to published methods.[20,199] Expression of H2A and H3 was performed in *E. coli* BL21 (DE3) cells. The expression culture was inoculated from an overnight culture to an OD_{600} = 0.05. Cells were grown to an OD_{600} = 0.3 at 37 °C and the expression was induced by the addition of IPTG (0.2 mM). After 3 -4 hours, cells were harvested by centrifugation, resuspended in a small volume of Milli-Q water and stored at -80 °C. Cell pellets were resuspended in core histone lysis buffer 1 (25 mL) and incubated at 30 °C for 30 minutes. After sonication (3x 15 seconds min, 8 cycles, 20 % power), the lysate was centrifuged (20 minutes, 27000 g, 4 °C) and the inclusion body pellet was washed with core histone lysis buffer 1 and twice with core histone lysis buffer 2. The cell pellet was resuspended in DMSO (350 µL), incubated at room temperature for 30 minutes and core histone unfolding buffer (13 mL) was added. After incubation at room temperature for 1 hour, the cell suspension was centrifuged (20 minutes, 25000 g, room temperature) and the extraction was repeated with 6.5 mL core histone unfolding buffer. The combined extracts were dialyzed (Snakeskin, 3500 MWCO, Thermo Fisher Scientific) against 2 L SAU 200. After sterile filtration (0.45 µm), the protein-containing solution was applied to HiTrap Q anion exchange column (5 mL, Cytiva). The flow-through and the first column volume was with SAU 200 were combined and applied to HiTrap SP HP cation exchange column (GE Life Sciences). After washing with 5 column volumes of SAU 200, histones were eluted with a binary gradient to SAU 1000. Histone-containing fractions were dialyzed (Snakeskin, 3500 MWCO, Thermo Fisher Scientific) against 5 L Milli-Q water at 4 °C overnight. H2B and H4 expression was carried out in *E. coli* BL21 (DE3) cells. Cultures were grown in SOC medium at 37 °C, transferred to LB medium (10 mL), grown for 1 hour at 37 °C and overnight at 30 °C. Cells were further grown at 37 °C to an OD_{600} = 1 and diluted with 50 mL pre-warmed LB

medium. After growth to OD_{600} = 1, cells were diluted with 1 L of LB medium to OD_{600} = 0.05, and grown at 37 °C to OD_{600} = 0.5. Protein expression was induced by addition of 1 mM IPTG and cells were harvested by centrifugation after 2 – 3 hours for H2B and 30 minutes for H4. Cell resuspension and DMSO solubilization was performed as described for H2A and H3. Solubilized cell pellets were diluted with 30 mL urea extraction buffer and incubated at 4 °C. Centrifugation (30 minutes, 21000 g, 4 °C) was performed followed by addition of the supernatant to cOmplete His-Tag Purification Resin (Roche, 4 mL for H2B, 2 mL for H4). After addition of imidazole to a final concentration of 5 mM, the samples were incubated at 4 °C overnight. A gradient of 8 mM to 1 M imidazole in the elution buffer was used for fractional elution of H2B and H4. Protein-containing fractions were pooled and dialyzed against Milli-Q water, followed by dialysis against TEV cleavage buffer (Snakeskin, 3500 MWCO, Thermo Fisher Scientific). TEV cleavage for H2B was performed by addition of TEV protease (1:15 wt/wt). After sterile filtration (0.45 µm), the solution was applied to HisTrap HP column (5 mL, GE Life Sciences). Cleaved His_6 tag and TEV protease were eluted with 500 mM imidazole in the TEV cleavage buffer and H2B was eluted with denaturing elution buffer. Protein-containing fractions were pooled and dialyzed against Milli-Q water at 4 °C overnight. H4 was cleaved with TEV protease (1:10 wt/wt) in TEV cleavage buffer and incubated at 30 °C for 5 hours. After dialysis against SAU 200 buffer at 4 °C overnight, H4 was applied to a HiTrap SP HP column (5 mL, GE Life Sciences). A binary gradient of 20 % to 70 % SAU 1000 eluted H4 in 7 column volumes. Protein-containing fractions were pooled and dialyzed (Snakeskin, 3500 MWCO, Thermo Fisher Scientific) against Milli-Q water at 4 °C overnight.

Core histone octamer was assembled according to a published procedure.[20] All 4 core histones were lyophilized prior to assembly. H2A (1.2 equivalents), H2B (1.2 equivalents), H3 (1.0 equivalents) and H4 (1.0 equivalents) were resuspended in octamer unfolding buffer and mixed to a final protein concentration of 1 mg/mL. Dialysis (Snakeskin, 3500 MWCO, Thermo Fisher Scientific) was performed 3 times against octamer refolding buffer at 4 °C overnight. The assembled core histone octamer was concentrated (10000 MWCO, Amicon, Merck) and applied to size exclusion chromatography (HiLoad 16/600 200 pg column, Cytiva). After addition of 10% glycerol, core histone octamer samples were stored at –80 °C.

5.2.2.13 Preparation of nucleosomal DNA

The 207 bp DNA for the nucleosome assembly was based on a published sequence containing a 601 bp nucleosome positioning sequence and 30 bp linkers on both sides, showing enhanced linker histone binding.[16-18,198] Nucleosomal DNA was amplified from pUC-18 backbone in a large scale PCR reaction in 96-well plates with a reaction size of 50 µL. Final concentrations in each reaction were 1x Thermopol buffer (NEB), 0.02 ng/µL template,

0.2 mM dNTPs (each), 0.25 mM primers (forward and reverse) and 0.025 U/µL Taq DNA polymerase (NEB). Initial denaturation was performed at 95 °C for 60 seconds, followed by 30 cycles of denaturation (15 seconds, 95 °C), annealing (20 seconds, 48.3 °C) and extension (5 minutes, 72 °C). The PCR product was purified using Nucleospin Gel and PCR Clean-up Kit (Macherey-Nagel) following the manufacturer's protocol. Final DNA concentration was determined by absorbance measurement at 260 nm (Nanodrop, Thermo Fisher Scientific).

5.2.2.14 Nucleosomal assembly

Nucleosomes were assembled by stepwise dialysis from high salt buffer (HSB) to low salt buffer (LSB) according to a published procedure.[19,20] Nucleosomal DNA (1.0 equivalents) was mixed with competitor DNA (crDNA, 0.05 equivalents, empty pUC-18 vector), BSA (3.85 equivalents, Thermo Fisher Scientific) and core histone octamer in HSB. Small scale assembly (9 µL) was performed to determine the ideal ratio of nucleosomal DNA to core histone octamer. Samples were dialyzed (Snakeskin, 3500 MWCO, Thermo Fisher Scientific) with decreasing salt concentration from 2 M to 0.23 M NaCl at 4 °C in 1 h intervals. Nucleosomes were then dialyzed at 4 °C overnight in LSB. Nucleosome concentration was determined by measuring total DNA concentration, which was converted to nucleosomal DNA concentration by the known ratio of nucleosomal to competitor DNA. Using the molecular weight of the nucleosomal DNA (133958.9 g/mol), the DNA concentration was transformed to the molar nucleosome concentration.

5.2.2.15 Chromatosome assembly

Chromatosome assembly was achieved by combining nucleosomes (0.4 µM in LSB) with linker histone variants H1.2 S150C, H1.2 mADPr and H1.2 diADPr in indicated ratios. Reaction mixtures were incubated at 19.5 °C for 35 minutes and analyzed by 7.5% native PAGE. The optimal ratio of nucleosome to linker histone was determined by small scale titration (7.5 µL), with the determined ratio being high enough to ensure complete conversion and low enough to avoid aggregation. The ratios between nucleosome and the linker histone variants were: H1.2 S150C 1:1, H1.2 mADPr 1:1.2 and H1.2 diADPr 1:2.

6 Appendix

6.1 Sequences

All DNA sequences are given from 5' to 3' and all protein sequences are given from N-terminus to C-terminus.

6.1.1 Linker histone variants

H1.2 WT (P16403)

The DNA sequence of the human linker histone variant H1.2 as cloned in pET-11a backbone, C-terminal His_6-tag is shown in blue.

ATGAGCGAAACCGCACCGGCAGCACCTGCTGCAGCACCTCCGGCAGAAAAAGCACCGGTTAAAAA
AAAAGCAGCCAAAAAAGCCGGTGGTACCCCGCGTAAAGCAAGCGGTCCTCCGGTTAGCGAACTGA
TTACCAAAGCAGTTGCAGCAAGCAAAGAACGTAGCGGTGTTAGCCTGGCAGCACTGAAAAAAGCA
CTGGCAGCAGCAGGTTATGATGTGGAAAAAAATAATAGCCGCATTAAACTGGGCCTGAAAAGCCT
GGTTAGCAAAGGCACCCTGGTTCAGACCAAAGGCACCGGTGCAAGCGGTTCATTTAAACTGAATA
AAAAAGCCGCAAGCGGTGAAGCAAAACCGAAAGTTAAAAAAGCGGGTGGCACCAAACCGAAAAAA
CCGGTTGGTGCAGCAAAAAAACCGAAAAAAGCAGCCGGTGGTGCAACCCCGAAAAAAAGCGCAAA
AAAAACGCCGAAAAAAGCCAAAAAACCGGCAGCAGCAACCGTTACCAAAAAAGTTGCAAAATCTC
CGAAAAAAGCGAAAGTTGCGAAACCGAAAAAGGCCGCAAAAAGCGCAGCAAAAGCAGTTAAACCG
AAAGCCGCTAAACCGAAAGTGGTTAAACCGAAGAAAGCGGCACCGAAAAAAAAA**CATCATCACC**
ATCACCACTAA

The amino acid sequence of human linker histone H1.2. The C-terminal His_6-tag is shown in blue. The first amino acid in the sequence (methionine) is cleaved during synthesis.

(M)SETAPAAPAAAPPAEKAPVKKKAAKKAGGTPRKASGPPVSELITKAVAASKERSGVSLAALKKA
LAAAGYDVEKNNSRIKLGLKSLVSKGTLVQTKGTGASGSFKLNKKAASGEAKPKVKKAGGTKPKKP
VGAAKKPKKAAGGATPKKSAKKTPKKAKKPAAATVTKKVAKSPKKAKVAKPKKAAKSAAKAVKP
KAAKPKVVKPKKAAPKKK**HHHHHH**

H1.2 S150C (P16403)

The DNA sequence of the human linker histone variant H1.2S150C (mutated codon shown in red) as cloned in pET11a backbone, C-terminal His_6-tag is shown in blue.

ATGAGCGAAACCGCACCGGCAGCACCTGCTGCAGCACCTCCGGCAGAAAAAGCACCGGTTAAAAA
AAAAGCAGCCAAAAAAGCCGGTGGTACCCCGCGTAAAGCAAGCGGTCCTCCGGTTAGCGAACTGA
TTACCAAAGCAGTTGCAGCAAGCAAAGAACGTAGCGGTGTTAGCCTGGCAGCACTGAAAAAAGCA
CTGGCAGCAGCAGGTTATGATGTGGAAAAAAATAATAGCCGCATTAAACTGGGCCTGAAAAGCCT
GGTTAGCAAAGGCACCCTGGTTCAGACCAAAGGCACCGGTGCAAGCGGTTCATTTAAACTGAATA
AAAAAGCCGCAAGCGGTGAAGCAAAACCGAAAGTTAAAAAAGCGGGTGGCACCAAACCGAAAAAA
CCGGTTGGTGCAGCAAAAAAACCGAAAAAAGCAGCCGGTGGTGCAACCCCGAAAAAATGCGCAAA
AAAAACGCCGAAAAAAGCCAAAAAACCGGCAGCAGCAACCGTTACCAAAAAAGTTGCAAAATCTC
CGAAAAAAGCGAAAGTTGCGAAACCGAAAAAGGCCGCAAAAAGCGCAGCAAAAGCAGTTAAACCG
AAAGCCGCTAAACCGAAAGTGGTTAAACCGAAGAAAGCGGCACCGAAAAAAAAA**CATCATCACC**
ATCACCACTAA

The amino acid sequence of the human linker histone variant H1.2S150C (mutation indicated in red). The C-terminal His_6-tag is shown in blue. The first amino acid in the sequence (methionine) is cleaved during synthesis.

(M)SETAPAAPAAAPPAEKAPVKKKAAKKAGGTPRKASGPPVSELITKAVAASKERSGVSLAALKKA
LAAAGYDVEKNNSRIKLGLKSLVSKGTLVQTKGTGASGSFKLNKKAASGEAKPKVKKAGGTKPKKP
VGAAKKPKKAAGGATPKKCAKKTPKKAKKPAAATVTKKVAKSPKKAKVAKPKKAAKSAAKAVKP
KAAKPKVVKPKKAAPKKKHHHHHH

6.1.2 Core histones

H2A (H2A 1-B/E, P04908)

The DNA sequence of the core histone H2A as cloned in pET11a backbone. The 5' NdeI and 3' BamHI cleavage sites are indicated in bold.

CATATGAGCGGTCGTGGTAAACAAGGTGGTAAAGCACGTGCAAAAGCAAAAACCCGTAGCAGCCG
TGCAGGTCTGCAGTTTCCGGTTGGTCGTGTTCATCGTCTGCTGCGTAAAGGTAATTATAGCGAAC
GTGTTGGTGCGGGTGCACCGGTTTATCTGGCAGCAGTTCTGGAATATCTGACCGCAGAAATTCTG
GAACTGGCAGGTAATGCAGCACGTGATAACAAAAAAACCCGCATTATTCCGCGTCATCTGCAGCT
GGCAATTCGTAATGATGAAGAACTGAATAAACTGCTGGGTCGTGTTACCATTGCGCAAGGTGGTG
TTCTGCCGAATATTCAGGCCGTTCTGCTGCCGAAAAAAACCGAAAGCCATCATAAAGCCAAAGGC
AAATAA**GGATCC**

The amino acid sequence of core histone H2A. The first amino acid in the sequence (methionine) is cleaved during synthesis.

(M)SGRGKQGGKARAKAKTRSSRAGLQFPVGRVHRLLRKGNYSERVGAGAPVYLAAVLEYLTAEILE
LAGNAARDNKKTRIIPRHLQLAIRNDEELNKLLGRVTIAQGGVLPNIQAVLLPKKTESHHKAKGK

H2B (H2B 1-J, P06899)

The DNA sequence of the core histone H2B as cloned in pET11a backbone. The 3' BamHI cleavage site are indicated in bold. The 5' NdeI cleavage site is removed by SDM during the incorporation of the TEV cleavage site (shown in green). The N-terminal His_6-tag is shown in blue.

ATGGGCAGCAGC**CATCATCATCATCATCAC**AGCAGCGGC**GAGAACCTGTACTTCCAGGGT**CCGG
AACCGGCAAAAAGCGCACCGGCACCGAAAAAAGGTAGCAAAAAAGCAGTTACCAAAGCGCAGAAA
AAAGACGGCAAAAAACGTAAACGTAGCCGCAAAGAAAGCTATAGCATCTATGTTTACAAAGTGCT
GAAACAGGTTCATCCGGATACCGGCATTAGCAGCAAAGCAATGGGTATTATGAATAGCTTCGTGA
ACGATATCTTTGAACGTATTGCCGGTGAAGCAAGCCGTCTGGCACATTATAACAAACGTAGCACC
ATTACCAGCCGTGAAATTCAGACCGCAGTTCGTCTGCTGCTGCCTGGTGAACTGGCAAAACATGCA
GTTAGCGAAGGCACCAAAGCCGTGACCAAATATACCAGCGCAAAATAA**GGATCC**

The amino acid sequence of core histone H2B. The first amino acid in the sequence (methionine) is cleaved during synthesis. The N-terminal His_6-tag is shown in blue and the TEV cleavage site is shown in red with the actual cleavage site marked by a vertical bar.

(M)GSS**HHHHHH**SSG**ENLYFQ**|**G**PEPAKSAPAPKKGSKKAVTKAQKKDGKKRKRSRKESYSIYVYK
VLKQVHPDTGISSKAMGIMNSFVNDIFERIAGEASRLAHYNKRSTITSREIQTAVRLLLPGELAKHAV
SEGTKAVTKYTSAK

H3 (H3.1, P68431)

The DNA sequence of the core histone H3 as cloned in pET11a backbone. The 5' NdeI and 3' BamHI cleavage sites are indicated in bold.

CATATGGCACGTACCAAACAGACCGCACGTAAAAGCACCGGTGGTAAAGCACCGCGTAAACAGCT
GGCAACCAAAGCAGCCCGTAAAAGCGCACCGGCAACCGGTGGTGTTAAAAAACCGCATCGTTATC
GTCCGGGTACAGTTGCACTGCGTGAAATTCGTCGTTATCAGAAAAGTACCGAACTGCTGATTCGT
AAACTGCCGTTTCAGCGTCTGGTTCGTGAAATTGCACAGGATTTCAAAACCGATCTGCGTTTTCAG
AGCAGCGCAGTTATGGCACTGCAAGAAGCATGCGAAGCATATCTGGTTGGCCTGTTTGAAGATAC
CAATCTGTGTGCAATTCATGCCAAACGTGTTACCATTATGCCGAAAGATATTCAGCTGGCACGTCG
TATTCGTGGTGAACGTGCATAA**GGATCC**

The amino acid sequence of core histone H3. The first amino acid in the sequence (methionine) is cleaved during synthesis.

(M)ARTKQTARKSTGGKAPRKQLATKAARKSAPATGGVKKPHRYRPGTVALREIRRYQKSTELLIR
KLPFQRLVREIAQDFKTDLRFQSSAVMALQEACEAYLVGLFEDTNLCAIHAKRVTIMPKDIQLARRI
RGERA

H4 (P62805)

The DNA sequence of the core histone H4 as cloned in pET11a backbone. The 3' BamHI cleavage site are indicated in bold. The 5' NdeI cleavage site is removed by SDM during the incorporation of the TEV cleavage site (indicated in green). The N-terminal His_6-tag is shown in blue.

ATGGGCAGCAGC**CATCATCATCATCATCAC**AGCAGCGGC**GAGAACCTGTACTTCCAGAGC**GGCC
GCGGCAAAGGTGGCAAAGGCCTGGGCAAGGGTGGCGCGAAACGCCATCGTAAAGTGCTGCGTGAT
AACATTCAGGGCATTACCAAACCGGCCATTCGTCGCCTGGCGCGTCGTGGCGGTGTGAAACGCATT
AGCGGTCTGATTTATGAAGAAACCCGTGGCGTGCTGAAAGTCTTTCTGGAAAACGTTATTCGTGA
TGCGGTGACCTATACCGAACATGCGAAACGCAAGACCGTGACGGCGATGGATGTTGTGTATGCAC
TGAAACGCCAGGGTCGCACCCTGTATGGTTTTGGCGGTTAA**GGATCC**

The amino acid sequence of core histone H4. The first amino acid in the sequence (methionine) is cleaved during synthesis. The N-terminal His_6-tag is shown in blue and the TEV cleavage site is shown in red with the actual cleavage site marked by a vertical bar.

(M)GSS**HHHHHH**SSG**ENLYFQ**|**S**GRGKGGKGLGKGGAKRHRKVLRDNIQGITKPAIRRLARRGGVK
RISGLIYEETRGVLKVFLENVIRDAVTYTEHAKRKTVTAMDVVYALKRQGRTLYGFGG

6.1.3 Nucleosomal DNA

Sequence of nucleosomal DNA used for affinity enrichment studies.[18] The 5' desthiobiotin (DTB) label is indicated in bold, the following 11 deoxythymidine spacers are underlined. The nucleosome positioning sequence is shown in light blue.

DTB-TTTTTTTTTTTATCTAATACTAGGACCCTATACGCGGCCGCATCGGAGAATCCCGGTGCCGA
GGCCGCTCAATTGGTCGTAGACAGCTCTAGCACCGCTTAAACGCACGTACGCGCTGTCCCCCGCGT
TTTAACCGCCAAGGGGATTACTCCCTAGTCTCCAGGCACGTGTCAGATATATACATCGATTGCATG
TGGATCCGAATTCATATTAATGAT

6.2 Supplementary schemes

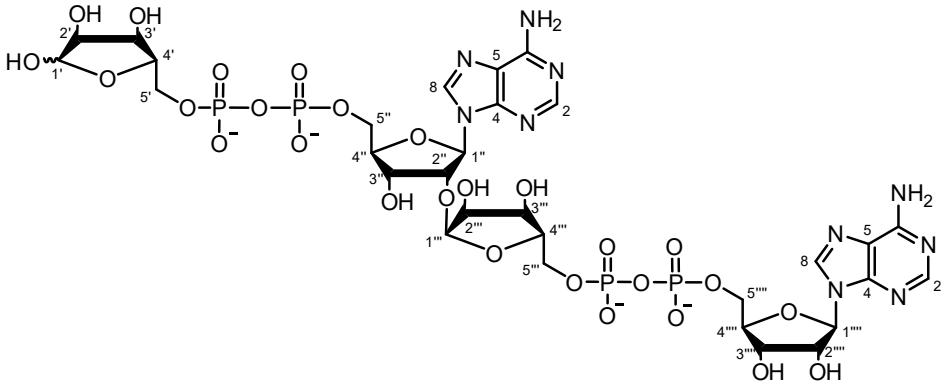

Scheme S1. Nomenclature for ADP-ribose dimer (diADPr).

6.3 Supplementary figures

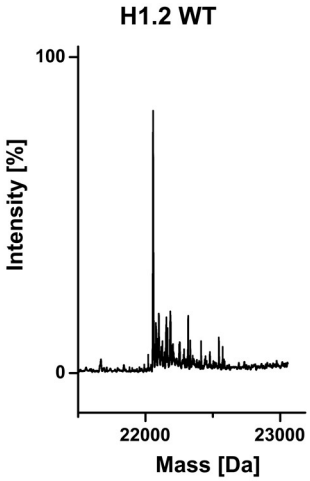

Figure S1 Full length protein MS measurement of the linker histone H1.2 WT. Calculated 22056 Da, measured 22056 Da.

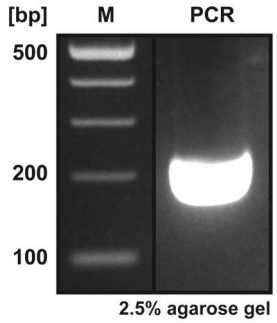

Figure S2. Agarose gel analysis of the PCR reaction producing the nucleosomal DNA. Nucleosomal DNA was produced by PCR and the product was applied to 2.5% agarose gel analysis revealing a band of the desired size (207 bp).

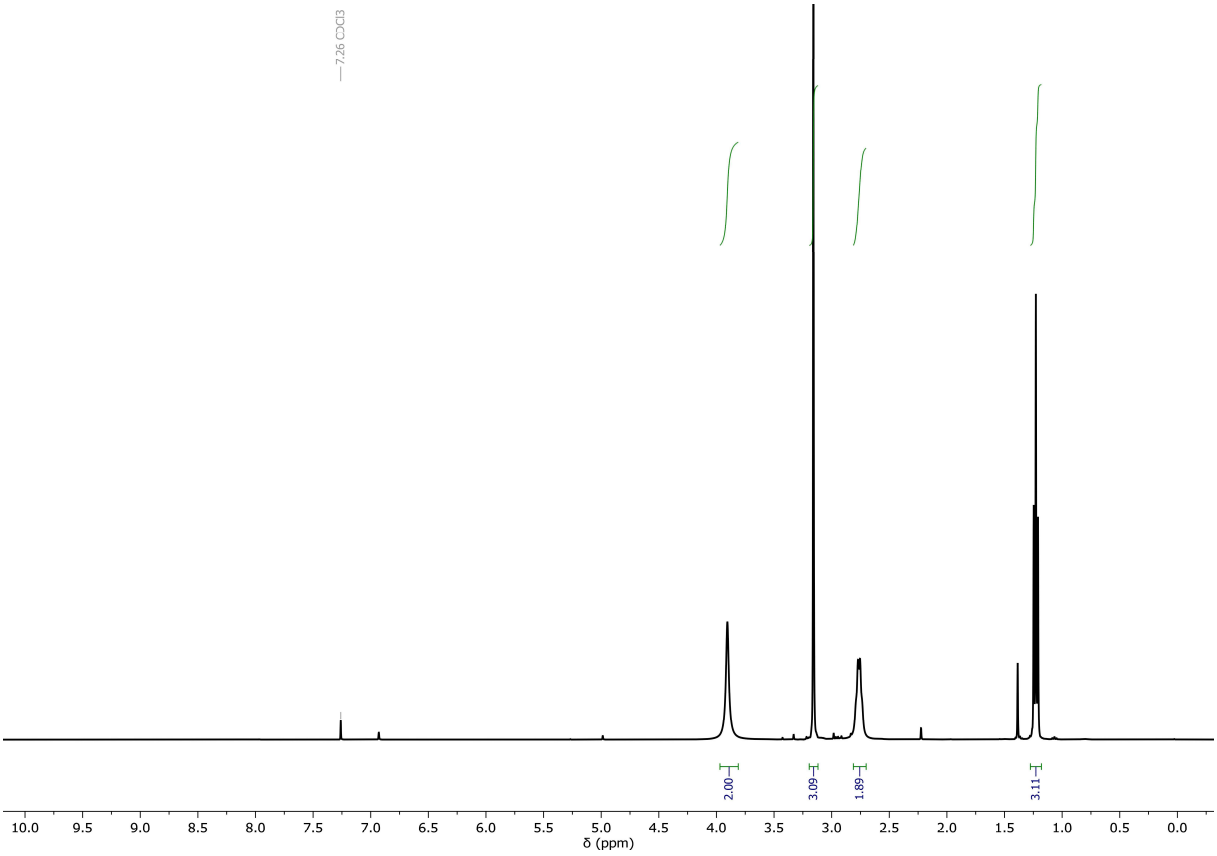

Figure S3. ^{1}H NMR spectrum of *S*-Ethyl α-methylhydrazide thiocarbamate.

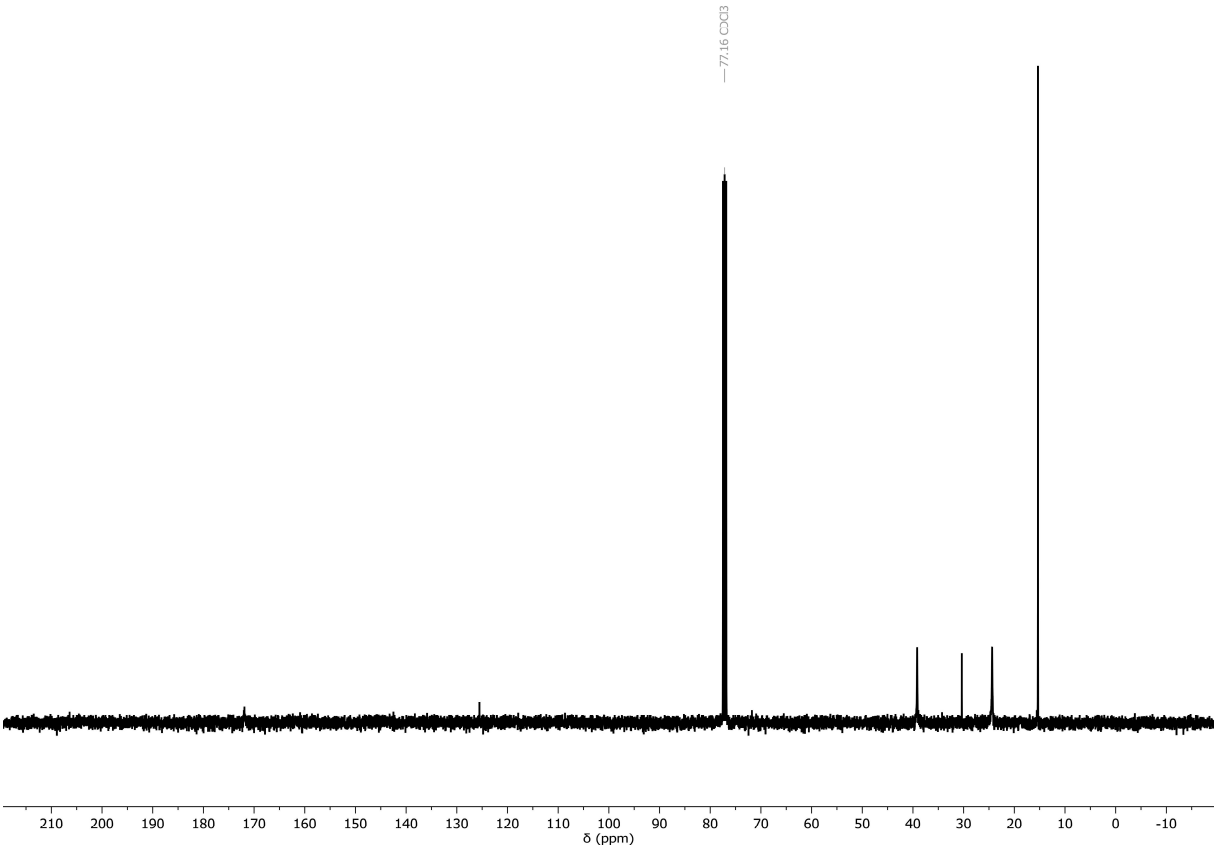

Figure S4. ^{13}C NMR spectrum of *S*-Ethyl α-methylhydrazide thiocarbamate.

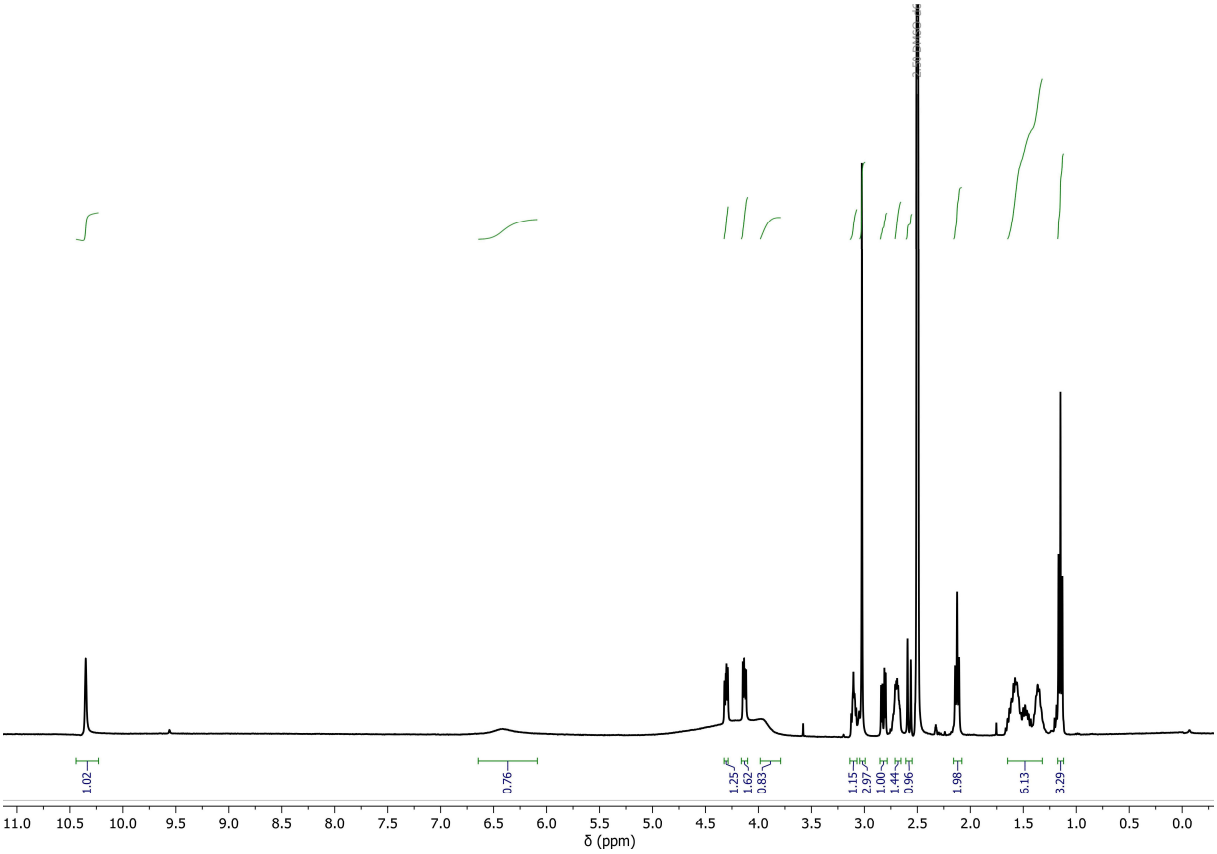

Figure S5. ^{1}H NMR spectrum of thiocarbamate linker modified biotin (TC-biotin).

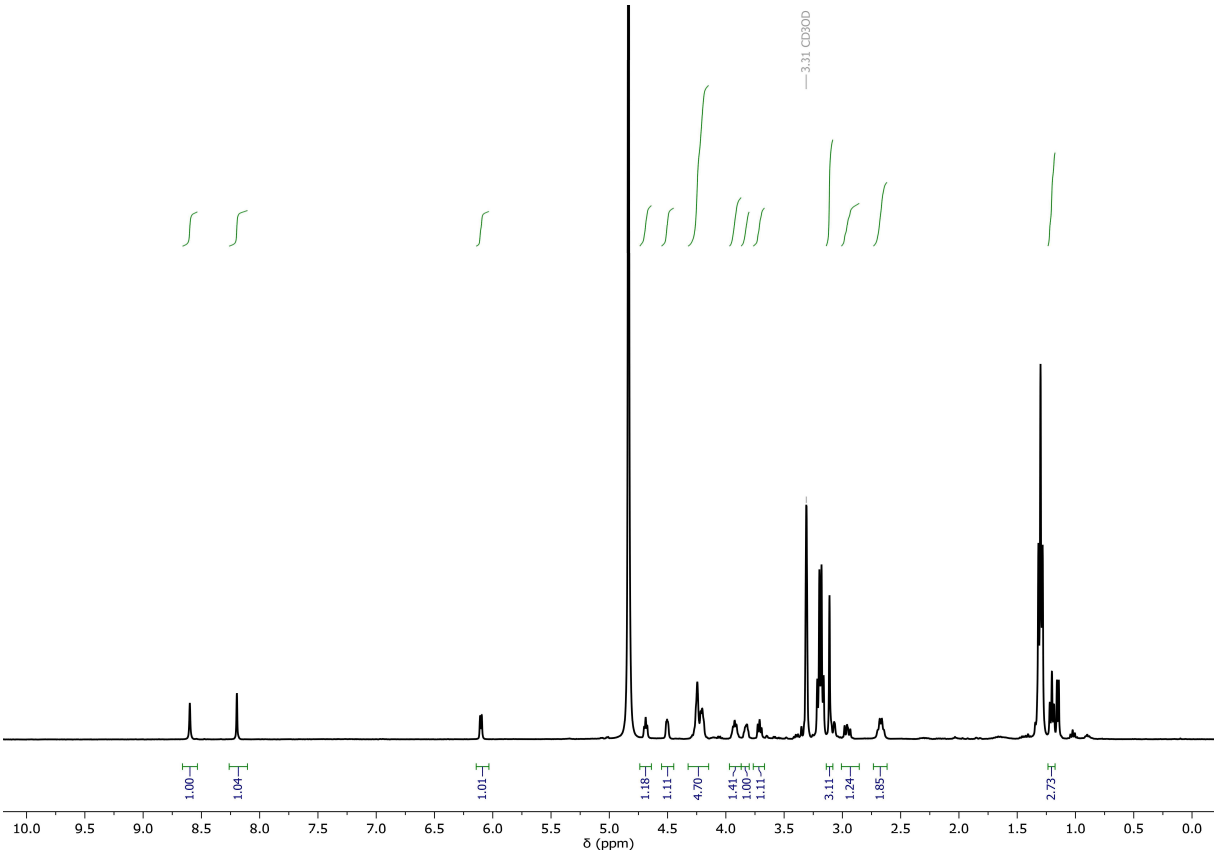

Figure S6. ^{1}H NMR spectrum of thiocarbamate linker modified mono-ADP-ribose (TC-mADPr).

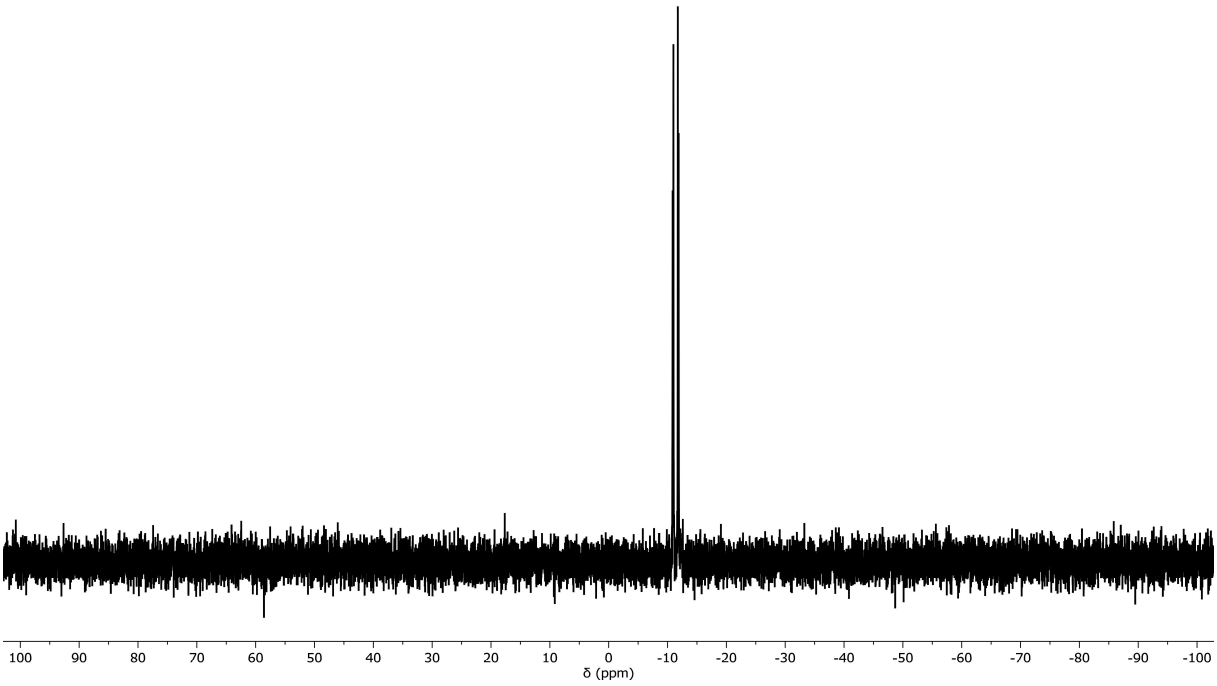

Figure S7. ^{31}P NMR spectrum of thiocarbamate linker modified mono-ADP-ribose (TC-mADPr).

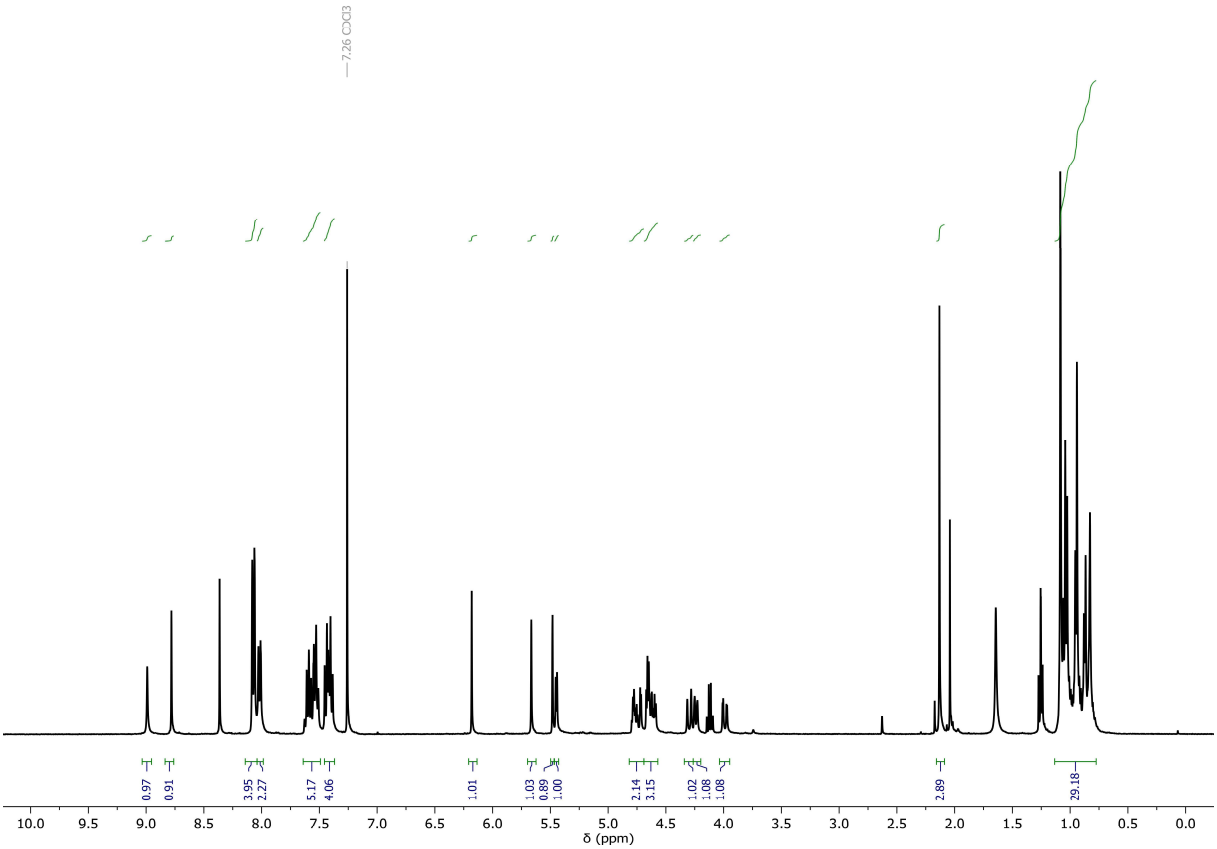

Figure S8. ^{1}H NMR spectrum of *N*^{6}-benzoyl-[3',5'-*O*-1,1,3,3-tetra-*iso*-propyl-disiloxane-1,3-diyl)-2'-*O*-α-D-(2''-*O*-acetyl-3'',5''-di-*O*-benzoyl-arabinofuranosyl)] –adenosine (13.3).

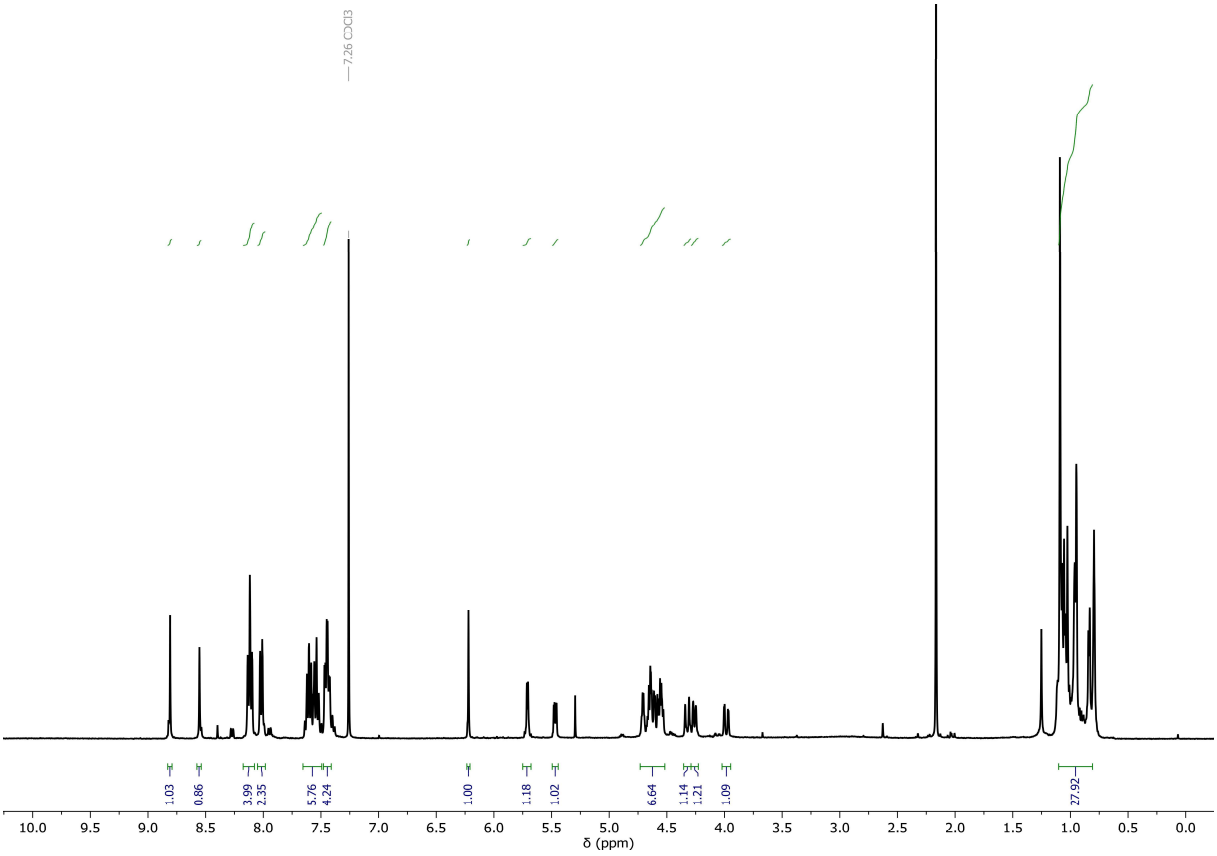

Figure S9. ^{1}H NMR spectrum of N^{6}-benzoyl-[3',5'-*O*-1,1,3,3-tetra-*iso*-propyl-disiloxane-1,3-diyl)-2'-*O*-α-D-(3'',5''-di-*O*-benzoyl-ribofuranosyl)] –adenosine (13.4).

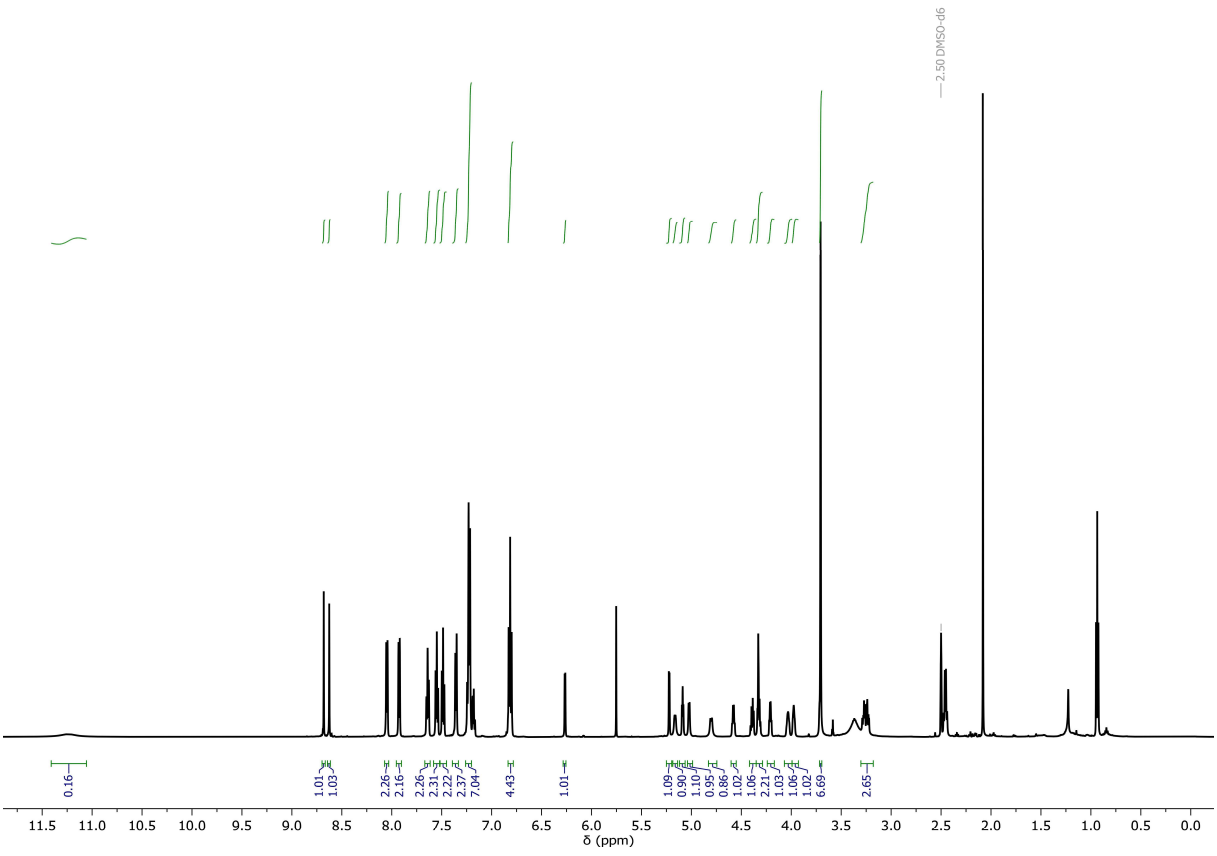

Figure S10. ^{1}H NMR spectrum of N^{6}-benzoyl-[5'-*O*-(4,4'-dimethoxytrityl)-2'-*O*-α-D-(5''-di-*O*-benzoyl-ribofuranosyl) –adenosine (13.6).

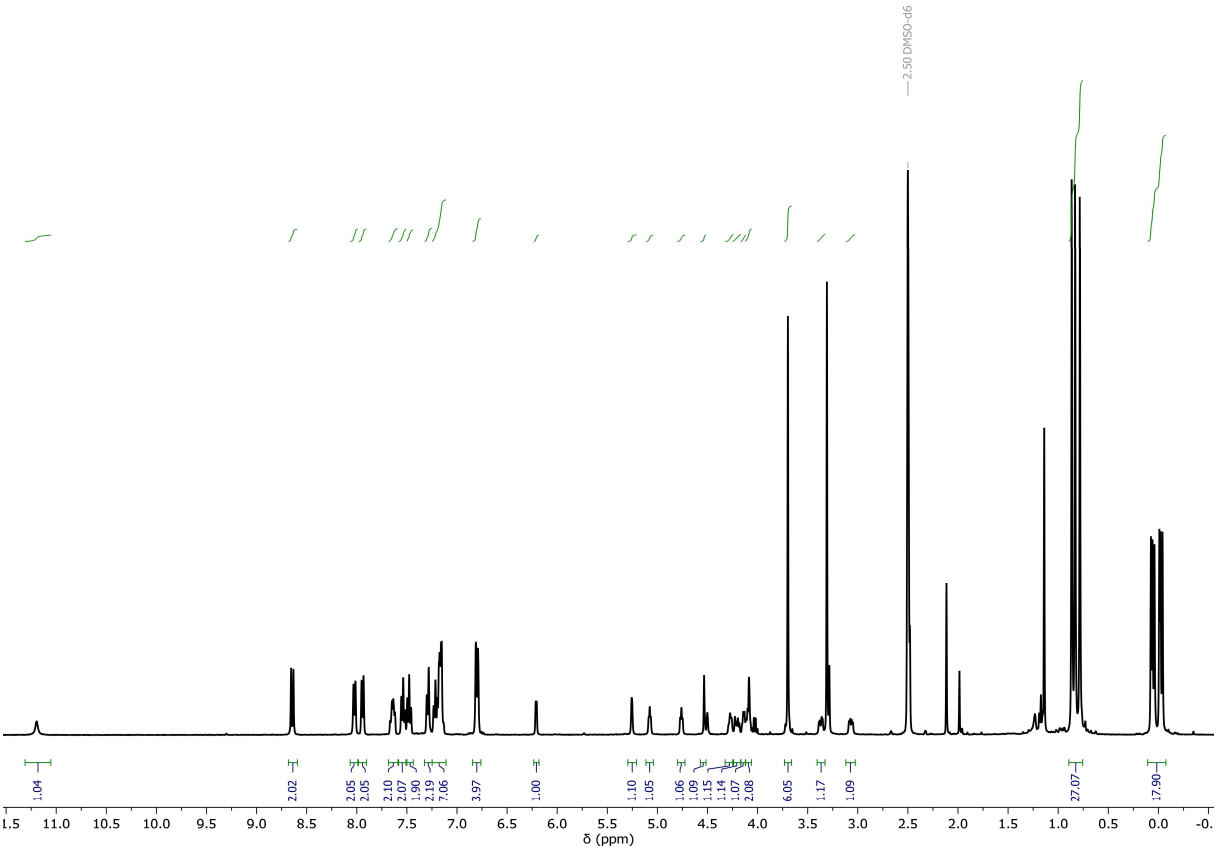

Figure S11. ^{1}H NMR spectrum of N^{6}-benzoyl-[3'-*O*-TBDMS-5'-*O*-(4,4'-dimethoxytrityl)-2'-*O*-α-D-(2'',3''-di-*O*-TBDMS-5''-di-*O*-benzoyl-ribofuranosyl) –adenosine (13.7).

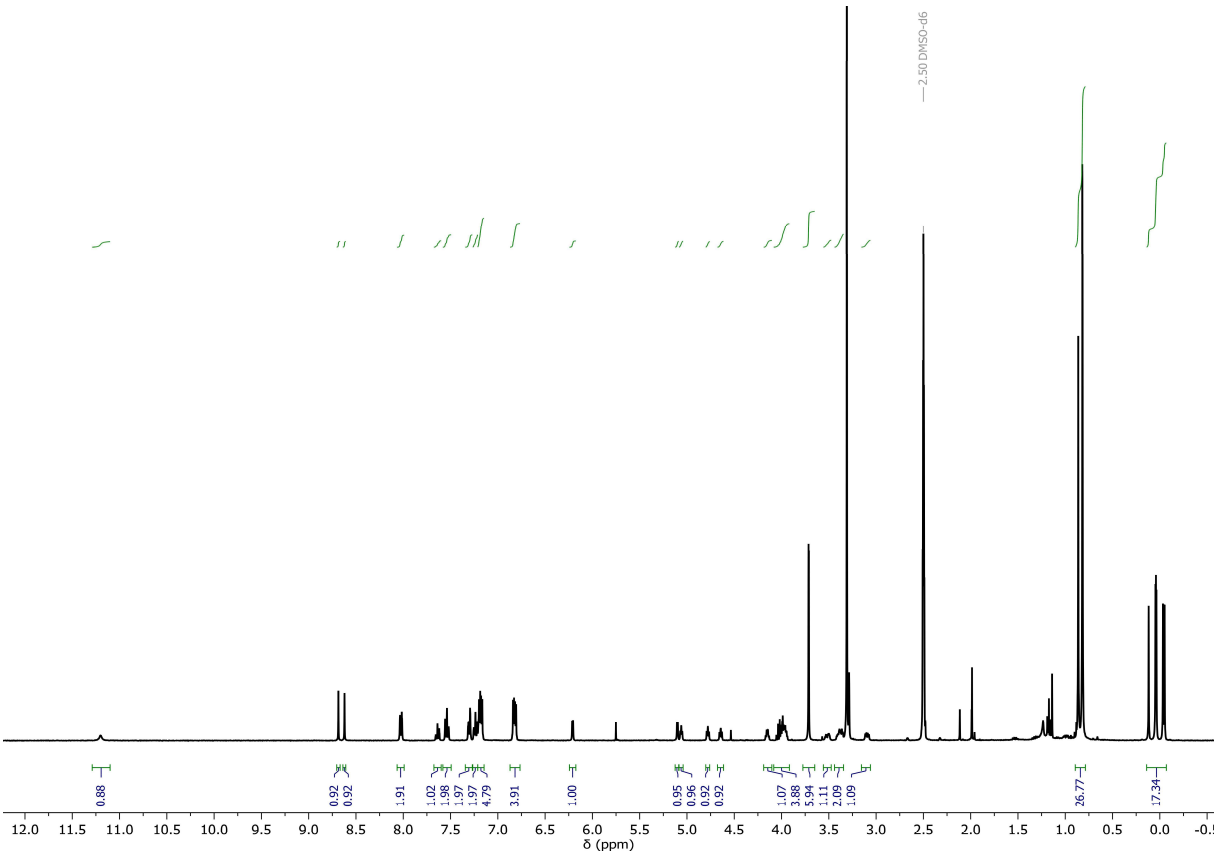

Figure S12. ^{1}H NMR spectrum of N^{6}-benzoyl-[3'-*O*-TBDMS-5'-*O*-(4,4'-dimethoxytrityl)-2'-*O*-α-D-(2'',3''-di-*O*-TBDMS-ribofuranosyl) –adenosine (13.8).

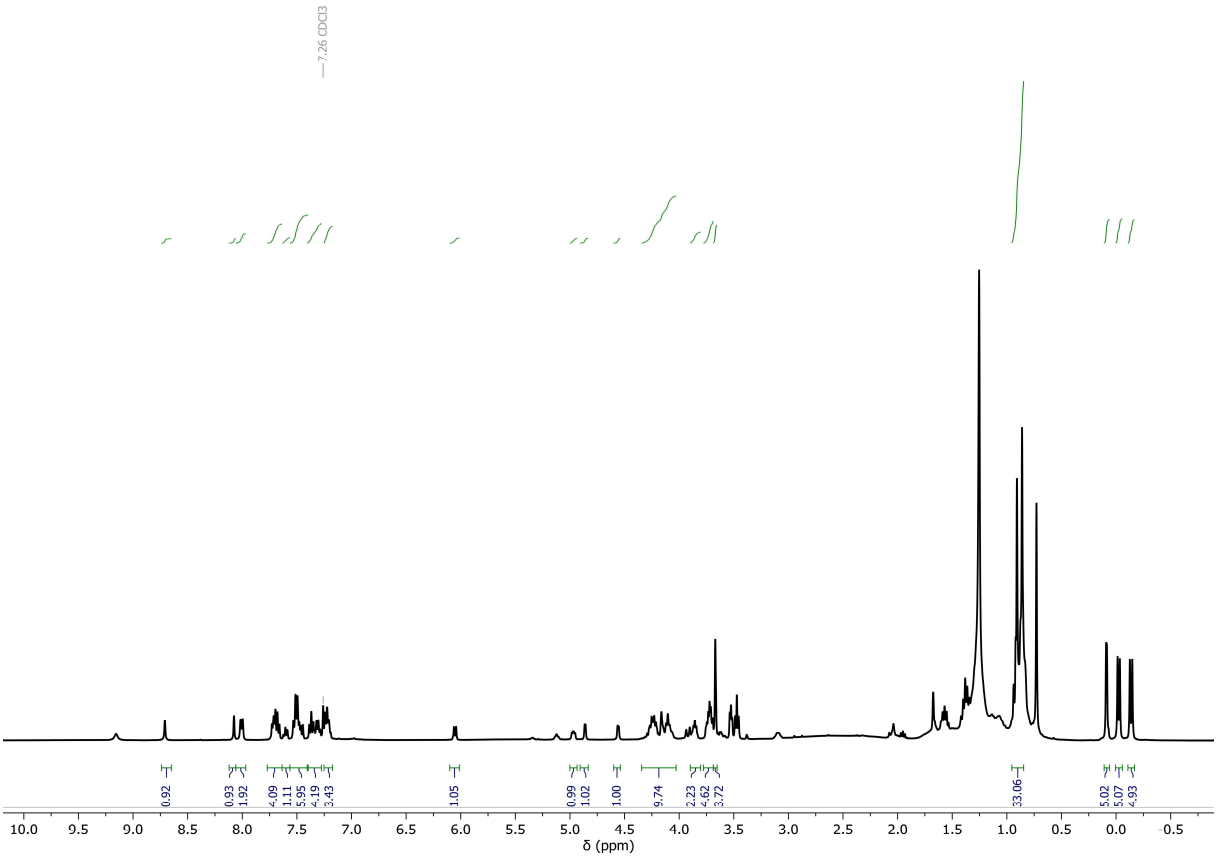

Figure S13. ^{1}H NMR spectrum of *N*^{6}-benzoyl-[3'-*O*-TBDMS-2'-*O*-α-D-(2'',3''-di-*O*-TBDMS-5''-*O*-(difluorenylmethyl)-phosphoryl-ribofuranosyl) –adenosine (13.9).

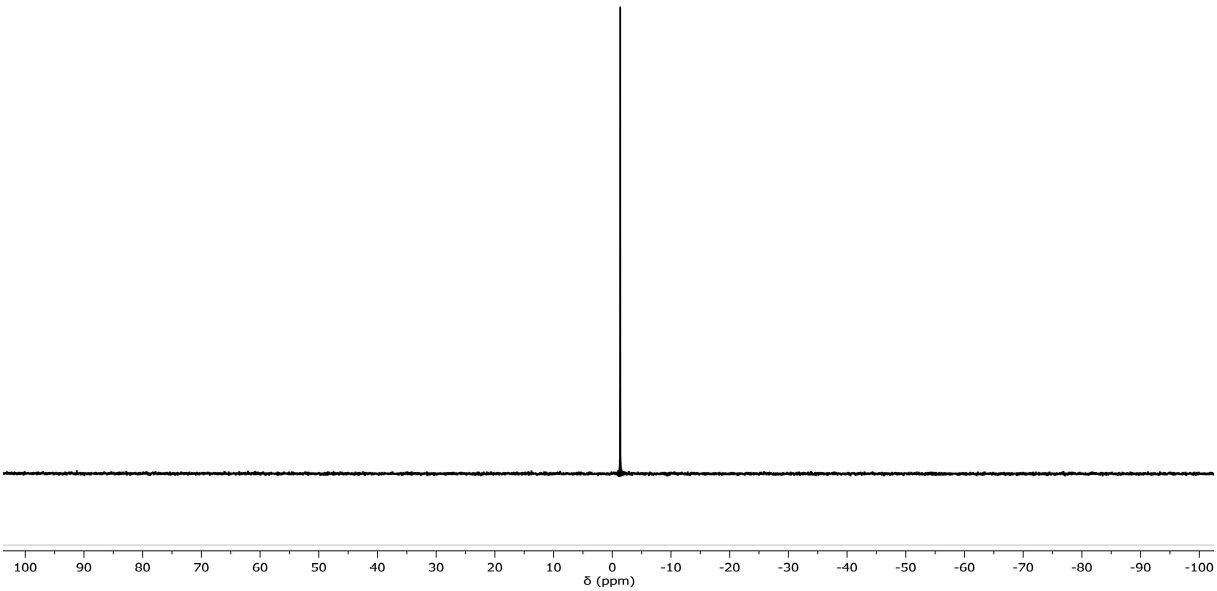

Figure S14. ^{31}P NMR spectrum of *N*^{6}-benzoyl-[3'-*O*-TBDMS-2'-*O*-α-D-(2'',3''-di-*O*-TBDMS-5''-*O*-(difluorenylmethyl)-phosphoryl-ribofuranosyl) –adenosine (13.9).

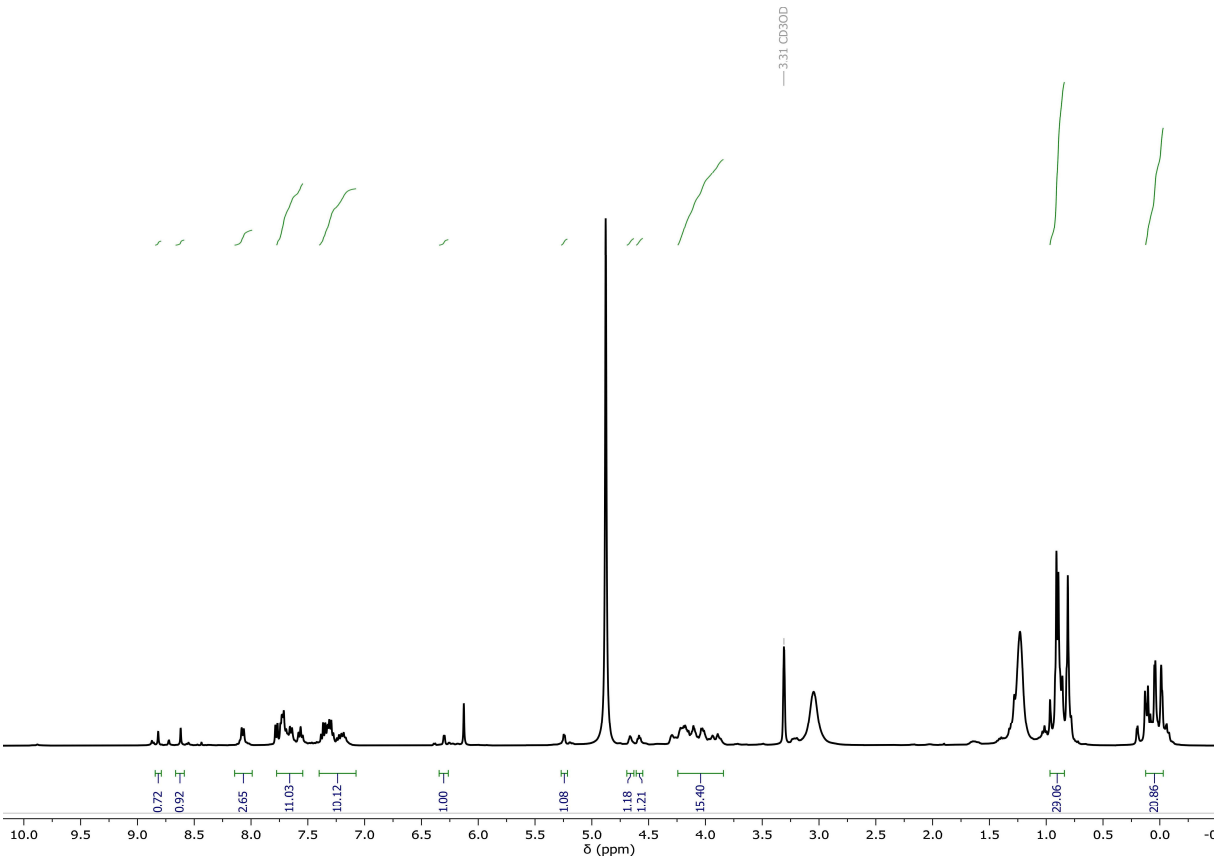

Figure S15. ^{1}H NMR spectrum of *N*^{6}-benzoyl-[3'-*O*-TBDMS-5'-*O*-phosphate-2'-*O*-α-D-(2'',3''-di-*O*-TBDMS-5''-*O*-di-fluorenylmethyl)-phosphoryl-ribofuranosyl) –adenosine (13.10).

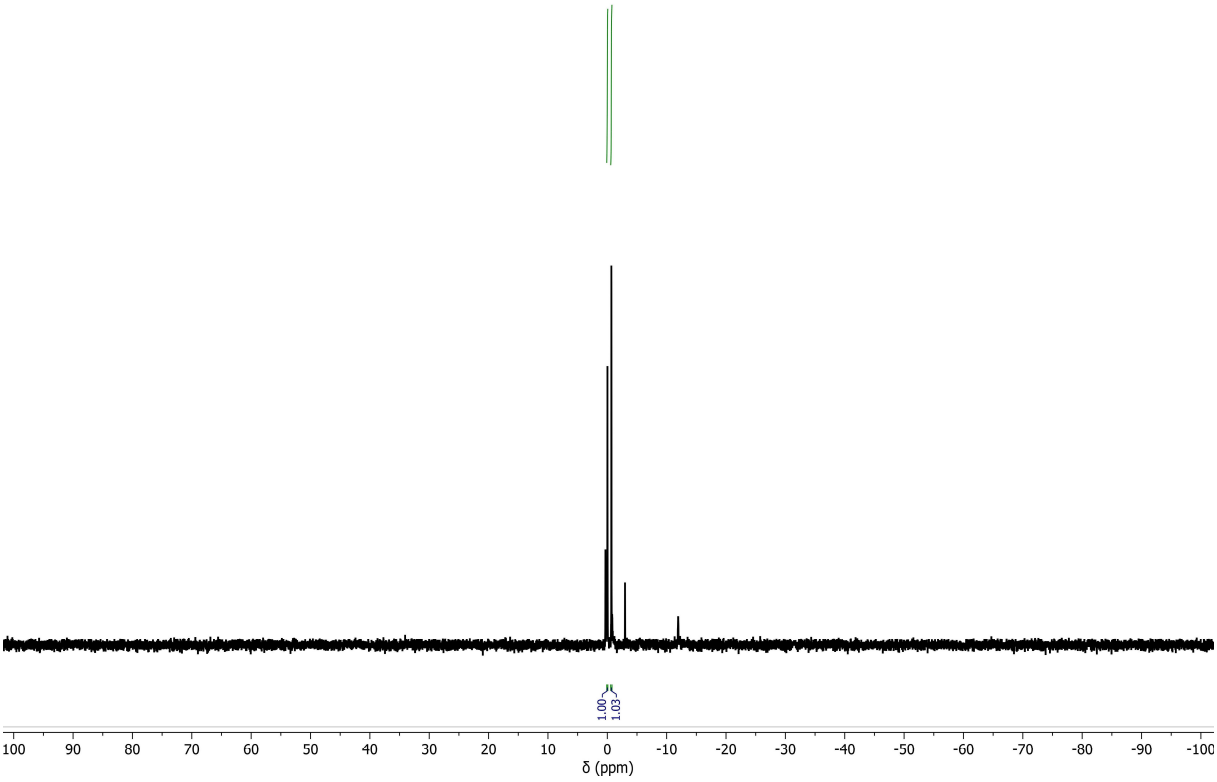

Figure S16. ^{31}P NMR spectrum of *N*^{6}-benzoyl-[3'-*O*-TBDMS-5'-*O*-phosphate-2'-*O*-α-D-(2'',3''-di-*O*-TBDMS-5''-*O*-di-fluorenylmethyl)-phosphoryl-ribofuranosyl) –adenosine (13.10).

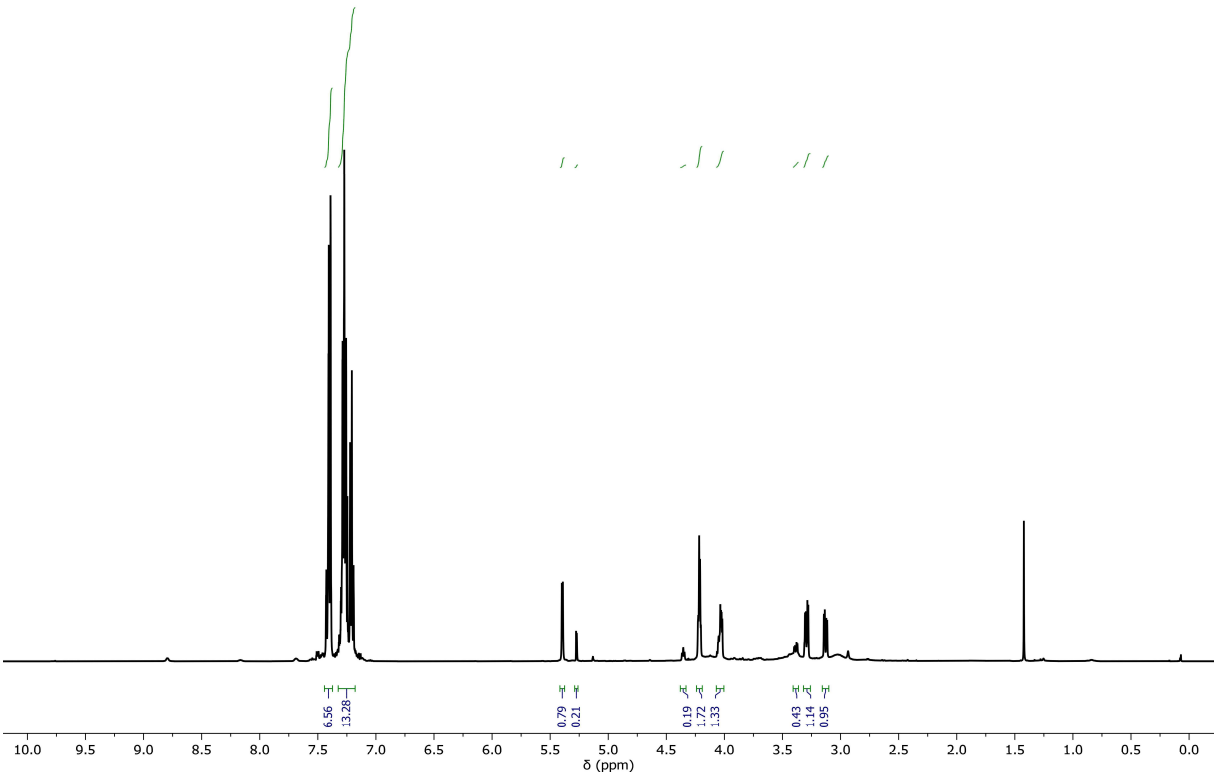

Figure S17. ^{1}H NMR spectrum of 5-*O*-triphenylmethyl-D-ribose (14.2).

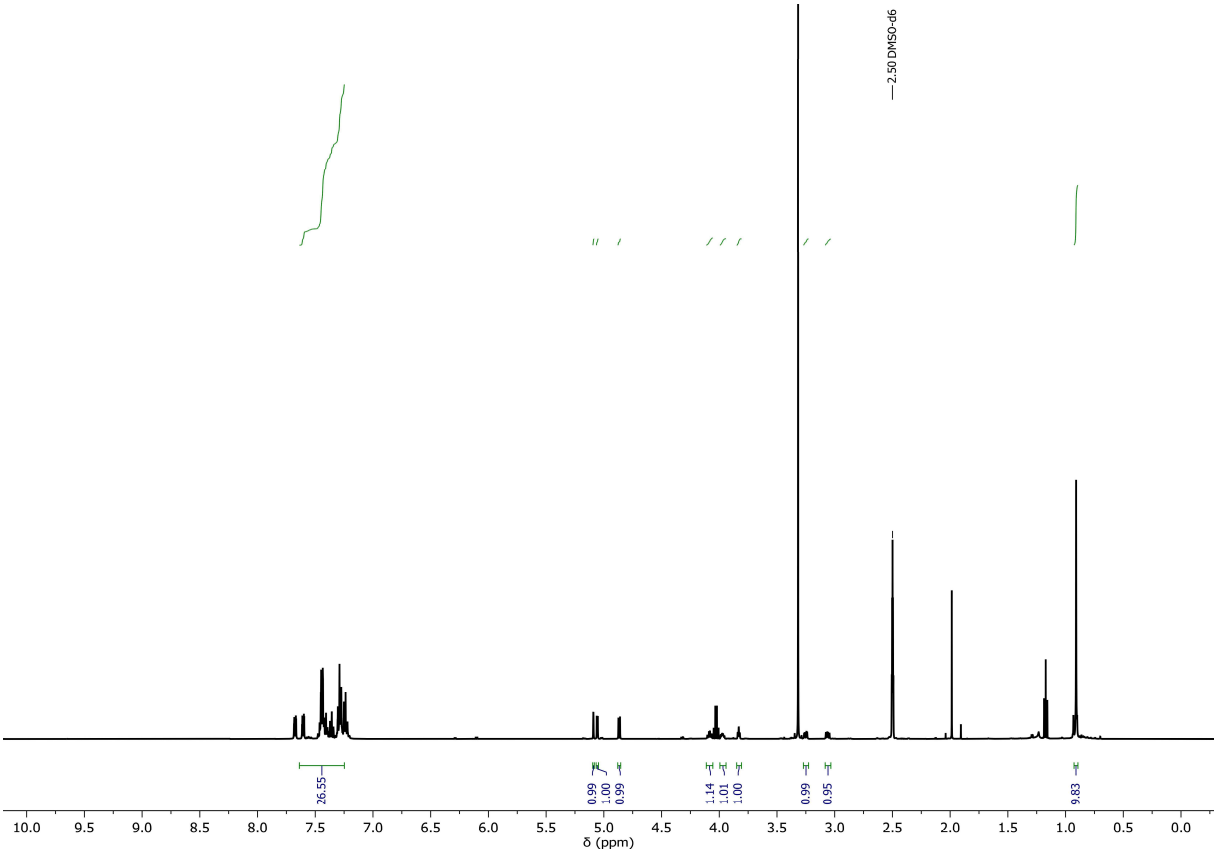

Figure S18. ^{1}H NMR spectrum of 1-*O*-TBDPS-5-*O*-triphenylmethyl-β-D-ribose (14.3).

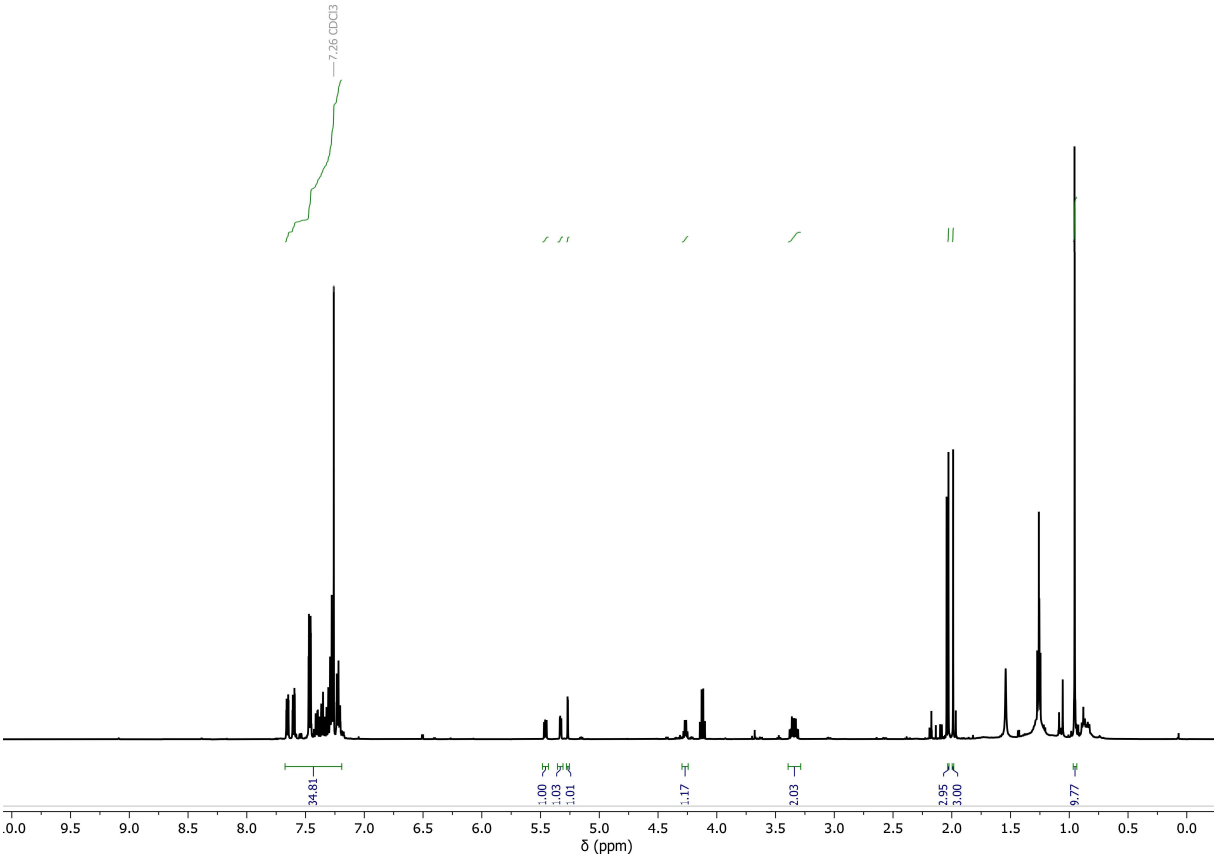

Figure S19. ^{1}H NMR spectrum of 1-*O*-TBDPS-2,3-di-*O*-acetyl-5-*O*-triphenylmethyl-β-D-ribose (14.4).

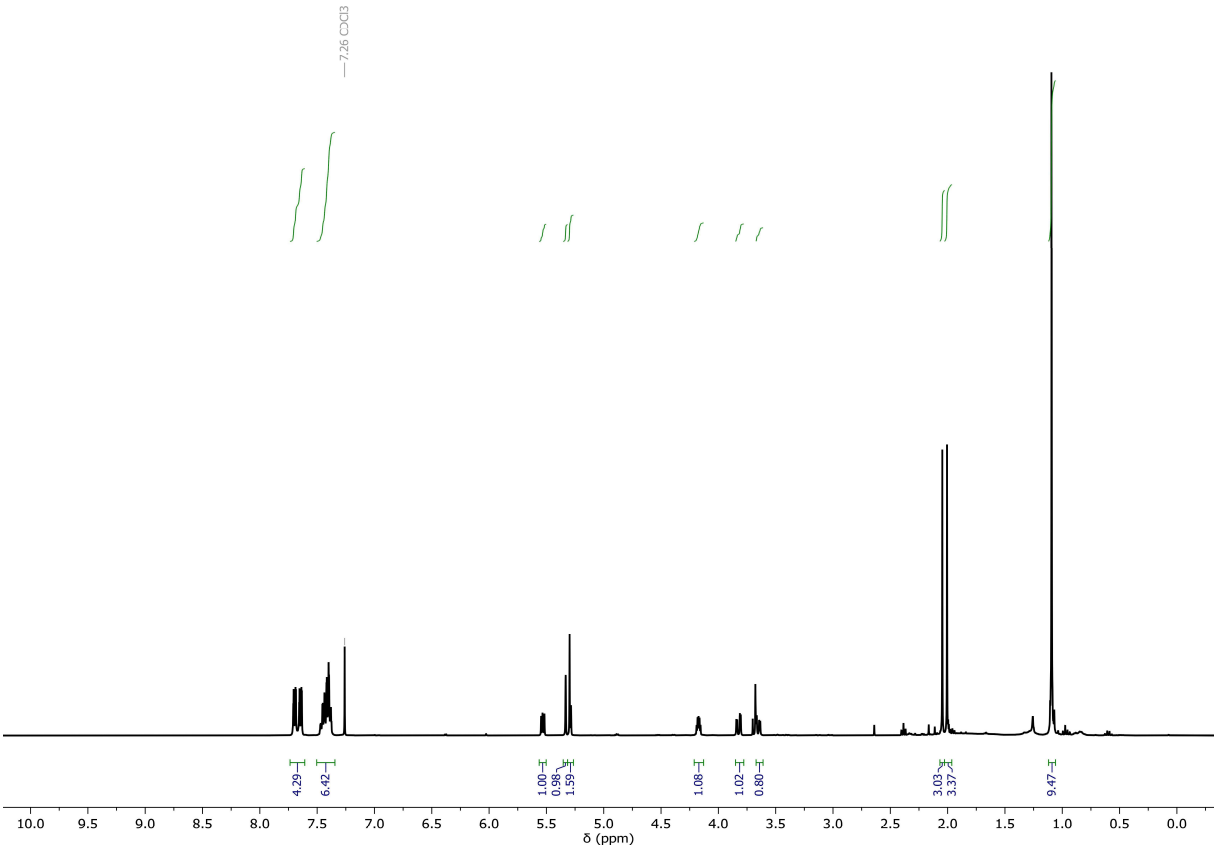

Figure S20. ^{1}H NMR spectrum of 1-*O*-TBDPS-2,3-di-*O*-acetyl-β-D-ribose (14.5).

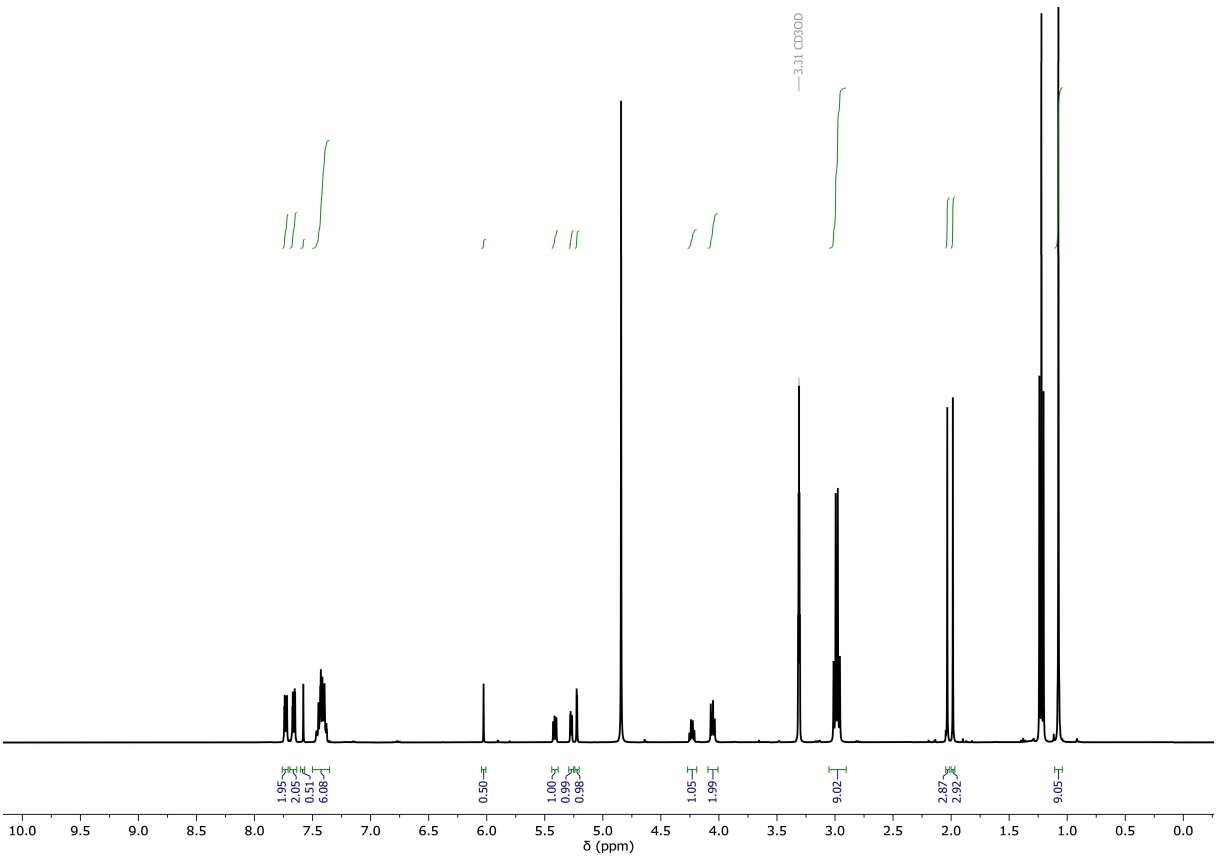

Figure S21. ^{1}H NMR spectrum of 1-*O*-TBDPS-2,3-di-*O*-acetyl-5-*O*-*H*-phosphonate-β-D-ribose (14.6).

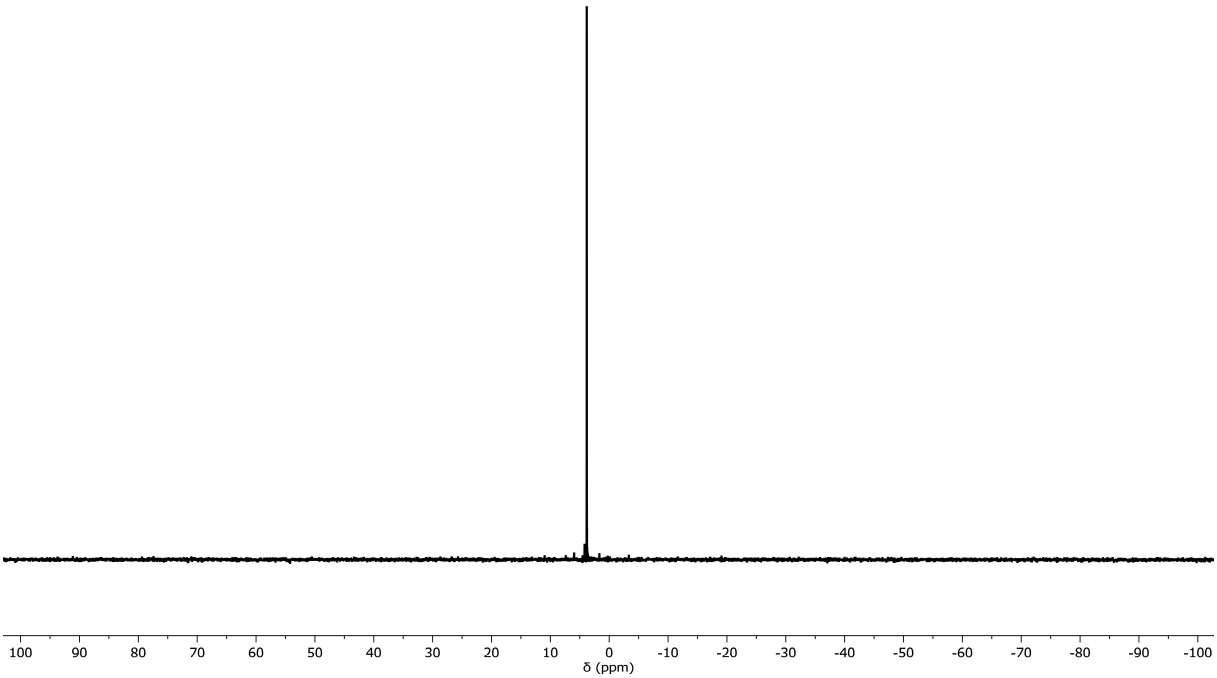

Figure S22. ^{31}P NMR spectrum of 1-*O*-TBDPS-2,3-di-*O*-acetyl-5-*O*-*H*-phosphonate-β-D-ribose (14.6).

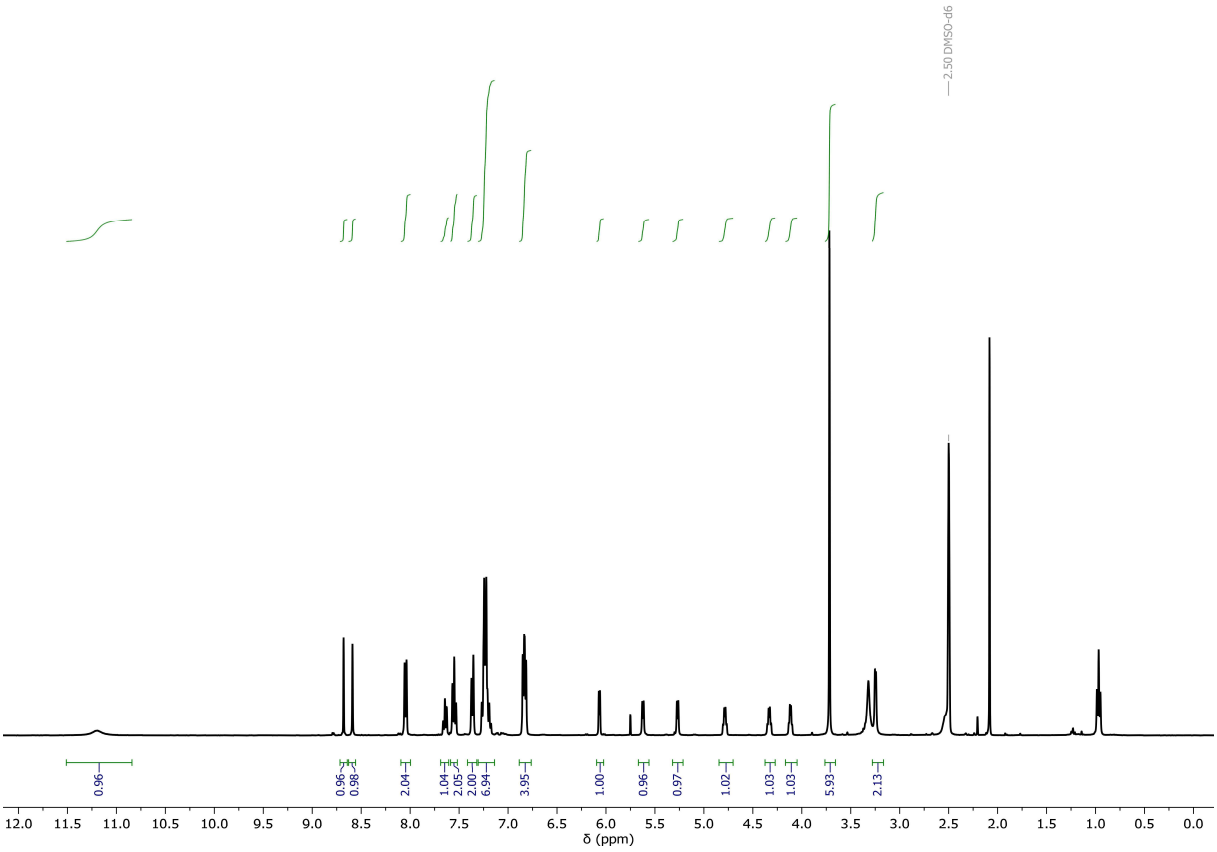

Figure S23. ^{1}H NMR spectrum of N^{6}-benzoyl-5'-*O*-(4,4'-dimethoxytrityl)-adenosine (15.2).

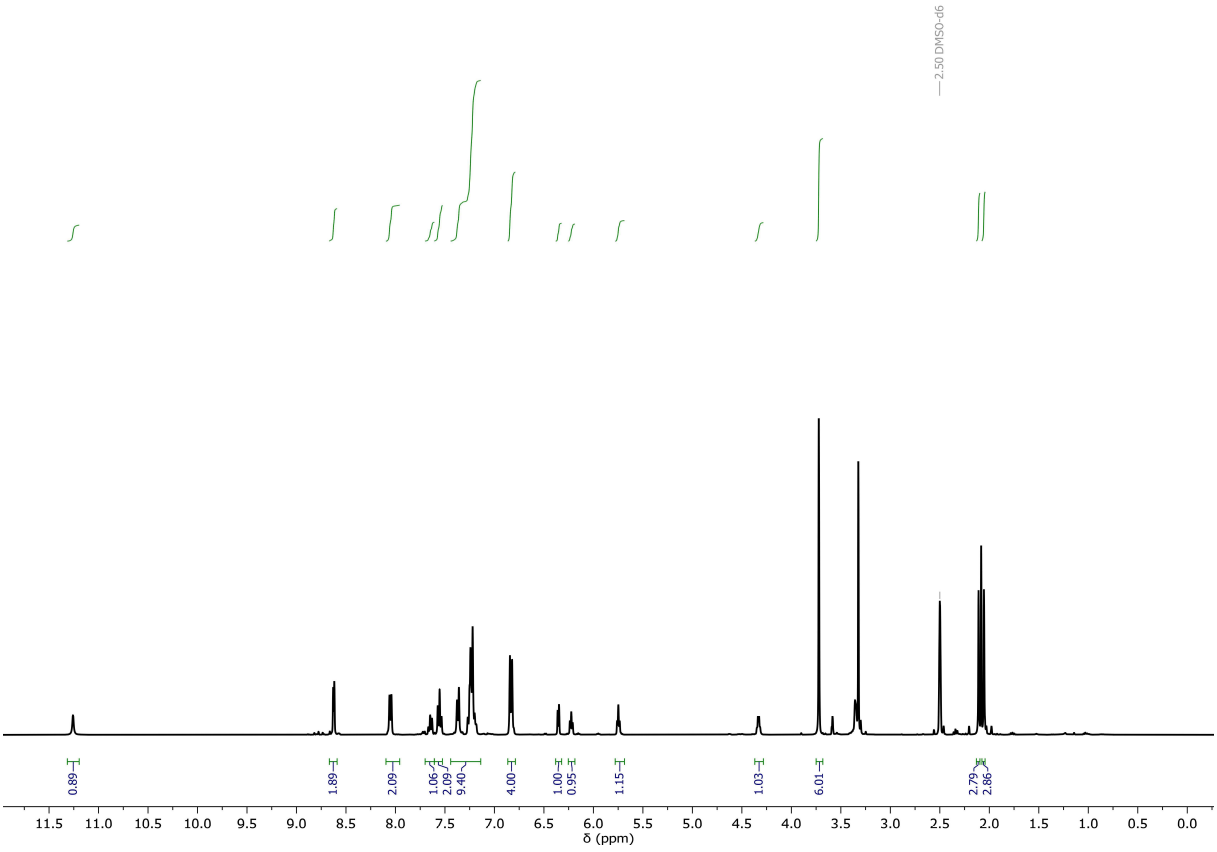

Figure S24. ^{1}H NMR spectrum of N^{6}-benzoyl-2',3'-di-*O*-acetyl-5'-*O*-(4,4'-dimethoxytrityl)-adenosine (15.3).

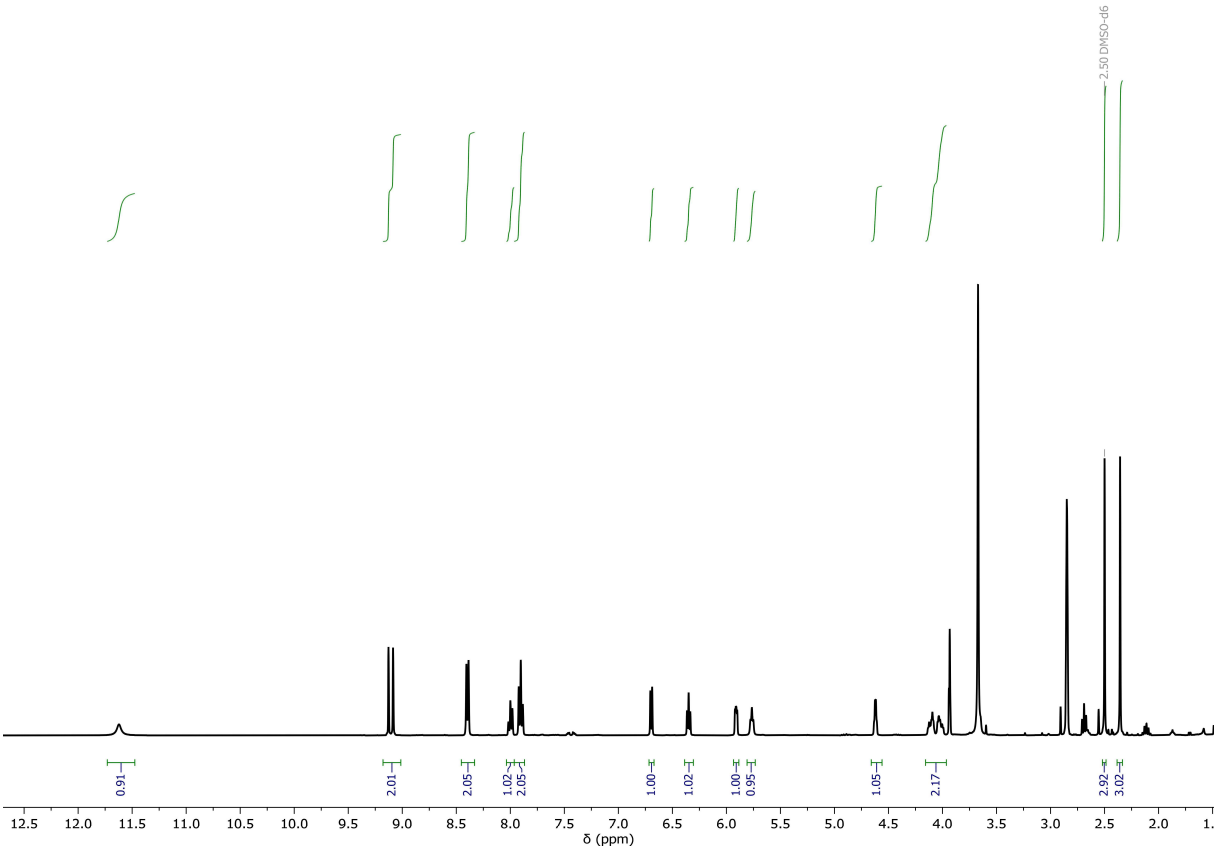

Figure S25. ^{1}H NMR spectrum of *N*^{6}-benzoyl-2',3'-di-*O*-acetyl-adenosine (15.4).

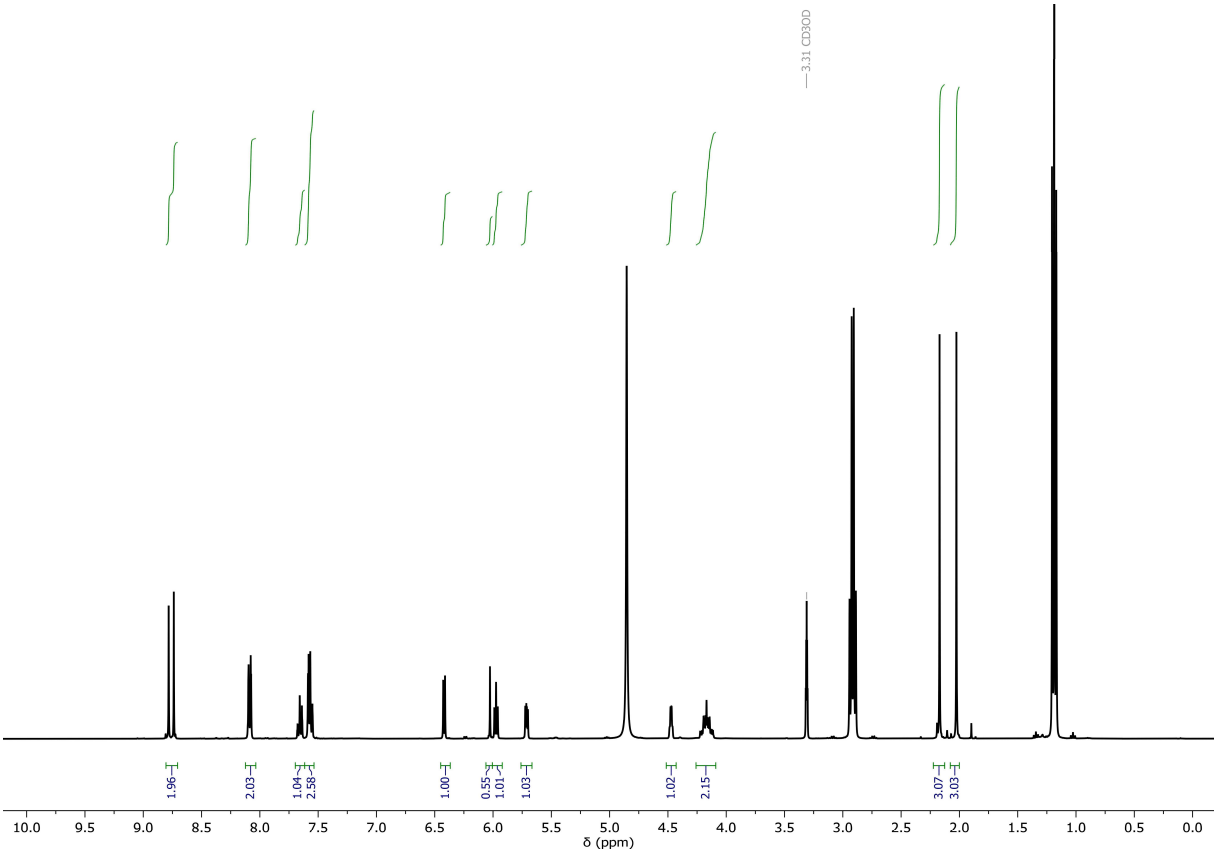

Figure S26. ^{1}H NMR spectrum of *N*^{6}-benzoyl-2',3'-di-*O*-acetyl-5'-*O*-*H*-phosphonate-adenosine (15.5).

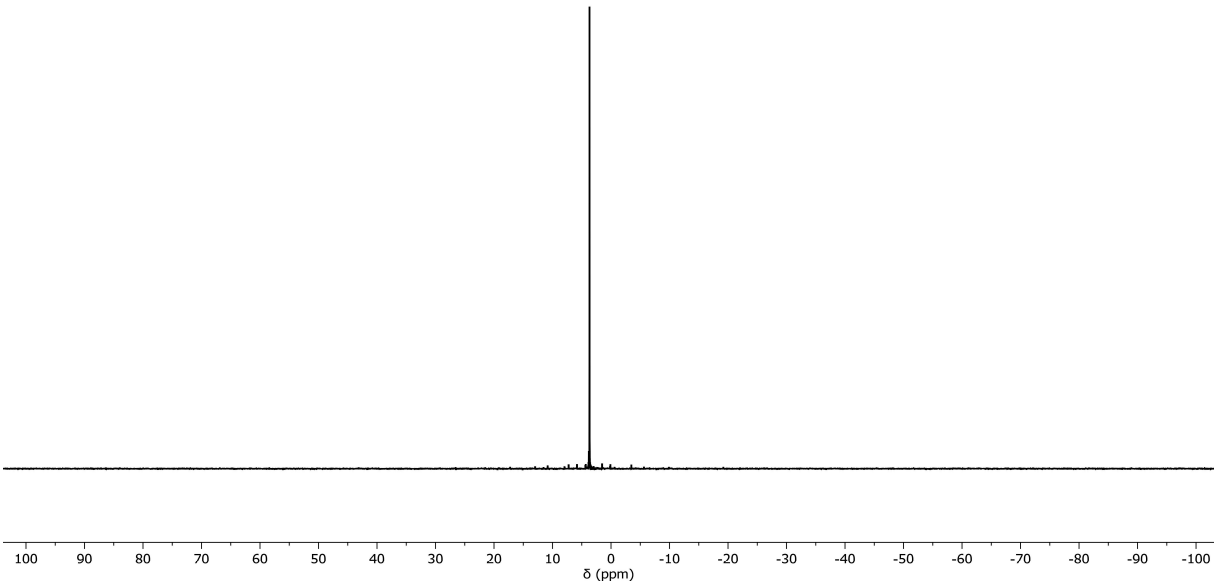

Figure S27. ^{31}P NMR spectrum of N^6-benzoyl-2',3'-di-*O*-acetyl-5'-*O*-*H*-phosphonate-adenosine (15.5).

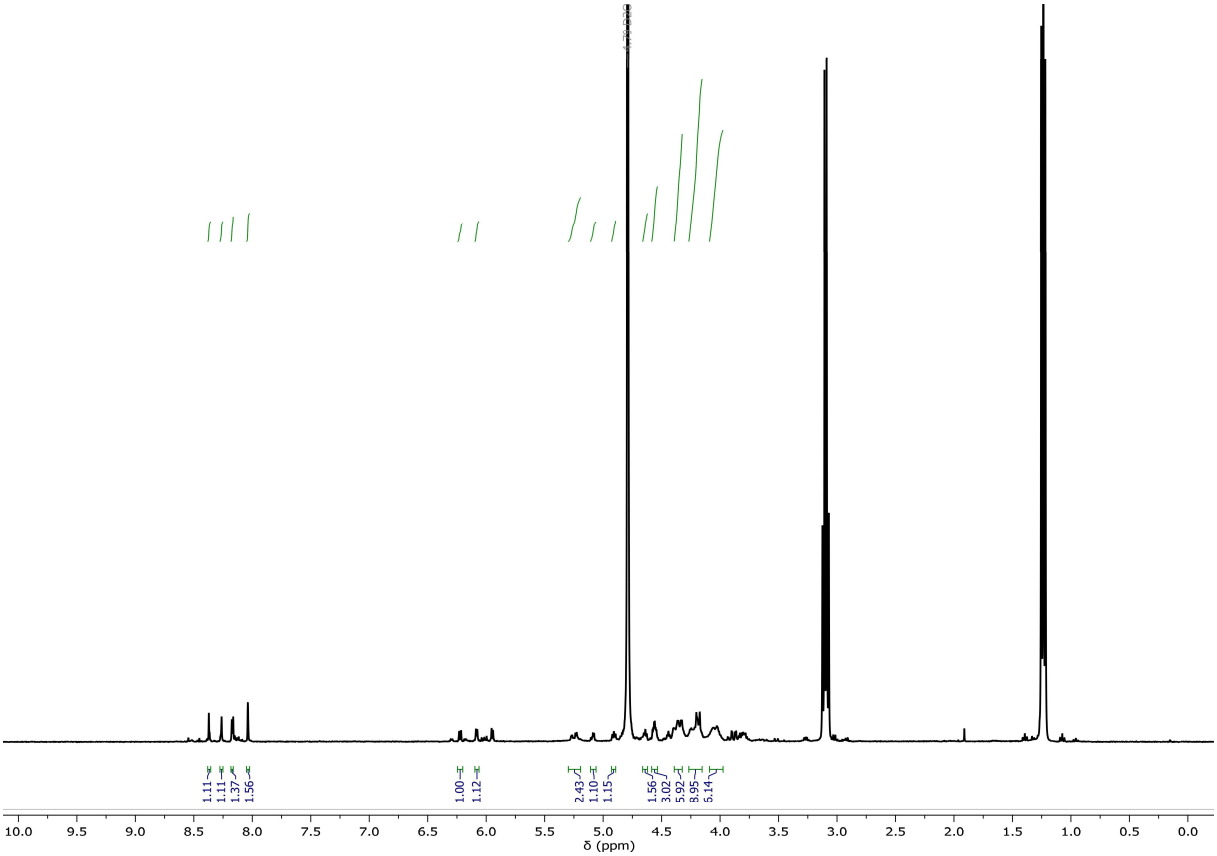

Figure S28. ^{1}H NMR of D-ribose adenosine dinucleotide-2''-*O*-α-D-ribose adenosine dinucleotide (diADPr).

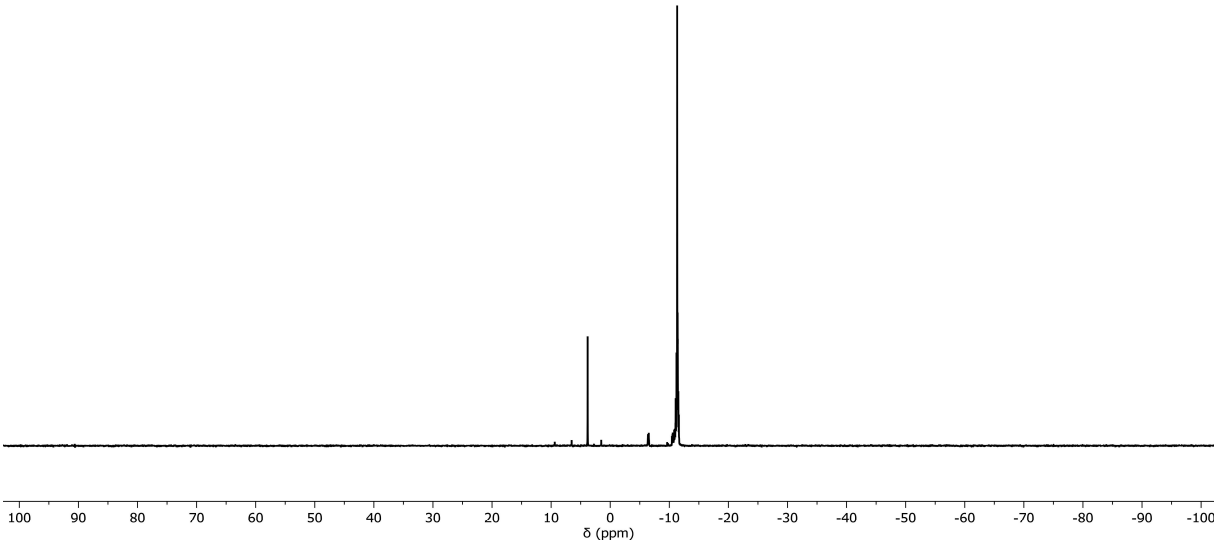

Figure S29. ^{31}P NMR of D-ribose adenosine dinucleotide-2''-*O*-α-D-ribose adenosine dinucleotide (diADPr).

7 References

1 Hottiger, M. O., Hassa, P. O., Lüscher, B., Schüler, H. & Koch-Nolte, F. Toward a unified nomenclature for mammalian ADP-ribosyltransferases. *Trends Biochem Sci* **35**, 208-219, doi:10.1016/j.tibs.2009.12.003 (2010).

2 Hottiger, M. O. ADP-ribosylation of histones by ARTD1: an additional module of the histone code? *FEBS Lett* **585**, 1595-1599, doi:10.1016/j.febslet.2011.03.031 (2011).

3 Lanz, J. *et al.* Disulfiram: Mechanisms, Applications, and Challenges. *Antibiotics (Basel)* **12**, doi:10.3390/antibiotics12030524 (2023).

4 Laps, S., Atamleh, F., Kamnesky, G., Sun, H. & Brik, A. General synthetic strategy for regioselective ultrafast formation of disulfide bonds in peptides and proteins. *Nat Commun* **12**, 870, doi:10.1038/s41467-021-21209-0 (2021).

5 Laps, S., Sun, H., Kamnesky, G. & Brik, A. Palladium-Mediated Direct Disulfide Bond Formation in Proteins Containing S-Acetamidomethyl-cysteine under Aqueous Conditions. *Angew Chem Int Ed Engl* **58**, 5729-5733, doi:10.1002/anie.201900988 (2019).

6 Hwang, Y. *et al.* A selective chemical probe for coenzyme A-requiring enzymes. *Angew Chem Int Ed Engl* **46**, 7621-7624, doi:10.1002/anie.200702485 (2007).

7 Mex, M. Expanding the Chemical Toolbox for the Investigation of Histone H1.2 ADP-Ribosylation. *PhD thesis, University of Konstanz* (2020).

8 Leidecker, O. *et al.* Serine is a new target residue for endogenous ADP-ribosylation on histones. *Nat Chem Biol* **12**, 998-1000, doi:10.1038/nchembio.2180 (2016).

9 Kistemaker, H. A. *et al.* Synthesis of well-defined adenosine diphosphate ribose oligomers. *Angew Chem Int Ed Engl* **54**, 4915-4918, doi:10.1002/anie.201412283 (2015).

10 Lambrecht, M. J. *et al.* Synthesis of dimeric ADP-ribose and its structure with human poly(ADP-ribose) glycohydrolase. *J Am Chem Soc* **137**, 3558-3564, doi:10.1021/ja512528p (2015).

11 Liu, Q. *et al.* Chemical synthesis of linear ADP-ribose oligomers up to pentamer and their binding to the oncogenic helicase ALC1. *Chem Sci* **12**, 12468-12475, doi:10.1039/d1sc02340c (2021).

12 Mikhailov, S. N., Drenichev, M. S., Oslovsky, V. E., Kulikova, I. V. & Herdewijn, P. Synthesis of Poly(ADP-ribose) Monomer Containing 2'-O-α-D-Ribofuranosyl Adenosine. *Curr Protoc Nucleic Acid Chem* **78**, e92, doi:10.1002/cpnc.92 (2019).

13 Mikhailov, S. N., Kulikova, I. V., Nauwelaerts, K. & Herdewijn, P. Synthesis of 2′-O-α-d-ribofuranosyladenosine, monomeric unit of poly(ADP–ribose). *Tetrahedron* **64**, 2871-2876, doi:doi.org/10.1016/j.tet.2008.01.028 (2008).

14 Zheng, M., Mex, M., Götz, K. H. & Marx, A. Synthesis of disaccharide nucleoside analogues as potential poly(ADP-ribose) polymerase-1 inhibitors. *Org Biomol Chem* **16**, 8904-8907, doi:10.1039/c8ob01894d (2018).

15 Saumer, P., Scheffner, M., Marx, A. & Stengel, F. Interactome of intact chromatosome variants with site-specifically ubiquitylated and acetylated linker histone H1.2. *Nucleic Acids Res* **52**, 101-113, doi:10.1093/nar/gkad1113 (2024).

16 Thåström, A., Bingham, L. M. & Widom, J. Nucleosomal locations of dominant DNA sequence motifs for histone-DNA interactions and nucleosome positioning. *J Mol Biol* **338**, 695-709, doi:10.1016/j.jmb.2004.03.032 (2004).

17 Lowary, P. T. & Widom, J. New DNA sequence rules for high affinity binding to histone octamer and sequence-directed nucleosome positioning. *J Mol Biol* **276**, 19-42, doi:10.1006/jmbi.1997.1494 (1998).

18 White, A. E., Hieb, A. R. & Luger, K. A quantitative investigation of linker histone interactions with nucleosomes and chromatin. *Sci Rep* **6**, 19122, doi:10.1038/srep19122 (2016).

19 Dyer, P. N. *et al.* Reconstitution of nucleosome core particles from recombinant histones and DNA. *Methods Enzymol* **375**, 23-44, doi:10.1016/s0076-6879(03)75002-2 (2004).

20 Luger, K., Rechsteiner, T. J. & Richmond, T. J. Preparation of nucleosome core particle from recombinant histones. *Methods Enzymol* **304**, 3-19, doi:10.1016/s0076-6879(99)04003-3 (1999).

21 Moyle, P. M. & Muir, T. W. Method for the synthesis of mono-ADP-ribose conjugated peptides. *J Am Chem Soc* **132**, 15878-15880, doi:10.1021/ja1064312 (2010).

22 Song, L. & Luo, Z. Q. Post-translational regulation of ubiquitin signaling. *J Cell Biol* **218**, 1776-1786, doi:10.1083/jcb.201902074 (2019).

23 Piovesan, A. *et al.* On the length, weight and GC content of the human genome. *BMC Res Notes* **12**, 106, doi:10.1186/s13104-019-4137-z (2019).

24 Venkatesh, S. & Workman, J. L. Histone exchange, chromatin structure and the regulation of transcription. *Nat Rev Mol Cell Biol* **16**, 178-189, doi:10.1038/nrm3941 (2015).

25 Takizawa, Y. & Kurumizaka, H. Chromatin structure meets cryo-EM: Dynamic building blocks of the functional architecture. *Biochim Biophys Acta Gene Regul Mech* **1865**, 194851, doi:10.1016/j.bbagrm.2022.194851 (2022).

26 Arents, G., Burlingame, R. W., Wang, B. C., Love, W. E. & Moudrianakis, E. N. The nucleosomal core histone octamer at 3.1 A resolution: a tripartite protein assembly and a left-handed superhelix. *Proc Natl Acad Sci U S A* **88**, 10148-10152, doi:10.1073/pnas.88.22.10148 (1991).

27 Oudet, P., Gross-Bellard, M. & Chambon, P. Electron microscopic and biochemical evidence that chromatin structure is a repeating unit. *Cell* **4**, 281-300, doi:10.1016/0092-8674(75)90149-x (1975).

28 Luger, K., Mäder, A. W., Richmond, R. K., Sargent, D. F. & Richmond, T. J. Crystal structure of the nucleosome core particle at 2.8 A resolution. *Nature* **389**, 251-260, doi:10.1038/38444 (1997).

29 Flaus, A., Luger, K., Tan, S. & Richmond, T. J. Mapping nucleosome position at single base-pair resolution by using site-directed hydroxyl radicals. *Proc Natl Acad Sci U S A* **93**, 1370-1375, doi:10.1073/pnas.93.4.1370 (1996).

30 Luger, K., Rechsteiner, T. J., Flaus, A. J., Waye, M. M. & Richmond, T. J. Characterization of nucleosome core particles containing histone proteins made in bacteria. *J Mol Biol* **272**, 301-311, doi:10.1006/jmbi.1997.1235 (1997).

31 Kornberg, R. D. Chromatin structure: a repeating unit of histones and DNA. *Science* **184**, 868-871, doi:10.1126/science.184.4139.868 (1974).

32 Noll, M. & Kornberg, R. D. Action of micrococcal nuclease on chromatin and the location of histone H1. *J Mol Biol* **109**, 393-404, doi:10.1016/s0022-2836(77)80019-3 (1977).

33 Fyodorov, D. V., Zhou, B. R., Skoultchi, A. I. & Bai, Y. Emerging roles of linker histones in regulating chromatin structure and function. *Nat Rev Mol Cell Biol* **19**, 192-206, doi:10.1038/nrm.2017.94 (2018).

34 Wu, C., Bassett, A. & Travers, A. A variable topology for the 30-nm chromatin fibre. *EMBO Rep* **8**, 1129-1134, doi:10.1038/sj.embor.7401115 (2007).

35 van Holde, K. & Zlatanova, J. Chromatin higher order structure: chasing a mirage? *J Biol Chem* **270**, 8373-8376, doi:10.1074/jbc.270.15.8373 (1995).

36 Adhireksan, Z., Sharma, D., Lee, P. L. & Davey, C. A. Near-atomic resolution structures of interdigitated nucleosome fibres. *Nat Commun* **11**, 4747, doi:10.1038/s41467-020-18533-2 (2020).

37 Tremethick, D. J. Higher-order structures of chromatin: the elusive 30 nm fiber. *Cell* **128**, 651-654, doi:10.1016/j.cell.2007.02.008 (2007).

38 Finch, J. T. & Klug, A. Solenoidal model for superstructure in chromatin. *Proc Natl Acad Sci U S A* **73**, 1897-1901, doi:10.1073/pnas.73.6.1897 (1976).

39 Robinson, P. J., Fairall, L., Huynh, V. A. & Rhodes, D. EM measurements define the dimensions of the "30-nm" chromatin fiber: evidence for a compact, interdigitated

structure. *Proc Natl Acad Sci U S A* **103**, 6506-6511, doi:10.1073/pnas.0601212103 (2006).

40 Bednar, J. *et al.* Nucleosomes, linker DNA, and linker histone form a unique structural motif that directs the higher-order folding and compaction of chromatin. *Proc Natl Acad Sci U S A* **95**, 14173-14178, doi:10.1073/pnas.95.24.14173 (1998).

41 Schlick, T., Hayes, J. & Grigoryev, S. Toward convergence of experimental studies and theoretical modeling of the chromatin fiber. *J Biol Chem* **287**, 5183-5191, doi:10.1074/jbc.R111.305763 (2012).

42 Schalch, T., Duda, S., Sargent, D. F. & Richmond, T. J. X-ray structure of a tetranucleosome and its implications for the chromatin fibre. *Nature* **436**, 138-141, doi:10.1038/nature03686 (2005).

43 Ou, H. D. *et al.* ChromEMT: Visualizing 3D chromatin structure and compaction in interphase and mitotic cells. *Science* **357**, doi:10.1126/science.aag0025 (2017).

44 Ricci, M. A., Manzo, C., García-Parajo, M. F., Lakadamyali, M. & Cosma, M. P. Chromatin fibers are formed by heterogeneous groups of nucleosomes in vivo. *Cell* **160**, 1145-1158, doi:10.1016/j.cell.2015.01.054 (2015).

45 Ohno, M. *et al.* Sub-nucleosomal Genome Structure Reveals Distinct Nucleosome Folding Motifs. *Cell* **176**, 520-534.e525, doi:10.1016/j.cell.2018.12.014 (2019).

46 Risca, V. I., Denny, S. K., Straight, A. F. & Greenleaf, W. J. Variable chromatin structure revealed by in situ spatially correlated DNA cleavage mapping. *Nature* **541**, 237-241, doi:10.1038/nature20781 (2017).

47 Fierz, B. & Poirier, M. G. Biophysics of Chromatin Dynamics. *Annu Rev Biophys* **48**, 321-345, doi:10.1146/annurev-biophys-070317-032847 (2019).

48 Baldi, S., Korber, P. & Becker, P. B. Beads on a string-nucleosome array arrangements and folding of the chromatin fiber. *Nat Struct Mol Biol* **27**, 109-118, doi:10.1038/s41594-019-0368-x (2020).

49 Fan, L. & Roberts, V. A. Complex of linker histone H5 with the nucleosome and its implications for chromatin packing. *Proc Natl Acad Sci U S A* **103**, 8384-8389, doi:10.1073/pnas.0508951103 (2006).

50 Clark, K. L., Halay, E. D., Lai, E. & Burley, S. K. Co-crystal structure of the HNF-3/fork head DNA-recognition motif resembles histone H5. *Nature* **364**, 412-420, doi:10.1038/364412a0 (1993).

51 Ramakrishnan, V., Finch, J. T., Graziano, V., Lee, P. L. & Sweet, R. M. Crystal structure of globular domain of histone H5 and its implications for nucleosome binding. *Nature* **362**, 219-223, doi:10.1038/362219a0 (1993).

52 Robinson, P. J. & Rhodes, D. Structure of the '30 nm' chromatin fibre: a key role for the linker histone. *Curr Opin Struct Biol* **16**, 336-343, doi:10.1016/j.sbi.2006.05.007 (2006).

53 Hergeth, S. P. & Schneider, R. The H1 linker histones: multifunctional proteins beyond the nucleosomal core particle. *EMBO Rep* **16**, 1439-1453, doi:10.15252/embr.201540749 (2015).

54 Marzluff, W. F. Metazoan replication-dependent histone mRNAs: a distinct set of RNA polymerase II transcripts. *Curr Opin Cell Biol* **17**, 274-280, doi:10.1016/j.ceb.2005.04.010 (2005).

55 Albig, W. & Doenecke, D. The human histone gene cluster at the D6S105 locus. *Hum Genet* **101**, 284-294, doi:10.1007/s004390050630 (1997).

56 Kasinsky, H. E., Lewis, J. D., Dacks, J. B. & Ausió, J. Origin of H1 linker histones. *Faseb j* **15**, 34-42, doi:10.1096/fj.00-0237rev (2001).

57 Clausell, J., Happel, N., Hale, T. K., Doenecke, D. & Beato, M. Histone H1 subtypes differentially modulate chromatin condensation without preventing ATP-dependent remodeling by SWI/SNF or NURF. *PLoS One* **4**, e0007243, doi:10.1371/journal.pone.0007243 (2009).

58 Catez, F., Ueda, T. & Bustin, M. Determinants of histone H1 mobility and chromatin binding in living cells. *Nat Struct Mol Biol* **13**, 305-310, doi:10.1038/nsmb1077 (2006).

59 Lobbia, V. R., Trueba Sanchez, M. C. & van Ingen, H. Beyond the Nucleosome: Nucleosome-Protein Interactions and Higher Order Chromatin Structure. *J Mol Biol* **433**, 166827, doi:10.1016/j.jmb.2021.166827 (2021).

60 Zhou, B. R. *et al.* Structural insights into the histone H1-nucleosome complex. *Proc Natl Acad Sci U S A* **110**, 19390-19395, doi:10.1073/pnas.1314905110 (2013).

61 Song, F. *et al.* Cryo-EM study of the chromatin fiber reveals a double helix twisted by tetranucleosomal units. *Science* **344**, 376-380, doi:10.1126/science.1251413 (2014).

62 Syed, S. H. *et al.* Single-base resolution mapping of H1-nucleosome interactions and 3D organization of the nucleosome. *Proc Natl Acad Sci U S A* **107**, 9620-9625, doi:10.1073/pnas.1000309107 (2010).

63 Zhou, B. R. *et al.* Structural Mechanisms of Nucleosome Recognition by Linker Histones. *Mol Cell* **59**, 628-638, doi:10.1016/j.molcel.2015.06.025 (2015).

64 Bednar, J. *et al.* Structure and Dynamics of a 197 bp Nucleosome in Complex with Linker Histone H1. *Mol Cell* **66**, 384-397.e388, doi:10.1016/j.molcel.2017.04.012 (2017).

65 Öztürk, M. A., Cojocaru, V. & Wade, R. C. Toward an Ensemble View of Chromatosome Structure: A Paradigm Shift from One to Many. *Structure* **26**, 1050-1057, doi:10.1016/j.str.2018.05.009 (2018).

66 Zlatanova, J. Histone H1 and the regulation of transcription of eukaryotic genes. *Trends Biochem Sci* **15**, 273-276, doi:10.1016/0968-0004(90)90053-e (1990).

67 Zlatanova, J., Caiafa, P. & Van Holde, K. Linker histone binding and displacement: versatile mechanism for transcriptional regulation. *Faseb j* **14**, 1697-1704, doi:10.1096/fj.99-0869rev (2000).

68 Mustafi, P. *et al.* Phosphorylation-dependent association of human chromatin protein PC4 to linker histone H1 regulates genome organization and transcription. *Nucleic Acids Res* **50**, 6116-6136, doi:10.1093/nar/gkac450 (2022).

69 Shen, X. & Gorovsky, M. A. Linker histone H1 regulates specific gene expression but not global transcription in vivo. *Cell* **86**, 475-483, doi:10.1016/s0092-8674(00)80120-8 (1996).

70 Ozgencil, M., Dullovi, A., Christiane Higos, R. C., Hořejší, Z. & Bellelli, R. The linker histone H1-BRCA1 axis is a crucial mediator of replication fork stability. *Life Sci Alliance* **6**, doi:10.26508/lsa.202301933 (2023).

71 Konishi, A. *et al.* Involvement of histone H1.2 in apoptosis induced by DNA double-strand breaks. *Cell* **114**, 673-688, doi:10.1016/s0092-8674(03)00719-0 (2003).

72 Prendergast, L. & Reinberg, D. The missing linker: emerging trends for H1 variant-specific functions. *Genes Dev* **35**, 40-58, doi:10.1101/gad.344531.120 (2021).

73 Lin, Q. *et al.* Reductions in linker histone levels are tolerated in developing spermatocytes but cause changes in specific gene expression. *J Biol Chem* **279**, 23525-23535, doi:10.1074/jbc.M400925200 (2004).

74 Millán-Zambrano, G., Burton, A., Bannister, A. J. & Schneider, R. Histone post-translational modifications - cause and consequence of genome function. *Nat Rev Genet* **23**, 563-580, doi:10.1038/s41576-022-00468-7 (2022).

75 Yang, Y., Zhang, M. & Wang, Y. The roles of histone modifications in tumorigenesis and associated inhibitors in cancer therapy. *J. Natl. Cancer Cent.* **2**, 277-290, doi:10.1016/j.jncc.2022.09.002 (2022).

76 Strahl, B. D. & Allis, C. D. The language of covalent histone modifications. *Nature* **403**, 41-45, doi:10.1038/47412 (2000).

77 Harshman, S. W., Young, N. L., Parthun, M. R. & Freitas, M. A. H1 histones: current perspectives and challenges. *Nucleic Acids Res* **41**, 9593-9609, doi:10.1093/nar/gkt700 (2013).

78 Wisniewski, J. R., Zougman, A., Krüger, S. & Mann, M. Mass spectrometric mapping of linker histone H1 variants reveals multiple acetylations, methylations, and phosphorylation as well as differences between cell culture and tissue. *Mol Cell Proteomics* **6**, 72-87, doi:10.1074/mcp.M600255-MCP200 (2007).

79 Turner, B. M. Decoding the nucleosome. *Cell* **75**, 5-8 (1993).

80 Bannister, A. J. & Kouzarides, T. Regulation of chromatin by histone modifications. *Cell Res* **21**, 381-395, doi:10.1038/cr.2011.22 (2011).

81 Martire, S. & Banaszynski, L. A. The roles of histone variants in fine-tuning chromatin organization and function. *Nat Rev Mol Cell Biol* **21**, 522-541, doi:10.1038/s41580-020-0262-8 (2020).

82 Rothbart, S. B. & Strahl, B. D. Interpreting the language of histone and DNA modifications. *Biochim Biophys Acta* **1839**, 627-643, doi:10.1016/j.bbagrm.2014.03.001 (2014).

83 Andrews, F. H., Strahl, B. D. & Kutateladze, T. G. Insights into newly discovered marks and readers of epigenetic information. *Nat Chem Biol* **12**, 662-668, doi:10.1038/nchembio.2149 (2016).

84 Prakash, K. & Fournier, D. Evidence for the implication of the histone code in building the genome structure. *Biosystems* **164**, 49-59, doi:10.1016/j.biosystems.2017.11.005 (2018).

85 Musselman, C. A., Lalonde, M. E., Côté, J. & Kutateladze, T. G. Perceiving the epigenetic landscape through histone readers. *Nat Struct Mol Biol* **19**, 1218-1227, doi:10.1038/nsmb.2436 (2012).

86 Hunter, T. The age of crosstalk: phosphorylation, ubiquitination, and beyond. *Mol Cell* **28**, 730-738, doi:10.1016/j.molcel.2007.11.019 (2007).

87 Portela, A. & Esteller, M. Epigenetic modifications and human disease. *Nat Biotechnol* **28**, 1057-1068, doi:10.1038/nbt.1685 (2010).

88 Cluntun, A. A. *et al.* The rate of glycolysis quantitatively mediates specific histone acetylation sites. *Cancer Metab* **3**, 10, doi:10.1186/s40170-015-0135-3 (2015).

89 Li, C. *et al.* Post-Translational Modification of Human Histone by Wide Tolerance of Acetylation. *Cells* **6**, doi:10.3390/cells6040034 (2017).

90 Dueva, R. *et al.* Neutralization of the Positive Charges on Histone Tails by RNA Promotes an Open Chromatin Structure. *Cell Chem Biol* **26**, 1436-1449.e1435, doi:10.1016/j.chembiol.2019.08.002 (2019).

91 Filippakopoulos, P. & Knapp, S. The bromodomain interaction module. *FEBS Lett* **586**, 2692-2704, doi:10.1016/j.febslet.2012.04.045 (2012).

92 Eberharter, A. & Becker, P. B. Histone acetylation: a switch between repressive and permissive chromatin. Second in review series on chromatin dynamics. *EMBO Rep* **3**, 224-229, doi:10.1093/embo-reports/kvf053 (2002).

93 Seto, E. & Yoshida, M. Erasers of histone acetylation: the histone deacetylase enzymes. *Cold Spring Harb Perspect Biol* **6**, a018713, doi:10.1101/cshperspect.a018713 (2014).

94 Rossetto, D., Avvakumov, N. & Côté, J. Histone phosphorylation: a chromatin modification involved in diverse nuclear events. *Epigenetics* **7**, 1098-1108, doi:10.4161/epi.21975 (2012).

95 Pawse, A. R., Ord, M. G. & Stocken, L. A. Histone kinase and cell division. *Biochem J* **122**, 713-719, doi:10.1042/bj1220713 (1971).

96 Manke, I. A., Lowery, D. M., Nguyen, A. & Yaffe, M. B. BRCT repeats as phosphopeptide-binding modules involved in protein targeting. *Science* **302**, 636-639, doi:10.1126/science.1088877 (2003).

97 Lopez, R. *et al.* Linker histone partial phosphorylation: effects on secondary structure and chromatin condensation. *Nucleic Acids Res* **43**, 4463-4476, doi:10.1093/nar/gkv304 (2015).

98 Ota, T. *et al.* Increased mitotic phosphorylation of histone H3 attributable to AIM-1/Aurora-B overexpression contributes to chromosome number instability. *Cancer Res* **62**, 5168-5177 (2002).

99 Byvoet, P., Shepherd, G. R., Hardin, J. M. & Noland, B. J. The distribution and turnover of labeled methyl groups in histone fractions of cultured mammalian cells. *Arch Biochem Biophys* **148**, 558-567, doi:10.1016/0003-9861(72)90174-9 (1972).

100 Fischle, W., Franz, H., Jacobs, S. A., Allis, C. D. & Khorasanizadeh, S. Specificity of the chromodomain Y chromosome family of chromodomains for lysine-methylated ARK(S/T) motifs. *J Biol Chem* **283**, 19626-19635, doi:10.1074/jbc.M802655200 (2008).

101 Paik, W. K. & Kim, S. E-N-dimethyllysine in histones. *Biochem. Biophy. Res. Commun.* **27**, 479-483, doi:doi.org/10.1016/S0006-291X(67)80010-X (1967).

102 Hempel, K., Lange, H. W. & Birkofer, L. [Epsilon-N-trimethyllysine, a new amino acid in histones]. *Naturwissenschaften* **55**, 37, doi:10.1007/bf00593411 (1968).

103 Borun, T. W., Pearson, D. & Paik, W. K. Studies of histone methylation during the HeLa S-3 cell cycle. *J Biol Chem* **247**, 4288-4298 (1972).

104 Gershey, E. L., Haslett, G. W., Vidali, G. & Allfrey, V. G. Chemical studies of histone methylation. Evidence for the occurrence of 3-methylhistidine in avian erythrocyte histone fractions. *J Biol Chem* **244**, 4871-4877 (1969).

105 Hyun, K., Jeon, J., Park, K. & Kim, J. Writing, erasing and reading histone lysine methylations. *Exp Mol Med* **49**, e324, doi:10.1038/emm.2017.11 (2017).

106 Tsukada, Y. *et al.* Histone demethylation by a family of JmjC domain-containing proteins. *Nature* **439**, 811-816, doi:10.1038/nature04433 (2006).

107 Taverna, S. D., Li, H., Ruthenburg, A. J., Allis, C. D. & Patel, D. J. How chromatin-binding modules interpret histone modifications: lessons from professional pocket pickers. *Nat Struct Mol Biol* **14**, 1025-1040, doi:10.1038/nsmb1338 (2007).

108 Hershko, A. & Ciechanover, A. The ubiquitin system. *Annu Rev Biochem* **67**, 425-479, doi:10.1146/annurev.biochem.67.1.425 (1998).

109 Li, W. & Ye, Y. Polyubiquitin chains: functions, structures, and mechanisms. *Cell Mol Life Sci* **65**, 2397-2406, doi:10.1007/s00018-008-8090-6 (2008).

110 Wang, H. *et al.* Role of histone H2A ubiquitination in Polycomb silencing. *Nature* **431**, 873-878, doi:10.1038/nature02985 (2004).

111 Lee, J. S. *et al.* Histone crosstalk between H2B monoubiquitination and H3 methylation mediated by COMPASS. *Cell* **131**, 1084-1096, doi:10.1016/j.cell.2007.09.046 (2007).

112 Atanassov, B. S., Koutelou, E. & Dent, S. Y. The role of deubiquitinating enzymes in chromatin regulation. *FEBS Lett* **585**, 2016-2023, doi:10.1016/j.febslet.2010.10.042 (2011).

113 Wielckens, K., Bredehorst, R., Adamietz, P. & Hilz, H. Protein-bound polymeric and monomeric ADP-ribose residues in hepatic tissues. Comparative analyses using a new procedure for the quantification of poly(ADP-ribose). *Eur J Biochem* **117**, 69-74, doi:10.1111/j.1432-1033.1981.tb06303.x (1981).

114 Koch-Nolte, F., Kernstock, S., Mueller-Dieckmann, C., Weiss, M. S. & Haag, F. Mammalian ADP-ribosyltransferases and ADP-ribosylhydrolases. *Front Biosci* **13**, 6716-6729, doi:10.2741/3184 (2008).

115 Rack, J. G. M., Palazzo, L. & Ahel, I. (ADP-ribosyl)hydrolases: structure, function, and biology. *Genes Dev* **34**, 263-284, doi:10.1101/gad.334631.119 (2020).

116 Mashimo, M., Kato, J. & Moss, J. Structure and function of the ARH family of ADP-ribosyl-acceptor hydrolases. *DNA Repair (Amst)* **23**, 88-94, doi:10.1016/j.dnarep.2014.03.005 (2014).

117 Ono, T., Kasamatsu, A., Oka, S. & Moss, J. The 39-kDa poly(ADP-ribose) glycohydrolase ARH3 hydrolyzes O-acetyl-ADP-ribose, a product of the Sir2 family of acetyl-histone deacetylases. *Proc Natl Acad Sci U S A* **103**, 16687-16691, doi:10.1073/pnas.0607911103 (2006).

118 Oka, S., Kato, J. & Moss, J. Identification and characterization of a mammalian 39-kDa poly(ADP-ribose) glycohydrolase. *J Biol Chem* **281**, 705-713, doi:10.1074/jbc.M510290200 (2006).

119 Mueller-Dieckmann, C. *et al.* The structure of human ADP-ribosylhydrolase 3 (ARH3) provides insights into the reversibility of protein ADP-ribosylation. *Proc Natl Acad Sci U S A* **103**, 15026-15031, doi:10.1073/pnas.0606762103 (2006).

120 Burzio, L. O., Riquelme, P. T. & Koide, S. S. ADP ribosylation of rat liver nucleosomal core histones. *J Biol Chem* **254**, 3029-3037 (1979).

121 Pan, P. W. *et al.* Structure and biochemical functions of SIRT6. *J Biol Chem* **286**, 14575-14587, doi:10.1074/jbc.M111.218990 (2011).

122 Hassa, P. O., Haenni, S. S., Elser, M. & Hottiger, M. O. Nuclear ADP-ribosylation reactions in mammalian cells: where are we today and where are we going? *Microbiol Mol Biol Rev* **70**, 789-829, doi:10.1128/mmbr.00040-05 (2006).

123 Messner, S. & Hottiger, M. O. Histone ADP-ribosylation in DNA repair, replication and transcription. *Trends Cell Biol* **21**, 534-542, doi:10.1016/j.tcb.2011.06.001 (2011).
124 Kleine, H. *et al.* Substrate-assisted catalysis by PARP10 limits its activity to mono-ADP-ribosylation. *Mol Cell* **32**, 57-69, doi:10.1016/j.molcel.2008.08.009 (2008).
125 Messner, S. *et al.* PARP1 ADP-ribosylates lysine residues of the core histone tails. *Nucleic Acids Res* **38**, 6350-6362, doi:10.1093/nar/gkq463 (2010).
126 Rulten, S. L. *et al.* PARP-3 and APLF function together to accelerate nonhomologous end-joining. *Mol Cell* **41**, 33-45, doi:10.1016/j.molcel.2010.12.006 (2011).
127 Boulikas, T. DNA strand breaks alter histone ADP-ribosylation. *Proc Natl Acad Sci U S A* **86**, 3499-3503, doi:10.1073/pnas.86.10.3499 (1989).
128 Nolan, N. L., Butt, T. R., Wong, M., Lambrianidou, A. & Smulson, M. E. Characterization of poly(ADP-ribose)--histone H1 complex formation in purified polynucleosomes and chromatin. *Eur J Biochem* **113**, 15-25, doi:10.1111/j.1432-1033.1980.tb06133.x (1980).
129 Ogata, N., Ueda, K., Kagamiyama, H. & Hayaishi, O. ADP-ribosylation of histone H1. Identification of glutamic acid residues 2, 14, and the COOH-terminal lysine residue as modification sites. *J Biol Chem* **255**, 7616-7620 (1980).
130 de Murcia, G. *et al.* Modulation of chromatin superstructure induced by poly(ADP-ribose) synthesis and degradation. *J Biol Chem* **261**, 7011-7017 (1986).
131 Wacker, D. A. *et al.* The DNA binding and catalytic domains of poly(ADP-ribose) polymerase 1 cooperate in the regulation of chromatin structure and transcription. *Mol Cell Biol* **27**, 7475-7485, doi:10.1128/mcb.01314-07 (2007).
132 Huletsky, A. *et al.* The effect of poly(ADP-ribosyl)ation on native and H1-depleted chromatin. A role of poly(ADP-ribosyl)ation on core nucleosome structure. *J Biol Chem* **264**, 8878-8886 (1989).
133 Hough, C. J. & Smulson, M. E. Association of poly(adenosine diphosphate ribosylated) nucleosomes with transcriptionally active and inactive regions of chromatin. *Biochemistry* **23**, 5016-5023, doi:10.1021/bi00316a029 (1984).
134 Aubin, R. J. *et al.* Correlation between endogenous nucleosomal hyper(ADP-ribosyl)ation of histone H1 and the induction of chromatin relaxation. *Embo j* **2**, 1685-1693, doi:10.1002/j.1460-2075.1983.tb01643.x (1983).
135 Kreimeyer, A., Wielckens, K., Adamietz, P. & Hilz, H. DNA repair-associated ADP-ribosylation in vivo. Modification of histone H1 differs from that of the principal acceptor proteins. *J Biol Chem* **259**, 890-896 (1984).
136 Jump, D. B., Butt, T. R. & Smulson, M. Nuclear protein modification and chromatin substructure. 3. Relationship between poly(adenosine diphosphate) ribosylation and different functional forms of chromatin. *Biochemistry* **18**, 983-990, doi:10.1021/bi00573a008 (1979).
137 Adamietz, P. & Rudolph, A. ADP-ribosylation of nuclear proteins in vivo. Identification of histone H2B as a major acceptor for mono- and poly(ADP-ribose) in dimethyl sulfate-treated hepatoma AH 7974 cells. *J Biol Chem* **259**, 6841-6846 (1984).
138 Altmeyer, M., Messner, S., Hassa, P. O., Fey, M. & Hottiger, M. O. Molecular mechanism of poly(ADP-ribosyl)ation by PARP1 and identification of lysine residues as ADP-ribose acceptor sites. *Nucleic Acids Res* **37**, 3723-3738, doi:10.1093/nar/gkp229 (2009).
139 Krupitza, G. & Cerutti, P. ADP-ribosylation of ADPR-transferase and topoisomerase I in intact mouse epidermal cells JB6. *Biochemistry* **28**, 2034-2040, doi:10.1021/bi00431a011 (1989).
140 Kalisch, T., Amé, J. C., Dantzer, F. & Schreiber, V. New readers and interpretations of poly(ADP-ribosyl)ation. *Trends Biochem Sci* **37**, 381-390, doi:10.1016/j.tibs.2012.06.001 (2012).
141 Barkauskaite, E., Jankevicius, G., Ladurner, A. G., Ahel, I. & Timinszky, G. The recognition and removal of cellular poly(ADP-ribose) signals. *Febs j* **280**, 3491-3507, doi:10.1111/febs.12358 (2013).
142 Malanga, M., Pleschke, J. M., Kleczkowska, H. E. & Althaus, F. R. Poly(ADP-ribose) binds to specific domains of p53 and alters its DNA binding functions. *J Biol Chem* **273**, 11839-11843, doi:10.1074/jbc.273.19.11839 (1998).

143 Pehrson, J. R. & Fried, V. A. MacroH2A, a core histone containing a large nonhistone region. *Science* **257**, 1398-1400, doi:10.1126/science.1529340 (1992).

144 Aravind, L. The WWE domain: a common interaction module in protein ubiquitination and ADP ribosylation. *Trends Biochem Sci* **26**, 273-275, doi:10.1016/s0968-0004(01)01787-x (2001).

145 Zhang, Y. *et al.* RNF146 is a poly(ADP-ribose)-directed E3 ligase that regulates axin degradation and Wnt signalling. *Nat Cell Biol* **13**, 623-629, doi:10.1038/ncb2222 (2011).

146 Kang, H. C. *et al.* Iduna is a poly(ADP-ribose) (PAR)-dependent E3 ubiquitin ligase that regulates DNA damage. *Proc Natl Acad Sci U S A* **108**, 14103-14108, doi:10.1073/pnas.1108799108 (2011).

147 Ahel, I. *et al.* Poly(ADP-ribose)-binding zinc finger motifs in DNA repair/checkpoint proteins. *Nature* **451**, 81-85, doi:10.1038/nature06420 (2008).

148 Rulten, S. L., Cortes-Ledesma, F., Guo, L., Iles, N. J. & Caldecott, K. W. APLF (C2orf13) is a novel component of poly(ADP-ribose) signaling in mammalian cells. *Mol Cell Biol* **28**, 4620-4628, doi:10.1128/mcb.02243-07 (2008).

149 Liu, Q., van der Marel, G. A. & Filippov, D. V. Chemical ADP-ribosylation: mono-ADPr-peptides and oligo-ADP-ribose. *Org Biomol Chem* **17**, 5460-5474, doi:10.1039/c9ob00501c (2019).

150 Bütepage, M., Eckei, L., Verheugd, P. & Lüscher, B. Intracellular Mono-ADP-Ribosylation in Signaling and Disease. *Cells* **4**, 569-595, doi:10.3390/cells4040569 (2015).

151 van der Heden van Noort, G. J., van der Horst, M. G., Overkleeft, H. S., van der Marel, G. A. & Filippov, D. V. Synthesis of mono-ADP-ribosylated oligopeptides using ribosylated amino acid building blocks. *J Am Chem Soc* **132**, 5236-5240, doi:10.1021/ja910940q (2010).

152 Kistemaker, H. A. *et al.* Synthesis and Macrodomain Binding of Mono-ADP-Ribosylated Peptides. *Angew Chem Int Ed Engl* **55**, 10634-10638, doi:10.1002/anie.201604058 (2016).

153 Voorneveld, J. *et al.* Synthetic α- and β-Ser-ADP-ribosylated Peptides Reveal α-Ser-ADPr as the Native Epimer. *Org Lett* **20**, 4140-4143, doi:10.1021/acs.orglett.8b01742 (2018).

154 Hananya, N., Daley, S. K., Bagert, J. D. & Muir, T. W. Synthesis of ADP-Ribosylated Histones Reveals Site-Specific Impacts on Chromatin Structure and Function. *J Am Chem Soc* **143**, 10847-10852, doi:10.1021/jacs.1c05429 (2021).

155 Tashiro, K., Mohapatra, J., Brautigam, C. A. & Liszczak, G. A Protein Semisynthesis-Based Strategy to Investigate the Functional Impact of Linker Histone Serine ADP-Ribosylation. *ACS Chem Biol* **17**, 810-815, doi:10.1021/acschembio.2c00091 (2022).

156 Liu, Q. *et al.* A General Approach Towards Triazole-Linked Adenosine Diphosphate Ribosylated Peptides and Proteins. *Angew Chem Int Ed Engl* **57**, 1659-1662, doi:10.1002/anie.201710527 (2018).

157 van der Heden van Noort, G. J., Overkleeft, H. S., van der Marel, G. A. & Filippov, D. V. Ribosylation of adenosine: an orthogonally protected building block for the synthesis of ADP-ribosyl oligomers. *Org Lett* **13**, 2920-2923, doi:10.1021/ol200971z (2011).

158 Kistemaker, H. A., Overkleeft, H. S., van der Marel, G. A. & Filippov, D. V. Branching of poly(ADP-ribose): Synthesis of the Core Motif. *Org Lett* **17**, 4328-4331, doi:10.1021/acs.orglett.5b02143 (2015).

159 Liu, Q., Kistemaker, H. A. V., Overkleeft, H. S., van der Marel, G. A. & Filippov, D. V. Synthesis of ribosyl-ribosyl-adenosine-5',5'',5'''(triphosphate)-the naturally occurring branched fragment of poly(ADP ribose). *Chem Commun (Camb)* **53**, 10255-10258, doi:10.1039/c7cc05755e (2017).

160 Miwa, M. *et al.* The branching and linear portions of poly(adenosine diphosphate ribose) have the same alpha(1 leads to 2) ribose-ribose linkage. *J Biol Chem* **256**, 2916-2921 (1981).

161 Miwa, M., Saikawa, N., Yamaizumi, Z., Nishimura, S. & Sugimura, T. Structure of poly(adenosine diphosphate ribose): identification of 2'-[1''-ribosyl-2''-(or 3''-)(1'''-ribosyl)]adenosine-5',5'',5'''-tris(phosphate) as a branch linkage. *Proc Natl Acad Sci U S A* **76**, 595-599, doi:10.1073/pnas.76.2.595 (1979).

162 Gold, H. *et al.* Synthesis of sugar nucleotides by application of phosphoramidites. *J Org Chem* **73**, 9458-9460, doi:10.1021/jo802021t (2008).

163 Xue, X. *et al.* Synthetic polyprenol-pyrophosphate linked oligosaccharides are efficient substrates for mycobacterial galactan biosynthetic enzymes. *Org Biomol Chem* **16**, 1939-1957, doi:10.1039/c8ob00316e (2018).

164 Wendicke, S., Warnecke, S. & Meier, C. Efficient synthesis of nucleoside diphosphate glycopyranoses. *Angew Chem Int Ed Engl* **47**, 1500-1502, doi:10.1002/anie.200703237 (2008).

165 Hofer, A. *et al.* A Modular Synthesis of Modified Phosphoanhydrides. *Chemistry* **21**, 10116-10122, doi:10.1002/chem.201500838 (2015).

166 Spicer, C. D. & Davis, B. G. Selective chemical protein modification. *Nat. Comm.* **5**, 4740, doi:10.1038/ncomms5740 (2014).

167 Gunnoo, S. B. & Madder, A. Chemical Protein Modification through Cysteine. *Chembiochem* **17**, 529-553, doi:10.1002/cbic.201500667 (2016).

168 McKay, C. S. & Finn, M. G. Click chemistry in complex mixtures: bioorthogonal bioconjugation. *Chem Biol* **21**, 1075-1101, doi:10.1016/j.chembiol.2014.09.002 (2014).

169 Hett, E. C. *et al.* Rational targeting of active-site tyrosine residues using sulfonyl fluoride probes. *ACS Chem Biol* **10**, 1094-1098, doi:10.1021/cb5009475 (2015).

170 Tang, K. C. *et al.* Tunable Amine-Reactive Electrophiles for Selective Profiling of Lysine. *Angew Chem Int Ed Engl* **61**, e202112107, doi:10.1002/anie.202112107 (2022).

171 Levine, P. M., Craven, T. W., Bonneau, R. & Kirshenbaum, K. Intrinsic bioconjugation for site-specific protein PEGylation at N-terminal serine. *Chem Commun (Camb)* **50**, 6909-6912, doi:10.1039/c4cc01928h (2014).

172 Bellucci, J. J., Bhattacharyya, J. & Chilkoti, A. A noncanonical function of sortase enables site-specific conjugation of small molecules to lysine residues in proteins. *Angew Chem Int Ed Engl* **54**, 441-445, doi:10.1002/anie.201408126 (2015).

173 Grant, G. A. Modification of Cysteine. *Curr Protoc Protein Sci* **87**, 15.11.11-15.11.23, doi:10.1002/cpps.22 (2017).

174 Lundell, N. & Schreitmüller, T. Sample preparation for peptide mapping--A pharmaceutical quality-control perspective. *Anal Biochem* **266**, 31-47, doi:10.1006/abio.1998.2919 (1999).

175 Boja, E. S. & Fales, H. M. Overalkylation of a protein digest with iodoacetamide. *Anal Chem* **73**, 3576-3582, doi:10.1021/ac0103423 (2001).

176 Shen, B. Q. *et al.* Conjugation site modulates the in vivo stability and therapeutic activity of antibody-drug conjugates. *Nat Biotechnol* **30**, 184-189, doi:10.1038/nbt.2108 (2012).

177 Bernardim, B. *et al.* Stoichiometric and irreversible cysteine-selective protein modification using carbonylacrylic reagents. *Nat Commun* **7**, 13128, doi:10.1038/ncomms13128 (2016).

178 Kenyon, G. L. & Bruice, T. W. Novel sulfhydryl reagents. *Methods Enzymol* **47**, 407-430, doi:10.1016/0076-6879(77)47042-3 (1977).

179 Davis, B. G., Maughan, M. A. T., Green, M. P., Ullman, A. & Jones, J. B. Glycomethanethiosulfonates: powerful reagents for protein glycosylation. *Tetrahedron: Asymmetry* **11**, 245-262, doi:doi.org/10.1016/S0957-4166(99)00497-8 (2000).

180 van Kasteren, S. I., Kramer, H. B., Gamblin, D. P. & Davis, B. G. Site-selective glycosylation of proteins: creating synthetic glycoproteins. *Nat Protoc* **2**, 3185-3194, doi:10.1038/nprot.2007.430 (2007).

181 Kaul, L., Süss, R., Zannettino, A. & Richter, K. The revival of dithiocarbamates: from pesticides to innovative medical treatments. *iScience* **24**, 102092, doi:10.1016/j.isci.2021.102092 (2021).

182 Veverka, K. A., Johnson, K. L., Mays, D. C., Lipsky, J. J. & Naylor, S. Inhibition of aldehyde dehydrogenase by disulfiram and its metabolite methyl diethylthiocarbamoyl-sulfoxide. *Biochem Pharmacol* **53**, 511-518, doi:10.1016/s0006-2952(96)00767-8 (1997).

183 Ahn, Y. H. *et al.* Electrophilic tuning of the chemoprotective natural product sulforaphane. *Proc Natl Acad Sci U S A* **107**, 9590-9595, doi:10.1073/pnas.1004104107 (2010).

184 Fontaine, S. D., Reid, R., Robinson, L., Ashley, G. W. & Santi, D. V. Long-term stabilization of maleimide-thiol conjugates. *Bioconjug Chem* **26**, 145-152, doi:10.1021/bc5005262 (2015).

185 Agten, S. M., Suylen, D. P. & Hackeng, T. M. Oxime Catalysis by Freezing. *Bioconjug Chem* **27**, 42-46, doi:10.1021/acs.bioconjchem.5b00611 (2016).

186 Abronina, P. I. *et al.* A Practical Silicon-Free Strategy for Differentiation of Hydroxy Groups in Arabinofuranose Derivatives. *Synthesis* **44**, 1219-1225, doi:10.1055/s-0031-1290752 (2012).

187 Albright, J. D. & Goldman, L. Dimethyl Sulfoxide-Acid Anhydride Mixtures. New Reagents for Oxidation of Alcohols1. *J. Am. Chem. Soc.* **87**, 4214-4216, doi:10.1021/ja01096a055 (1965).

188 Markiewicz, W. T. & Wiewiórowski, M. A new type of silyl protecting groups in nucleoside chemistry. *Nucleic Acids Res.* **5**, s185-s190, doi:10.1093/nar/1.suppl_1.s185 (1978).

189 Watanabe, Y., Nakamura, T. & Mitsumoto, H. Protection of phosphate with the 9-fluorenylmethyl group. Synthesis of unsaturated-acyl phosphatidylinositol 4,5-bisphosphate. *Tetrahedron Lett.* **38**, 7407-7410, doi:10.1016/S0040-4039(97)85781-4 (1997).

190 Appy, L., Chardet, C., Peyrottes, S. & Roy, B. Synthetic Strategies for Dinucleotides Synthesis. *Molecules* **24**, doi:10.3390/molecules24234334 (2019).

191 Sekine, M., Aoyagi, M., Ushioda, M., Ohkubo, A. & Seio, K. Chemically stabilized phenylboranylidene groups having a dimethoxytrityl group as a colorimetrically detectable protecting group designed for cis-1,2-diol functions of ribonucleosides in the solid-phase synthesis of m2(2,2)G5'ppT. *J Org Chem* **70**, 8400-8408, doi:10.1021/jo051202m (2005).

192 Wada, T., Sato, Y., Honda, F., Kawahara, S. & Sekine, M. Chemical Synthesis of Oligodeoxyribonucleotides Using N-Unprotected H-Phosphonate Monomers and Carbonium and Phosphonium Condensing Reagents: O-Selective Phosphonylation and Condensation. *J. Am. Chem. Soc.* **119**, 12710-12721, doi:10.1021/ja9726015 (1997).

193 Le Corre, S. S., Berchel, M., Couthon-Gourvès, H., Haelters, J. P. & Jaffrès, P. A. Atherton-Todd reaction: mechanism, scope and applications. *Beilstein J Org Chem* **10**, 1166-1196, doi:10.3762/bjoc.10.117 (2014).

194 O'Sullivan, J. *et al.* Emerging roles of eraser enzymes in the dynamic control of protein ADP-ribosylation. *Nat Commun* **10**, 1182, doi:10.1038/s41467-019-08859-x (2019).

195 Singh, H. R. *et al.* A Poly-ADP-Ribose Trigger Releases the Auto-Inhibition of a Chromatin Remodeling Oncogene. *Mol Cell* **68**, 860-871.e867, doi:10.1016/j.molcel.2017.11.019 (2017).

196 Gibson, B. A., Conrad, L. B., Huang, D. & Kraus, W. L. Generation and Characterization of Recombinant Antibody-like ADP-Ribose Binding Proteins. *Biochemistry* **56**, 6305-6316, doi:10.1021/acs.biochem.7b00670 (2017).

197 Struhl, K. & Segal, E. Determinants of nucleosome positioning. *Nat Struct Mol Biol* **20**, 267-273, doi:10.1038/nsmb.2506 (2013).

198 Saumer, P. Elucidating the chromatosome interactome: A modular platform for the investigation of linker histone modifications. *PhD thesis* (2023).

199 Klinker, H., Haas, C., Harrer, N., Becker, P. B. & Mueller-Planitz, F. Rapid purification of recombinant histones. *PLoS One* **9**, e104029, doi:10.1371/journal.pone.0104029 (2014).

200 Tanaka, Y. *et al.* Expression and purification of recombinant human histones. *Methods* **33**, 3-11, doi:10.1016/j.ymeth.2003.10.024 (2004).

201 Flaus, A. Principles and practice of nucleosome positioning in vitro. *Front. Life Sci.* **5**, 5-27, doi:10.1080/21553769.2012.702667 (2011).

202 Claudet, C., Angelov, D., Bouvet, P., Dimitrov, S. & Bednar, J. Histone octamer instability under single molecule experiment conditions. *J Biol Chem* **280**, 19958-19965, doi:10.1074/jbc.M500121200 (2005).

203 Brehove, M. *et al.* DNA sequence influences hexasome orientation to regulate DNA accessibility. *Nucleic Acids Res* **47**, 5617-5633, doi:10.1093/nar/gkz283 (2019).

204 Frouws, T. D., Barth, P. D. & Richmond, T. J. Site-Specific Disulfide Crosslinked Nucleosomes with Enhanced Stability. *J Mol Biol* **430**, 45-57, doi:10.1016/j.jmb.2017.10.029 (2018).

205 Zhou, B. R. *et al.* Distinct Structures and Dynamics of Chromatosomes with Different Human Linker Histone Isoforms. *Mol Cell* **81**, 166-182.e166, doi:10.1016/j.molcel.2020.10.038 (2021).
206 Mohapatra, J. *et al.* Serine ADP-ribosylation marks nucleosomes for ALC1-dependent chromatin remodeling. *Elife* **10**, doi:10.7554/eLife.71502 (2021).
207 Poirier, G. G., de Murcia, G., Jongstra-Bilen, J., Niedergang, C. & Mandel, P. Poly(ADP-ribosyl)ation of polynucleosomes causes relaxation of chromatin structure. *Proc Natl Acad Sci U S A* **79**, 3423-3427, doi:10.1073/pnas.79.11.3423 (1982).
208 D'Amours, D., Desnoyers, S., D'Silva, I. & Poirier, G. G. Poly(ADP-ribosyl)ation reactions in the regulation of nuclear functions. *Biochem J* **342 (Pt 2)**, 249-268 (1999).
209 Liu, C., Vyas, A., Kassab, M. A., Singh, A. K. & Yu, X. The role of poly ADP-ribosylation in the first wave of DNA damage response. *Nucleic Acids Res* **45**, 8129-8141, doi:10.1093/nar/gkx565 (2017).
210 Kraus, W. L. & Lis, J. T. PARP goes transcription. *Cell* **113**, 677-683, doi:10.1016/s0092-8674(03)00433-1 (2003).